NAVAL POSTGRADUATE SCHOOL

MONTEREY, CALIFORNIA

THESIS

THE IMPACTS OF MULTIPLE SIMULTANEOUS CLIMATE VARIATIONS

by

Richard E. Ilczuk Jr.

December 2016

Thesis Advisor: Tom Murphree
Co-Advisor: Megan Hutchins

THIS PAGE INTENTIONALLY LEFT BLANK

REPORT DOCUMENTATION PAGE			*Form Approved OMB No. 0704–0188*

1. AGENCY USE ONLY *(Leave blank)*	**2. REPORT DATE** December 2016	**3. REPORT TYPE AND DATES COVERED** Master's thesis

4. TITLE AND SUBTITLE THE IMPACTS OF MULTIPLE SIMULTANEOUS CLIMATE VARIATIONS	**5. FUNDING NUMBERS**
6. AUTHOR(S) Richard E. Ilczuk Jr.	
7. PERFORMING ORGANIZATION NAME(S) AND ADDRESS(ES) Naval Postgraduate School Monterey, CA 93943-5000	**8. PERFORMING ORGANIZATION REPORT NUMBER**
9. SPONSORING /MONITORING AGENCY NAME(S) AND ADDRESS(ES) Earth System Prediction capability Program of the Office of Naval Research and Naval Research Program of the Naval Postgraduate School	**10. SPONSORING / MONITORING AGENCY REPORT NUMBER**

11. SUPPLEMENTARY NOTES The views expressed in this thesis are those of the author and do not reflect the official policy or position of the Department of Defense or the U.S. Government. IRB number ____N/A____.

12a. DISTRIBUTION / AVAILABILITY STATEMENT Approved for public release. Distribution is unlimited.	**12b. DISTRIBUTION CODE**

13. ABSTRACT (maximum 200 words)

Climate variations—such as El Niño–La Niña (ENLN), the Madden–Julian Oscillation (MJO), and the Arctic Oscillation (AO)—have significant impacts on environmental conditions and operating environments around the globe. However, relatively little is known about how climate variations interact and alter each other's impacts. We used several multi-decadal reanalysis data sets to investigate the interactions between ENLN and MJO events. We analyzed the interactions by season, and by event amplitude and phase. We found substantial constructive and destructive interference between the tropical convection and subsidence centers of ENLN and MJO events, and the tropical and extratropical low-frequency wave responses to the events. This interference causes large differences in the anomalies that are commonly thought to characterize the events—for example, changes in the patterns, locations, magnitudes, and even signs of the wind, precipitation, and ocean surface wave anomalies associated with EN, LN, and the eight MJO phases. Our results indicate that analyses and forecasts of one type of climate variation need to account for the simultaneous occurrence of other types of climate variations. The data sets, methods, and results of this study will be used to improve operational climate and long range support products.

14. SUBJECT TERMS climate, climate variations, El Niño, El Nino, La Niña, La Nina, long range forecasting, Madden–Julian Oscillation, operational climate support	**15. NUMBER OF PAGES** 195
	16. PRICE CODE

17. SECURITY CLASSIFICATION OF REPORT	**18. SECURITY CLASSIFICATION OF THIS PAGE**	**19. SECURITY CLASSIFICATION OF ABSTRACT**	**20. LIMITATION OF ABSTRACT**
Unclassified	Unclassified	Unclassified	UU

NSN 7540-01-280-5500 Standard Form 298 (Rev. 2-89)
Prescribed by ANSI Std. 239-18

THIS PAGE INTENTIONALLY LEFT BLANK

Approved for public release. Distribution is unlimited.

THE IMPACTS OF MULTIPLE SIMULTANEOUS CLIMATE VARIATIONS

Richard E. Ilczuk Jr.
Lieutenant Commander, United States Navy
B.S., United States Naval Academy, 2006

Submitted in partial fulfillment of the
requirements for the degree of

MASTER OF SCIENCE IN METEOROLOGY AND PHYSICAL OCEANOGRAPHY

from the

NAVAL POSTGRADUATE SCHOOL
December 2016

Approved by: Tom Murphree
Thesis Advisor

Megan Hutchins
Co-Advisor

Wendell Nuss
Chair, Department of Meteorology

THIS PAGE INTENTIONALLY LEFT BLANK

ABSTRACT

Climate variations—such as El Niño–La Niña (ENLN), the Madden–Julian Oscillation (MJO), and the Arctic Oscillation (AO)—have significant impacts on environmental conditions and operating environments around the globe. However, relatively little is known about how climate variations interact and alter each other's impacts. We used several multi-decadal reanalysis data sets to investigate the interactions between ENLN and MJO events. We analyzed the interactions by season, and by event amplitude and phase. We found substantial constructive and destructive interference between the tropical convection and subsidence centers of ENLN and MJO events, and the tropical and extratropical low-frequency wave responses to the events. This interference causes large differences in the anomalies that are commonly thought to characterize the events—for example, changes in the patterns, locations, magnitudes, and even signs of the wind, precipitation, and ocean surface wave anomalies associated with EN, LN, and the eight MJO phases. Our results indicate that analyses and forecasts of one type of climate variation need to account for the simultaneous occurrence of other types of climate variations. The data sets, methods, and results of this study will be used to improve operational climate and long range support products.

THIS PAGE INTENTIONALLY LEFT BLANK

TABLE OF CONTENTS

LIST OF FIGURES

THIS PAGE INTENTIONALLY LEFT BLANK

LIST OF TABLES

THIS PAGE INTENTIONALLY LEFT BLANK

LIST OF ACRONYMS AND ABBREVIATIONS

ACAF	Advanced Climate Analysis and Forecasting
AL	Aleutian Low
AMIP-II	Atmospheric Model Intercomparison Project-II
AO	Arctic Oscillation
AOR	area of operations
AS	American Samoa
BOM	Australian Government Bureau of Meteorology
CFSR	Climate Forecast System Reanalysis
CMSP	Coastal and Marine Spatial Planning
CNMI	Commonwealth of the Northern Mariana Islands
DOD	Department of Defense
DOE	Department of Energy
EM	electromagnetic
EN	El Nino
ENLN	El Nino-La Niña
ENSO	El Nino Southern Oscillation
EOF	empirical orthogonal function
ESRL	Earth System Research Laboratory
ETC	extratropical cyclone
FNMOC	Fleet Numerical Meteorology and Oceanography Center
GPH	geopotential height
GSI	Gridpoint Statistical Interpolation
HWC	Hadley-Walker Circulation
IL	lcelandic Low
IOD	Indian Ocean Dipole
ITCZ	Intertropical Convergence Zone
JAS	July, August, September
JFM	January, February, March
LN	La Niña
LTM	long term mean

mb	millibars
MC	maritime continent
MEI	Multivariate ENSO Index
METOC	meteorology and oceanography
MJO	Madden–Julian Oscillation
NAO	North Atlantic Oscillation
NCAR	National Center for Atmospheric Research
NCEI	National Centers for Environmental Information
NCEP	National Centers for Environmental Prediction
NOAA	National Oceanic Atmospheric Administration
NPH	North Pacific High
OLR	outgoing longwave radiation
PERSIANN-CDR	Precipitation Estimation from Remotely Sensed Information using Artificial Neural Networks Climate Date Record
PNA	Pacific-North American
PR	precipitation rate
PRA	precipitation rate anomaly
R1	NCEP/NCAR Reanalysis 1
R2	NCEP/DOE AMIP-II Reanalysis
RMM	Real-time Multivariate MJO
SLP	sea level pressure
SLPA	sea level pressure anomaly
SPCZ	South Pacific Convergence Zone
SPH	South Pacific High
SST	sea surface temperature
SSTA	sea surface temperature anomaly
SWA	southwest Asia
SWH	significant wave height
SWHA	significant wave height anomaly
TC	tropical cyclone
U.S.	United States

ACKNOWLEDGMENTS

I would like to thank Professor Tom Murphree and Megan Hutchins for their guidance and expertise during the entire thesis process. I received a tremendous amount of assistance from Mary Jordan, whose Matlab knowledge enabled us to process countless numbers of data sets with ease. Thank you, Mary! Many thanks to Bruce Ford and Justin Dennison of Clear Science, Inc., who developed a process to composite and plot multiple non-consecutive dates using the CFSR forced WW3 reanalysis data set. I would also like to acknowledge Earth System Research Laboratory/Physical Sciences Division, for providing me daily composites of numerous variables for this research. My beautiful wife, Meghan, deserves a lot of credit for her continuous support and patience during the past 29 months. Thank you, Meghan! This research was supported in part by the Earth System Prediction Capabilities Program of the Office of Naval Research and the Naval Research Program of the Naval Postgraduate School.

THIS PAGE INTENTIONALLY LEFT BLANK

I. INTRODUCTION

A. MOTIVATION AND BACKGROUND

Long-range forecasts of environmental conditions are an increasingly important set of products for operational forecasting centers, such as the U.S. Navy's Fleet Numerical Meteorology and Oceanography Center (FNMOC). Long-range forecast are especially important in long-range planning of operations, such as Department of Defense (DOD) exercises and operations. Many months prior to an operational deployment, military meteorology and oceanography (METOC) specialists begin identifying the expected climatological conditions for the area of operations (AOR) and for the transits to and from the AOR. These conditions are often described in terms of the operating limits, or thresholds, for the people and equipment that will be used in the operation—for example, in terms of the probability that temperatures will exceed the limits within which operations can be safely and effectively conducted. Long term mean (LTM) conditions are a common way to represent expected climate conditions (e.g., the temperature based on an average of several decades of temperature records). But the climate system experiences substantial intraseasonal, interannual, decadal, and longer variations from long term mean conditions, such as El Nino–La Niña (ENLN), Madden–Julian Oscillation (MJO), North Atlantic Oscillation (NAO), Arctic Oscillation (AO), and Indian Ocean Dipole (IOD) events (Bridgman and Oliver 2006). These climate variations need to be accounted for in operational climate support because they can lead to large deviations, or anomalies, from long term mean conditions (Van den Dool 2007).

The impacts of climate variation can extend over large regions of the globe. For example, ENLN events centered in the tropical Pacific can significantly alter temperatures, precipitation, and many other variables throughout the globe (Horel and Wallace 1981; Philander 1990). These interactions over large distances are known as climate teleconnections. The mechanisms for climate teleconnections tend to involve relatively low frequency Rossby and Kelvin waves in the atmosphere and ocean (Horel and Wallace 1981; Sardeshmukh and Hoskins 1988; Stepanek 2006; Zhang 2013). Climate variation can trigger such wave activity, and two climate variations occurring at

the same time can trigger waves that constructively and/or destructively interfere with each other. For example, Stepanek (2006) identified constructive and destructive interference in the anomalous extratropical Rossby waves initiated by simultaneous MJO and ENLN events. However, relatively few studies have been done to investigate how multiple simultaneous climate variations interact with each other and how they alter each other's impacts around the globe (Stepanek 2006; Johnson 2011; Moon et al. 2011). In this research, we have investigated these interactions by analyzing the global scale anomalies associated with simultaneous MJO and ENLN events. Our main motivations for this research were: (1) build a research foundation for analyzing and forecasting the impacts of multiple simultaneous climate variations; and (2) increase operational climate and long range support capabilities at FNMOC and elsewhere by improving data sets, methods, and tools for accounting for the effects of multiple simultaneous climate variations.

One operational application of improved information about the impacts of multiple simultaneous climate variations is in coastal and marine spatial planning (CMSP). CMSP uses information from subject matter experts, government policy documents, and science-related tools, such as geographic information systems (GIS), to address specific ocean management challenges and advance goals for economic development and conservation (NOAA 2016). CMSP is a collaborative effort that includes state officials, private companies, local partners, and federal organizations, including the U.S. Navy (Obama 2010). DOD is involved in CMSP in accordance with Executive Order 13547, Stewardship of the Ocean, our Coasts, and the Great Lakes (19 July 2010). The Assistant Secretary of the Navy for Energy, Installations, and Environment Program established guidelines for implementing federal coastal and ocean policy. CMSP involves the development of environmental data sets, and wide access to those data sets and to visualization and analysis tools. This environmental information is critical in developing and implementing plans for use of the coastal and marine environment by a wide range of organizations and individuals, including commercial, national security, and recreational users. CMSP is being conducted for the U.S. affiliated Pacific islands—Hawaii, Guam, Commonwealth of the Northern Mariana Islands

(CNMI), and American Samoa (AS) (Pacific Islands Regional Planning Body 2016). These Pacific island regions are important for cultural, historic, economic, and national security reasons. From a DOD perspective, CMSP is important for these regions to help plan exercises and other operations, and to minimize conflicts between national security operations and other operations (e.g., conflicts between Navy exercises and offshore energy, aquaculture and recreational operations). The environmental information developed by climate research, such as our research project, is important in developing coastal marine spatial plans that account for long term mean and climate variation conditions, including conditions associated with multiple climate variations. Much of our research is focused on the tropical Pacific and thus has a high potential to contribute to the environmental information needed for Pacific islands CMSP.

B. MJO OVERVIEW AND CLASSIFICATION

The MJO, first identified by Madden and Julian (1971, 1994), is a major intraseasonal climate variation of the tropical atmosphere and ocean with substantial impacts in the extratropics (Stepanek 2006; Pohl and Matthews 2007; Johnson 2011; Zhang 2005, 2013). MJO events have convective and subsidence components centered near the equator that propagate eastward around the globe in about 30 to 60 days (Hendon and Salby 1994; Zhang 2013; Gottschalck et al. 2016). Figures 1 and 2 show examples of the anomalies that are typically used to characterize MJO events. Figure 1 shows the sea level pressure (SLP) anomalies (SLPAs) associated with eight phases of the MJO for November–March and May–September. The convective [subsidence] component is represented by the tropical region of negative [positive] SLPAs. The eight phases are represented by the eight panels for each period, November–March and May–September. The location of the convective component is represented by the phase name. For example, phase 2 is labeled West Indian Ocean, phase 4 is labeled West Maritime Continent, and phase 8 is labeled East Pacific Ocean. Note the eastward progression of these components from one phase to the next. The SLPA patterns indicate that the MJO has characteristics of an anomalous tropical Rossby-Kelvin wave response to heating anomalies centered on the equator (Matsuno 1966; Gill 1982). Figure 2 shows the

corresponding precipitation anomalies for the eight MJO phases. Note that areas of anomalously low [high] SLP tend to be areas of anomalously high [low] precipitation.

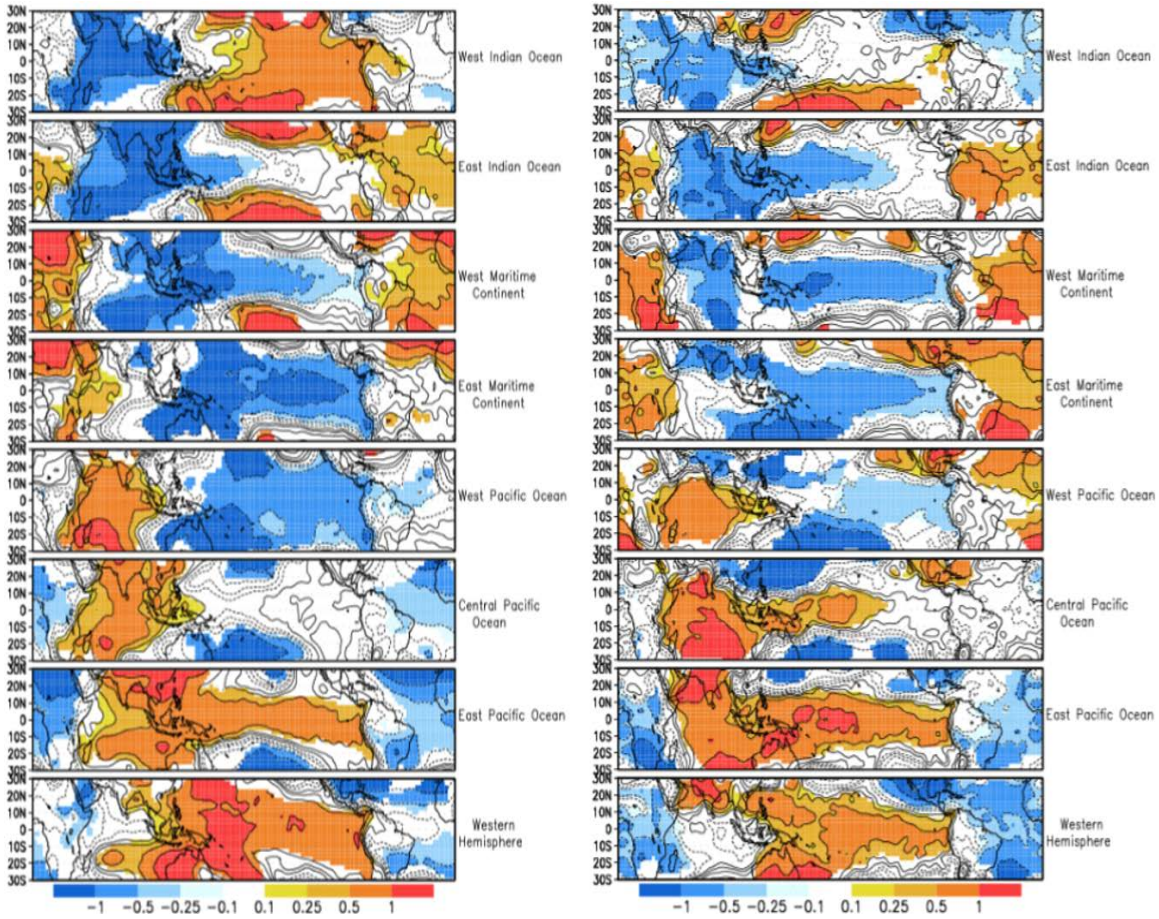

Composite SLP anomalies (mb) for eight phases of the MJO cycle based on data for November-March 1979–2004 (left panels) and May-September 1979–2004 (right panels).

Figure 1. SLP (mb) Anomalies for Eight MJO Phases. Source: Gottschalck et al. (2016).

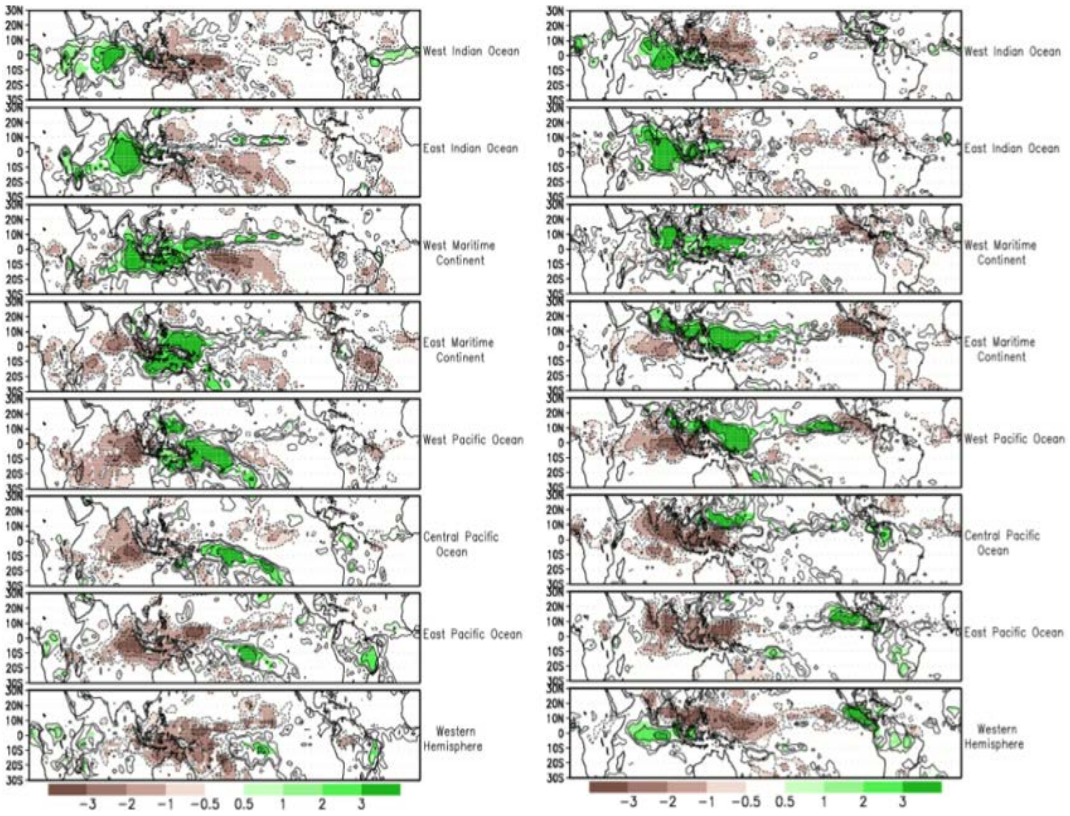

Composite precipitation anomalies (mm) for eight phases of the MJO cycle based on data for November-March 1979–2004 (left panels) and May-September 1979–2004 (right panels.

Figure 2. Precipitation Anomalies for Eight MJO Phases.
Source: Gottschalck et al. (2016).

Figure 3 shows the basic structures associated with the MJO. The convective component (left side of Figure 3) is characterized by anomalous deep convection with upward vertical motion and precipitation over and near the equator, a pair of negative SLPAs that straddle the equator, and a pair of anomalous upper tropospheric anticyclones that straddle the equator. The subsidence component (right side of Figure 3) is characterized by opposite anomalies—anomalously downward vertical motion, anomalously clear skies, negative precipitation anomalies, positive SLPAs straddling the equator, and negative upper tropospheric height anomalies straddling the equator.

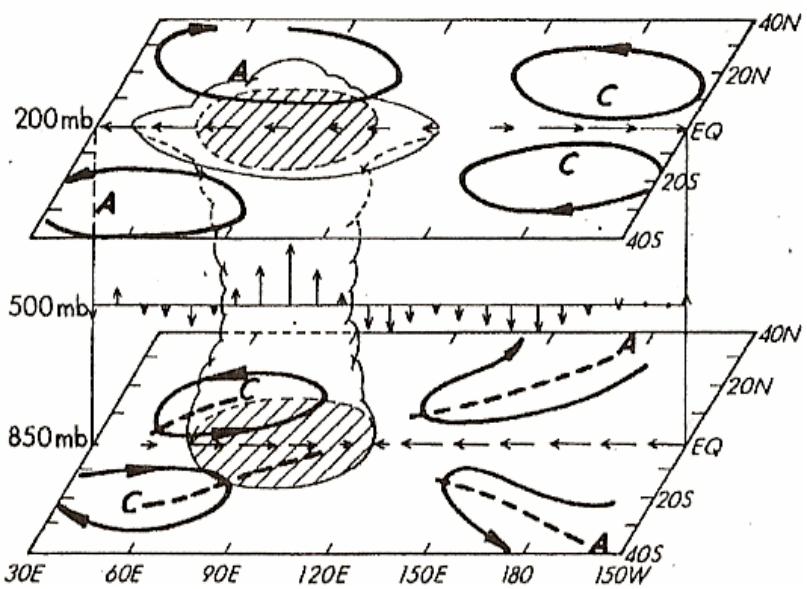

The convective and subsidence components of the MJO along the equator as it propagates eastward. The cloud represents the anomalous convection, thick black arrows represent anomalous winds at 850 mb and 200 mb, and smaller black arrows depict vertical motions at 500 mb. The anticyclonic and cyclonic circulation centers are depicted with an "A" or "C" with troughs and ridges shown as dashed lines.

Figure 3. Convective and Subsidence Components of the MJO.
Source: Rui and Wang (1990).

MJO events are centered in the tropics but can have significant impacts on extratropical conditions (Madden and Julian 1994; Kayano and Kousky 1999; Wang et al. 2002; Stepanek 2006; Zhang 2013; Gottschalck et al. 2016). These impacts occur in large part by the initiation of teleconnections in which tropical heating and circulation anomalies lead to the triggering of anomalous extratropical Rossby waves that then alter tropospheric circulations, temperature and moisture advection, precipitation, and other variables (Sardeshmukh and Hoskins 1988; Hendon and Salby 1994; Kayano and Kousky 1999; Stepanek 2006). Figure 4 shows the characteristic 200 mb geopotential height anomalies for MJO phase 4 during October-March. In the extratropics, the height anomalies have an equivalent barotropic structure, so the sign and spatial distribution of the 200 mb height anomalies are representative of the corresponding lower tropospheric height anomalies. The alternating positive and negative anomalies marked by the black arrow indicate an anomalous extratropical Rossby wave train that is a response to the warming and cooling anomalies that are associated with the convective and subsidence

components. The height anomalies represent corresponding circulation anomalies that lead to anomalies in temperature, moisture advection, precipitation, and other variables. For example, the negative height anomalies centered near Alaska and the northeastern Pacific indicate positive moisture advection anomalies into, and precipitation anomalies over, much of northwestern North America (Stepanek 2006).

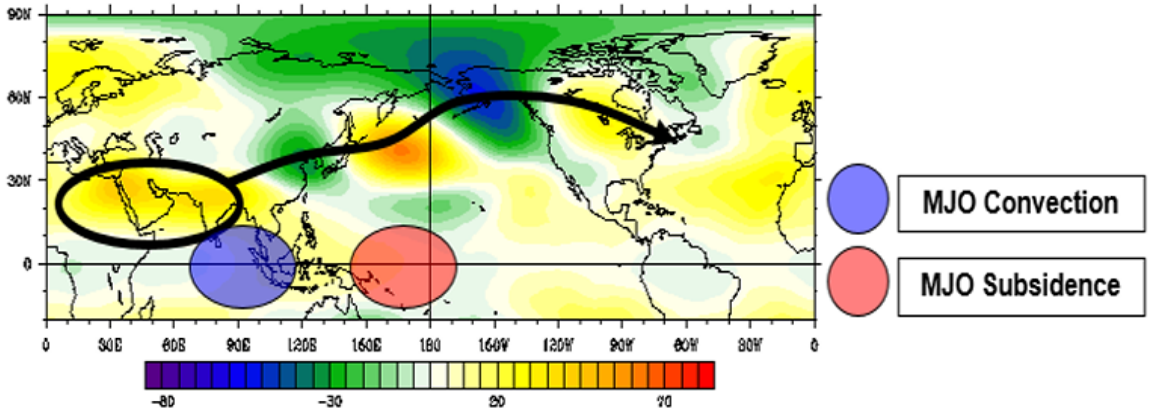

Characteristic 200 mb height anomalies (m) for MJO phase 3 in October-March. Blue and pink ovals show the positons of the MJO convective and subsidence components. Alternating positive and negative anomalies marked by black arrow indicate anomalous extratropical Rossby wave train extending northward and eastward from southwest Asia to North America.

Figure 4. 200 mb Height Anomalies (m) for MJO Phase 3 during October-March. Source: Stepanek, Murphree, and Wash (2006).

Wheeler and Herndon (2004) developed an index of the MJO phase and amplitude that is widely used in research and operations. The index is derived from an empirical orthogonal function (EOF) analysis of near-real time equatorial anomalies of 850 mb zonal wind, 200 mb zonal wind, and satellite-observed outgoing longwave radiation (OLR). The index is routinely updated by the Australian Government Bureau of Meteorology (BOM; BOM 2016). The main results of the EOF analysis are two real-time multivariate MJO (RMM) EOFs termed RMM1 and RMM2 that provide a multivariate description of the MJO phase and amplitude (BOM 2016). The phase indicates the location of the convective component and, by implication, the location of the convective component to the east (or west) of the convective component. Figure 5 shows an example of how that index is used to graphically represent the state of MJO. The index value for

an individual day is indicated by a point on the colored curve. The location of a point within the eight triangular regions indicates the phase. The distance of a point from the center indicates the amplitude or strength of the MJO, with greater distances indicating greater amplitudes. Figure 5 shows the index values for 01 January-31 March 1997 (red for January, green for February, blue for March). Note the generally eastward propagation and the amplitude variations during this three month period. The extratropical impacts of MJO events depend in part on the MJO phase and amplitude, and the season in which the MJO occurs (Stepanek 2006).

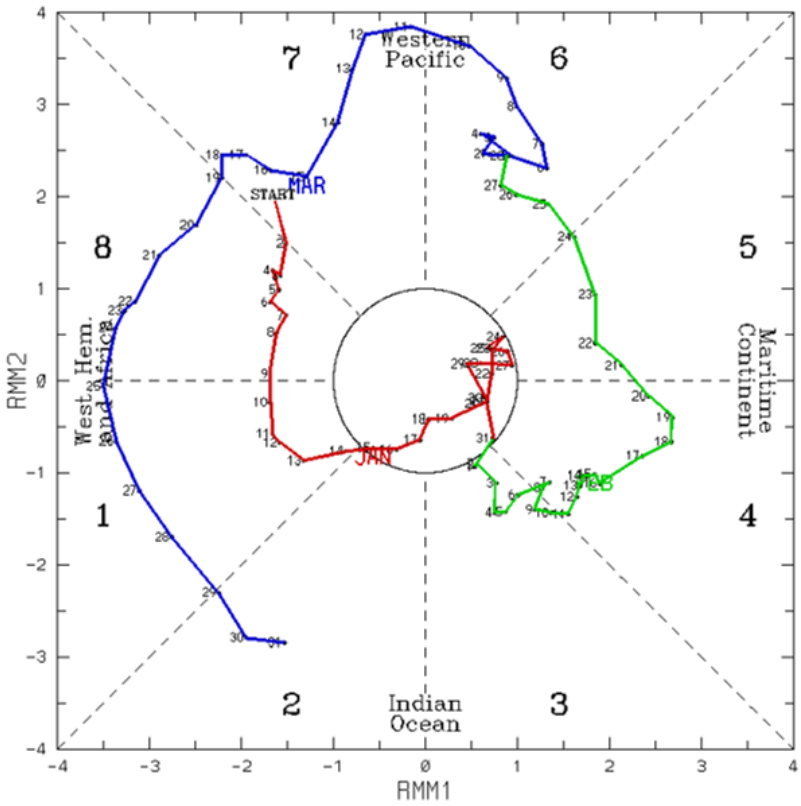

MJO and amplitude phase diagram for 01 January 1997–31 March 1997 based (red for Jan, green for Feb, and blue for Mar). A point on the colored curve represents the MJO for a single day. The phase for that day is indicated by the triangular region (1–8) in which the point occurs. The amplitude is indicated by the distance of the point for the center of the diagram (greater distance indicates greater amplitude). Points within the central circle indicate weak amplitudes.

Figure 5. MJO Phase and Amplitude Diagram for 01 January 1997 through 31 March 1997. Source: Commonwealth of Australia Bureau of Meteorology (2016).

C. IMPACTS OF SIMULTANEOUS CLIMATE VARIATIONS

There have been many studies of individual climate variations, such as ENLN, MJO, and AO (e.g., Philander 1990; Madden and Julian 1994; Wang et al. 2002; Bridgman and Oliver 2006; Camargo et al. 2009; Zhang 2013). But there have been far fewer studies of the combined effects, or impacts, of multiple simultaneous climate variations, especially of the combined extratropical impacts. The studies of individual climate variations have characterized the anomalies associated with each variation by composting the anomalies for multiple days during which the variation has occurred (e.g., Horel and Wallace 1981). But many of these composites have not been filtered to remove days in which other climate variations occurred, especially climate variations with similar frequencies. Thus, the characteristic anomalies derived from these composite analyses may include effects from other climate variations that were occurring on the composited days. Thus, the resulting anomalies may misrepresent the anomalies that are actually characteristic of the climate variation for which the compositing was done.

Climate variations often occur simultaneously, and it is highly likely that the climate anomalies that occur under those conditions are different than those that occur when only one variation is occurring or when some other combination of variations is occurring. Thus, it is important from a research perspective and an operational analysis and forecasting perspective to be able to distinguish the characteristic anomalies associated with: (a) individual climate variations; and (b) different combinations of two or more climate variations. For example, it is important to distinguish EN and MJO precipitation anomalies from each other, and to distinguish the precipitation anomalies that occur when EN and MJO phase 4 is occurring from EN and MJO phase 8, from LN and MJO phase 3, from negative AO and MJO phase 5, etc.

Kessler and Kleeman (1999) used numerical model experiments to conclude that MJO events can enhance EN events, and thus lead to a coupling of MJO and EN processes. Zhang (2005) summarized the results of studies that have looked at the interactions of ENLN and MJO in the tropics—for example, the potential for MJO events to initiate EN events through the triggering of equatorial ocean Kelvin waves and of EN events to affect the intensity of MJO events. Moon et al. (2011) found that the impacts of

MJO phases 3 and 7 on east Asia and western North America can be altered by the simultaneous occurrence of EN or LN. Stepanek (2006) analyzed the extratropical impacts of MJO events according to the state of ENLN, as well as according to MJO phase, amplitude, and the season. Stepanek found that the anomalous extratropical Rossby wave trains associated with the different MJO phases were substantially affected by the presence or absence of EN and LN, which led to large differences in extratropical precipitation anomalies associated with the phases. Marshal et al. (2015, 2016) assessed the impact of the MJO on global ocean wind waves, including the combined impacts of MJO and NAO events, and found evidence of interactions between the two climate variations and their impacts on ocean surface waves, especially in the North Atlantic.

A number of new climate data sets have become available since these prior studies of simultaneous MJO and ENLN events. These data sets provide improved accuracies, spatial and temporal resolutions, spatial and temporal coverage, and additional variables. The data sets include, for example, the National Centers for Environmental Prediction (NCEP) Climate Forecast System Reanalysis (CFSR; Saha et al. 2006, 2010) and Climate Forecast System Version 2 (CFSV2; Saha et al. 2014), NCEP WaveWatch III hindcasts with CFSR wind forcing (WW3; Chawla et al. 2103), and the Precipitation Estimation from Remotely Sensed Information using Artificial Neural Networks Climate Date Record (PERSIANN-CDR; Ashouri et al. 2014). These new data sets have the potential to improve analyses and forecasts of climate variations and their individual and combined impacts.

D. RESEARCH QUESTIONS

We designed our study to exploit the new climate data sets to better determine how multiple simultaneous climate variations affect each other's impacts. We focused our study on variables that are important in the development of climate and long range support for national security operations and Pacific islands CMSP (for example, precipitation and ocean surface waves). We focused on MJO and ENLN events, but our methods are applicable to many other climate variations.

Our main research questions were:

1. How are the impacts of MJO affected by the simultaneous occurrence of ENLN events, and vice versa?

2. How do these effects vary by:

    a. MJO phase

    b. season

    c. variable

    d. location

3. How large are these effects?

4. What dynamical processes lead to these effects?

5. How can operational support centers, such as FNMOC, optimally provide information about these effects to their customers?

6. How can information about these variations be optimally conveyed to improve decision support?

E. THESIS ORGANIZATION

Chapter II describes the study period and regions, followed by a summary of our data sets and methods. Chapter III describes our main results for sea surface temperature (SST), sea level pressure (SLP), 200 mb geopotential height (Z200), precipitation rate (PR), and significant wave height (SWH) for MJO phase 4 during January, February, and March (JFM). Chapter IV provides our conclusions and recommendations for further work. Appendices A-C provide, respectively, results for phase 8 during JFM, for phases 4 and 8 during July, August, and September (JAS), and for precipitation in southwest Asia (SWA).

THIS PAGE INTENTIONALLY LEFT BLANK

II. DATA AND METHODS

A. STUDY REGIONS AND PERIODS

We focused on three main study regions: (1) the entire globe; (2) the tropical Pacific (30°S–30°N, 100°E–70°W); and (3) southwest Asia (0°N–50°N, 20°E–110°E). There were some deviations from these regions to account for data set limitations—for example, limitations in the spatial coverage of the PERSIANN-CDR data set.

Our study period was July 1974-March 2016. Our focus months were January, February, and March (JFM) and July, August, and September (JAS). There were some deviations from these years to account for data set limitations—for example, limitations in the temporal coverage of the CFSR and WW3 data sets. The July 1974 start of the study periods was determined by the start of the RMM MJO index data set that we used. We chose to focus on JFM and JAS because these months tend to represent extremes in the: (1) seasonal cycle of the climate system; (2) activity of MJO and ENLN; and (3) impacts of MJO and ENLN in the extratropics and elsewhere.

B. VARIABLES AND DATA SETS

Our focus variables and data sets are summarized in Table 1. In this table, R1 is the NCEP/National Center for Atmospheric Research (NCAR) reanalysis (Kalnay et al. 1996; Kistler et al. 2001), WW3 is the NCEP WaveWatch III hindcasts with CFSR wind forcing (Chawla et al. 2013), and PERSIANN-CDR is the Precipitation Estimation from Remotely Sensed Information using Artificial Neural Networks Climate Date Record (Ashouri et al. 2014). The LTM period is the period used for calculating the long term means which we then used to calculate climate anomalies. The LTM period is also the period covered by the data set, except for R1 for which the period covered is 1948-present. The analysis tools in Table 1 refer to the main tools we used to access, download, and/or process the data. ESRL stands for two websites of the NOAA Earth System Research Laboratory Physical Science Division (PSD) at which we composited, plotted, and downloaded data and figures (http://www.esrl.noaa.gov/psd/cgi-bin/data/composites/printpage.pl and http://www.esrl.noaa.gov/psd/data/composites/day). ACAF

stands for Advanced Climate Analysis and Forecasting, a restricted access website of the U.S. Navy's FNMOC, at which climate data sets can be accessed, visualized, composited, and analyzed. CSI stands for Clear Science, Inc., a research and development organization involved in developing ACAF and in cooperative research with the Naval Postgraduate School (NPS). CSI assisted us in developing composites of the WW3 data. Matlab is the data analysis and visualization software package from MathWorks.

Table 1. Variables and Data Sets Used in Study

Focus Variables	Data Sets	LTM Periods	Analysis Tools
Sea Surface Temperature (SST)	R1	1981–2010	ESRL
Sea Level Pressure (SLP)	R1	1981–2010	ESRL
200 mb Geopotential Height (Z200)	R1	1981–2010	ESRL
Precipitation Rate (PR)	PERSIANN-CDR	1983–2015	Matlab
Significant Wave Height (SWH)	WW3	1979–2007	ACAF / CSI / Matlab

The details of the data sets are well described by the references cited. But some aspects of the data sets affected our selection and use of the data sets. We chose to use R1 instead of CFSR because the R1 data was readily available via the ESRL sites for producing composites of hundreds of days of data. This availability significantly increased our ability to analyze multiple simultaneous climate variation impacts. For precipitation, we chose to use the PERSIANN-CDR data set instead of the R1 or CFSR data sets because the PERSIANN-CDR data set: (a) has a higher horizontal resolution (0.25°, compared to 2.5° for R1 and 0.5° for CFSR); and (b) has fewer of the reanalysis artifacts that are apparent in the R1 and CFSR precipitation data, especially over land (Kalnay et al. 1996; Kistler et al. 2001; Ashouri et al. 2014). The PERSIANN-CDR data is limited spatially to 60°S–60°N, and there are spatial gaps within this latitude range where insufficient satellite data was available for our analyses—for example, in central Asia north of Afghanistan and Pakistan.

We selected the focus variables to provide representations of the main processes that: (a) characterize MJO and ENLN (e.g., SST, SLP, Z200, PR); (b) characterize the extratropical impacts of these climate variations (e.g., SST, SLP, Z200, PR, SWH); and (c)

are important in the planning of national security operations and in CMSP (e.g., SST, SLP, Z200, PR, SWH). We initially analyzed other variables, including 850 mb geopotential height (Z850) and outgoing longwave radiation (OLR) but decided that our five focus variables were sufficient for the scope of this research project. We used daily mean values for each of the variables from which we then computed monthly and three-monthly means.

C. MJO AND ENLN INDICES

We focused on MJO and ENLN climate variations. We used the RMM index (BOM 2016) to identify MJO days, phases, and amplitudes at a daily resolution. We used RMM index data for the period July 1974-March 2016, but minus the period March-December 1978 for which no data was available due to missing satellite observations (BOM 2016). We obtained the RMM index data at: htttp://www.bom.gov.au/climate/mjo/graphics/rmm.74toRealtime.txt.

We used the Multivariate ENSO Index (MEI) to identify ENLN periods, phases, and amplitudes. The MEI is a bimonthly index based on six variables: sea level pressure, zonal and meridional components of the surface wind, sea surface temperature, surface air temperature, and total cloudiness fraction of the sky (Wolter and Timlin 2011). We obtained the MEI data at: http://www.esrl.noaa.gov/psd/enso/mei/. We interpolated the MEI bimonthly values to daily values for comparison to the daily values for the MJO index. We used the MEI magnitude to determine the ENLN state, as shown in Table 2. In this table, the number of days describes the number of days that we identified for each ENLN state in our July 1974-March 2016 study period. The total number of days in that study period was 14,960.

Table 2. Determination of ENLN State

MEI Value Range	ENLN State	Number of Days in Study Period
> +0.5	EN	6,076
-0.5 to +0.5	Neutral	5,933
< -0.5	LN	2,951

Table 3 shows the number of days in each ENLN state for JFM and JAS in the study period.

Table 3. Number of EN, Neutral, and LN Days for JFM and JAS

Season	EN	Neutral	LN
JFM	1,308	1,474	994
JAS	1,688	1,442	642

D. CONDITIONAL COMPOSITES

We determined the MJO and ENLN state for each day of the study period, and then identified the days for which different MJO and ENLN conditions were met. We did this identification of dates for a number of cases, with each case representing a different set of conditions. For example, we identified the days in JFM during the study period on which both of the following two conditions were met: (a) MJO phase 4 with amplitude greater than or equal to 1.0 occurred; ***and*** (b) a moderate to strong EN occurred.

We then composited, or averaged together, the daily values for each focus variable for the days we had identified for each case. The results were conditional composite values representing the mean conditions during the days in which the specified conditions were met.

We focused our analyses on the conditional composite anomalies for each case. An anomaly is the conditional composite mean minus the LTM for the specified season and for

each grid point. For example, the SWH anomaly for MJO phase 4 during JFM is calculated as: SWH $\text{Anomaly}_{\text{JFM\_Phase4}}$ = $\text{SWH}_{\text{JFM\_Phase4}}$ - LTM SWH_{JFM}. We focused on the anomalies because: (a) they are a standard way of characterizing climate variations and their impacts; and (b) they are the standard target for long range forecasts (i.e., the standard variable that is forecasted in long range forecasts) (Van den Dool 2007). Skill in forecasting anomalies indicates the forecast is more skillful than a forecast based on long term means (i.e., on climatology) (Wilks 2007).

E. CASE DESCRIPTIONS

We analyzed the conditional composite anomalies for 25 cases. The cases represented different seasons and regions, and different combinations of MJO and ENLN conditions. Case types 1–9 are for all variables, for the globe, and for JFM and JAS. Case type 10 is for precipitation rate in the southwest Asian region in JFM.

1. LTM values. The LTM cases represent a combination of all EN, LN, and Neutral periods and all MJO periods, with no filtering out of any days within the LTM period for each variable. These cases represent what are generally called climatological conditions.

2. EN anomalies for MEI > +0.5. This case represents a combination of EN and all MJO conditions (no filtering out of any MJO days). Represents what are generally called EN anomaly conditions but actually includes anomalies due to MJO and other climate variations.

3. LN anomalies for MEI < -0.5. This case represents a combination of LN and all MJO conditions (no filtering out of any MJO days). Represents what are generally called LN anomaly conditions but actually includes anomalies due to MJO and other climate variations.

4. Neutral anomalies for MEI ≥ -0.5 and ≤ +0.5. This case represents a combination of Neutral and all MJO conditions (no filtering out of any MJO days). Represents what are generally called Neutral anomaly conditions but actually includes anomalies due to MJO and other climate variations.

5. MJO Phase 4 anomalies for MJO amplitudes ≥ +1.0 and all MEI values (EN/LN/Neutral). This case represents a combination of MJO phase 4 and EN, LN, Neutral conditions (other MJO phases and amplitudes filtered out). Represents what are generally called MJO phase 4 anomaly conditions but actually includes anomalies due to EN, LN, and Neutral conditions and other climate variations.

6. MJO Phase 4 anomalies for MJO amplitudes ≥ +1.0 and EN. This case represents a combination of MJO phase 4 and EN conditions (LN, Neutral, and other MJO phases and amplitudes filtered out). Represents MJO phase 4 anomaly conditions when combined with EN anomaly conditions.

7. MJO Phase 4 anomalies for Amplitudes ≥ +1.0 and LN. This case represents a combination of MJO phase 4 and LN conditions (EN, Neutral, and other MJO phases and amplitudes filtered out). Represents MJO phase 4 anomaly conditions when combined with LN anomaly conditions.

8. MJO Phase 4 anomalies for MJO amplitudes ≥ +1.0 and Neutral. This case represents a combination of MJO phase 4 and Neutral conditions (EN, LN, and other MJO phases and amplitudes filtered out). Represents MJO phase 4 conditions when combined with Neutral conditions. This case comes the closest to representing MJO phase 4 anomalies all by themselves (that is, pure MJO phase 4 anomaly conditions in the absence of EN and LN). This case however does not represent entirely pure MJO phase 4 conditions because other climate variations have not been filtered out (AO, IOD, etc., have not been filtered out).

9. The same as case types 5–8 but for MJO Phase 8.

10. MJO Phase 4 and Phase 8 anomalies for MJO amplitudes ≥ +1.0 for precipitation rate in southwest Asia (SWA) during JFM. This case type is similar to case types 2–3 and 6–8 but for just precipitation rate, just SWA, and just JFM.

Table 4 summarizes each of the 25 cases and indicates where in this report these main results for each case can be found.

Table 4. Case Descriptions

Case	Composite Type	Months	MJO Phase	MJO Amplitude	ENLN State	Location in this Report
1	LTM	JFM	-	-	-	Chapter III
2	Anomaly	JFM	-	-	EN	Chapter III
3	Anomaly	JFM	-	-	LN	Chapter III
4	Anomaly	JFM	-	-	Neutral	Chapter III
5	Anomaly	JFM	4	≥ +1.0	EN + LN + Neutral	Chapter III
6	Anomaly	JFM	4	≥ +1.0	EN	Chapter III
7	Anomaly	JFM	4	≥ +1.0	LN	Chapter III
8	Anomaly	JFM	4	≥ +1.0	Neutral	Chapter III
9	Anomaly	JFM	8	≥ +1.0	EN + LN + Neutral	Appendix A
10	Anomaly	JFM	8	≥ +1.0	EN	Appendix A
11	Anomaly	JFM	8	≥ +1.0	LN	Appendix A
12	Anomaly	JFM	8	≥ +1.0	Neutral	Appendix A
13	LTM	JAS	-	-	-	Appendix B
14	Anomaly	JAS	-	-	EN	Appendix B
15	Anomaly	JAS	-	-	LN	Appendix B
16	Anomaly	JAS	-	-	Neutral	Appendix B
17	Anomaly	JAS	4	≥ +1.0	EN + LN + Neutral	Appendix B
18	Anomaly	JAS	4	≥ +1.0	EN	Appendix B
19	Anomaly	JAS	4	≥ +1.0	LN	Appendix B
20	Anomaly	JAS	4	≥ +1.0	Neutral	Appendix B
21	Anomaly	JAS	8	≥ +1.0	EN + LN + Neutral	Appendix B
22	Anomaly	JAS	8	≥ +1.0	EN	Appendix B
23	Anomaly	JAS	8	≥ +1.0	LN	Appendix B
24	Anomaly	JAS	8	≥ +1.0	Neutral	Appendix B
25.a	Anomaly (SWA)	JFM	-	-	EN LN	Appendix C
25.b	Anomaly (SWA)	JFM	4, 8	≥ +1.0	EN + LN + Neutral	Appendix C

The number of days used to develop the composites for each case varied. This was because there was an uneven distribution of the different conditions represented by the cases—for example, there were more EN days than Neutral days or LN days (Table 2). Of course, the more conditions that we applied for a given case, the smaller the number of days in the study period that would be likely to meet all the conditions. For example, we would expect, and we found, that the number of days that are both EN and MJO phase 4 days would be less than the number of days that are just EN days. The differing numbers of days was problematic because comparisons of two or more composites is most straightforward when each composite uses the same number of days.

We considered several options for addressing this problem, including: (1) subtracting days from composites that had a large number of days by removing days that were least comparable to the comparison days (e.g., removing strong EN days so that the EN and LN composites each involved an equal number of weak and moderate days); (2) working with percentages instead of actual values; and (3) working with unequal numbers of days but focusing on the signs and patterns of the anomalies rather than the specific magnitudes of the anomalies. We chose to use: (a) method 2 for our results concerning the distribution of MJO amplitudes by ENLN state; and (b) method 3 for analyses of the focus variable anomalies. For the focus variable anomaly results, our main focus was on the anomaly signs and patterns, with less focus on the anomaly magnitudes.

III. RESULTS

A. ANALYSIS CHARACTERISTICS

One of our first steps was to determine the distribution of MJO activity by MJO amplitude, ENLN state (EN, LN, and Neutral), and season (JFM and JAS). This analysis helped us select the range of MJO amplitudes and the season on which to focus, and to assess the extent to which differing numbers of days for the cases would be a problem. Figures 6 and 7 show examples of the results from these analyses—in particular, the percentage of days, by MJO amplitude, in which MJO phase 4 occurred simultaneously with EN, LN, or Neutral conditions for JFM (Figure 6) and JAS (Figure 7). Note that the percentage of days varied considerably by MJO amplitude, ENLN state, and season. Based on these type of initial analyses, we decided to focus our study on MJO amplitudes ≥ 1.0, all three ENLN states (EN, LN, and Neutral), and the two extreme seasons (JFM and JAS).

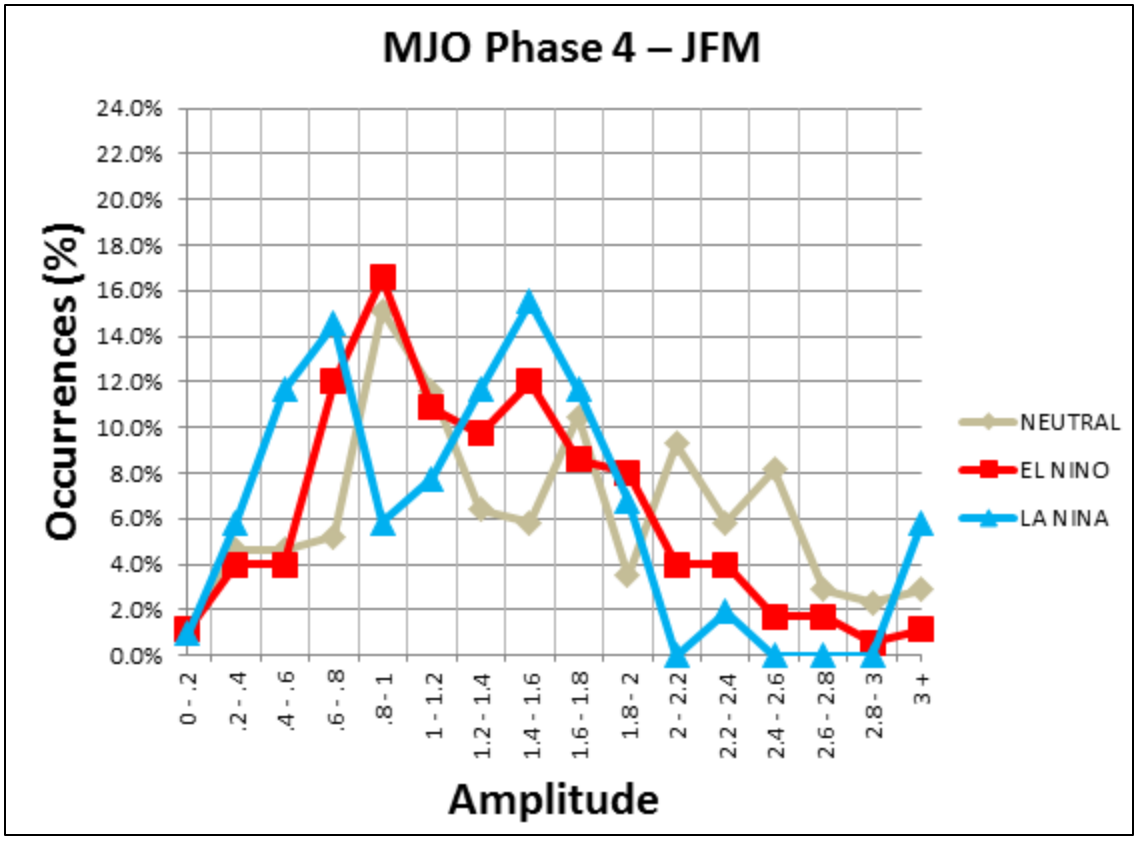

Percentage of MJO Phase 4 days in JFM by MJO amplitude and by ENLN state (EN, LN, and Neutral).

Figure 6. Percentage of MJO Phase 4 Days by Amplitude and ENLN State for JFM

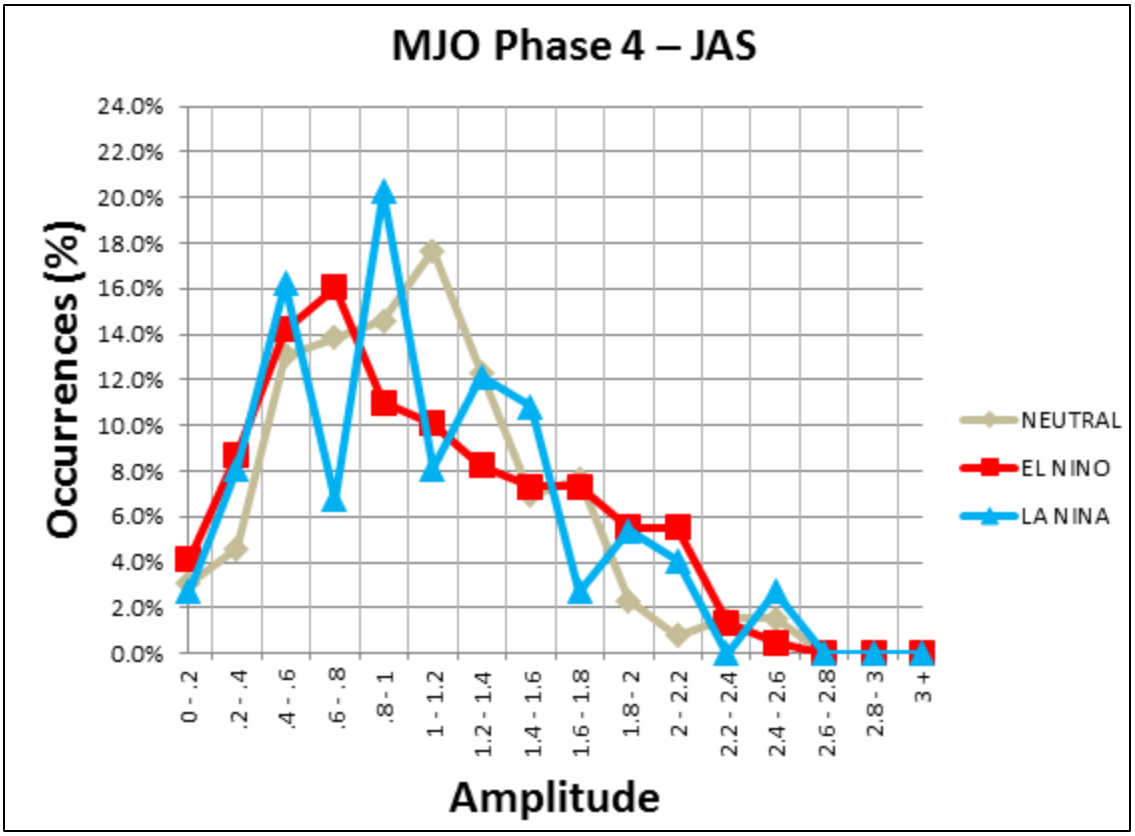

Percentage of MJO Phase 4 days in JAS by MJO amplitude and by ENLN state (EN, LN, and Neutral).

Figure 7. Percentage of MJO Phase 4 Days by Amplitude and ENLN State for JAS

In the following eight sections, the results from cases 1–8 (Table 5) are presented. We have plotted the anomaly results to facilitate the comparison of the results from the different cases—for example, using the same contouring range and interval for the Z200 anomaly figures for each of the cases. This meant that some figures show relatively little detail in the areas where the anomalies have high magnitudes. We decided that this was acceptable because our focus in this study was mainly on the anomaly patterns and signs of the anomalies, with a lesser focus on the magnitudes (see Chapter II, section E).

B. CASE 1: CHARACTERISTIC JFM LONG TERM MEANS

To understand the results of our climate variation analyses, it is useful to first examine the LTM climatological patterns and processes that are related to our focus variables. Figures 8–12 show the LTM values for the focus variables for JFM. The JFM

LTM SST (Figure 8) shows: (a) higher values of SST in the tropics and especially near the maritime continent (MC) in the western tropical Pacific and eastern tropical Indian basins; and (b) lower values in the eastern parts of the tropical and subtropical Pacific. Note in particular the higher SSTs in the western equatorial Pacific and lower SSTs in the eastern equatorial Pacific. Still lower values of SST are found in the extratropics.

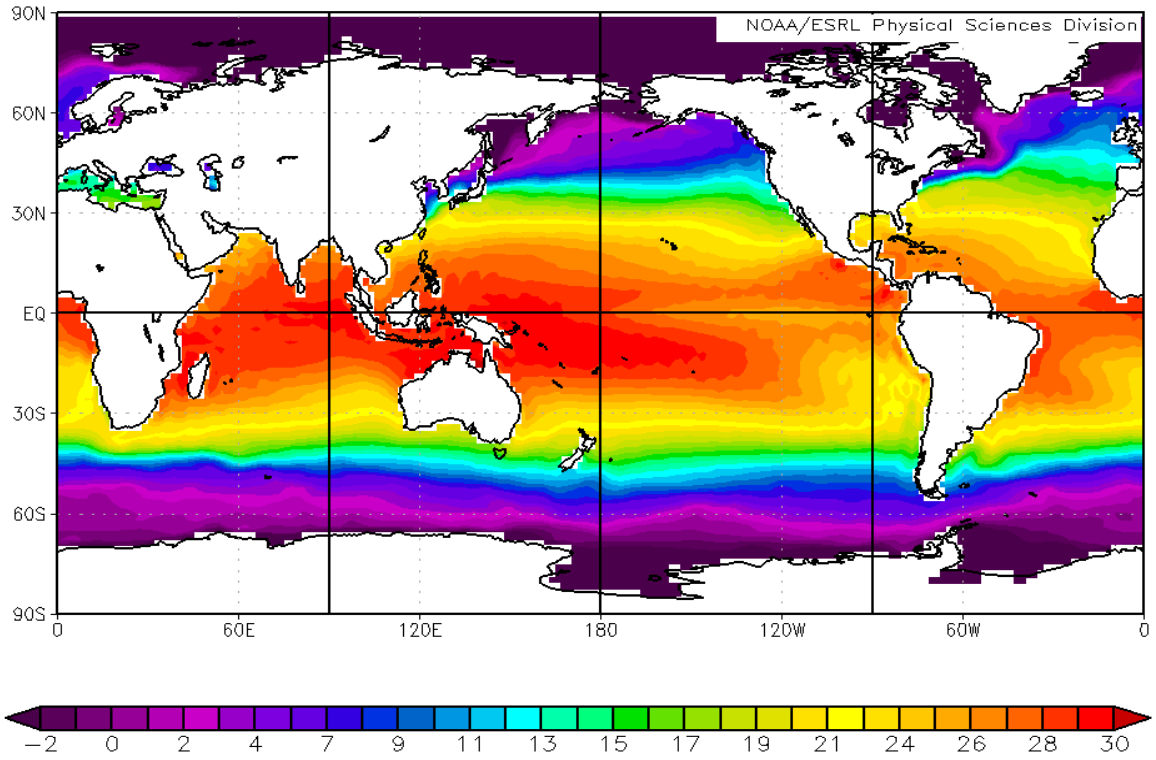

Note the relatively high SSTs in the tropics, especially in the tropical Indian and western Pacific basins.

Figure 8. LTM Sea Surface Temperature (SST; °C) for JFM.

The LTM JFM SLP (Figure 9) has lower values in the tropics, especially where the corresponding SSTs are high near the MC (Figure 8). The low tropical values can be used to infer the locations of: (a) the ITCZ—for example, just north of the equator in the Pacific basin, just south of the equator in the Indian basin, and over tropical Africa and South America; and (b) the SPCZ extending southeastward from the MC. Relatively high values of SLP occur in: (a) the subtropics—for example, in the subtropical eastern North and South Pacific basins, where the North Pacific High (NPH) and South Pacific High

(SPH) occur, respectively; (b) in the subtropical South Indian basin where the Mascarene High occurs; and (c) over the winter continents of Eurasia and North America, where the Asian High and North American High occur, respectively. The relatively high SLP values correspond to relatively low temperatures at the surface and in the lower troposphere (e.g., Figure 8). Low values of SLP occur in the subpolar ocean regions—for example, near the Aleutians and near Iceland where the Aleutian Low (AL) and Icelandic Low (IL) occur respectively. These low values occur where SSTs are relatively warm compared to nearby land areas and where extratropical cyclone (ETC) activity (not shown) is high.

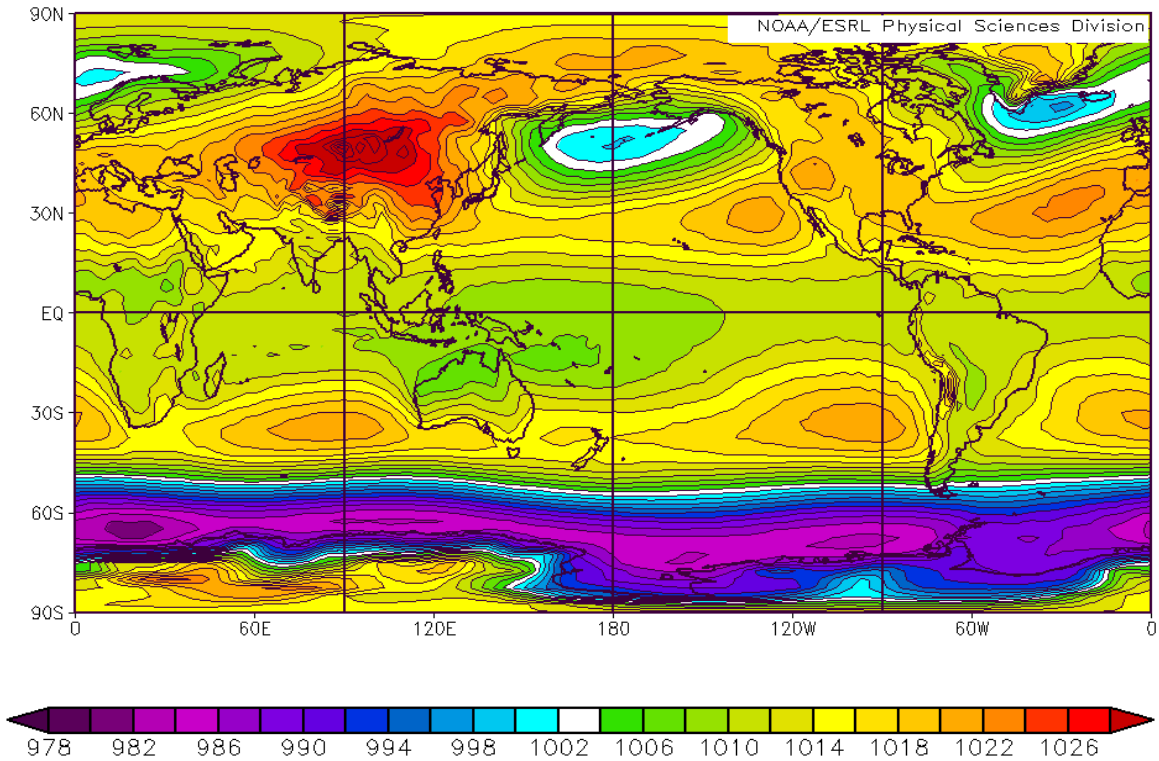

Note the high pressure regions centered in and near the subtropics, and the low pressure regions centered in the tropics and subpolar regions.

Figure 9. LTM Sea Level Pressure (SLP; mb) for JFM.

The SLP figure can be used to infer the corresponding lower tropospheric wind directions and speeds—in particular: (a) the trade winds flowing westward and equatorward from the subtropical highs into the tropical lows; (b) southward and southwestward winds out of the Asian High; and (c) the extratropical westerlies flowing

along the poleward flanks of the subtropical highs and equatorward flanks of the subpolar lows. These winds represent, in part, the Hadley-Walker Circulation (HWC) in which air flows equatorward and westward in the tropical lower troposphere, and poleward and eastward in the tropical upper troposphere.

The LTM JFM Z200 (Figure 10) shows high values in the tropics, especially over the low SLP values that occur near the MC. Relatively low values of Z200 are found over the subtropical highs. Still lower values occur in the extratropics, especially: (a) in the polar regions; and (b) on the eastern flanks of the Asian High and North American High. The zonal variations in Z200 reveal LTM wave patterns, in particular: (a) a tropical Rossby-Kelvin wave pattern associated with relatively high Z200 values over the MC and tropical Africa and South America, and relatively low Z200 values in between these three areas (for example, over the eastern tropical Pacific); and (b) an extratropical Rossby wave pattern associated with relatively low values [troughs] over eastern Asian and eastern North America and relatively high values [ridges] in between these areas (for example, over western North America and western Eurasia).

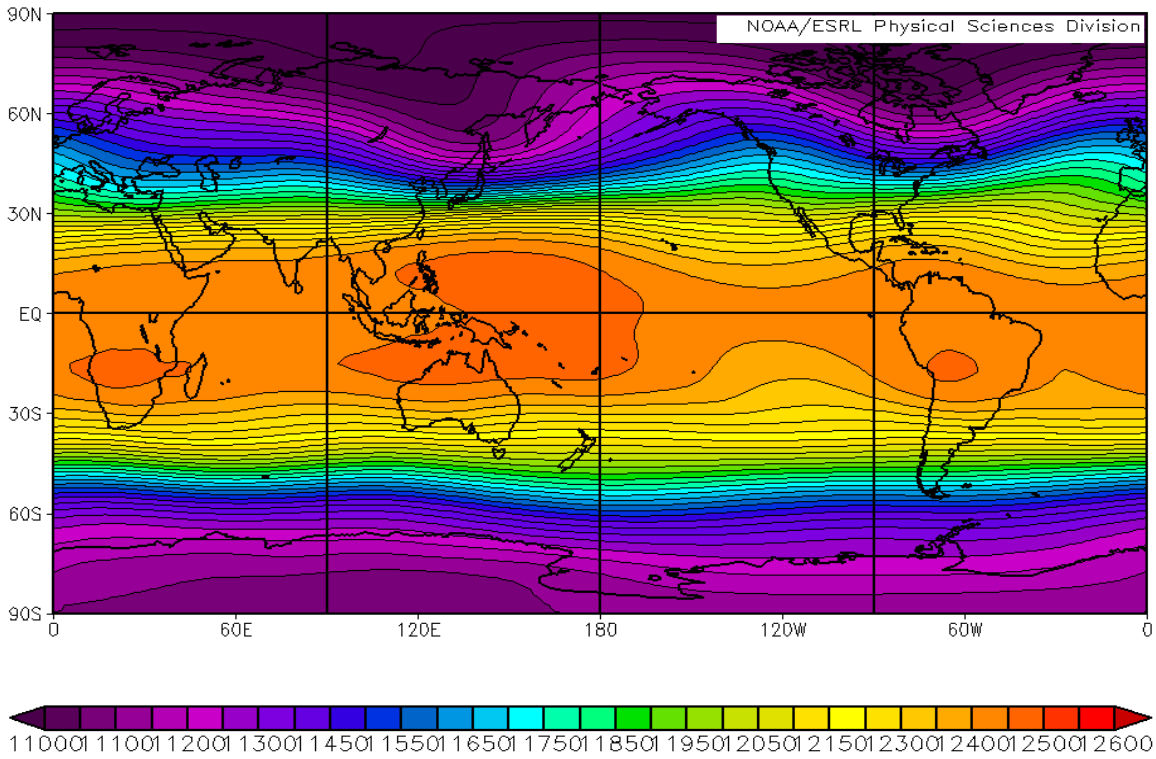

Note the long wave patterns in the tropics and the extratropical northern hemisphere.

Figure 10. LTM 200 mb Geopotential Height (Z200; m) for JFM.

The Z200 figure can be used to infer the corresponding upper tropospheric wind directions and speeds—in particular: (a) the predominance of eastward winds in the extratropics and parts of the tropics (for example, the eastern tropical Pacific); (b) the east Asian-North Pacific jet between the trough over east Asia and the ridge over the MC; and (c) westward winds in the equatorial areas where the Z200 values are high (for example, over and near the MC). These winds represent, in part, the upper tropospheric component of the HWC.

The LTM JFM PR (Figure 11) shows higher values where SLP is lower—for example, over and near the MC, in the ITCZ and SPCZ, and between the subtropical high and subpolar lows where the extratropical storm tracks occur. Lower PR values tend to occur where SLP is higher—for example, over and near the subtropical highs. The PR values can be used to infer latent heating values—for example, high latent heating in the tropical areas with high PR values. Note that the triangular white areas near 70°E in

Figure 11 are areas in which insufficient data was available (see Chapter II, section B for more information on this issue).

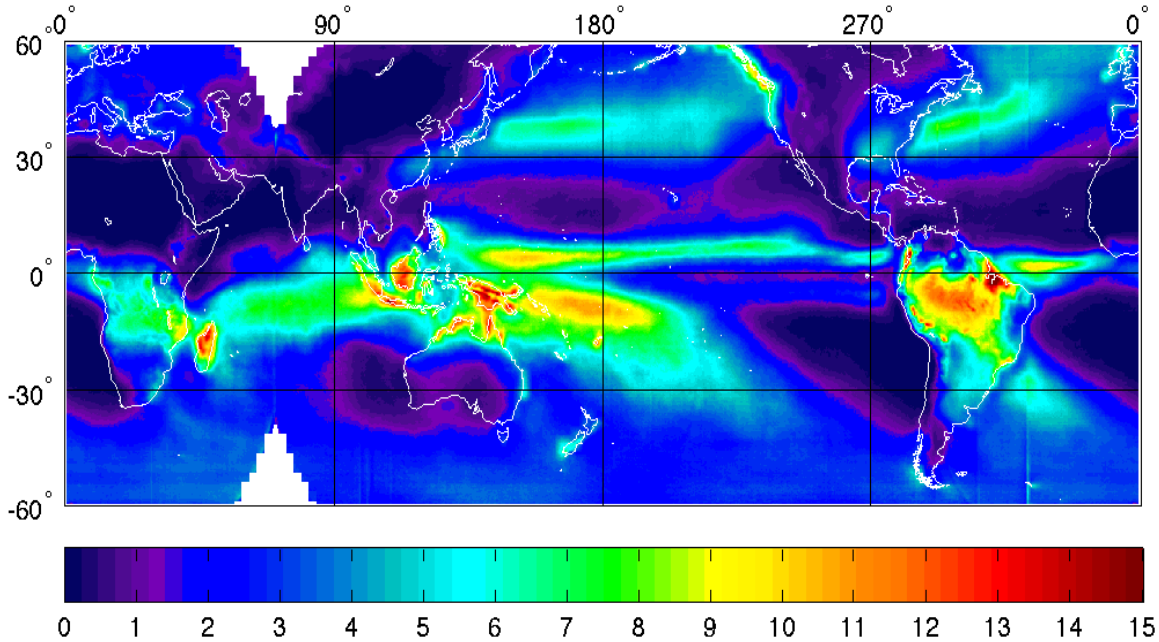

Note the relatively high precipitation rates in the tropics, especially over and near the maritime continent and Amazon, in the ITCZ and SPCZ, and in the extratropical storm tracks over the North Pacific and North Atlantic.

Figure 11. LTM Precipitation Rate (PR; mm/day) for JFM.

The LTM JFM SWH (Figure 12) shows higher values where the inferred SLP gradient and low tropospheric winds are strong (cf. Figure 9)—for example, between the subtropical highs and subpolar lows where the extratropical storm tracks occur, especially in the winter hemisphere. Lower SWH values occur where the inferred SLP gradient and lower tropospheric winds are weak (cf. Figure 9). Ocean surface waves tend to propagate away from their formation regions, so wave propagation may lead to relatively high SWH values in areas of relatively low SLP gradient. This may explain the occurrence of relatively high SWH values in the central-eastern tropical Pacific where waves may have propagated in from formation regions in the extratropical North and South Pacific. The LTM JFM wave directions (not shown) indicate that the dominant wave directions in the central-eastern tropical Pacific are from the northwest, west, and southwest, even though

the dominant wind direction in this area is from the east (cf. Figure 9). This suggests that extratropical wind stress is a significant factor determining SWH values in the central-eastern tropical Pacific.

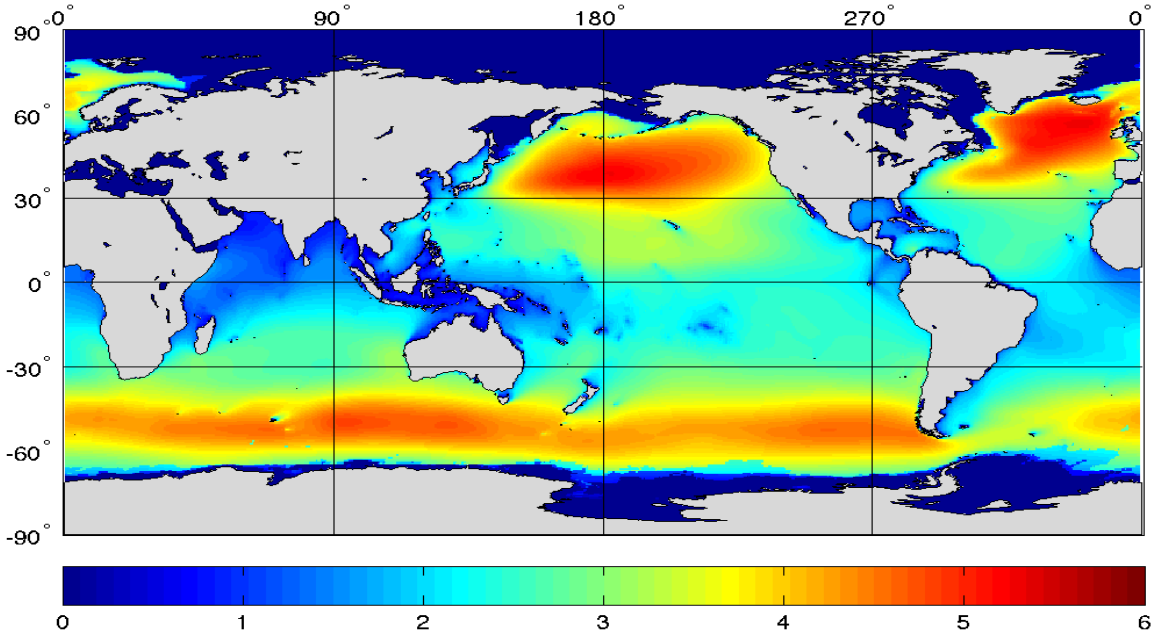

Note the areas of high significant wave heights in the extratropical North Pacific and North Atlantic.

Figure 12. LTM Significant Wave Height (SWH; m) for JFM.

Comparisons of the JFM LTM SST, SLP, Z200, PR, and SWH (Figures 8–12) indicate that these five variables are dynamically related. For example, the figures imply that, in the tropics, higher SSTs would tend to produce lower overlying SLP values, stronger trade winds, higher values of lower tropospheric wind convergence and moisture convergence (not shown), higher Z200, higher upper tropospheric divergence (not shown), higher PRs, higher tropospheric heating via latent heating, (not shown), and higher tropical ocean surface wave heights due to stronger trade winds. These dynamical relationships also indicate that when one of these variables is altered by a climate variation, then the other variables are likely to be altered too (cf. Philander 1990).

C. CASE 2: CHARACTERISTIC JFM EN ANOMALIES

Figures 13–17 show the characteristic anomalous values for the focus variables for JFM during EN years. The JFM EN SST anomalies (SSTAs; Figure 13) show: (a) positive anomalies in the central-eastern tropical Pacific, in the tropical Indian Ocean, and along the west coasts of North and South America; and (b) negative anomalies in the western tropical Pacific that extend poleward and eastward into the central North and South Pacific. Note that the tropical Pacific SSTAs represent an anomalous *decrease* in the west-east SST gradient seen in LTM SST (cf. Figure 8).

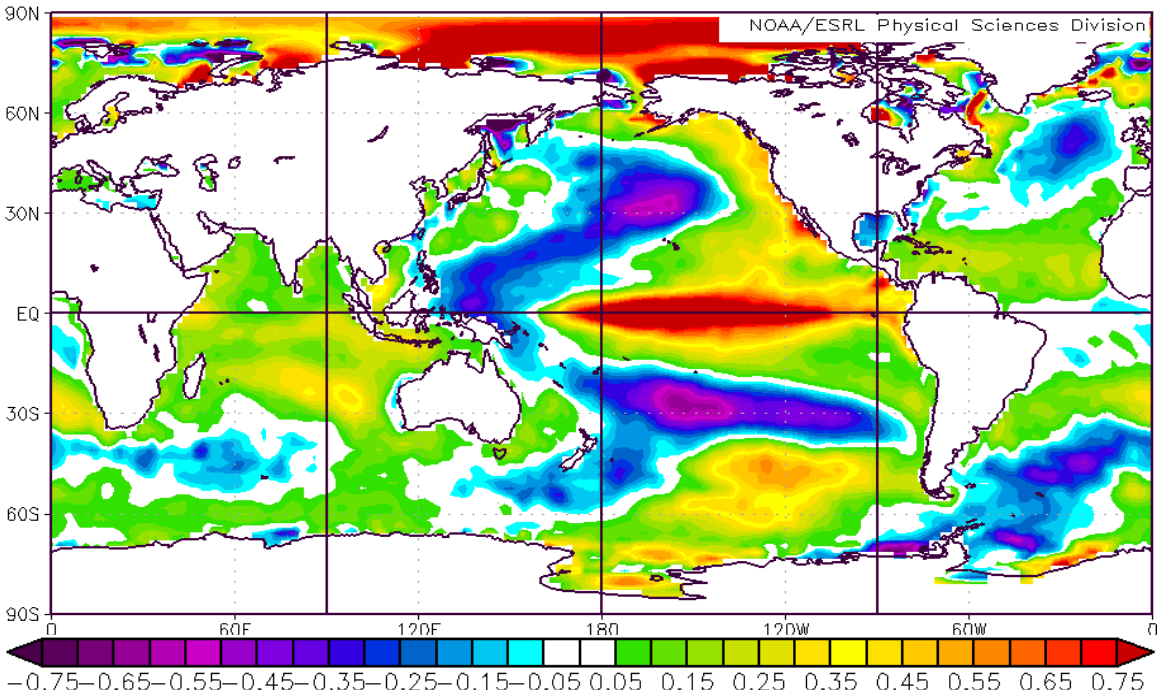

Note: (a) the positive SSTAs in the Indian Ocean, the central-eastern tropical Pacific basin, and along the west coast of North America; and (b) the negative SSTAs in the western tropical Pacific and central North and South Pacific.

Figure 13. SST Anomalies (SSTAs; °C) for EN Years during JFM.

The JFM EN SLP anomalies (SLPAs; Figure 14) show: (a) negative anomalies in the tropical central-eastern Pacific, the eastern subtropical and midlatitude Pacific, and the midlatitude North Atlantic; and (b) positive anomalies in the western tropical Pacific and most of the tropical eastern hemisphere. Note that the SLPAs represent: (a) a

reduction in the strength of the western tropical Pacific Low, the NPH, and SPH; and (b) an increase in the strength of the AL (Figure 9). Note too that the tropical Pacific SLP anomalies are dynamically consistent with the corresponding SST anomalies (cf. Figure 13), with negative [positive] tropical SLPAs over positive [negative] tropical SSTAs. The SLPAs can be used to infer the corresponding lower tropospheric wind anomalies—for example: (a) positive wind speed anomalies on the southern flank of the negative SLPA in the northeast Pacific, where the anomalous SLP gradient leads to an anomalous strengthening of the westerlies; and (b) negative wind speed anomalies in the tropical Pacific trade wind region, where the anomalously weak subtropical and tropical SLP gradient leads to anomalously weak trade winds.

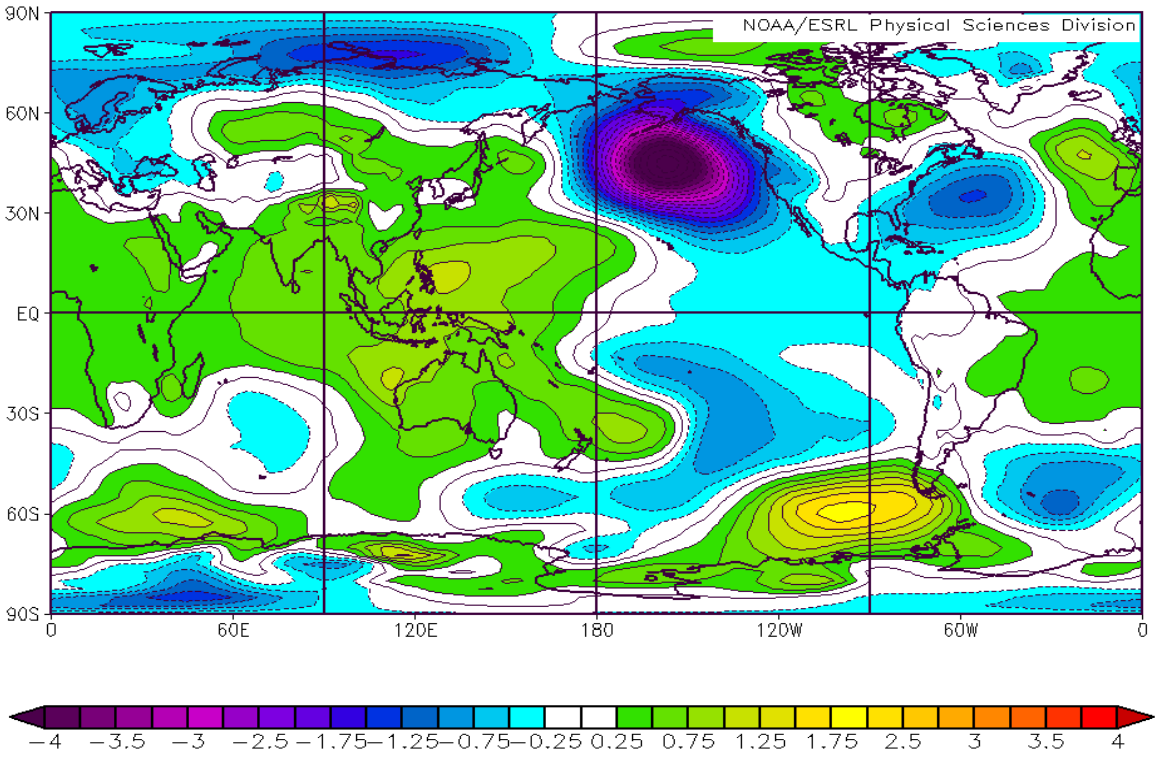

Note the positive SLPAs in much of the eastern hemisphere and the negative SLPAs in much of the western hemisphere, especially in the northeast Pacific and western North Atlantic.

Figure 14. SLP Anomalies (SLPAs; mb) for EN Years during JFM.

The JFM EN 200 mb geopotential height anomalies (ZA200s; Figure 15) show: (a) positive anomalies throughout most of the tropics, especially over the negative SLPAs

in the central-eastern tropical Pacific (Figure 14), where the twin positive Z200 anomalies straddling the equator indicate an anomalous Rossby-Kelvin wave; and (b) positive and negative anomalies in the extratropics that indicate anomalous Rossby wave trains—for example, an anomalous wave train extending across the North Pacific, North America, and the North Atlantic—and the positive phase of the Pacific-North American (PNA) pattern (Philander 1990; Leathers et al. 1991). Note that in the extratropics the ZA200s are similar in pattern and sign to the SLPAs (Figure 14)—for example, negative [positive] SLPAs and ZA200s in the AL region, southeastern U.S., and western North Atlantic [central Russia, Canada]. This correspondence between the SLP and Z200 anomalies indicates equivalent barotropic structure in these extratropical areas. The ZA200s can also be used to infer the corresponding upper tropospheric wind anomalies—for example, an anomalous *increase* in the strength of the subtropical jet from the dateline eastward to about 40°W (cf. Figure 10).

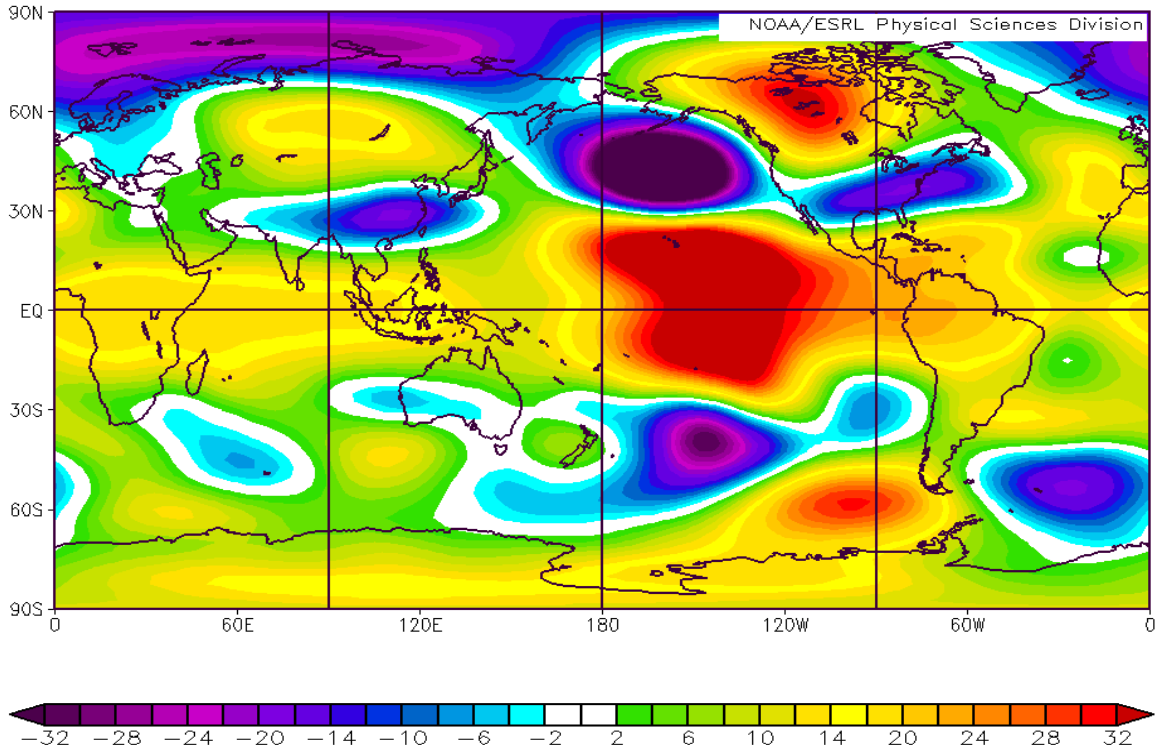

Note the twin positive anomalies in the eastern tropical Pacific, indicating an anomalous tropical Rossby-Kelvin wave and evidence of the positive phase of the PNA.

Figure 15. Z200 Anomalies (ZA200; m) for EN Years during JFM.

The JFM EN PR anomalies (PRAs; Figure 16) show: (a) positive anomalies in the central-eastern tropical Pacific; and (b) negative anomalies in the western and off-equatorial tropical Pacific. These PRAs are consistent with the known PRAs for EN events (Philander 1990; Chung and Power 2016). These PRAs are also dynamically consistent with the corresponding SSTAs and SLPAs, with positive [negative] SSTAs and negative [positive] SLPAs corresponding to positive PRAs (Figures 13, 14). Note that many of the PRAs represent shifts in the locations of the ITCZ and the SPCZ—for example, a southward shift of the ITCZ in the central-eastern tropical Pacific, and an eastward shift of the SPCZ. There are also notable PRAs in southern Africa, northern South America, and to the west and east of midlatitude North America. These PRAs are consistent with the corresponding anomalies in SLP and ZA200 (Figures 14, 15) and in related low level moisture advection and upper tropospheric jets (not shown). The tropical PRAs are also consistent with the ZA200s—in particular, the positive PRAs in the central-eastern tropical Pacific indicate positive latent heating anomalies and positive ZA200s (Figure 15).

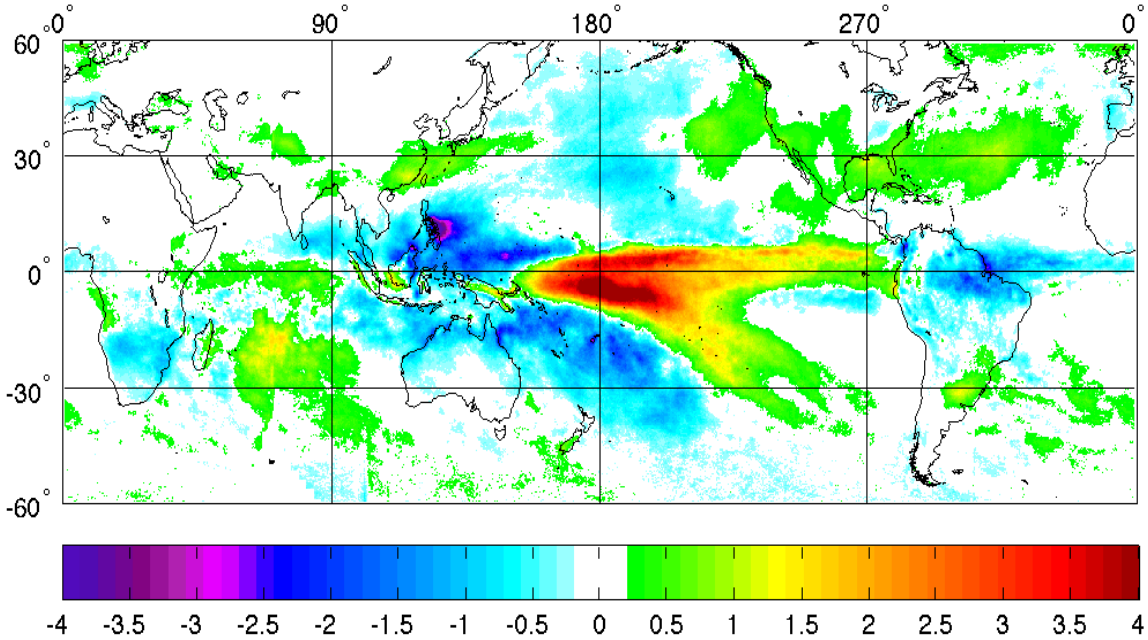

Note the negative and positive anomalies in the tropics, especially over the maritime continent and central-eastern tropical Pacific.

Figure 16. PR Anomalies (PRAs; mm/day) for EN Years during JFM.

The JFM EN SWH anomalies (SWHAs) (Figure 17) show positive anomalies in the central North and South Pacific where the SLPA gradients are relatively strong and indicate an *increase* in the lower tropospheric westerly winds of those regions (Figure 9). Negative SWHAs occur in areas where the SLPA gradients lead to anomalously weak lower tropospheric winds—for example, east and west of the northern Philippines. There are also positive SWHAs in the central-eastern tropical Pacific, even though the anomalous SLP gradients are weak there. This may be due to anomalously strong propagation of high waves into this region from other regions—in particular from the positive SWHA regions in the extratropical North and South Pacific. This speculation is supported by the JFM EN wave direction anomalies (not shown), which are mainly from the north in the central-eastern tropical Pacific.

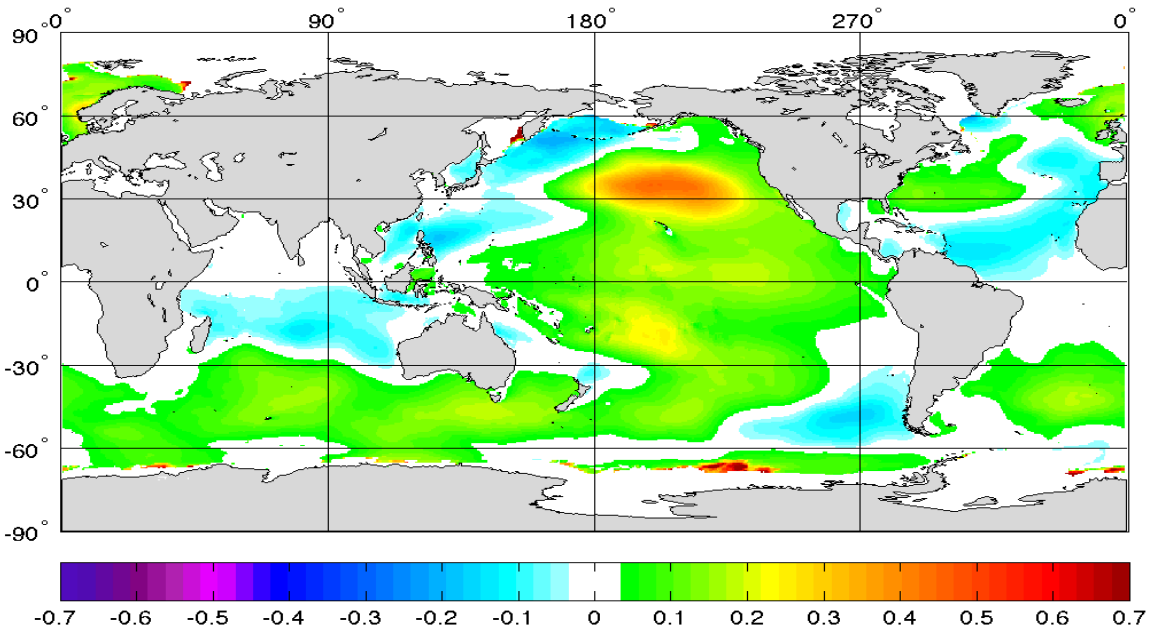

Note the positive anomalies in most of the Pacific and the negative anomalies in parts of the tropical Indian and western Pacific basins.

Figure 17. SWH Anomalies (SWHAs; m) for EN Years during JFM.

Similar to the LTM analyses, comparisons of the JFM EN anomalies for SST, SLP, Z200, PR, and SWH indicate the anomalies in these five variables are dynamically related. For example, during EN events, the Pacific subtropical highs tend to become

anomalously low and/or the western tropical Pacific and southeast Asian lows tend to become anomalously high, so that the Pacific trade winds become anomalously weak, and SSTs become anomalously cool [warm] in the western [eastern] tropical Pacific. These anomalies lead to anomalous Rossby and Kelvin wave activity, and anomalous transports of energy, moisture, and momentum between the tropics and extratropics that produce anomalous extratropical conditions, such as anomalous storm tracks and precipitation (Horel and Wallace 1981; Philander 1990; Leathers et al. 1991).

D. CASE 3: CHARACTERISTIC JFM LN ANOMALIES

Figures 18–22 show the characteristic anomalous values for the focus variables for JFM during LN years. The JFM LN SSTAs (Figure 18) show: (a) negative anomalies in the central-eastern tropical Pacific, in the tropical Indian Ocean, and along the west coasts of North and South America; and (b) positive anomalies in the western tropical Pacific that extend poleward and eastward into the central North and South Pacific. Note that the tropical Pacific SSTAs represent an anomalous *increase* in the west-east SST gradient seen in the LTM SST (Figure 8). Note also that the LN SSTAs are generally opposite in sign to the EN SSTAs (Figure 13).

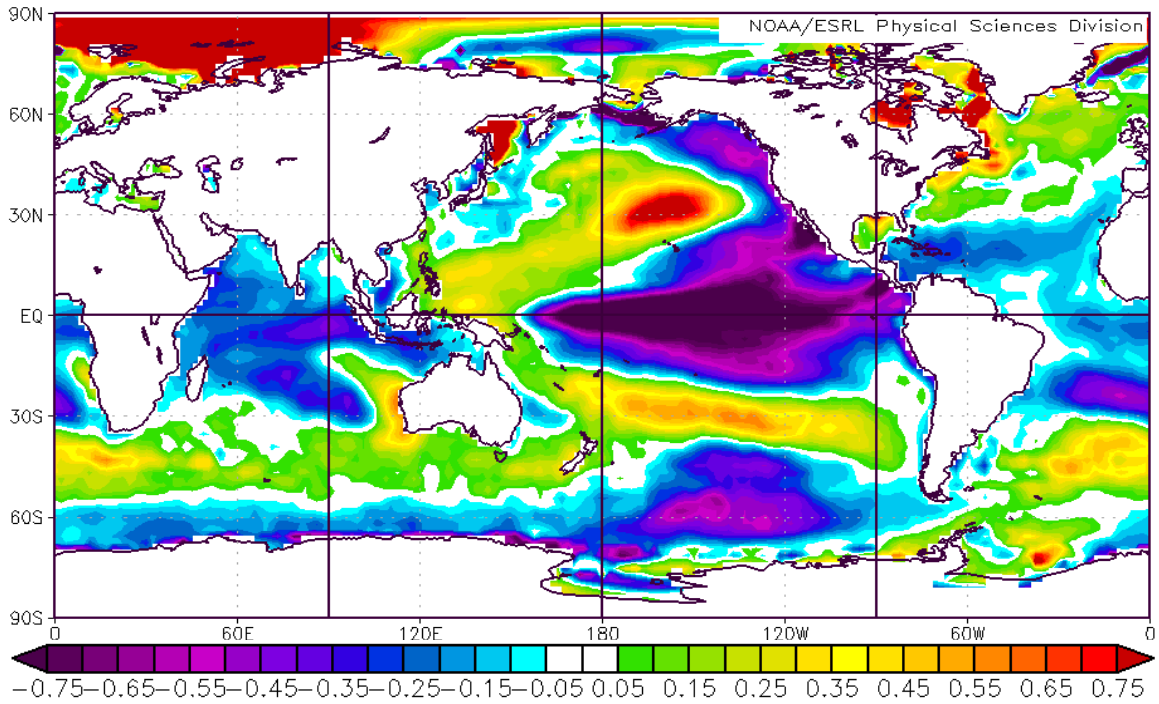

Note: (a) the negative SSTAs in the Indian Ocean, the central-eastern tropical Pacific basin, and along the west coast of North America; and (b) the positive SSTAs in the western tropical Pacific and central North and South Pacific.

Figure 18. SST Anomalies (°C) for LN Years during JFM.

The JFM LN SLPAs (Figure 19) show: (a) positive anomalies in the tropical central-eastern Pacific, the eastern subtropical and midlatitude Pacific, and the midlatitude North Atlantic; and (b) negative anomalies in the western tropical Pacific and most of tropical eastern hemisphere. Note that the SLPAs represent: (a) an increase in the strength of the western tropical Pacific Low, the NPH, and SPH; and (b) a decrease in the strength of the AL (Figure 9). Note too that the tropical Pacific SLP anomalies are dynamically consistent with the corresponding SST anomalies (see Figure 18), with negative [positive] tropical SLPAs over positive [negative] tropical SSTAs. The SLPAs can be used to infer the corresponding lower tropospheric wind anomalies—for example: (a) negative wind speed anomalies on the southern flank of the positive SLPA in the northeast Pacific, where the anomalous SLP gradient leads to an anomalous weakening of the westerlies; and (b) positive wind speed anomalies in the tropical Pacific trade wind region, where the anomalously strong subtropical-tropical SLP gradient leads to

anomalously strong trade winds. Note also that the LN SPAs are generally opposite in sign to the EN SLPAs (Figure 14).

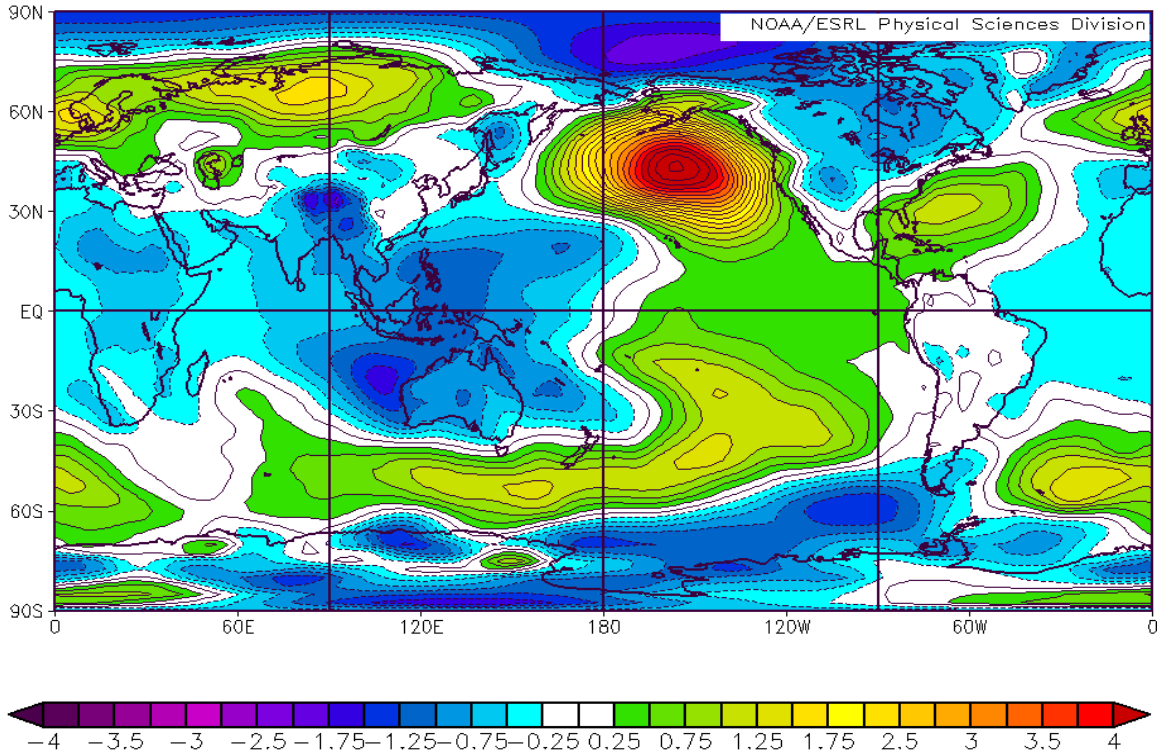

Note the positive anomalies in the tropical central-eastern Pacific, the eastern subtropical and midlatitude Pacific, and the midlatitude North Atlantic and negative anomalies in the western tropical Pacific and most of tropical eastern hemisphere.

Figure 19. SLP Anomalies (mb) for LN Years during JFM.

The JFM LN ZA200s (Figure 20) show: (a) negative anomalies throughout most of the tropics, especially over the negative SLPAs in the central-eastern tropical Pacific where the twin negative anomalies straddling the equator indicate an anomalous Rossby-Kelvin wave; and (b) positive and negative anomalies in the extratropics that indicate anomalous Rossby wave trains—for example, an anomalous wave train extending across the North Pacific, North America, and the North Atlantic—and the negative phase of the PNA pattern (Leathers et al. 1991). Note that in the extratropics, the ZA200s are similar in pattern and sign to the SLPAs (Figure 19)—for example, positive [negative] SLP and ZA200s in the AL region and, subtropical western North Atlantic [Canada]. This

correspondence between the SLP and ZA200s indicates equivalent barotropic structure in these extratropical areas. The ZA200s can also be used to infer the corresponding upper tropospheric wind anomalies—for example, an anomalous *decrease* in the strength of the subtropical jet from the dateline eastward to about 40°W (cf. Figure 10). Note also that the LN ZA200s are generally opposite in sign to the EN ZA200s (Figure 15).

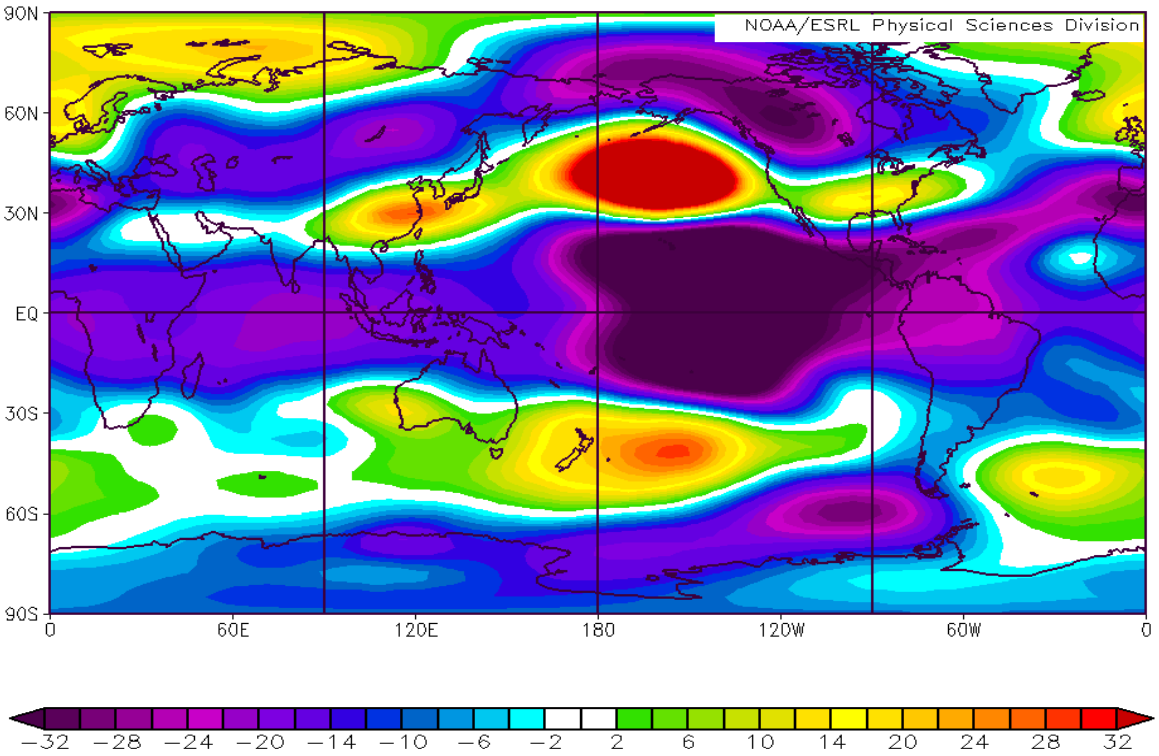

Note the twin negative anomalies in the eastern tropical Pacific, tropical Rossby-Kelvin wave response, which induces an anomalous wave train in the subtropics.

Figure 20. Z200 Anomalies (m) for LN Years during JFM.

The JFM LN PR anomalies (PRAs; Figure 21) show: (a) negative anomalies in the central-eastern tropical Pacific; and (b) positive anomalies in much of the western tropical Pacific and SPCZ region. These PRAs are consistent with the known PRAs for LN events (Philander 1990). These PRAs are also dynamically consistent with the corresponding SSTAs and SLPAs, with negative [positive] SSTAs and positive [negative] SLPAs corresponding to negative [positive] PRAs (Figures 18, 19). Note that many of the PRAs represent shifts in the location of the ITCZ and SPCZ—for example, a

northward shift of the ITCZ in the central-eastern tropical Pacific, and a westward shift of the SPCZ. There are also notable PRAs over southern Africa, northern South America, and over the southeastern U.S. These PRAs are consistent with the corresponding anomalies in SLP and Z200 (Figures 19, 20) and in related low level moisture advection and upper tropospheric jets (not shown). The tropical PRAs are also consistent with the ZA200s—in particular, the negative PRAs in the central-eastern tropical Pacific indicate negative latent heating anomalies and negative ZA200s (Figure 20). Note also that the LN PRAs are generally opposite in sign to the EN PRAs (Figure 16).

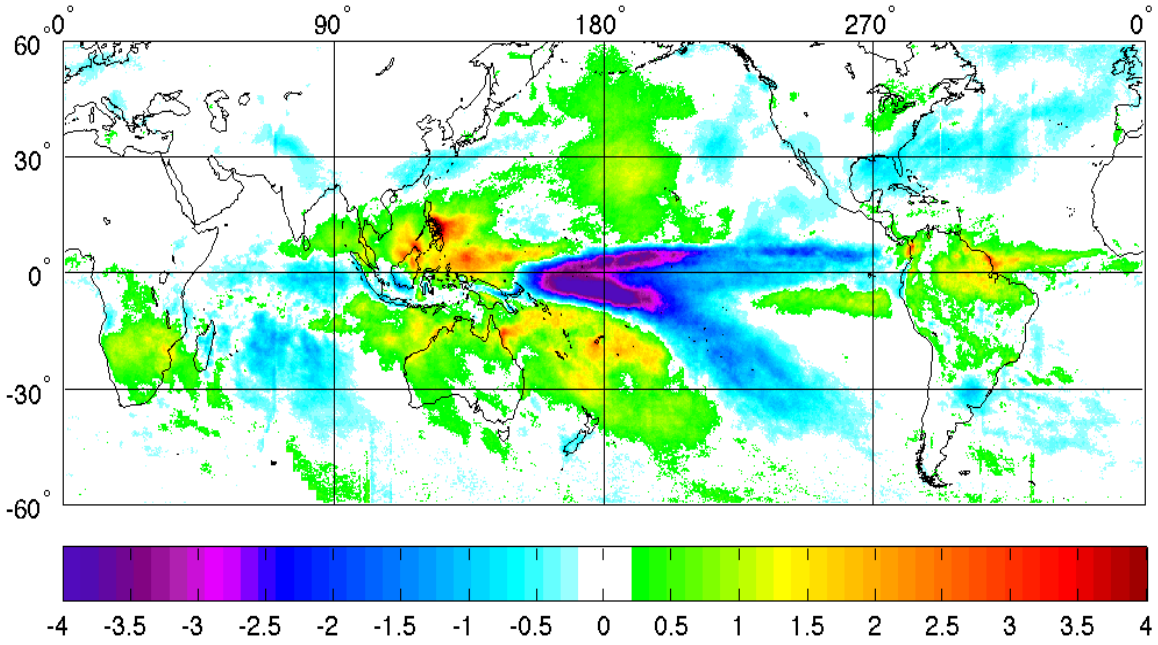

Note the positive and negative anomalies in the tropics, especially over the maritime continent and central-eastern tropical Pacific.

Figure 21. PR Anomalies (mm/day) for LN Years during JFM.

The JFM LN SWHAs (Figure 22) show negative SWHAs in the central North Pacific, where the SLPA gradients are relatively strong and indicate a *decrease* in the lower tropospheric winds in this region (Figure 9). Positive SWHAs occur in areas where the SLPA gradients lead to anomalously strong lower tropospheric winds—for example, just south of the Aleutians and east and west of the northern Philippines. There are also negative SWHAs in the central-eastern tropical Pacific, even though the anomalous SLP

gradients are weak there. This may be due to anomalously weak propagation of high waves into this region from other regions—in particular from the negative SWHA regions in the extratropical North Pacific. Note also that the LN SWHAs are generally opposite in sign to the EN SWHAs (Figure 17).

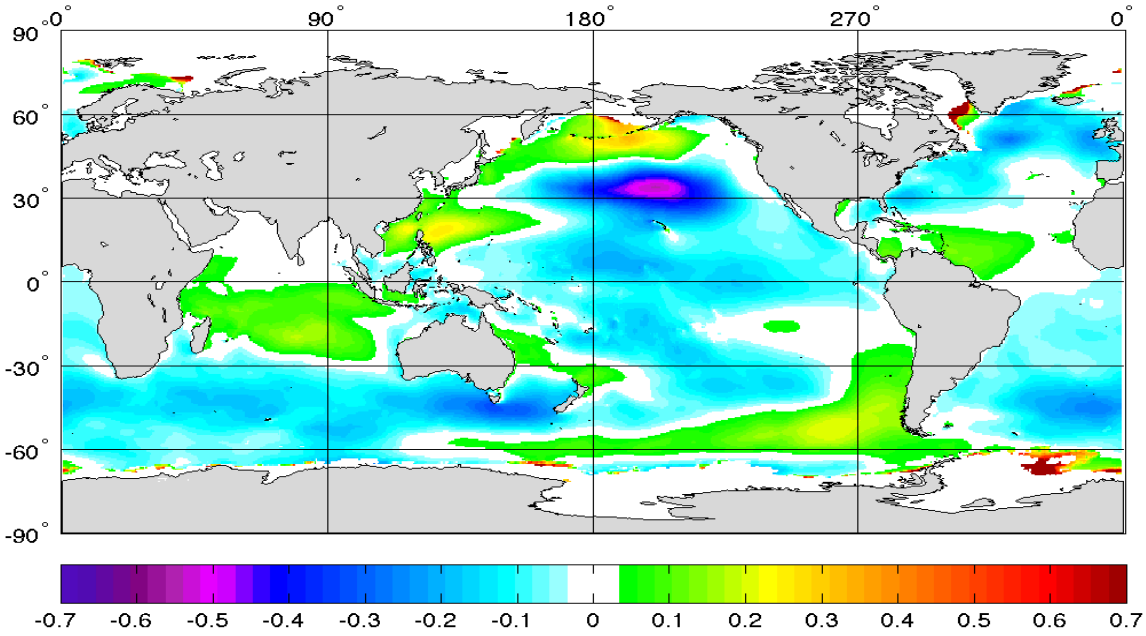

Note the negative anomalies in most of the Pacific and the positive anomalies in parts of the tropical Indian and western Pacific basins.

Figure 22. SWH Anomalies (m) for LN Years during JFM.

As with the EN anomalies, comparisons of the JFM LN anomalies for SST, SLP, Z200, PR, and SWH indicate that the anomalies in these five variables are dynamically related. For example, during LN events, the Pacific subtropical highs tend to become anomalously high and/or the western tropical Pacific and southeast Asian lows tend to become anomalously low, so that the Pacific trade winds become anomalously strong, SSTs become anomalously warm [cool] in the western [eastern] tropical Pacific. These anomalies lead to anomalous Rossby and Kelvin wave activity, and anomalous transports of energy, moisture, and momentum between the tropics and extratropics that produce anomalous extratropical conditions, such as anomalous storm tracks and precipitation (Horel and Wallace 1981; Philander 1990).

E. CASE 4: CHARACTERISTIC JFM NEUTRAL ANOMALIES

Figures 23–27 show the characteristic anomalous values for the focus variables for JFM during Neutral years. The JFM Neutral SSTAs (Figure 23) show: (a) a mix of negative and positive SSTAs in the tropical Pacific, with negative SSTAs in the far western tropical Pacific in the MC region, positive SSTAs in the central tropical Pacific, and negative SSTAs in the eastern tropical Pacific; and (b) a mix of negative and positive SSTAs in the extratropical North Pacific, with negative SSTAs in the western subtropical North Pacific and positive SSTAs in the central and northeastern North Pacific. Compared to the EN and LN SSTAs (Figures 13, 18) the Neutral SSTA patterns are smaller scale, less coherent, and weaker. This is consistent with the concept that EN and LN are major factors in determining interannual climate variability (Philander 1990; Bridgman and Oliver 2006).

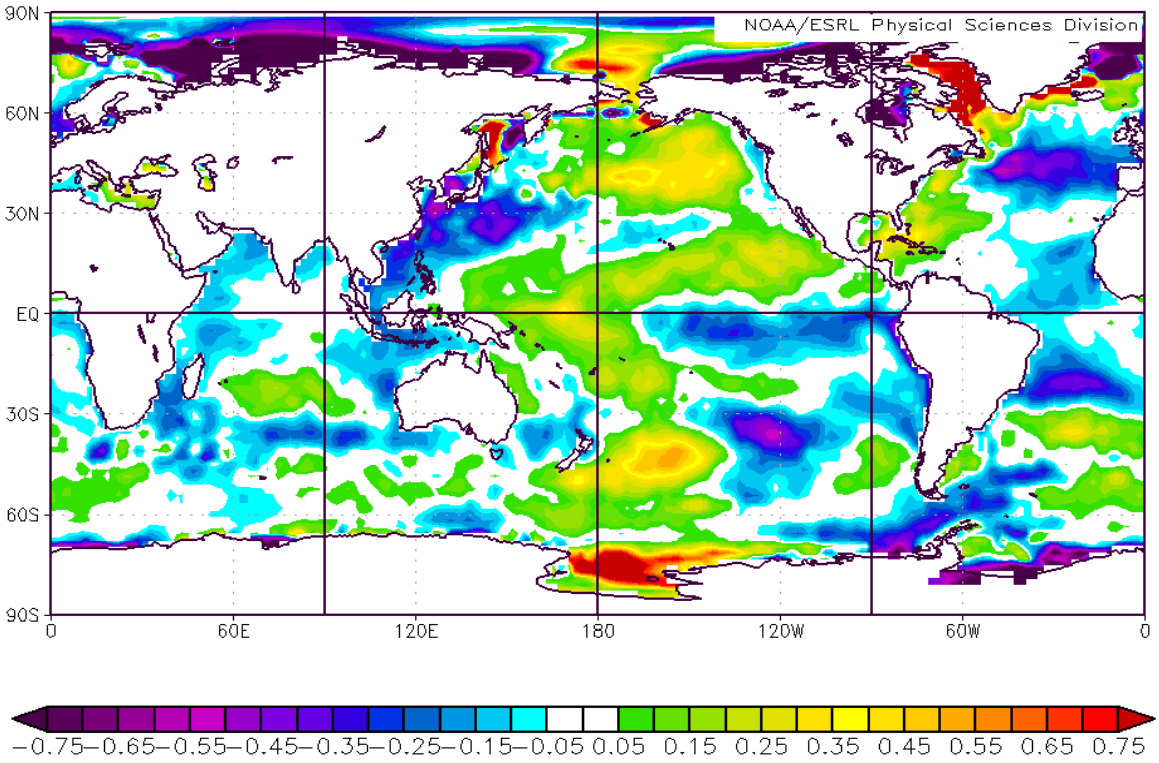

Note the mix of SST anomalies over the tropical Pacific and subtropical North Pacific and subtropical North Atlantic.

Figure 23. SST Anomalies (°C) for Neutral Years during JFM.

The JFM Neutral SLPAs (Figure 24) show: (a) weak anomalies in the tropics; (b) positive anomalies in the Arctic and Gulf of Alaska; and (c) negative anomalies over western Europe and much of the northern midlatitudes. The positive SLPA in the Aleutian Low region and the negative SLPA in the western tropical Pacific are similar to the SLPAs associated with LN (Figure 14). The Arctic and northern midlatitude SLPA pattern is similar to the SLPAs associated with the negative phase of the AO (Bridgman and Oliver 2006). The negative SLPAs in the western Pacific over and near the Philippine Sea are consistent with the positive SSTAs in that region (Figure 23). Overall, in the tropics and midlatitudes, the Neutral SPLAs are smaller scale, less coherent, and weaker than for the EN and LN cases.

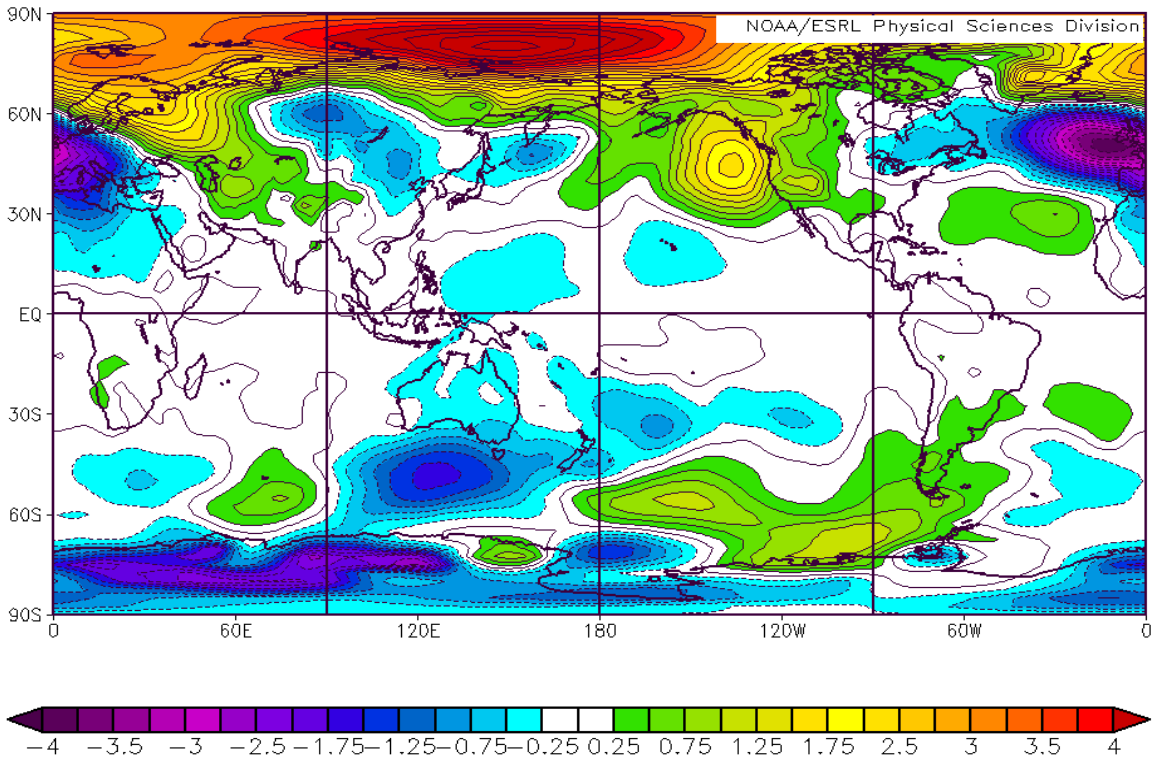

Note the small anomalies in the tropics, and a mix of positive and negative anomalies in the extratropics.

Figure 24. SLP Anomalies (mb) for Neutral Years during JFM.

The JFM Neutral ZA200s (Figure 25) show: (a) generally weak negative anomalies throughout the tropics; (b) positive anomalies in the Arctic; and (c) negative

anomalies in much of the northern midlatitudes. The Arctic and northern midlatitude ZA200 pattern is similar to the ZA200 pattern associated with the negative phase of the AO (Hu and Feng 2010). Note that in the extratropics, the ZA200 anomalies are similar in pattern and sign to the SLPAs (Figure 24)—for example, positive [negative] SLP and Z200 anomalies in the Arctic [northern midlatitudes]. This correspondence between the SLP and Z200 anomalies indicates equivalent barotropic structure in these extratropical areas.

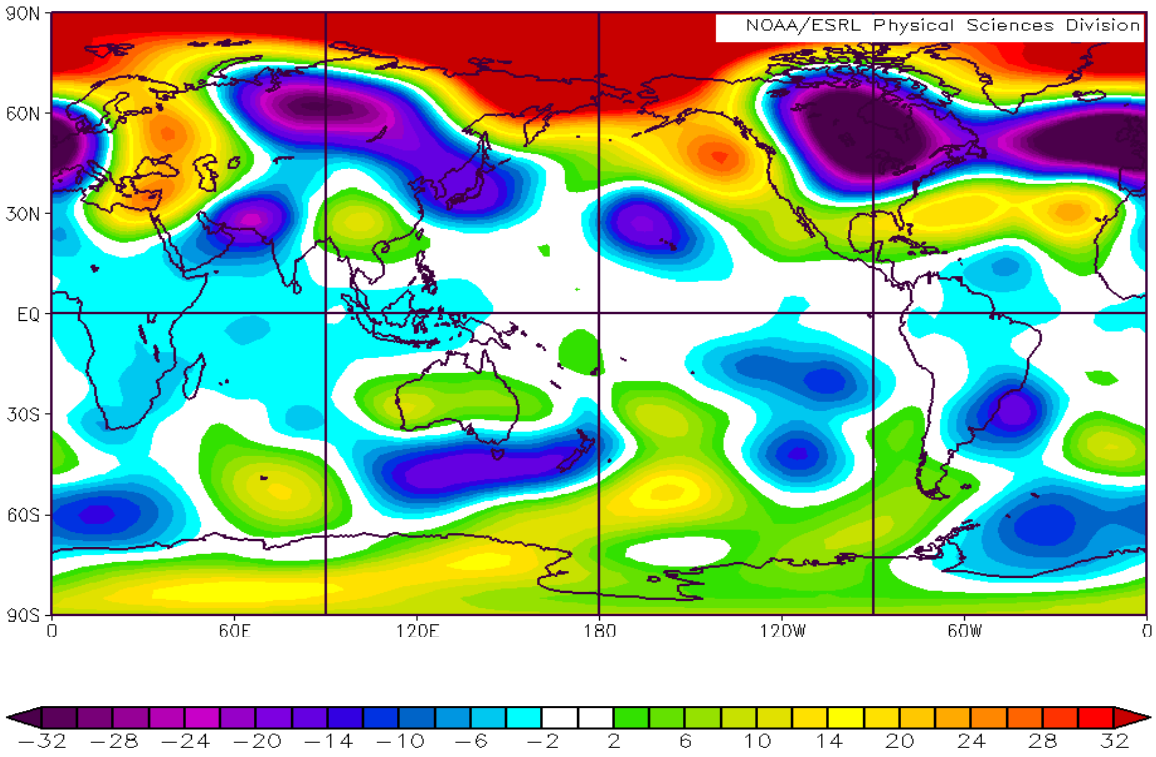

Note the generally small anomalies in the tropics, and a mix of positive and negative anomalies in the extratropics..

Figure 25. Z200 Anomalies (m) for Neutral Years during JFM.

The JFM Neutral PR anomalies (PRAs; Figure 26) are generally weak and with little clear large scale structure. But there is a pattern of negative PRAs centered over the South China Sea, positive PRAs in the western tropical Pacific over and east of MC region; and negative PRAs in much of the central-eastern tropical Pacific. These tropical Pacific PRAs are dynamically consistent with the corresponding SSTAs and SLPAs, with

negative [positive] SSTAs and positive [negative] SLPAs corresponding to negative [positive] PRAs (Figures 23, 24). In particular, the positive PRAs between the Philippines and the dateline are consistent with the positive SSTAs and negative SLPAs in that region (Figures 23, 24).

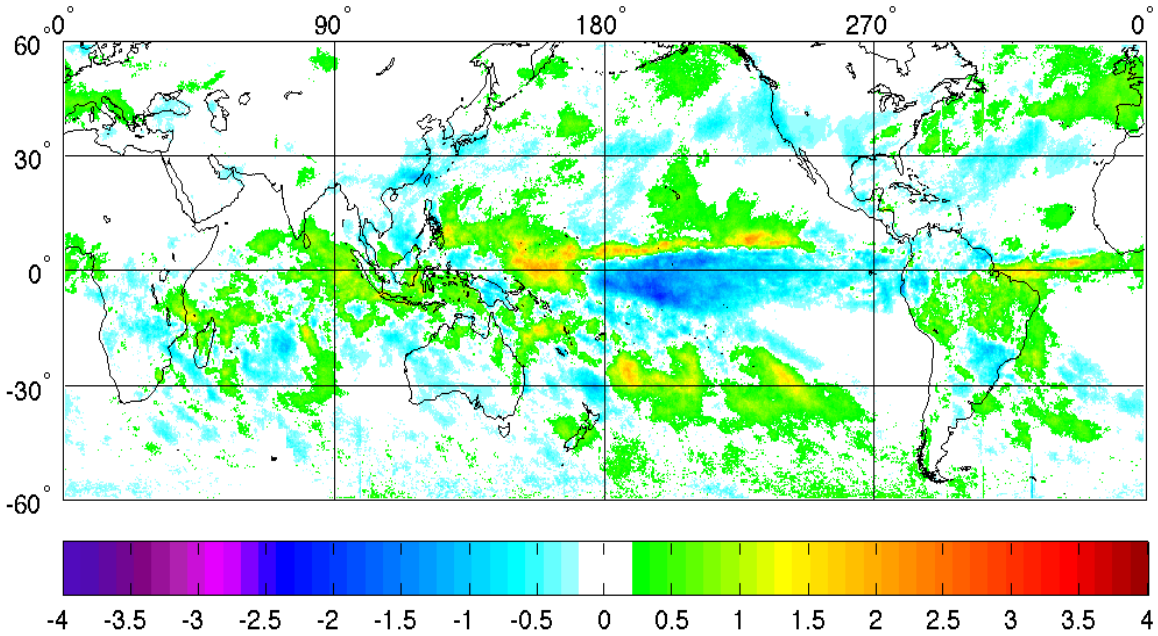

Note the relatively small anomalies in the tropics, and even smaller anomalies in the extratropics.

Figure 26. PR Anomalies (mm/day) for Neutral Years during JFM.

The JFM Neutral SWHAs (Figure 27) show generally weak SLPAs and SWHAs, and with little clear large scale structure. The SLPAs in the North Pacific and North Atlantic are dynamically consistent with the corresponding SWHAs in those regions. For example, the negative SWHAs in the central North Pacific are consistent with the weakened westerlies indicated by the positive SLPAs in the Aleutian Low region. Overall, in the tropics and midlatitudes, the Neutral SWHAs are smaller scale, less coherent, and weaker than for the EN and LN cases.

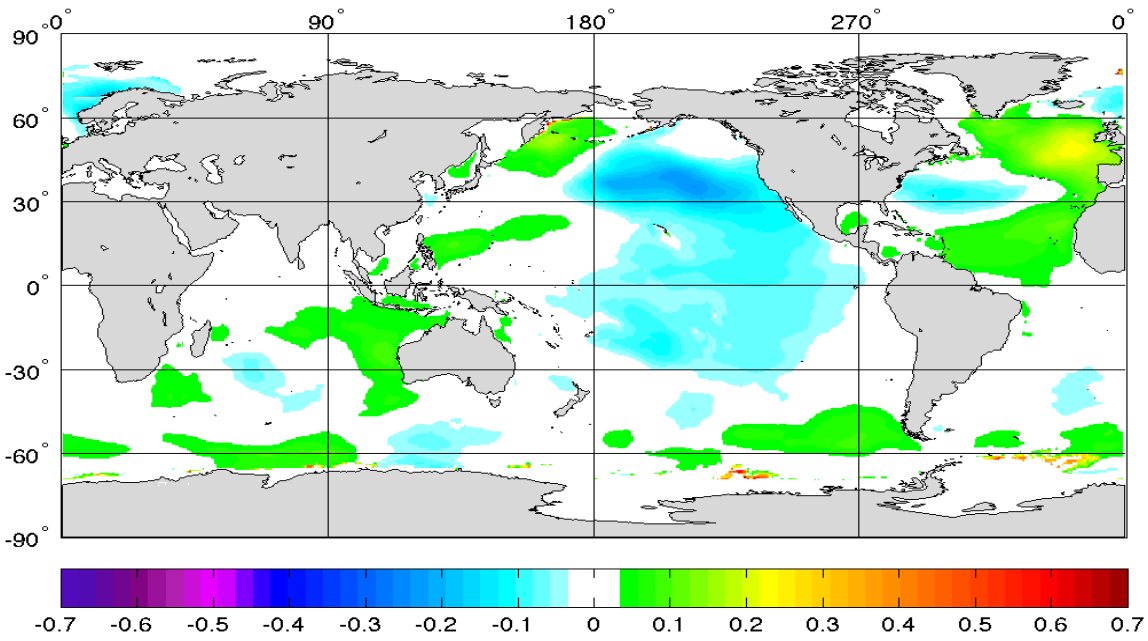

Note the relatively small anomalies, but with somewhat larger anomalies in the midlatitude North Pacific and Atlantic.

Figure 27. SWH Anomalies (m) for Neutral Years during JFM.

F. CASE 5: CHARACTERISTIC JFM PHASE 4 ANOMALIES

Figures 28–32 show the characteristic anomalous values for the focus variables for JFM when the MJO is in Phase 4 with an amplitude greater than or equal to +1.0, and for all EN, LN, and Neutral periods (that is, for all values of the MEI; see case 5 description in Chapter II, section E). The JFM Phase 4 SST anomalies (SSTAs; Figure 28) show, in the tropics and midlatitudes, SSTAs that are generally weak and with little large scale structure compared to the EN and LN SSTAs (Figures 13, 18). But there is a weak pattern of SSTAs with positive SSTAs from the MC into the central tropical Pacific, with negative SSTAs to the west in the tropical Indian Ocean and to the east of the MC in the eastern tropical Pacific.

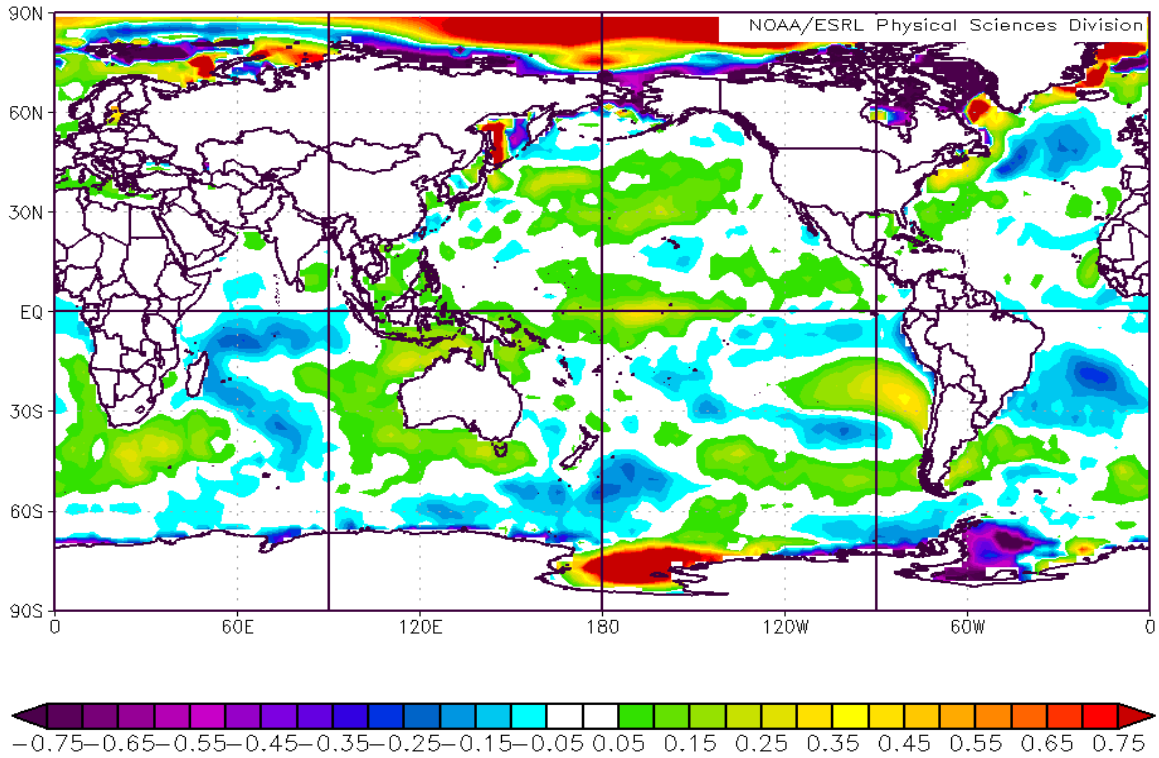

Note the generally weak and small scale anomalies outside of the polar regions.

Figure 28. SST Anomalies (°C) for MJO Phase 4 and all EN, LN, and Neutral Years during JFM.

The JFM Phase 4 SLPAs (Figure 29) show: (a) negative anomalies in most of the Indian Ocean, most of Eurasia, tropical Pacific, western subtropical North Pacific, subpolar South Pacific, and subpolar North Atlantic; and (b) positive anomalies in the subtropical North and South Pacific, most of the tropical and subtropical Atlantic basin, and most of Africa. Note that the SLPAs represent: (a) an increase in the strength of the tropical low in the Indian and Pacific, NPH, SPH, Azores High, and IL; and (b) a decrease in the strength of the Asian High, AL, and Mascarene High over the subtropical South Indian Ocean (Figure 9). The negative SLPA pattern in the tropical Pacific, east Asia, South Indian Ocean, and Australia indicates an anomalous Rossby-Kelvin wave and anomalous tropospheric warming centered near the MC (Chapter I, section B; Philander 1990). The pattern of alternating negative and positive SLPAs extending eastward and poleward from east Asia to the North Pacific, North America, and North Atlantic indicates an anomalous extratropical Rossby wave train (Chapter I, section B;

Philander 1990). The SLPAs can be used to infer the corresponding lower tropospheric wind anomalies—for example: (a) negative wind speed anomalies on the southern flank of the positive SLPA in the northeast Pacific, where the anomalous SLP gradient leads to an anomalous weakening of the westerlies; and (b) positive wind speed anomalies in the tropical Pacific trade wind region, where the anomalously strong subtropical-tropical SLP gradient leads to anomalously strong trade winds.

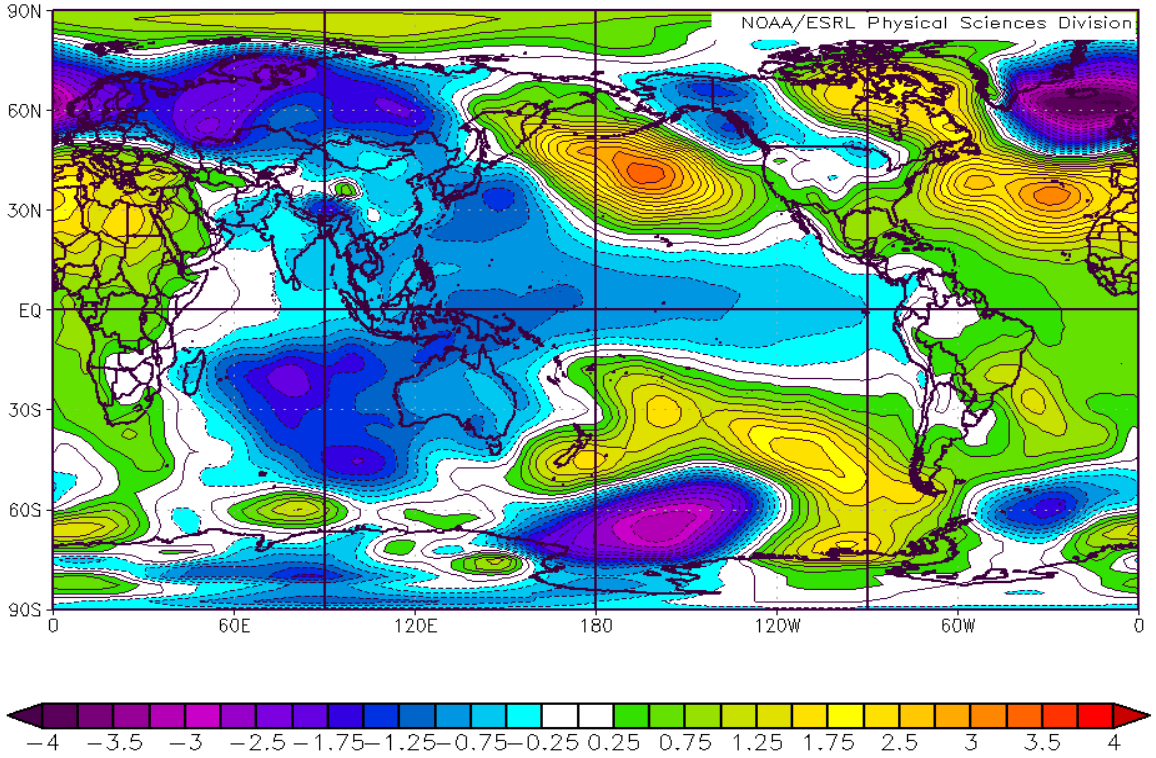

Note the negative anomaly pattern in the tropical Pacific, western subtropical, midlatitude Pacific, and most of the Indian Ocean indicative of anomalous Rossby and Kelvin waves.

Figure 29. SLP Anomalies (mb) for MJO Phase 4 and all EN, LN, and Neutral Years during JFM.

The JFM Phase 4 ZA200s (Figure 30) show: (a) positive anomalies in the western tropical Pacific and MC; (b) positive anomalies over subtropical south Asia and the subtropical South Indian Ocean that straddle the equator in most of the eastern hemisphere and that merge with the positive anomalies over the western tropical Pacific; (c) negative anomalies along the equator over Africa and the Indian Ocean; and (d)

negative anomalies that straddle the equator in the central Pacific. The ZA200s that straddle the equator and that lie over the equator from Africa eastward to South America indicate an anomalous tropical Rossby-Kelvin wave, consistent with the indications from the corresponding SLPA results (Figure 29). The alternating negative and positive ZA200s in the extratropics indicate anomalous extratropical Rossby waves—for example, an anomalous Rossby wave train extending eastward from east Asia into the North Atlantic, and another arching over the South Pacific and southern South America. Note the indications of equivalent barotropic structure in the extratropics (compare Figures 29 and 30)—for example, over the North Pacific, North America, and North Atlantic. The ZA200s can also be used to infer the corresponding upper tropospheric wind anomalies—for example, an anomalously strong subtropical jet over south Asia, from the Mediterranean Sea to Japan, and an anomalously weak subtropical jet over the central North Pacific and southern North America, from about 170°E to the eastern U.S. (cf. Figure 10).

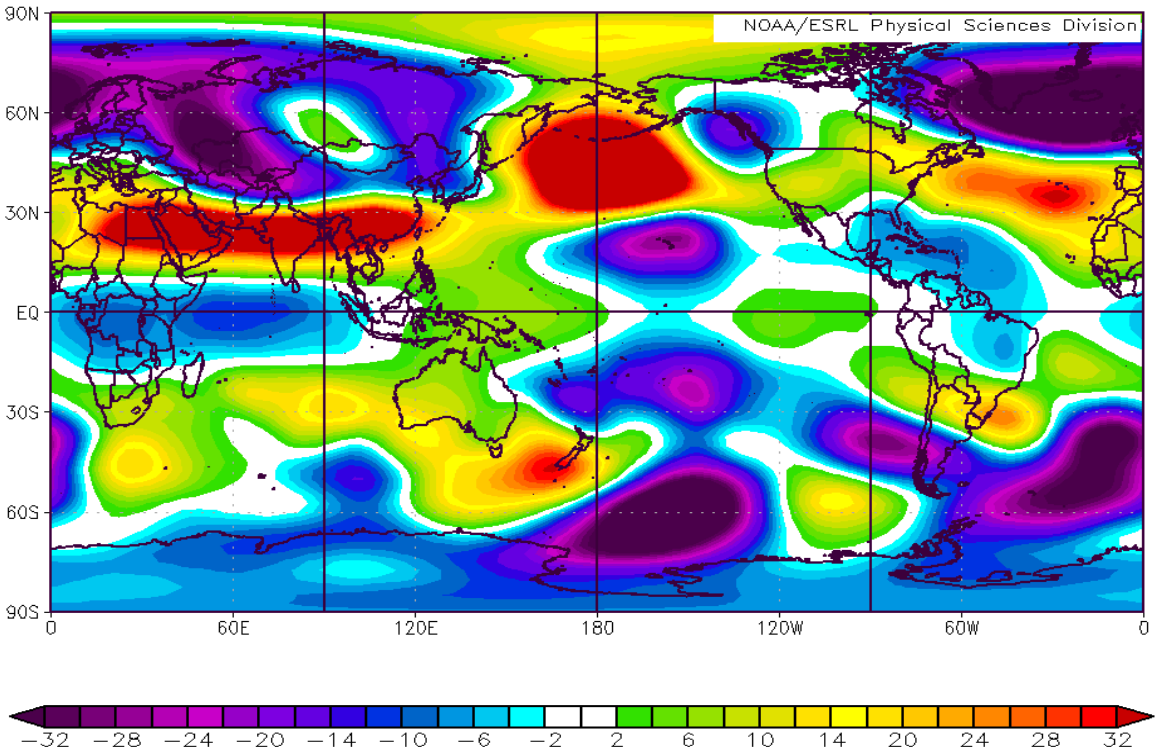

Note the evidence of anomalous tropical Rossby-Kelvin waves and extratropical Rossby waves in both the northern and southern hemispheres.

Figure 30. Z200 Anomalies (mb) for MJO Phase 4 and all EN, LN, and Neutral Years during JFM.

The JFM Phase 4 PR anomalies (PRAs; Figure 31) show: (a) positive anomalies over the MC and over most of nearby tropical Indian and western tropical Pacific; (b) positive anomalies just north of the equator in the central-eastern Pacific; (c) positive anomalies over much of northern Europe, the central North Pacific and over and near British Columbia and the Pacific Northwest region of the U.S.; (d) negative anomalies near the dateline in the tropical South Pacific and in the eastern tropical Pacific; (e) negative anomalies over most of tropical Africa and tropical South America; and (f) negative anomalies over much of southwest Asia and east Asia. The tropical PRAs are consistent with the known PRAs for MJO Phase 4 (Stepanek 2006; Zhang 2013; Gottschalck et al. 2016). The PRAs indicate a westward shift of the SPCZ and a northward shift of the ITCZ in the western and central Pacific. The PRAs are also consistent with the corresponding anomalies in SLP and Z200 (Figures 29, 30) and in

related low level moisture advection and upper tropospheric jets (not shown)—for example: (a) anomalously strong dry air from central Asia into east Asia leading to negative PRAs there; and (b) anomalously strong moist air from the North Atlantic into northern Europe leading to positive PRAs there. The tropical PRAs are also consistent with the ZA200s—in particular, the positive PRAs over and near the MC indicate positive latent heating anomalies and positive Z200 anomalies there (Figure 30). Note that the PRAs are nearly opposite to the EN PRAs (Figure 16) in many parts of the tropics, especially from the eastern Indian Ocean to about 150°W.

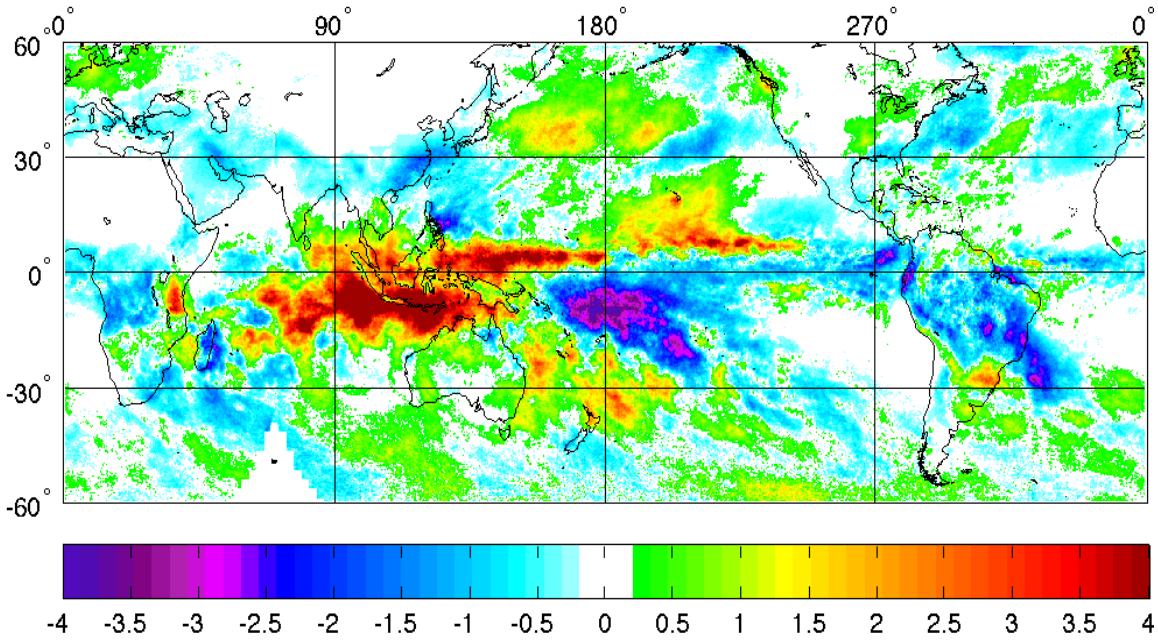

Note: (a) the positive anomalies in the tropics over and near the eastern Indian, basin, MC, and western Pacific; and (b) the negative anomalies in much of the tropical central-eastern Pacific.

Figure 31. PR Anomalies (mm/day) for MJO Phase 4 and all EN, LN, and Neutral Years during JFM.

The JFM Phase 4 SWHAs (Figure 32) show: (a) positive anomalies in much of the South Indian Ocean, parts of the tropical Pacific (especially between the Philippines and the dateline), much of the tropical North Atlantic, and west of northern Europe; and (b) negative anomalies in the central North Pacific, and much of the South Pacific and the midlatitude western North Atlantic. These SWHAs are consistent with the wind

anomalies indicated by the corresponding SLPAs (compare Figures 9 and 29)—for example: (a) an increase in the northward flow into the ITCZ in the South Indian Ocean leading to positive SWHAs there; (b) a decrease in the midlatitude westerlies in the central North Pacific leading to negative SWHAs there; and (c) an increase in the midlatitude westerlies in the midlatitude subpolar North Atlantic leading to positive SWHAs there.

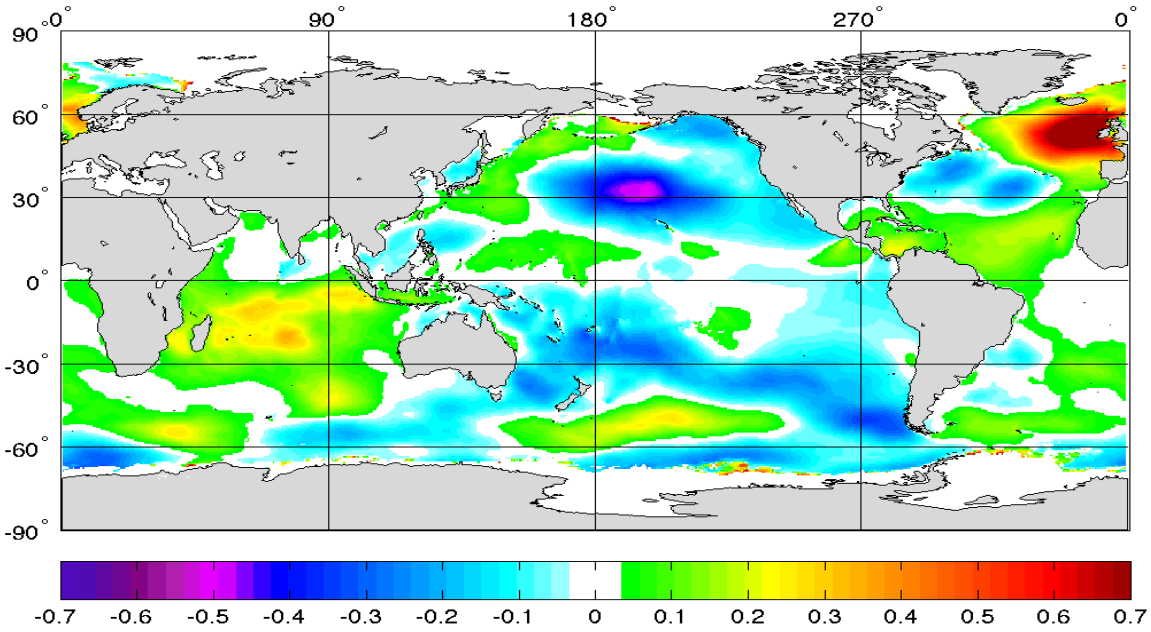

Note the positive anomalies in the South Indian Ocean and midlatitude North Atlantic, and negative anomalies in the central-eastern midlatitude Pacific.

Figure 32. SWH Anomalies (m) for MJO Phase 4 and all EN, LN, and Neutral Years during JFM.

The JFM Phase 4 anomalies (Figures 28–32) show dynamical consistency between the different anomalies. For example, the positive PRAs in the MC region are consistent with the negative SLPAs and the positive ZA200s in that region. The ZA200s also reveal anomalous Rossby and Kelvin wave activity, and anomalous interactions that affect transports of energy, moisture, and momentum between the tropics and extratropics, and that lead, in turn, to anomalous extratropical conditions, such as anomalous storm tracks, precipitation, and ocean surface waves.

The JFM Phase 4 anomalies reveal the anomalies that are commonly used to characterize MJO Phase 4 conditions. However, these anomalies also include anomalies associated with other climate variations—for example, anomalies associated with EN, LN, AO, and IOD. So these anomalies may not be the best indicator of MJO Phase 4 conditions. The following sections present MJO Phase 4 anomalies when EN, LN, and Neutral conditions are selectively included and excluded.

G. CASE 6: CHARACTERISTIC JFM EN PHASE 4 ANOMALIES

Figures 33–37 show the characteristic anomalous values for the focus variables for JFM during EN when the MJO is in Phase 4 with an amplitude greater than or equal to +1.0 (see case 6 description in Chapter II, section E). The JFM EN-Phase 4 SSTAs (Figure 33) show: (a) positive anomalies in the central-eastern tropical Pacific, in the tropical Indian Ocean, and along the west coasts of North and South America; and (b) negative anomalies in the western tropical Pacific that extend poleward and eastward into the central North and South Pacific. Note that the tropical Pacific SSTAs represent an anomalous *decrease* in the west-east SST gradient area seen in the LTM SST (Figure 8). Also note that the overall SSTA patterns are very similar to those in EN years (Figure 13) and very different from those in LN and Neutral years (Figures 18 and 23). This indicates that MJO Phase 4 has a relatively small impact on SSTAs compared to EN, and the EN impacts on SST are dominant over MJO phase 4 impacts when EN and MJO Phase 4 are occurring simultaneously.

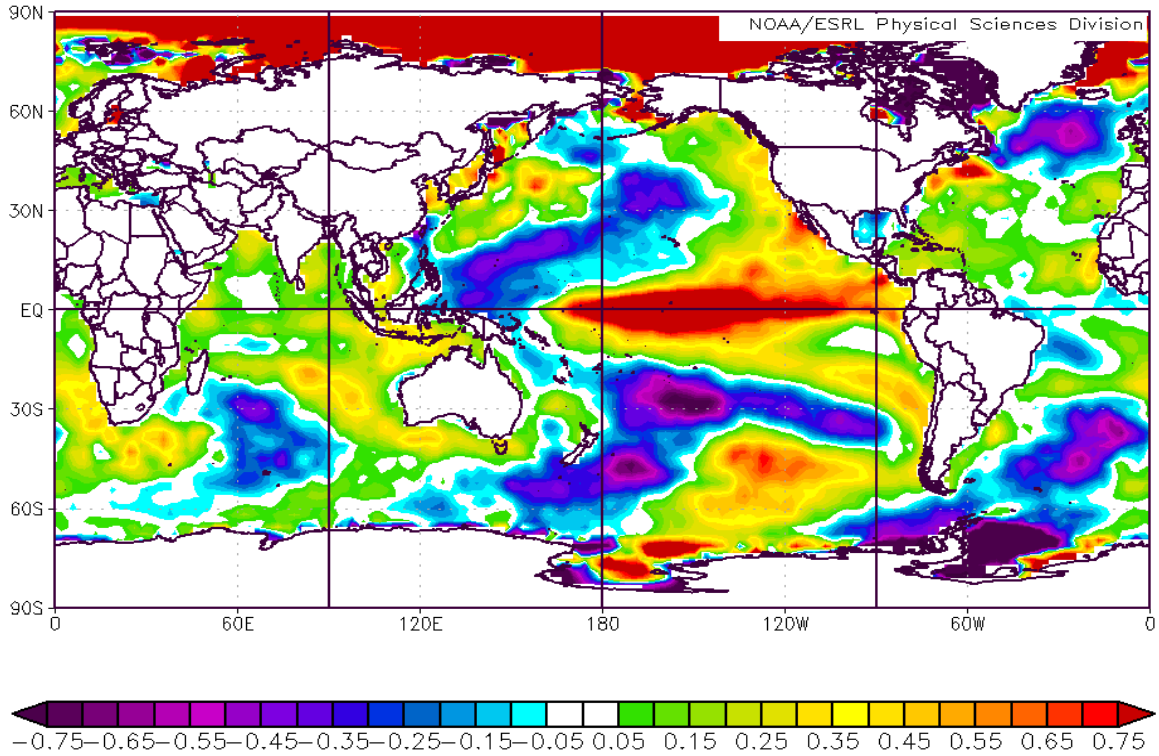

Note the similarities to the SSTAs in the EN composite (Figure 13).

Figure 33. SST Anomalies (°C) for MJO Phase 4 and EN Years during JFM.

The JFM EN-Phase 4 SLPAs (Figure 34) show: (a) negative anomalies in the tropical central-eastern Pacific, the eastern subtropical and midlatitude Pacific, southern Indian Ocean, southeast of Japan, eastern U.S., subpolar North Atlantic, and northern Eurasia; and (b) positive anomalies in much of the Atlantic basin, especially in the midlatitude North Atlantic, much of the western half of North America, Africa, and tropical Indian Ocean. Note that the SLPAs represent: (a) a reduction in the strength of the NPH, SPH, Siberian High, and Mascarene High; and (b) an increase in the strength of the AL and IL (Figure 9) and central-eastern tropical Pacific Low. Note too that the tropical Pacific SLP anomalies are dynamically consistent with the corresponding SST anomalies (cf. Figure 33), with negative [positive] tropical SLPAs over positive [negative] tropical SSTAs. The SLPAs can be used to infer the corresponding lower tropospheric wind anomalies—for example: (a) positive wind speed anomalies on the southern flank of the negative SLPA in the northeast Pacific, where the anomalous SLP gradient leads to an anomalous strengthening of the westerlies; and (b) negative wind

speed anomalies in the tropical Pacific trade wind region, where the anomalously weak subtropical—tropical SLP gradient leads to anomalously weak trade winds.

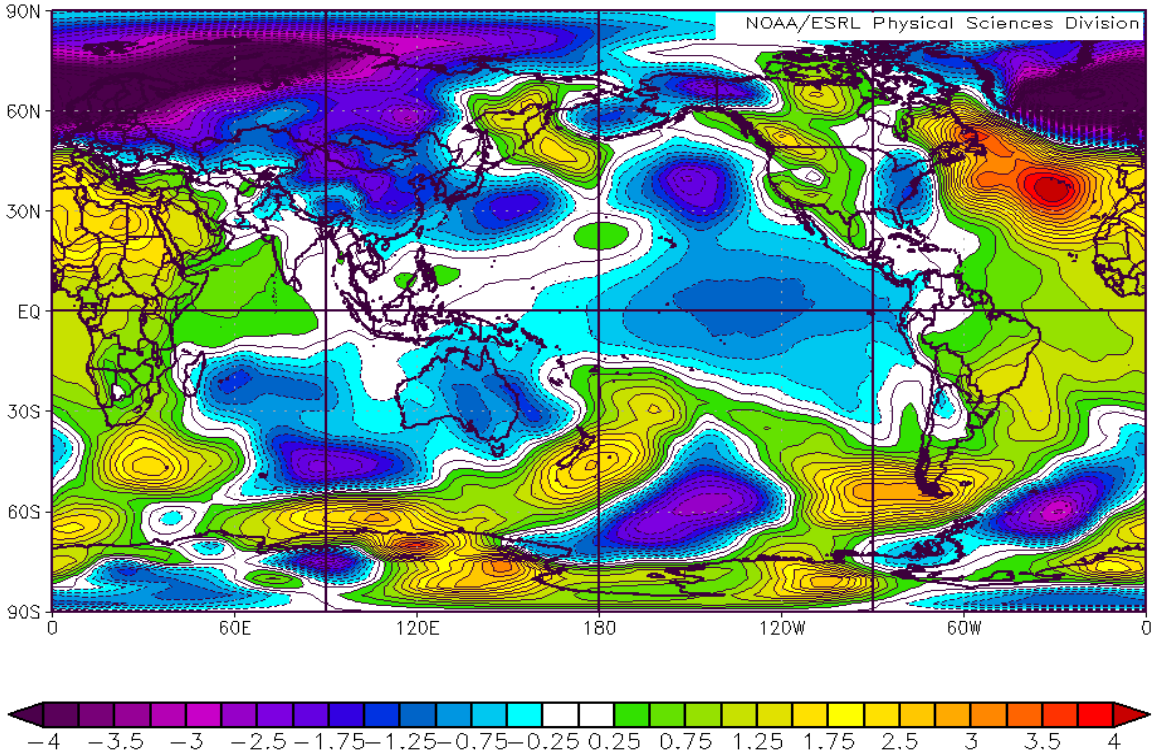

Note the differences between these anomalies and those in the EN composite (Figure 14).

Figure 34. SLP Anomalies (mb) for MJO Phase 4 and EN Years during JFM.

Figure 34 also shows that the overall SLPA patterns are different in many ways from those in EN years (Figure 14). In some regions, the MJO impacts on SLP are opposite to those of EN, as indicated by regions in which the EN-Phase 4 SLPAs are opposite to the EN SLPAs. This is especially clear in: (a) the tropics and subtropics between 90°E and the dateline, where the EN SLPAs are positive but the EN-Phase 4 SLPAs are negative; and (b) the midlatitude North Pacific where the EN SLPAs are strongly negative but the EN-Phase 4 SLPAs are less strongly negative. In other regions, the SLPAs are very similar to those for Phase 4 (Figure 29), indicating that MJO Phase 4 impacts dominate over EN impacts. This is especially clear in the North Atlantic. These overall results are consistent with what might have been expected from Figures 1 and 29.

But, Figure 34 helps clarify: (a) the spatial extent and magnitude of the MJO Phase 4 impacts on SLP when EN is also occurring; (b) the regions in which MJO Phase 4 impacts apparently interfere constructively and destructively with EN impacts; and (c) the regions in which MJO Phase 4 impacts dominate over EN impacts. Overall, these results indicate that MJO Phase 4 has global impacts on SLPA that are at least comparable in magnitude to that of EN, and that the MJO Phase 4 impacts and EN impacts can significantly enhance and suppress each other.

The JFM EN-Phase 4 ZA200s (Figure 35) show: (a) positive anomalies throughout most of the tropics, especially over the negative SLPAs in the central-eastern tropical Pacific (Figure 34), where the positive anomalies straddling the equator indicate an anomalous Rossby-Kelvin wave; and (b) positive and negative anomalies in the extratropics that indicate anomalous Rossby wave trains—for example, an anomalous wave train centered at about 30–40°N and extending eastward from central Asia. The ZA200s can also be used to infer the corresponding upper tropospheric wind anomalies—for example, an anomalous *increase* in the strength of the subtropical jet from northwest Africa eastward to southern China (cf. Figure 10).

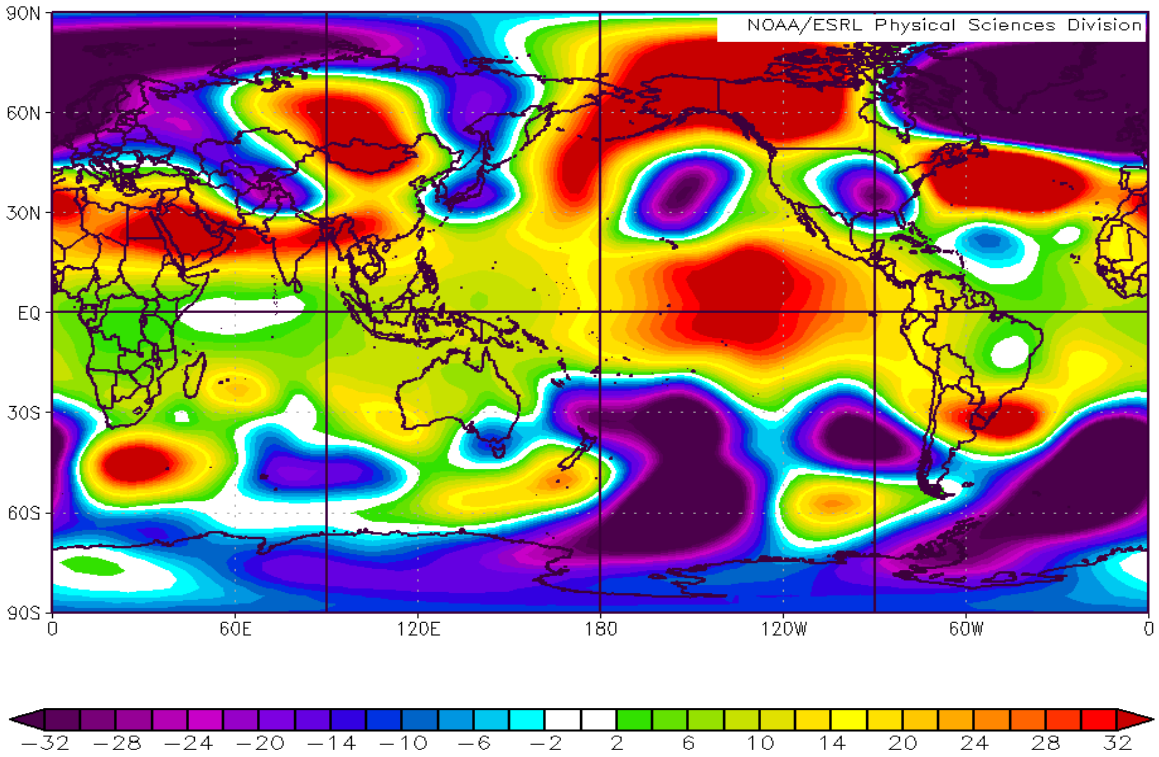

Note the differences between these anomalies and those in the EN composite (Figure 15).

Figure 35. Z200 Anomalies (mb) for MJO Phase 4 and EN Years during JFM.

Comparisons of the ZA200 results for EN, Phase 4, and EN-Phase 4 cases (Figures 15, 30, 35) show that the EN-Phase 4 anomalies are approximately what would be expected from adding the anomalies for the other two cases, and from constructive and destructive interference of the impacts from EN and MJO Phase 4. For example, the dominance of positive ZA200s in the tropics during EN is apparently weakened by the negative ZA200s in much of the tropics during MJO Phase 4, so that the EN-Phase 4 ZA200s (Figure 35) are weaker positive or negative in much of the tropics compared to the EN ZA200s (Figure 15). As another example, a positive PNA pattern during EN (Figure 15) is apparently countered by nearly opposite anomalies during Phase 4 (Figure 30), so that there is less evidence of the PNA during EN-Phase 4 case (Figure 35) than in the EN case. However, the strong anomalies over the Arctic and neighboring subpolar regions in the EN-Phase 4 case appear to be the result of constructive interference

between the responses to EN and the responses to MJO Phase 4 (compare Figures 15, 30, and 35).

The JFM EN-Phase 4 PR anomalies (PRAs; Figure 36) show: (a) positive anomalies in much of the central-eastern tropical Pacific, and tropical Indian Ocean extending into the MC; and (b) negative anomalies in the western and off-equatorial tropical Pacific east of the Philippines, and in the SPCZ region. These PRAs are approximately consistent with the corresponding SSTAs and SLPAs in several areas, with positive [negative] SSTAs and negative [positive] SLPAs corresponding to positive PRAs (Figures 33, 34). Note that many of the PRAs represent shifts in the locations of the ITCZ and the SPCZ—for example, a northward shift of the ITCZ in the central-eastern tropical Pacific, and possible westward and eastward shifts of the SPCZ. There are also notable negative PRAs in the eastern Mediterranean, southwest Asia, eastern China, southern Africa, and northern South America. These PRAs are consistent with the corresponding anomalies in SLP and ZA200 (Figures 34, 35) and in related low level moisture advection and upper tropospheric jets (not shown). The tropical PRAs are also consistent with the ZA200s—in particular, the positive PRAs in the central-eastern tropical Pacific indicate positive latent heating anomalies and positive ZA200s (Figure 35).

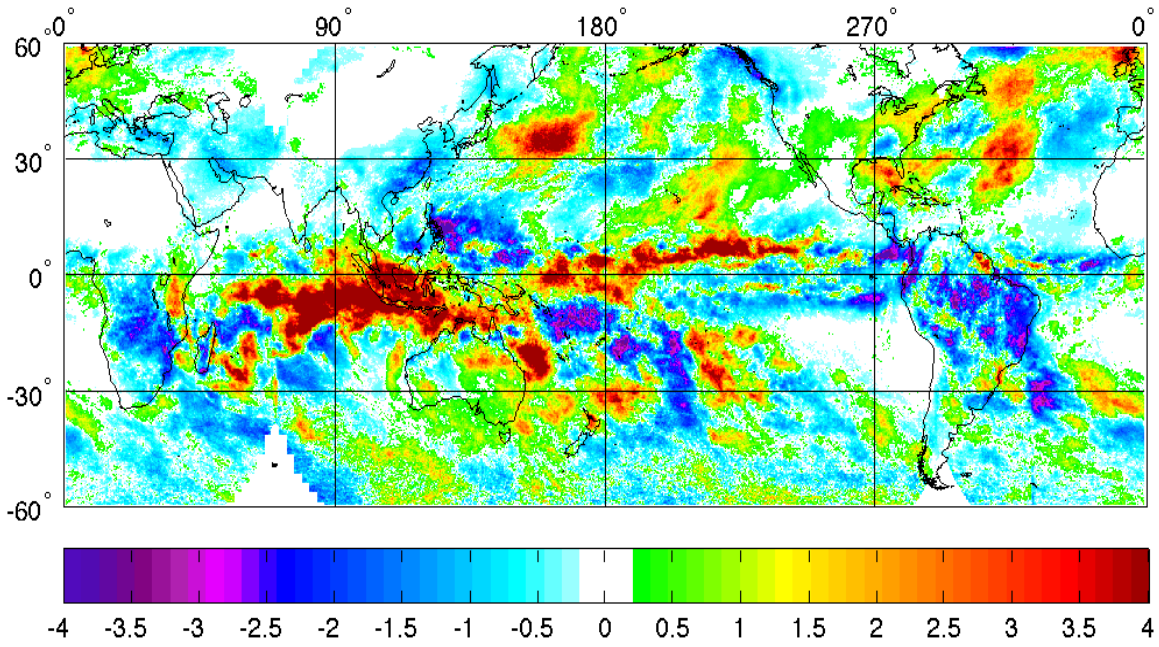

Note the differences between these anomalies and those in the EN composite (Figure 16).

Figure 36. PR Anomalies (mm/day) for MJO Phase 4 and EN Years during JFM.

Comparisons of the PRAs for EN-Phase 4 (Figure 36) with those for EN only (Figure 16) and Phase 4 (Figure 31) show that the MJO Phase 4 anomalies and EN anomalies destructively interfere in some regions (for example, the southern MC, from northern Borneo east to the dateline, eastern China) and constructively interfere in other regions (for example, in much of the SPCZ region, over and east of the northern Philippines, northern South America). In other regions, the anomalies of one case are dominant because the corresponding anomalies from the other case are weak—for example, over the eastern Mediterranean and southwest Asia, where MJO Phase 4 PRAs dominate. The overall results indicate that the EN PRAs in many regions are substantially altered by the simultaneous occurrence of MJO Phase 4, and vice versa.

The JFM EN-Phase 4 SWHAs (Figure 37) show notable: (a) positive anomalies in the South Indian Ocean, the central-eastern tropical Pacific, and the northeast Atlantic; and (b) negative anomalies in much of the western tropical-subtropical Pacific, the northeast and southeast Pacific, and the western North Atlantic. Theses anomalies are

consistent with the corresponding SLPA gradients (Figure 9) and the implied wind anomalies, and with propagation of waves away from their formation regions.

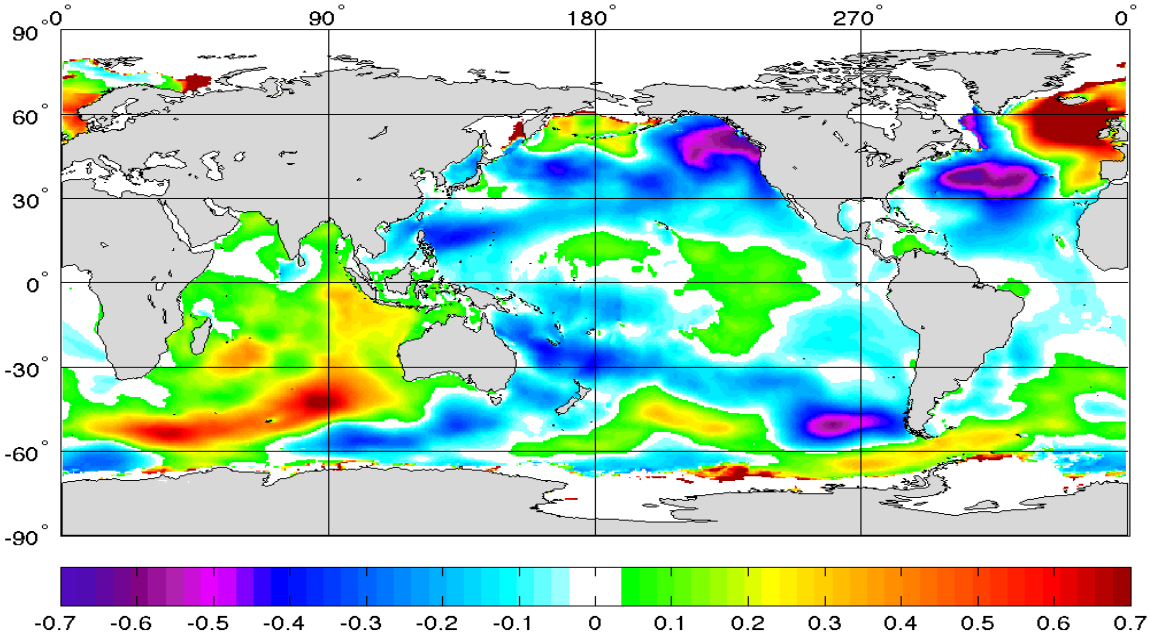

Note the similarities between these anomalies and those in the Phase 4 composite (Figure 32).

Figure 37. SWH Anomalies (m) for MJO Phase 4 and EN Years during JFM.

Comparisons of the SWHAs for EN-Phase 4 (Figure 37) with those for EN only (Figure 17) and Phase 4 (Figure 32) indicate that the EN and Phase 4 impacts on SWHs: (a) destructively interfere in many regions, such as the Southern Indian Ocean, much of the extratropical North and South Pacific, and much of the tropical and midlatitude North Atlantic; and (b) constructively interfere in some regions (for example, parts of the central-eastern tropical Pacific, west and east of the northern Philippines, the northeast Atlantic). The over similarity in pattern and sign of the SWH anomalies for Phase 4 SWHAs (Figure 32) and for EN-Phase 4 (Figure 37) indicate that the EN-Phase SWHAs are dominated by the impacts of phase 4 on SWH. Note that the EN-Phase 4 SWHAs (Figure 37) in the Gulf of Alaska and northeast Atlantic have larger magnitudes than in the EN case (Figure 17) or the Phase 4 case (Figure 32). This may be the result of fewer

days being composited for the EN-Phase 4 case than the other two cases (see Chapter II, section E).

H. CASE 7: CHARACTERISTIC JFM LN PHASE 4 ANOMALIES

Figures 38–42 show the characteristic anomalous values for the focus variables for JFM during LN when the MJO is in Phase 4 with an amplitude greater than or equal to +1.0 (see case 7 description in Chapter II, section E). The JFM LN-Phase 4 SSTAs (Figure 38) show (a) negative anomalies in the central-eastern tropical Pacific, in the tropical Indian Ocean, and along the west coasts of North and South America; and (b) positive anomalies in the western tropical Pacific that extend poleward and eastward into the central North and South Pacific. Note that the tropical Pacific SSTAs represent an anomalous *increase* in the west-east SST gradient area seen in the LTM SST (Figure 8). Also note that the overall SSTA patterns are very similar to those in LN years (Figure 18) and very different from those in EN, Neutral, and EN-Phase 4 years (Figures 13, 23, and 33). This indicates that MJO Phase 4 has a relatively small impact on SSTAs compared to LN, and that LN dominates the SSTAs when LN and MJO Phase 4 are occurring simultaneously.

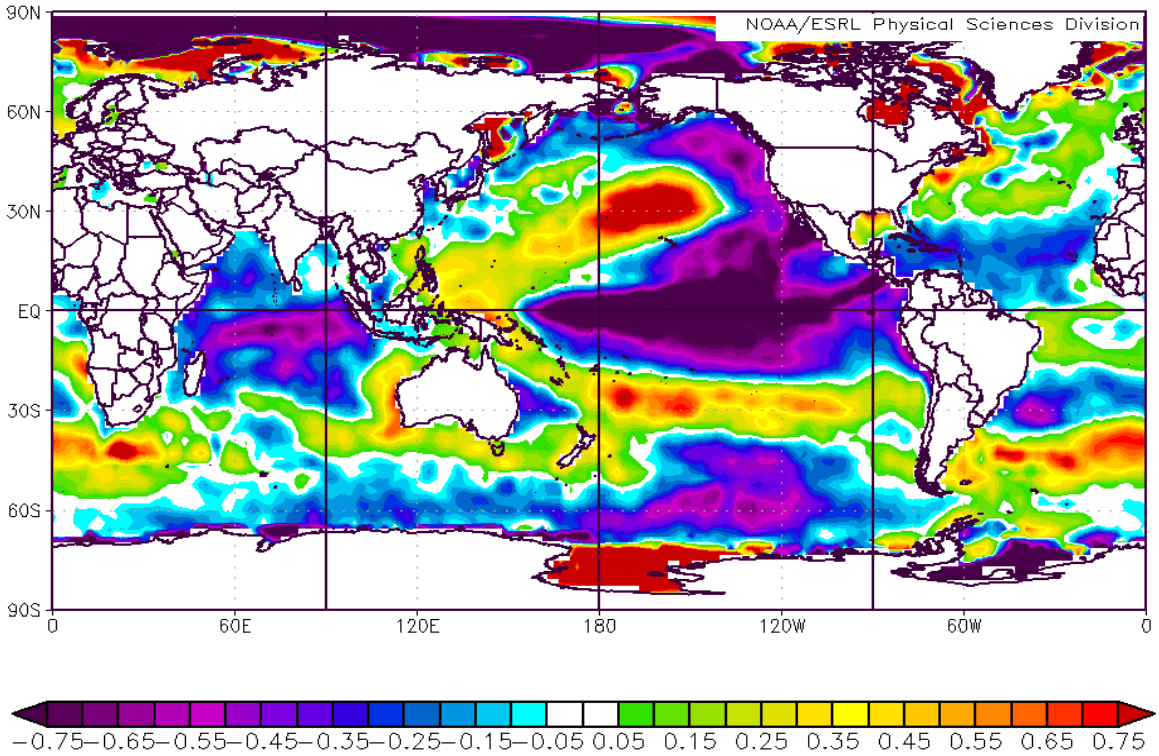

Note the similarities between these anomalies and those in the LN composite (Figure 18).

Figure 38. SST Anomalies (°C) for MJO Phase 4 and LN Years during JFM.

The JFM LN-Phase 4 SLPAs (Figure 39) show: (a) positive anomalies in the eastern subtropical-midlatitude North and South Pacific, northeastern North America, Greenland, the Arctic, and the midlatitude North Atlantic; and (b) negative anomalies in much of the western tropical Pacific, the Indian Ocean, western Eurasia, western and southern North America. Note that the SLPAs represent: (a) an overall decrease in the strength of the AL, IL, and Mascarene High; and (b) an increase in the strength of the NPH and SPH, and the Siberian High (Figure 9). Note too that the tropical western Pacific SLP anomalies are dynamically consistent with the corresponding SST anomalies (see Figure 38), with negative SLPAs over positive SSTAs.

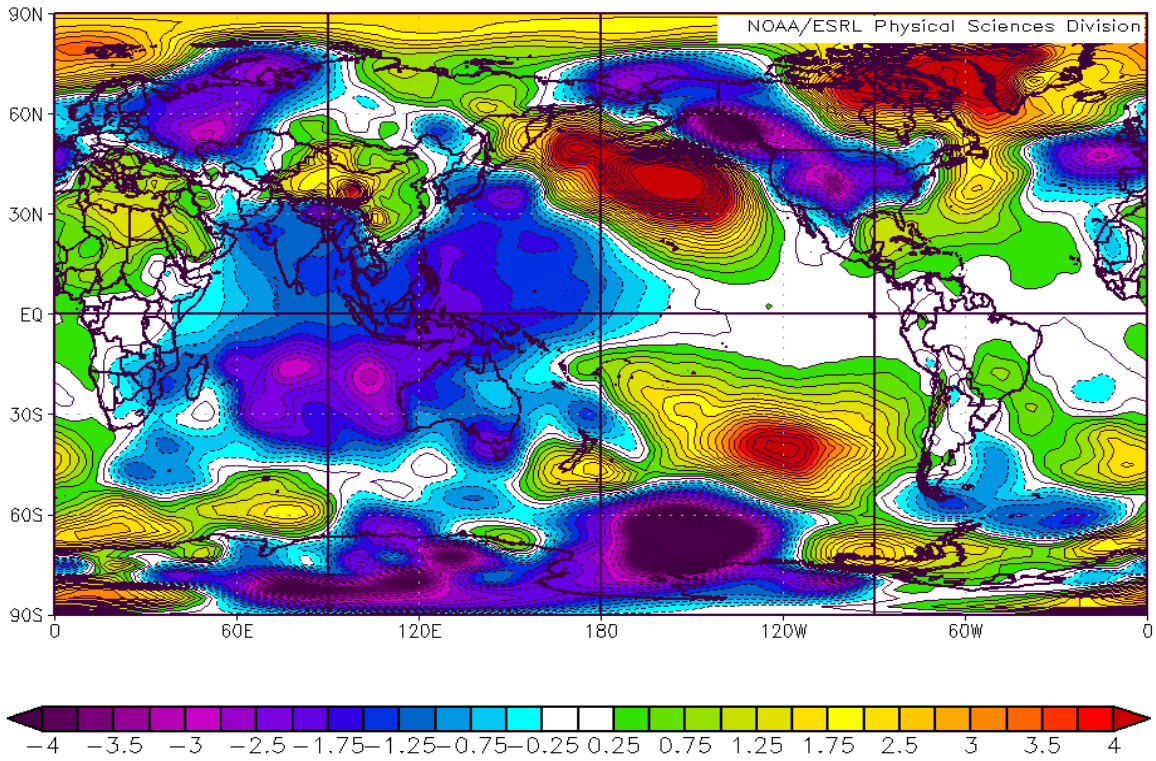

Note the similarities between these anomalies and those in the Phase 4 composite (Figure 29).

Figure 39. SLP Anomalies (mb) for MJO Phase 4 and LN Years during JFM.

The overall SLPA patterns in Figure 39 are similar in many ways to those in MJO phase 4 (Figure 29) and, to a lesser extent, those in LN years (Figure 19). This indicates that the LN-Phase 4 SLPAs are: (a) dominated by the impacts of MJO phase 4; and (b) are constructively interfered with by the impacts of LN. Figure 39 helps clarify: (a) the spatial extent and magnitude of the MJO Phase 4 impact on SLP when LN is also occurring; (b) the regions in which MJO Phase 4 impacts constructively and destructively interfere with LN impacts; and (c) the regions in which MJO Phase 4 impacts dominate over LN impacts. Overall, these results indicate that MJO Phase 4 has global impacts on SLPA that are at least comparable in magnitude to that of LN, and that the MJO Phase 4 impacts and LN impacts can significantly enhance and suppress each other.

The JFM LN-Phase 4 ZA200s (Figure 40) show: (a) negative anomalies throughout most of the tropics, with negative anomalies straddling the equator in the tropical Pacific that indicate an anomalous Rossby-Kelvin wave; and (b) alternating

positive and negative anomalies in the extratropics that indicate anomalous Rossby wave trains—in particular, a very clear anomalous wave train in the northern midlatitudes that extends eastward from east Eurasia to the North Atlantic and western Eurasia. The ZA200s can be used to infer corresponding upper tropospheric wind anomalies—for example, an anomalous *increase* in the strength of the subtropical jet from northwest Africa eastward to southern Japan and an anomalous *decrease* in the strength of the subtropical jet over the central North Pacific ab diver southern North America and the western North Atlantic (cf. Figure 10).

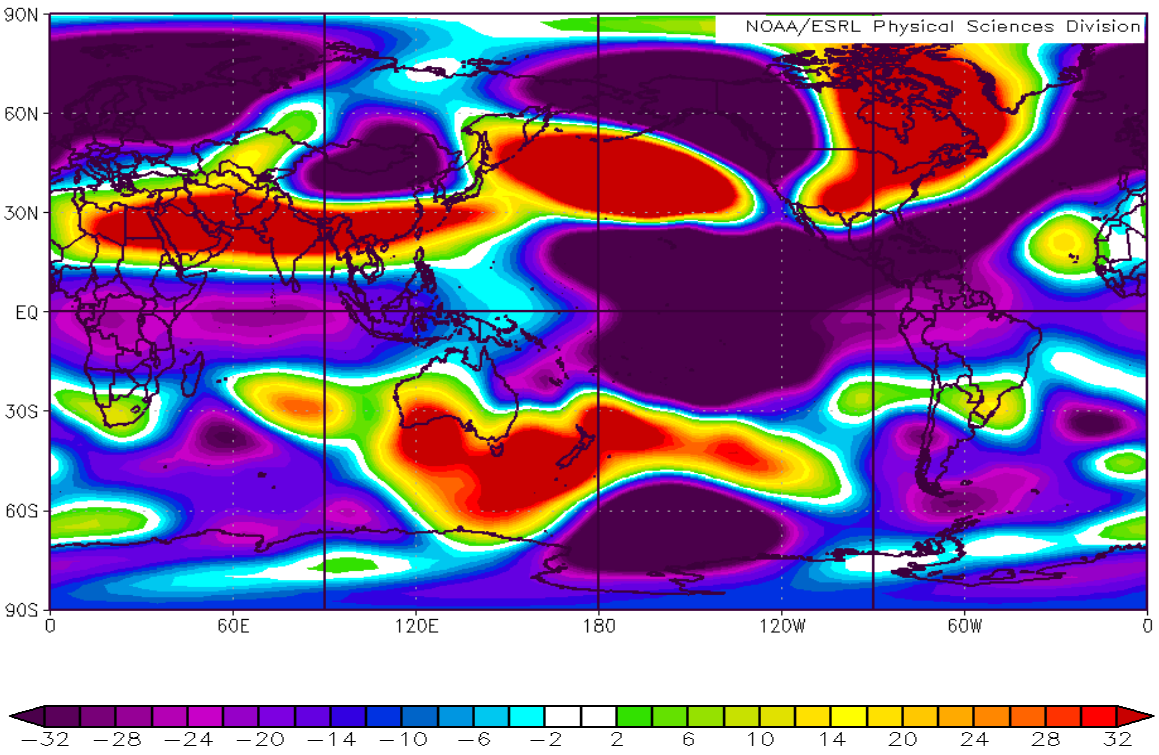

Note: (a) the similarities between these anomalies and those in the LN and Phase 4 composites (Figures 20 and 30); and (b) the pronounced anomalous Rossby wave train extending eastward from eastern Eurasia to western Eurasia.

Figure 40. Z200 Anomalies (mb) for MJO Phase 4 and LN Years during JFM.

Comparisons of the ZA200 results for LN, Phase 4, and LN-Phase 4 (Figures 20, 30, 40) show that the LN-Phase 4 anomalies are similar to what would be expected from adding the anomalies for the other two cases (i.e., from constructive and destructive

interference of the impacts from LN and MJO Phase 4). For example, the dominance of negative ZA200s in the tropics during LN case is apparently weakened by the positive ZA200s near the MC during MJO Phase 4, so that the LN-Phase 4 ZA200s are less negative or positive over the MC. As another example, the positive anomalies over northern Africa southern Asia, and the central North Pacific in the LN and Phase 4 cases lead to very pronounced positive anomalies in those regions in the LN-Phase 4 case.

The JFM-LN Phase 4 PR anomalies (PRAs; Figure 41) show: (a) positive anomalies in southern Africa, tropical South Indian Ocean, MC and western tropical Pacific; and (b) negative anomalies in the central-eastern tropical Pacific and SPCZ region. The tropical Pacific PRAs are dynamically consistent with the corresponding SSTAs and SLPAs, with positive [negative] SSTAs and negative [positive] SLPAs corresponding to positive PRAs (Figures 38, 39), especially over the MC. However, the positive PRAs in and near the ITCZ in the tropical South Indian basin overlie negative SSTAs. Note that many of the PRAs represent shifts in the locations of the ITCZ and the SPCZ—for example, a northward shift of the ITCZ in the central-eastern tropical Pacific, and a westward shift of the SPCZ. These are consistent with what is expected during LN events (Figure 19; Philander 1990) and with what is expected during Phase 4 (Figure 31; Gottschalck et al. 2016). There are also notable negative PRAs in the eastern Mediterranean, southwest Asia, eastern China, western Africa, and the U.S. Gulf Coast. The tropical PRAs are also consistent with the ZA200s—in particular, the negative PRAs in the central-eastern tropical Pacific indicate negative latent heating anomalies and negative ZA200s (Figure 40).

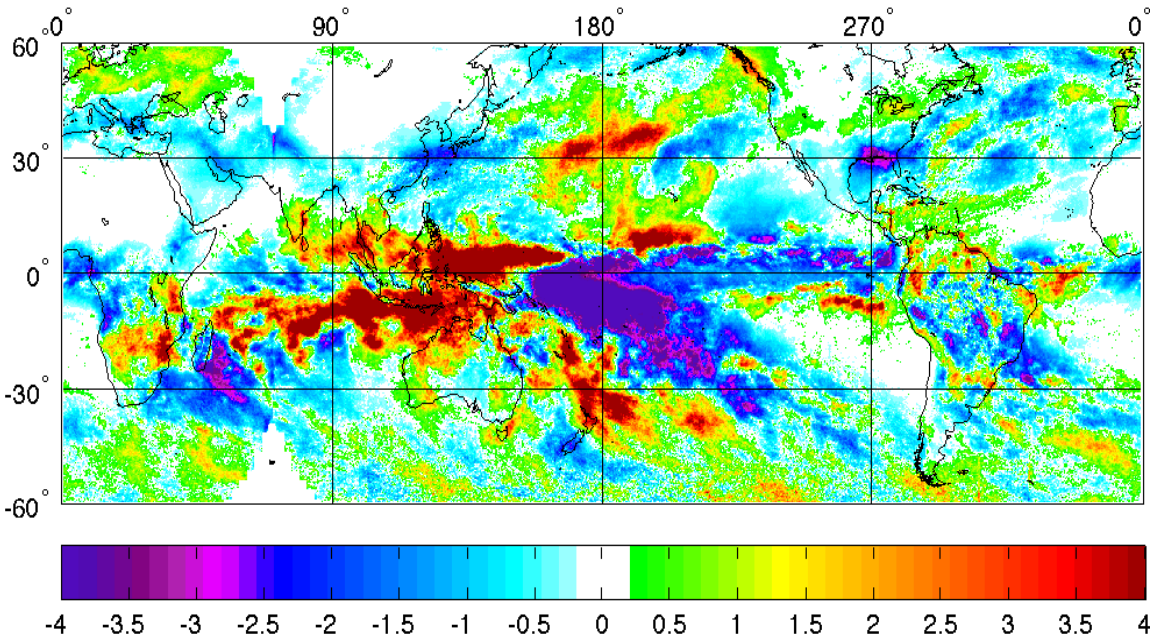

Note the similarities between these anomalies and those in the LN and Phase 4 composites (Figures 21 and 31).

Figure 41. PR Anomalies (mm/day) for MJO Phase 4 and LN Years during JFM.

Comparisons of the PRAs for LN-Phase 4 (Figure 41) with those for LN only (Figure 21) and Phase 4 (Figure 31) show that the MJO Phase 4 anomalies and LN anomalies: (a) constructively interfere in many regions—for example, the MC, central-eastern tropical Pacific, the SPCZ region, and eastern China; and (b) destructively interfere in some regions—for example, much of the Philippine Sea, southern Africa, and South America. In some regions, the anomalies of one case may dominate—for example, over the eastern Mediterranean and southwest Asia, where MJO Phase 4 PRAs may dominate. The overall results indicate that the LN PRAs in many regions are substantially altered by the simultaneous occurrence of MJO Phase 4, and vice versa.

The JFM LN-Phase 4 SWHAs (Figure 42) show notable: (a) positive anomalies near the Horn of Africa, and in the South Indian Ocean, midlatitude North Pacific, and tropical North Atlantic; and (b) negative anomalies centered in the SPCZ region, central North Pacific and extratropical North Atlantic. These anomalies are generally consistent with the corresponding SLPA gradients (Figure 39) and the implied wind anomalies, and

with propagation of waves away from their formation regions. For example, the SWHAs in the North Pacific (Figure 42) are consistent with the positive SLPAs in that region (Figure 39) and the corresponding lower tropospheric wind anomalies (not shown).

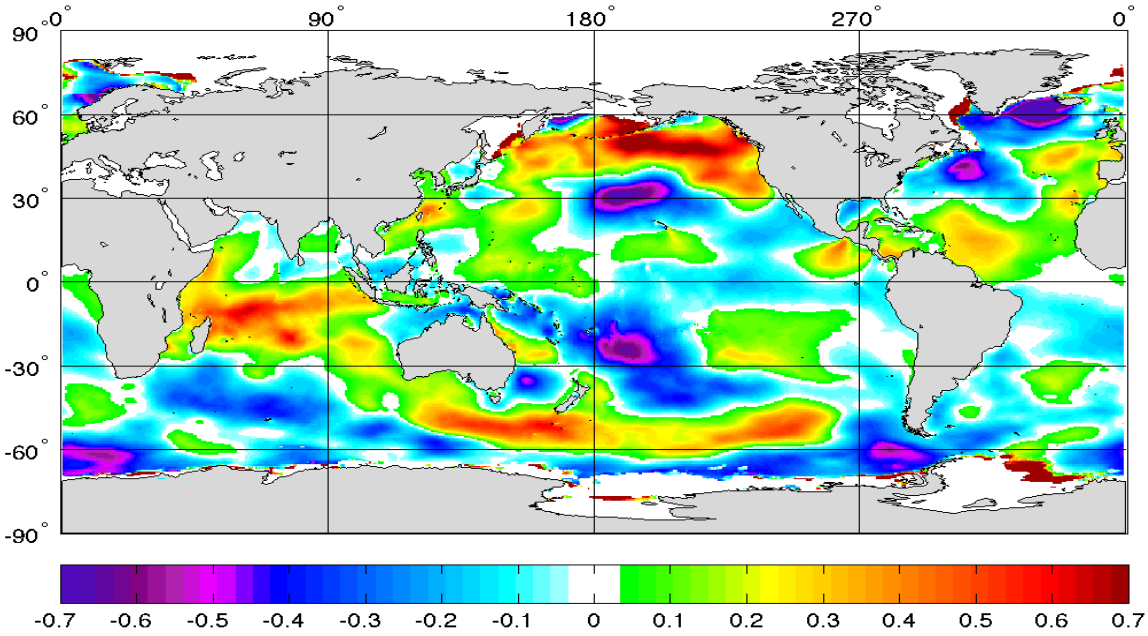

Note the similarities between these anomalies and those in the LN and Phase 4 composites (Figures 22 and 32).

Figure 42. SWH Anomalies (m) for MJO Phase 4 and LN Years during JFM.

Comparisons of the SWHAs for LN-Phase 4 (Figure 42) with those for LN only (Figure 22) and Phase 4 (Figure 32) show that the Phase 4 anomalies and LN anomalies constructively interfere in many regions—for example, the South Indian Ocean, the central North and South Pacific, and the western North Atlantic. In other regions, the anomalies of one case dominate over those of the other case—for example, the Gulf of Alaska and the North Atlantic where LN impacts appear to dominate. The overall results indicate that the impacts of LN and Phase 4 on SWHAs constructively interfere in many regions; and (b) the SWH impacts of LN may substantially alter those of Phase 4, and vice versa.

I. CASE 8: CHARACTERISTIC JFM NEUTRAL PHASE 4 ANOMALIES

Figures 43–47 show the characteristic anomalous values for the focus variables for JFM during Neutral periods when the MJO is in Phase 4 with an amplitude greater than or equal to +1.0 (see case 8 description in Chapter II, section E). Note that these case 8 anomalies represent MJO phase 4 anomalies without impacts from simultaneous EN or LN events. So the case 8 anomalies reveal the relatively pure impacts of phase 4 (as discussed in Chapter II, section E). The JFM Neutral-Phase 4 SSTAs (Figure 43) show: (a) negative anomalies in the eastern tropical Pacific, western subtropical Pacific, in the tropical South Indian Ocean, the midlatitude western North Pacific, west coasts of North and South America; and much of the tropical to midlatitude Atlantic; and (b) positive anomalies in the western tropical Pacific that extend poleward and eastward into the central North and South Pacific, and in the subpolar North Atlantic. Note that the tropical Pacific SSTAs represent an anomalous *increase* in the west-east SST gradient area seen in the LTM SST (Figure 8). Also note that the overall SSTA patterns are very similar to the Neutral patterns (Figure 23) and similar to the Phase 4 patterns (Figure 28). This indicates that: (a) the EN and LN impacts on SST tend to cancel out each other; and (b) Phase 4 impacts on SST are relatively small compared to EN and LN impacts, consistent with the conclusions based on Figures 33 and 38.

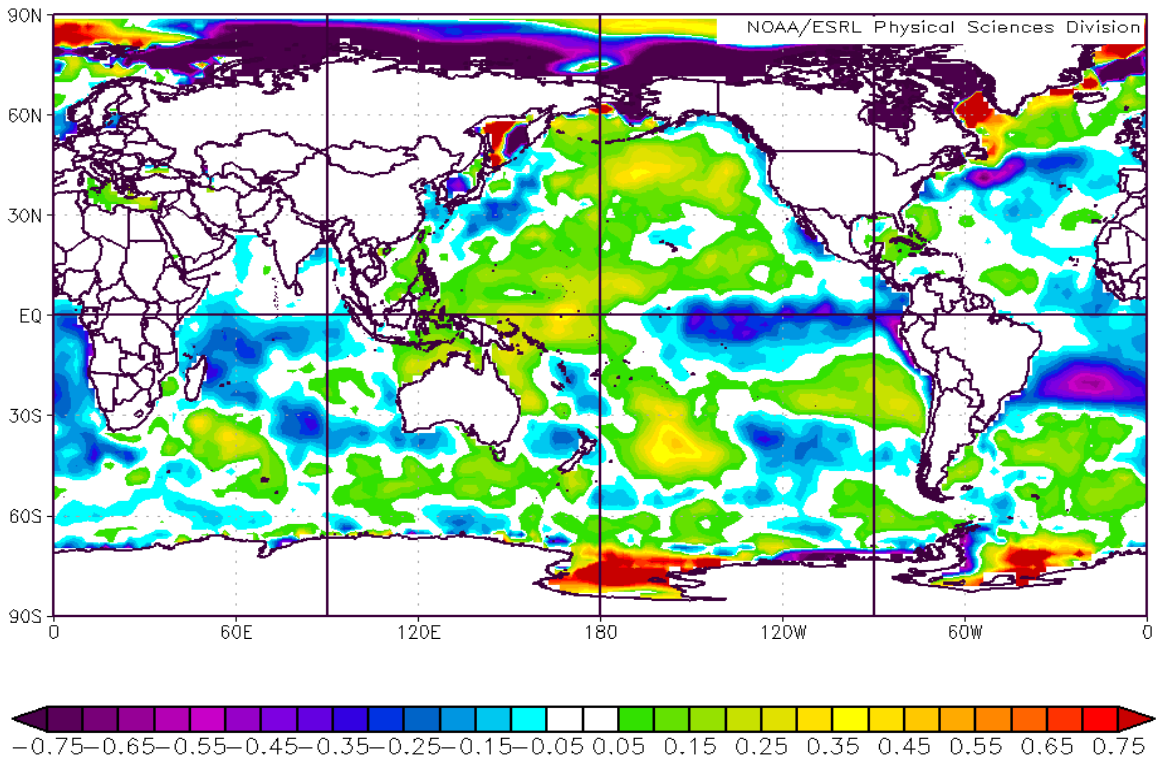

Note the similarities between these anomalies and those in the Neutral and Phase 4 composites (Figures 23 and 28).

Figure 43. SST Anomalies (°C) for MJO Phase 4 and Neutral Years during JFM.

The JFM Neutral-Phase 4 SLPAs (Figure 44) show: (a) negative anomalies in most of the Indian Ocean, most of Eurasia, tropical Pacific, western subtropical North Pacific, subpolar South Pacific, and subpolar North Atlantic; and (b) positive anomalies in the subtropical North and South Pacific, most of the tropical and subtropical Atlantic basin, and most of Africa. Note that the SLPAs represent: (a) an increase in the strength of the tropical low in the Indian and Pacific, NPH, SPH, Azores High, and IL; and (b) a decrease in the strength of the Asian High, AL, and Mascarene High (Figure 9). Note too that the tropical Pacific SLP anomalies are dynamically consistent with the corresponding SST anomalies (cf. Figure 43), with negative [positive] tropical SLPAs over positive [negative] tropical SSTAs. The negative SLPA pattern in the tropical Pacific, east Asia, South Indian Ocean, and Australia indicates an anomalous Rossby-Kelvin wave and anomalous tropospheric warming centered near the MC (Chapter I, section B; Philander

1990). The pattern of alternating negative and positive SLPAs extending eastward and poleward from east Asia to the North Pacific, North America, and North Atlantic indicates an anomalous extratropical Rossby wave train (Chapter I, section B; Philander 1990). The SLPAs in Figure 44 can be used to infer the corresponding lower tropospheric wind anomalies—for example: (a) negative wind speed anomalies on the southern flank of the positive SLPA in the northeast Pacific, where the anomalous SLP gradient leads to an anomalous weakening of the westerlies; and (b) positive wind speed anomalies in the tropical Pacific trade wind region, where the anomalously strong subtropical-tropical SLP gradient leads to anomalously strong trade winds.

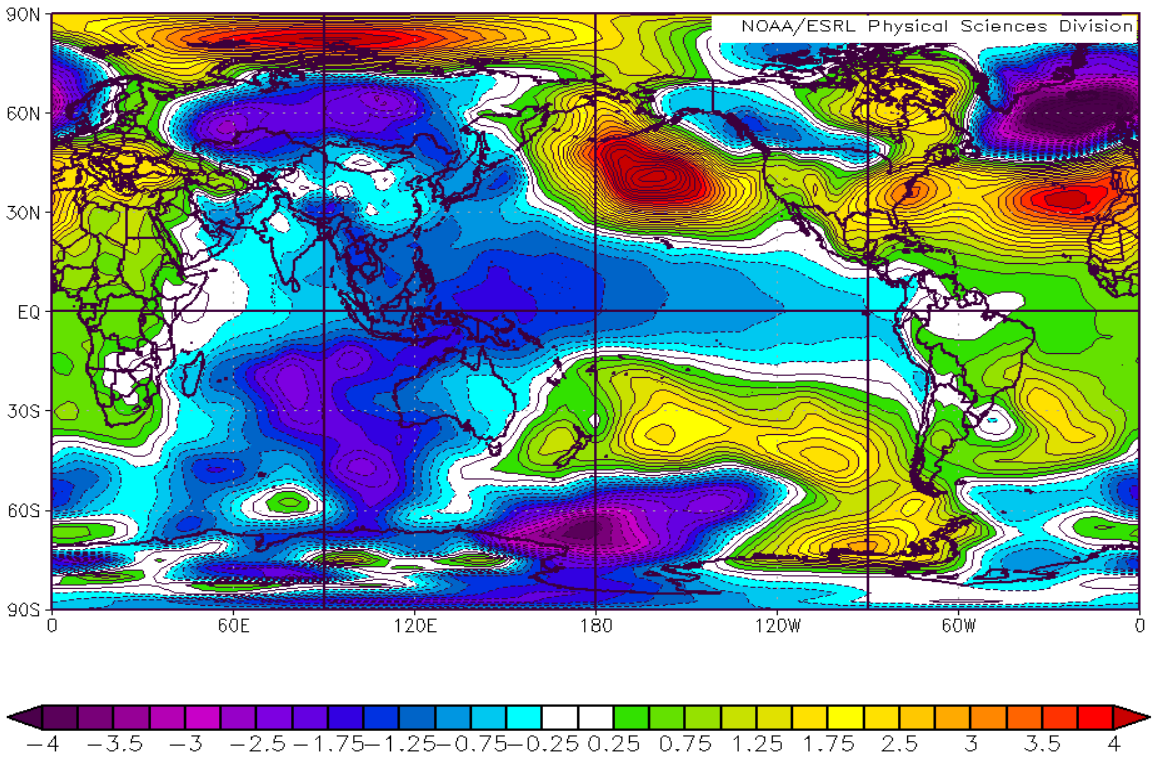

Note the pronounced similarities between these anomalies and those in the Phase 4 composite (Figure 29).

Figure 44. SLP Anomalies (mb) for MJO Phase 4 and Neutral Years during JFM.

The SLPAs in Figure 44 are: (a) strikingly similar to those in Phase 4 (Figure 29); and (b) similar to those in LN (Figure 19) and LN-Phase 4 (Figure 39). This indicates

that: (a) the phase 4 impacts on SLP are similar in pattern, sign, and magnitude to those of LN; (b) SLPAs from phase 4 and LN are likely to strongly reinforce each other; and (c) the impacts on SLP from EN and LN tend to cancel out each other.

The JFM Neutral-Phase 4 ZA200s (Figure 45) show: (a) positive anomalies in the western tropical Pacific and MC; (b) positive anomalies over subtropical south Asia and the subtropical South Indian Ocean that straddle the equator in most of the eastern hemisphere and that merge with the positive anomalies over the western tropical Pacific; (c) negative anomalies along the equator over Africa and the Indian Ocean; and (d) negative anomalies that straddle the equator in the central Pacific. The ZA200s that straddle the equator and that lie over the equator from Africa eastward to South America indicate an anomalous tropical Rossby-Kelvin wave, consistent with the indications from the corresponding SLPA results (Figure 44). The alternating negative and positive ZA200s in the extratropics indicate anomalous extratropical Rossby waves—for example, an anomalous Rossby wave train extending eastward from east Asia into the North Atlantic, and another arching over the South Pacific and southern South America. Note the indications of equivalent barotropic structure in the extratropics (compare Figures 44 and 45)—for example, over the North Pacific, North America, and North Atlantic. The ZA200s can also be used to infer the corresponding upper tropospheric wind anomalies—for example, an anomalously strong subtropical jet over south Asia, from the Mediterranean Sea to Japan, and an anomalously weak subtropical jet over the central North Pacific and southern North America, from about 170°E to the eastern U.S. west (cf. Figure 10). Note the ZA200 patterns in Figure 45 are strikingly similar to those in the Phase 4 case (Figure 30), indicating that the impacts of EN and LN on Z200 tend to cancel out each other.

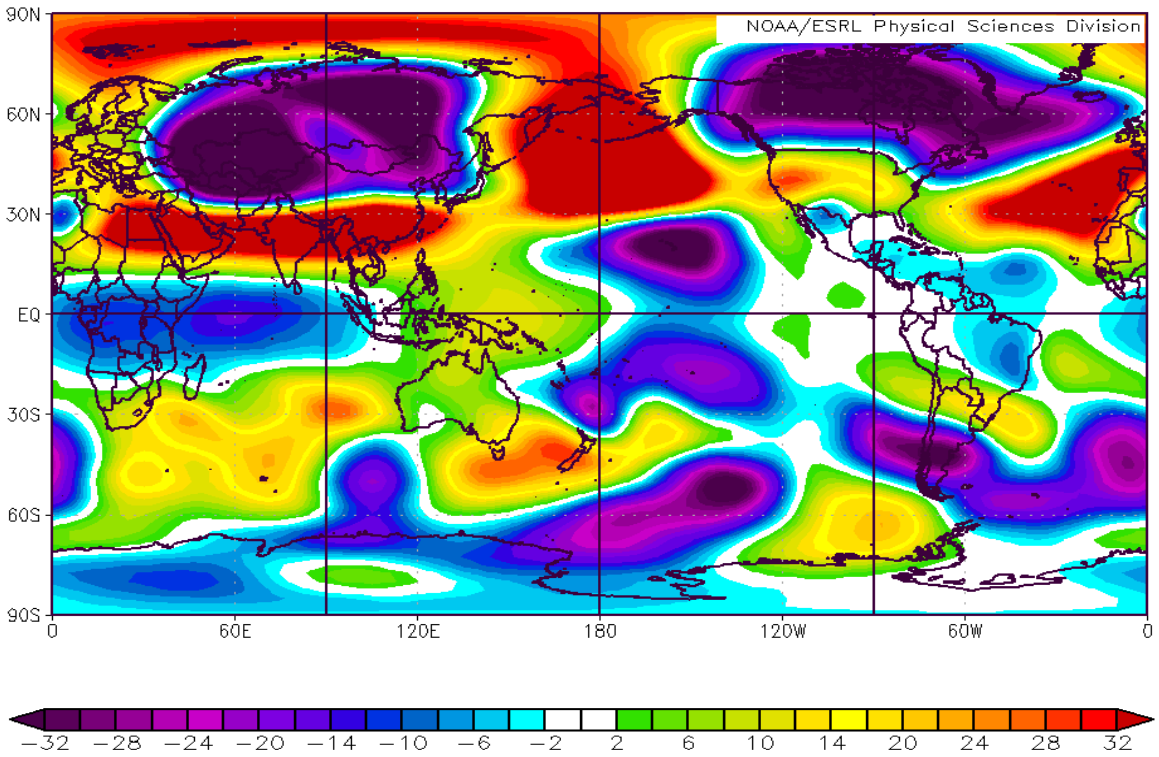

Note the striking similarities between these anomalies and those in the Phase 4 composite (Figure 30).

Figure 45. Z200 Anomalies (mb) for MJO Phase 4 and Neutral Years during JFM.

The JFM Neutral-Phase 4 PR anomalies (PRAs; Figure 46) are: (a) very similar to those in Phase 4 (Figure 31) and LN-Phase 4 (Figure 41); and (b) somewhat similar to those in LN (Figure 21). This indicates that: (a) the phase 4 impacts on PR are similar in pattern, sign, and magnitude to those of LN; (b) PRAs from phase 4 and LN are likely to strongly reinforce each other; and (c) the impacts on PR from EN and LN tend to cancel out each other.

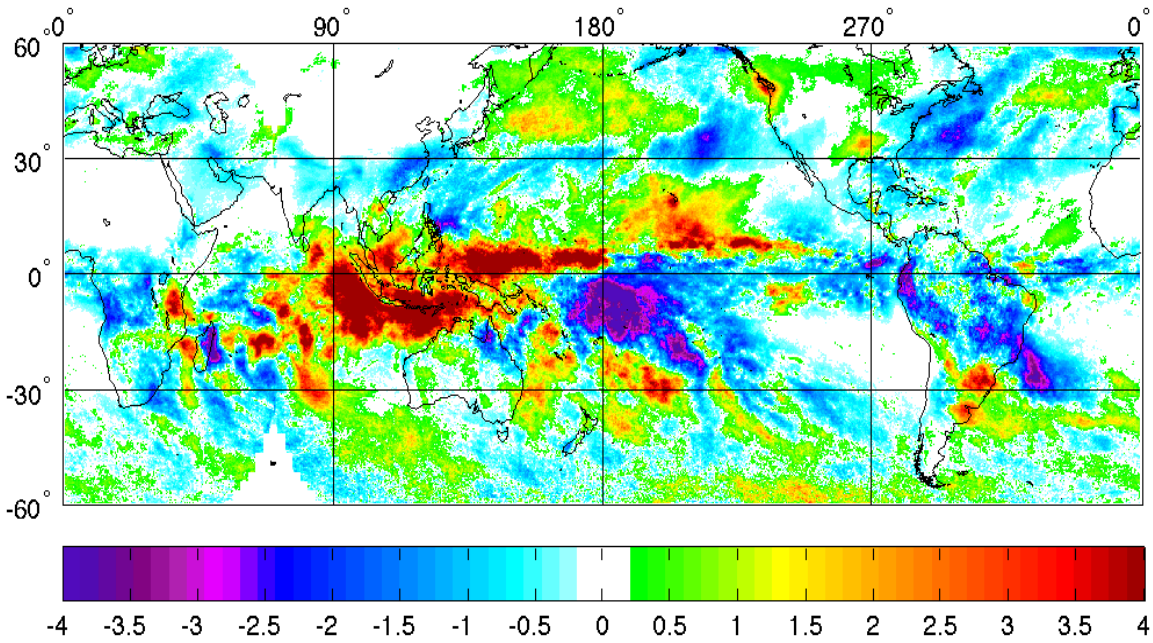

Note the clear similarities between these anomalies and those in the Phase 4 and LN-Phase 4 composites (Figures 31 and 41).

Figure 46. PR Anomalies (mm/day) for MJO Phase 4 and Neutral Years during JFM.

The JFM Neutral-Phase 4 SWHAs (Figure 47) are very similar to those in the Phase 4 case (Figure 32), indicating that the impacts of EN and LN on SWH tend to cancel out each other.

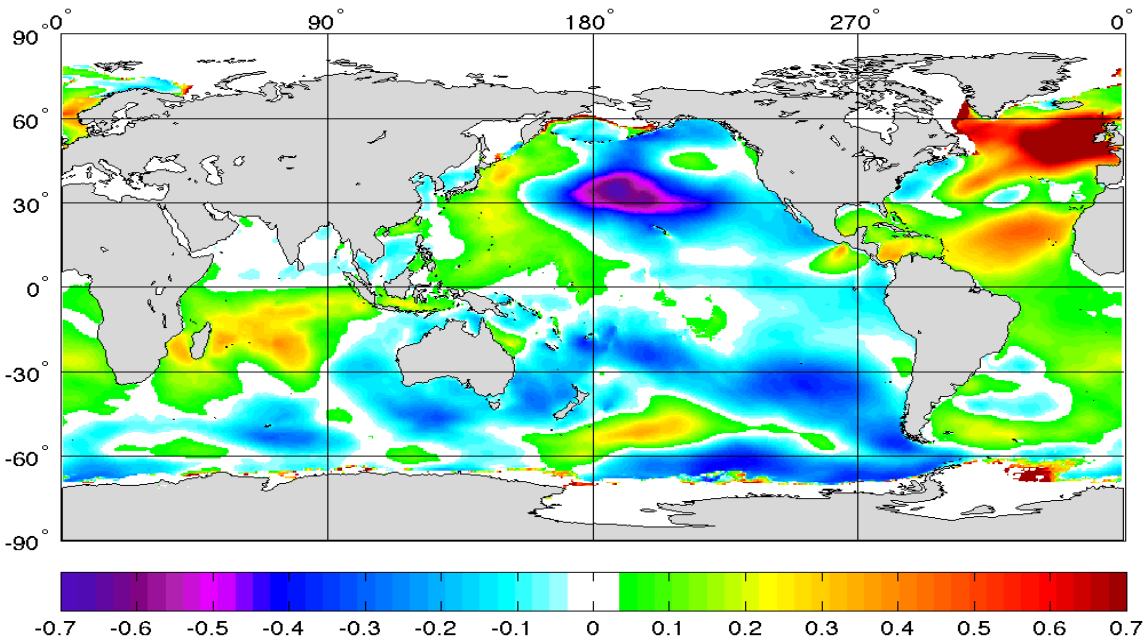

Note the mix of significant wave height anomalies in the tropical Pacific, positive anomalies in the southern Indian Ocean western North Pacific, strong positive anomalies in the midlatitude North Atlantic, and negative anomalies in the central-eastern midlatitude Pacific.

Figure 47. SWH Anomalies (m) for MJO Phase 4 and Neutral Years during JFM.

The results from cases 9–25 (Table 5) are presented in Appendices A-C. The precipitation rate anomalies for southwest Asia shown in Appendix C provide some especially clear evidence of the importance at regional scales of accounting for multiple simultaneous climate variations.

THIS PAGE INTENTIONALLY LEFT BLANK

IV. SUMMARY, CONCLUSIONS, AND RECOMMENDATIONS

We examined the effects of multiple simultaneous climate variations—in particular, the MJO and ENLN. We identified the days during our study period in which different climate variation conditions were met—for example, when MJO phase 4 and LN occurred simultaneously and when MJO phase 8 occurred without EN or LN. We analyzed global and regional climate anomalies for 25 specific conditional cases involving a range of conditions involving: (a) MJO phases 4 and 8; (b) EN, LN, and Neutral conditions; and (c) JFM and JAS (northern winter and summer). Our focus variables were SST, SLP, Z200, PR, and SWH. Our results indicate that the anomalies that are commonly associated with an individual climate variation (EN, LN, or one of the MJO phases) can be substantially different from the anomalies that occur when that climate variations occurs at the same time as another climate variation. In particular, there can be: (a) enhancements and reductions of the individual variation anomalies; and (b) shifts in the patterns and signs of the individual variation anomalies. These conclusions indicate that multiple simultaneous climate variations need to be accounted for in: (a) climate research; (b) in the development of operational climate support products, such as the products provided by the climate division of FNMOC; and (c) the use of climate products in operational planning, such as planning of national security operations and CMSP. The impacts of multiple simultaneous climate variations can be especially pronounced in: (1) areas of interest for national security, such as the Horn of Africa, eastern Mediterranean, southwest Asia, east Asia, and South China Sea; and (2) in the U.S. affiliated Pacific islands, where CMSP is underway.

Our results indicate that FNMOC's ACAF system for developing climate support products would benefit from the ability to account for multiple simultaneous climate variations. This new capability would build on the existing ACAF capability to develop products based on the ENLN state. The new capability should eventually include the ability to account for all major climate variations individually and in multiple combinations. Some of these variations include ENLN, MJO, AO, NAO, and IOD.

The ability to understand and predict the impacts of climate variations at global and regional scales is important to ensure successful planning processes by federal, state, and local agencies, and other organizations. Military planning and planning for humanitarian assistance and disaster relief (HADR) are examples of planning that would benefit from improved predictions of climate variation impacts.

A. RECOMMENDATIONS FOR FUTURE RESEARCH

They are many opportunities to expand this research further and to address a number of additional climate concerns. First, there are six additional MJO phases that were not analyzed in this research. These six phases could be analyzed in a similar fashion and provide further information about the effects of multiple simultaneous climate variations. Second, seasonal variations also affect climate variations and their impacts. Our results show that there are seasonal differences in the impacts of multiple simultaneous climate variations, but we only examined two seasons, JFM and JAS. So we recommend additional research to examine other times of the year. Third, additional atmospheric, oceanic, atmospheric electromagnetic (EM), and ocean acoustic variables should be examined using the approach we applied in our study. From a research perspective, it would be useful to examine OLR and velocity potential, since they are strongly affected by, and used to characterize, the MJO. Tropical cyclone (TC) variables would also be useful to examine, since ENLN and MJO affect TC formations, intensities, and tracks (e.g., Camargo et al. 2007; Johnson 2011; Gottschalck et al. 2016). ENLN and MJO also affect EM ducting in the atmosphere and acoustic ducting in the ocean (Ramsaur 2009; Turek 2008; Heidt 2009; McKeon 2013), so it would be useful to examine EM and acoustic variables (e.g., EM ducting characteristics, acoustic parameters). The undersea warfare operators, for instance, could find the results of such research useful in long range planning (e.g., results concerning sonic layer depth and ambient noise).

We conducted an analysis of the effects on PR in southwest Asia of multiple climate variations (Appendix C). We recommend that additional regional analyses be conducted, since they can reveal impacts from multiple climate variations that are

difficult to identify from global scale analyses. This research would extend both our work and that of Stepanek (2006). This work would be especially useful from an operational perspective, since most operational planning occurs at regional and local scales.

There are a number of climate variations besides ENLN and MJO that should be investigated, such as the AO, NAO, and IOD, to name a few. In addition, combinations of more than two climate variations (e.g., EN, MJO, and AO) should be studied, since such combinations are common.

Finally, research is needed to determine how best to develop and provide to customers information about the effects of multiple simultaneous climate variations. For example, research on how to develop products at different lead times while accounting for the differences in the time scales and predictabilities of different climate variations (e.g., longer time scales for ENLN than for MJO, more skill at long lead forecasts of EN and LN events, once they have started, than for MJO events once they have started). These differences are likely to impact the products that are produced at different lead times prior to the start of operations and could introduce variations in forecasts as lead times decrease that are problematic for customers planning (e.g., forecasts that are weighted toward EN or LN impacts at longer lead times but then shift toward a greater MJO weighting as lead times decrease).

THIS PAGE INTENTIONALLY LEFT BLANK

APPENDIX A. JFM PHASE 8 RESULTS

A. CASE 9: CHARACTERISTIC JFM PHASE 8 ANOMALIES

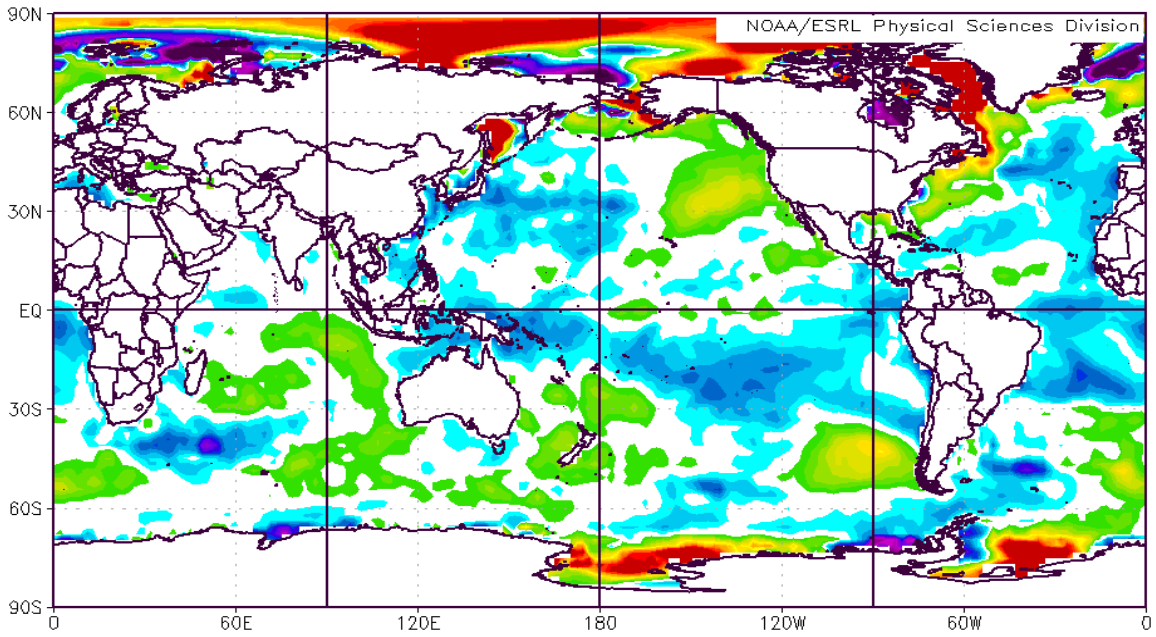

Figure 48. SST Anomalies (°C) for MJO Phase 8 and all EN, LN, and Neutral Years during JFM.

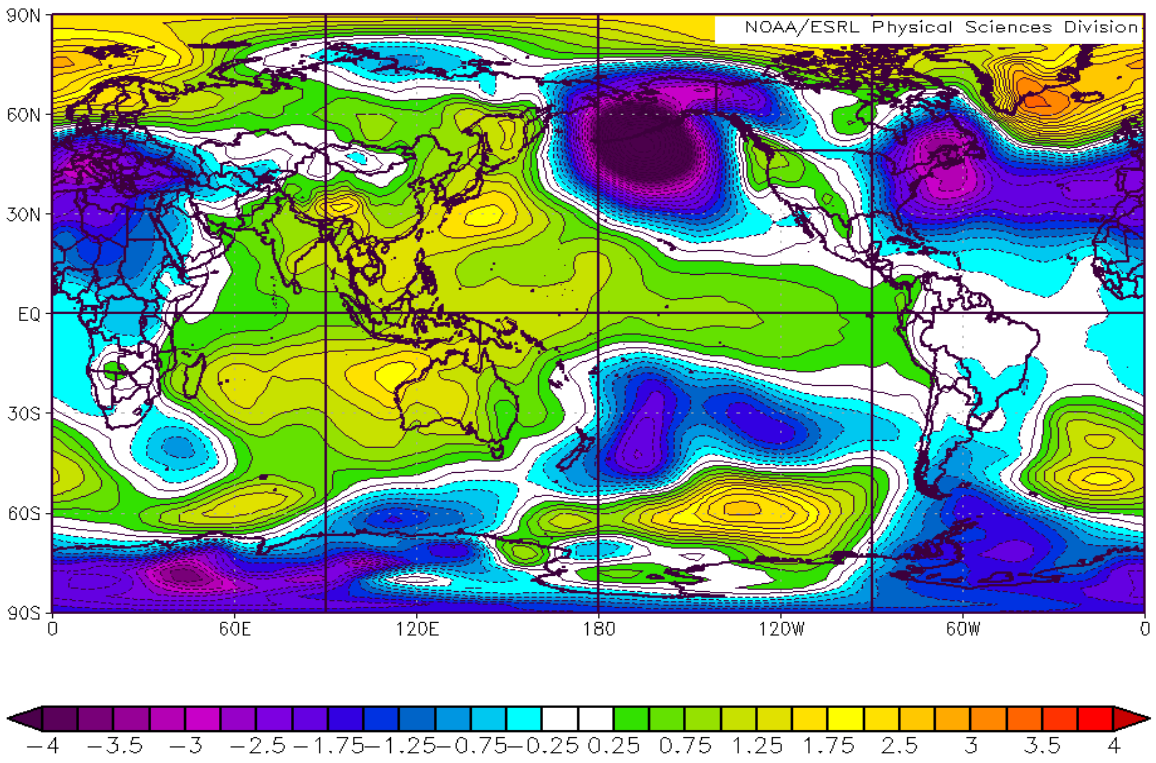

Figure 49. SLP Anomalies (mb) for MJO Phase 8 and all EN, LN, and Neutral Years during JFM.

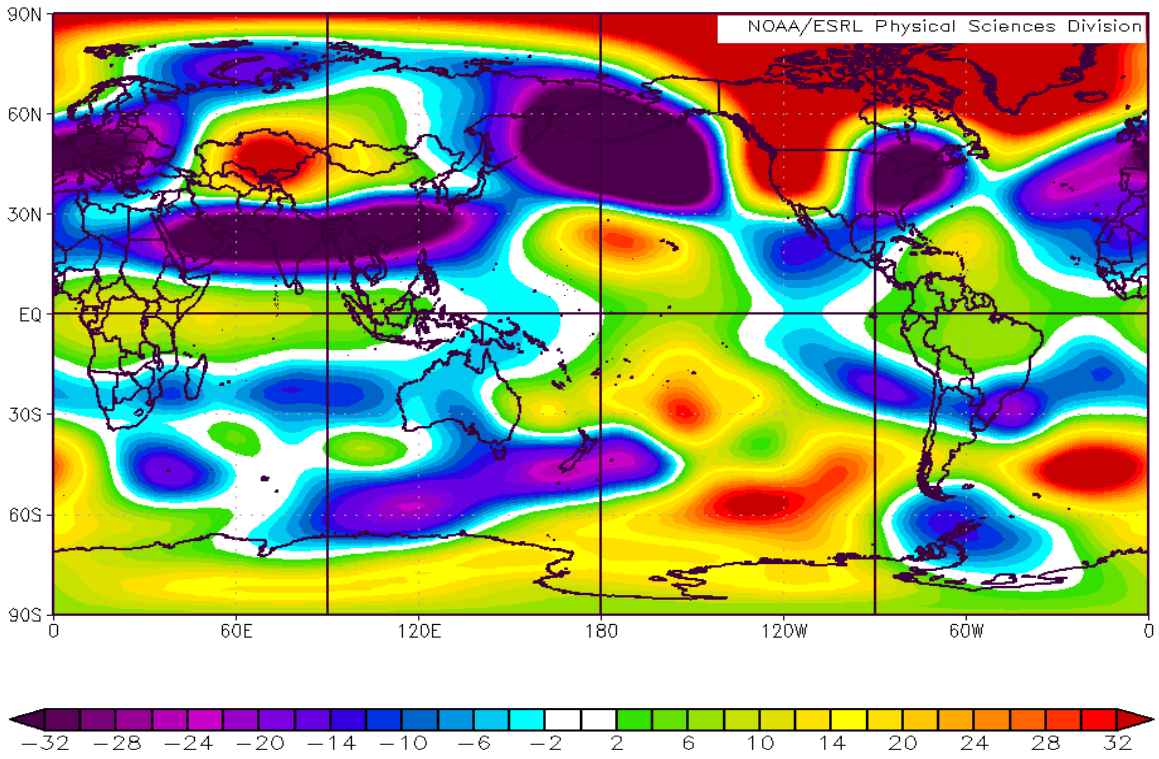

Figure 50. Z200 Anomalies (mb) for MJO Phase 8 and all EN, LN, and Neutral Years during JFM.

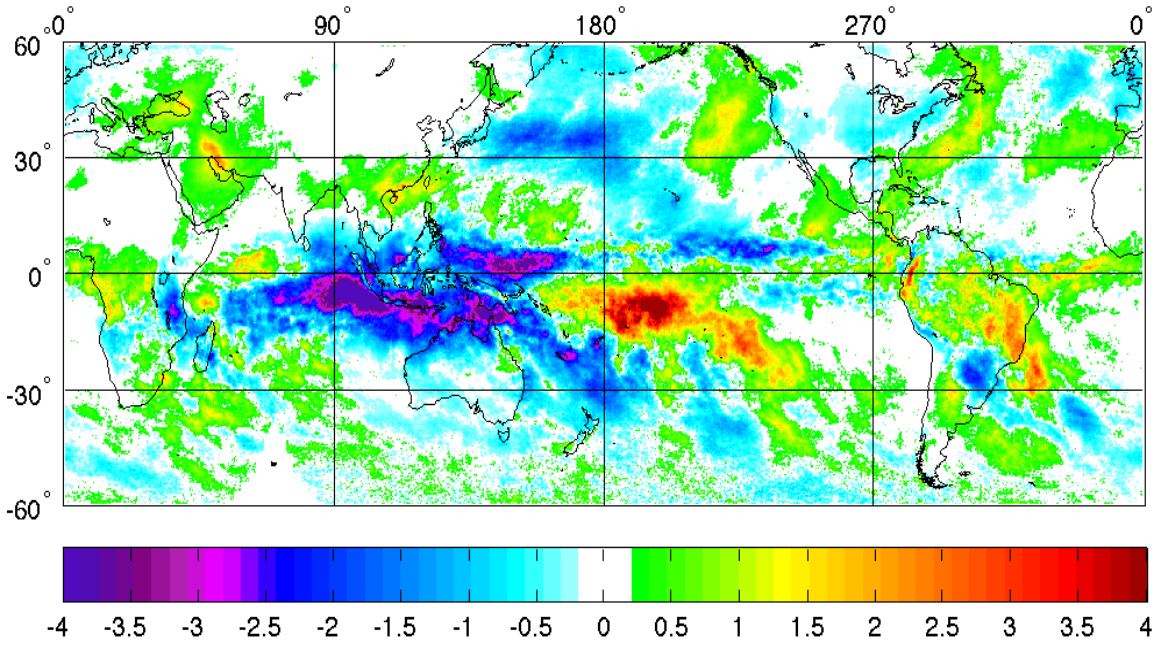

Figure 51. PR Anomalies (mm/day) for MJO Phase 8 and all EN, LN, and Neutral Years during JFM.

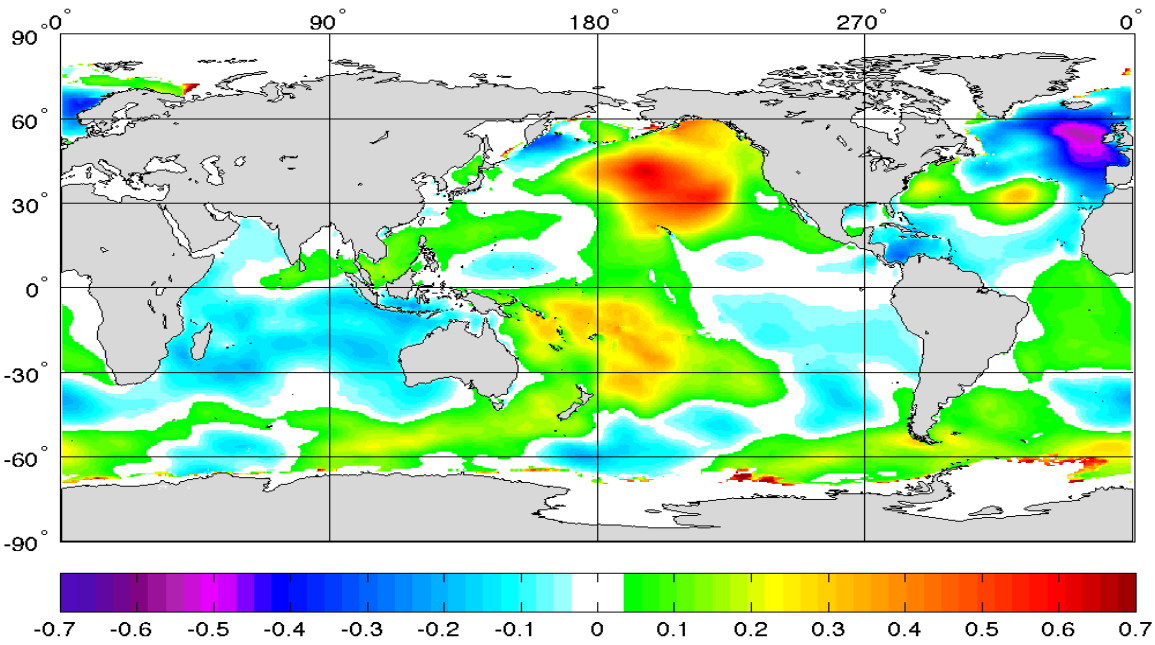

Figure 52. SWH Anomalies (m) for MJO Phase 8 and all EN, LN, and Neutral Years during JFM.

B. CASE 10: CHARACTERISTIC JFM EN PHASE 8 ANOMALIES

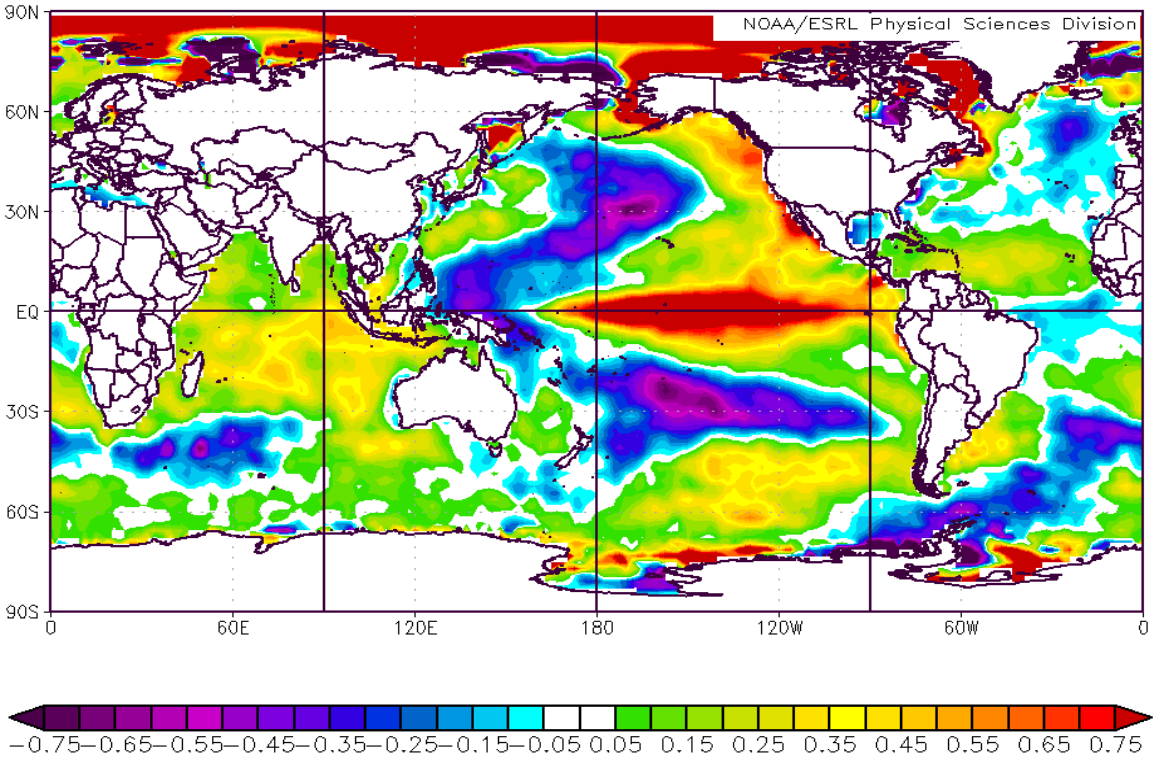

Figure 53. SST Anomalies (°C) for MJO Phase 8 and EN Years during JFM.

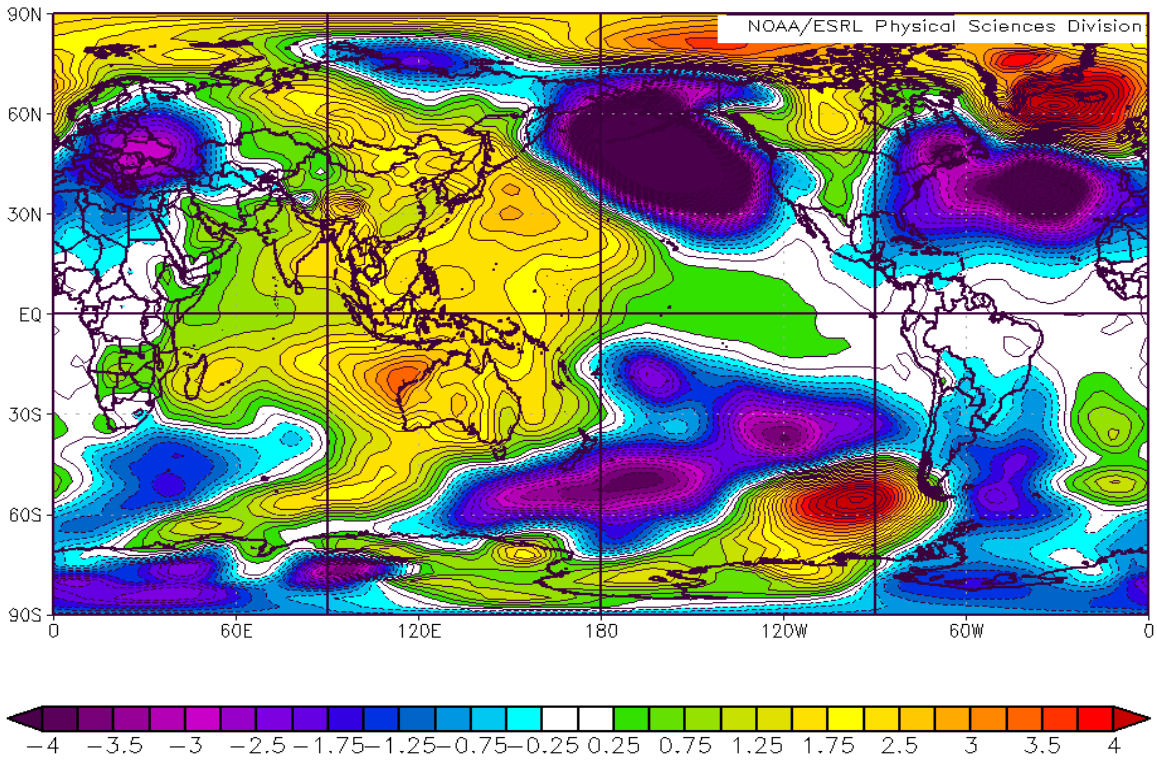

Figure 54. SLP Anomalies (mb) for MJO Phase 8 and EN Years during JFM.

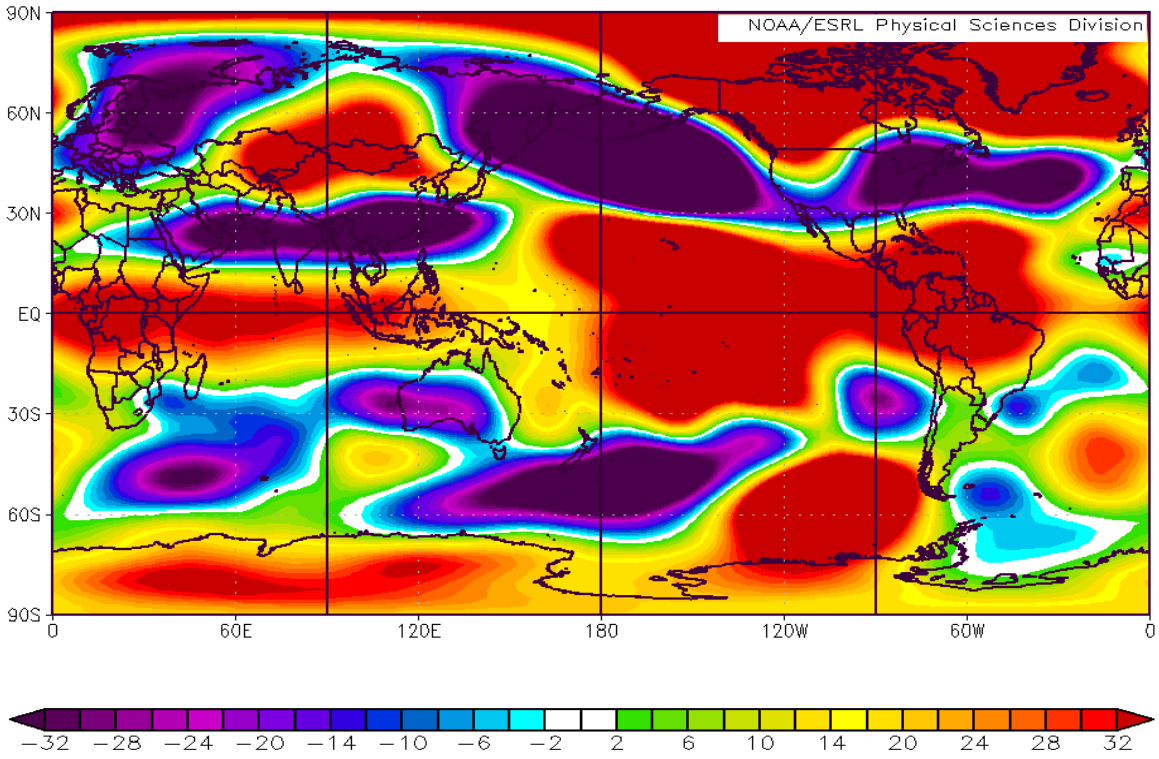

Figure 55. Z200 Anomalies (mb) for MJO Phase 8 and EN Years during JFM.

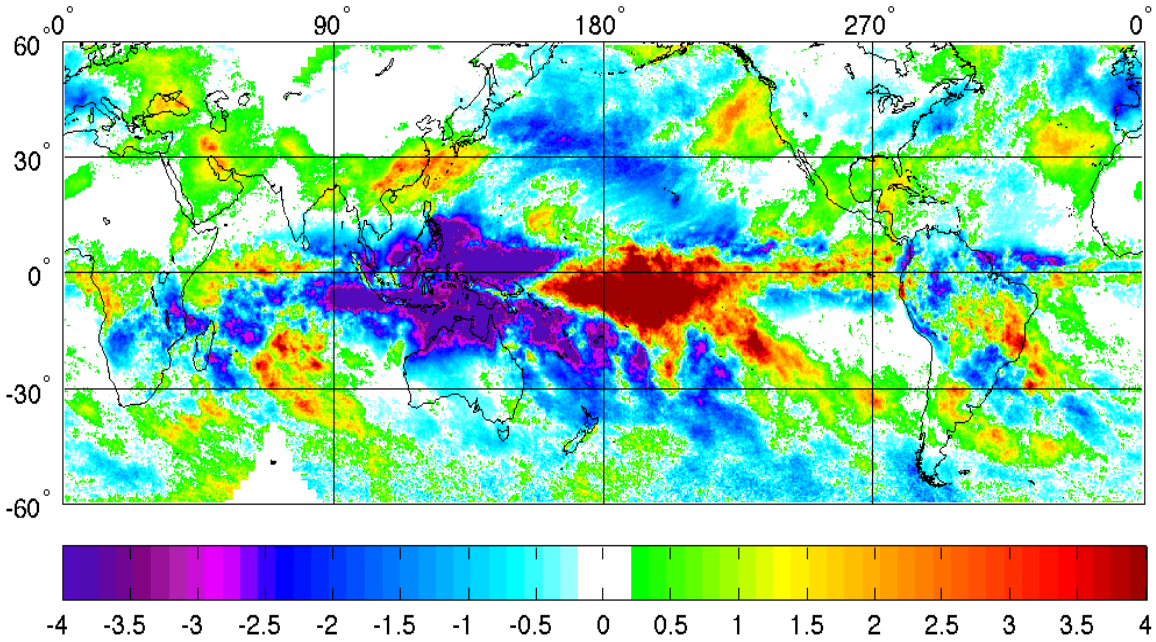

Figure 56. PR Anomalies (mm/day) for MJO Phase 8 and EN Years during JFM.

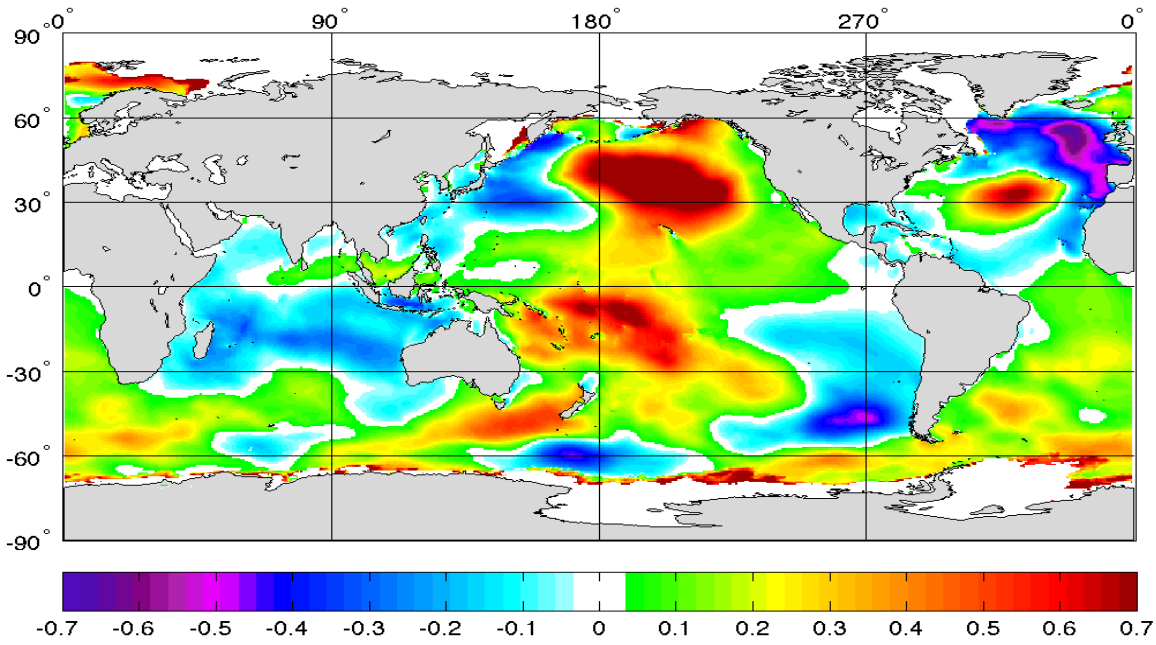

Figure 57. SWH Anomalies (m) for MJO Phase 8 and EN Years during JFM.

C. CASE 11: CHARACTERISTIC JFM LN PHASE 8 ANOMALIES

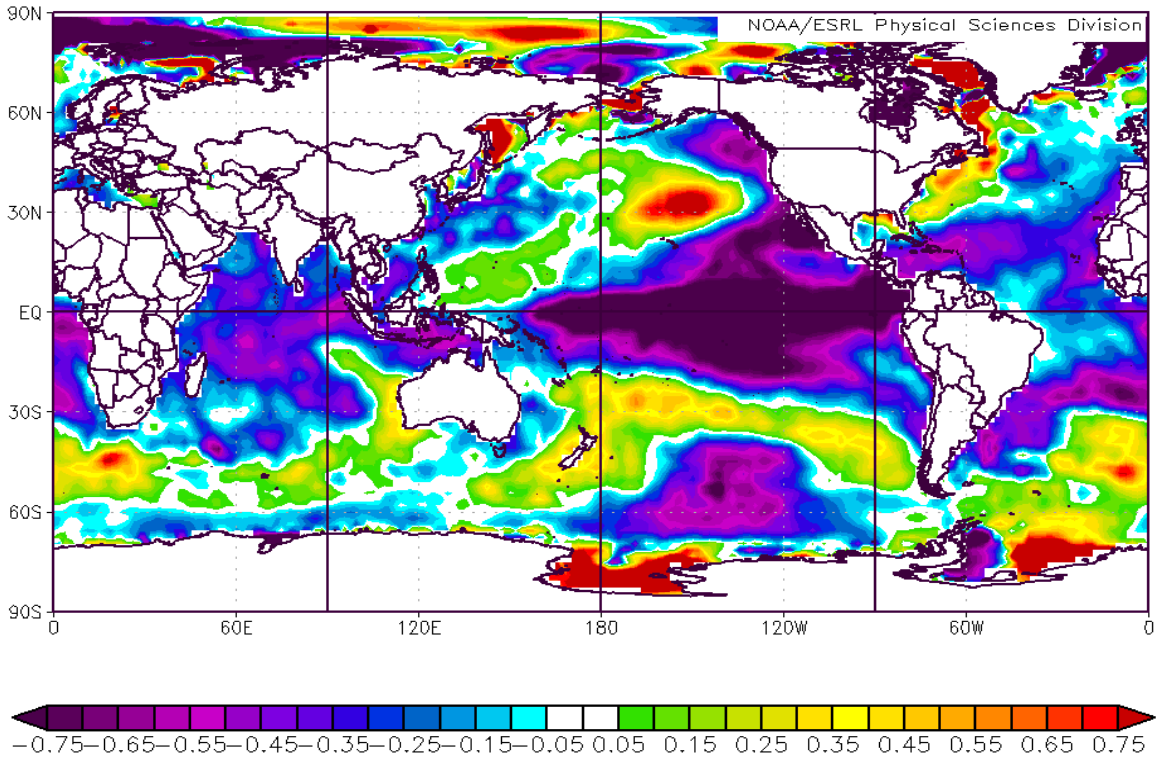

Figure 58. SST Anomalies (°C) for MJO Phase 8 and LN Years during JFM.

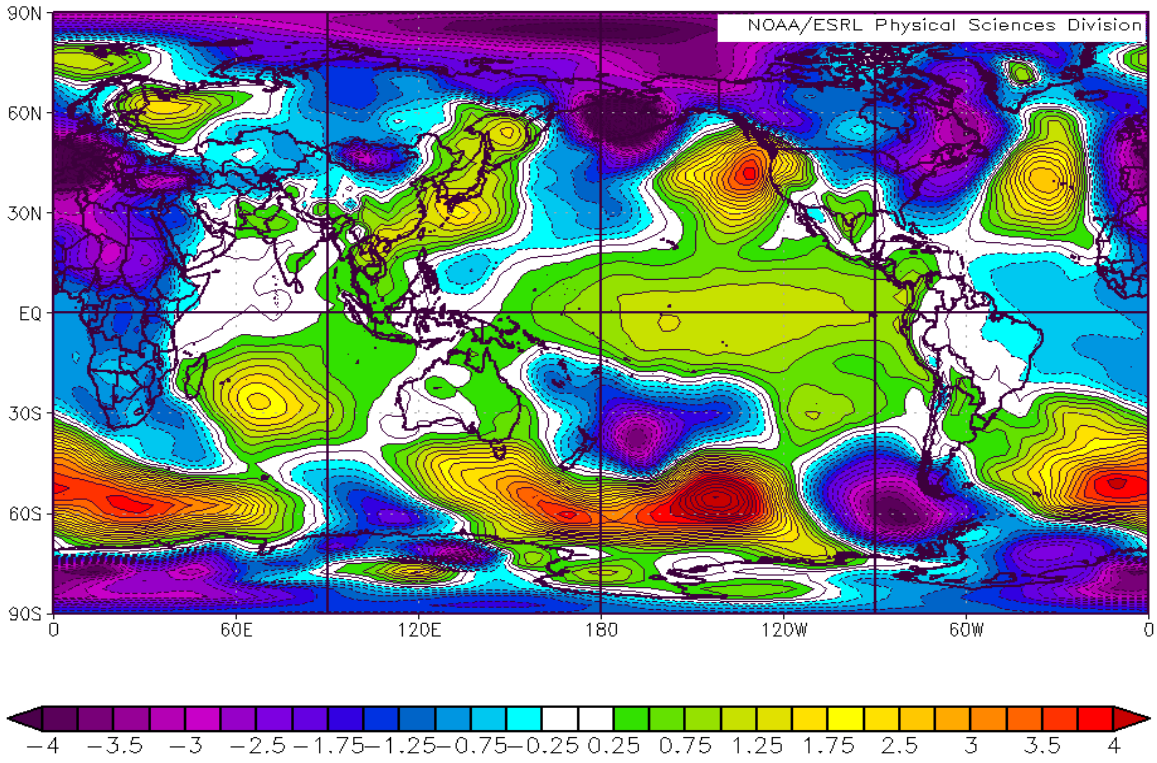

Figure 59. SLP Anomalies (mb) for MJO Phase 8 and LN Years during JFM.

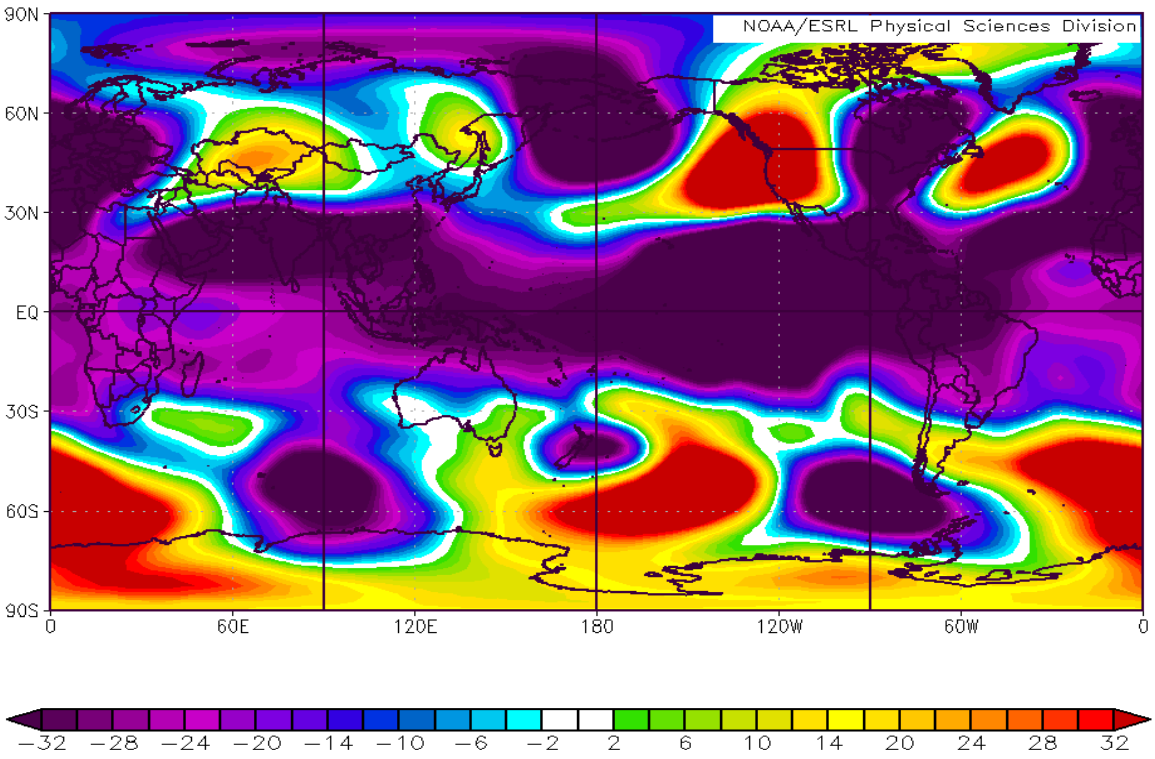

Figure 60. Z200 Anomalies (mb) for MJO Phase 8 and LN Years during JFM.

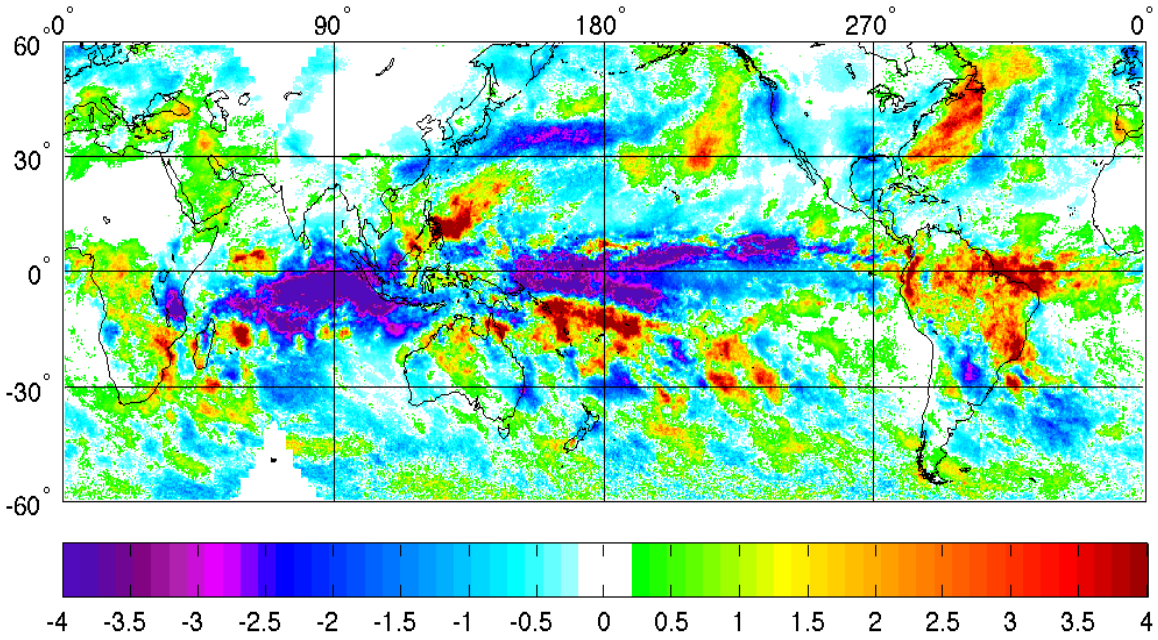

Figure 61. PR Anomalies (mm/day) for MJO Phase 8 and LN Years during JFM.

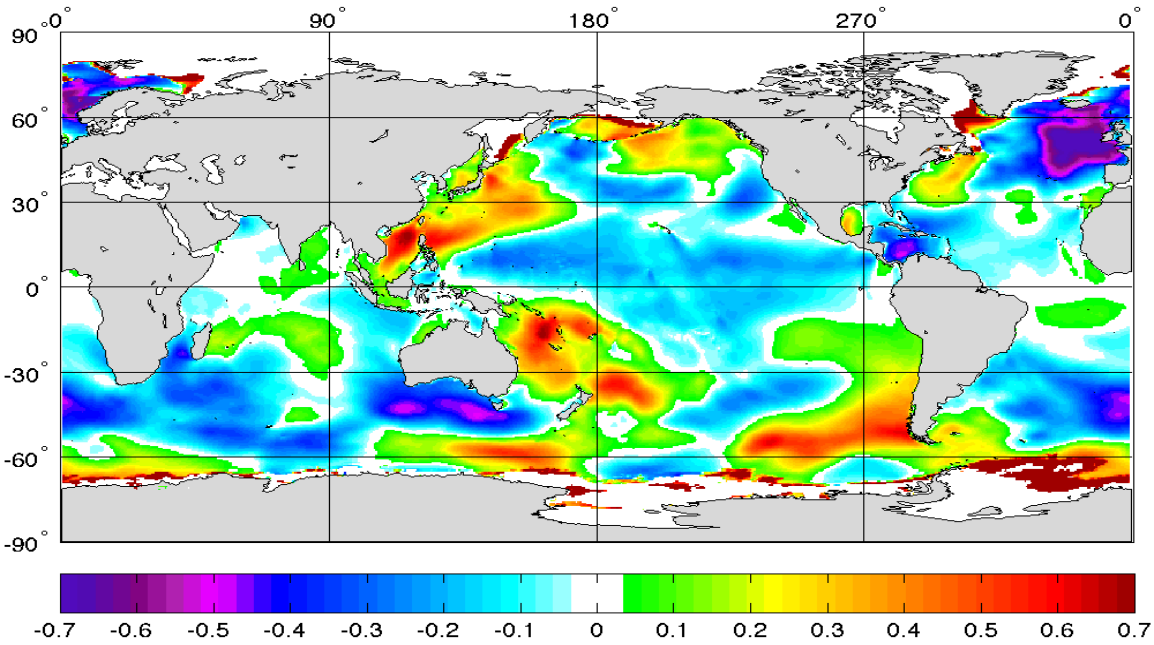

Figure 62. SWH Anomalies (m) for MJO Phase 8 and LN Years during JFM.

D. CASE 12: CHARACTERISTIC JFM NEUTRAL PHASE 8 ANOMALIES

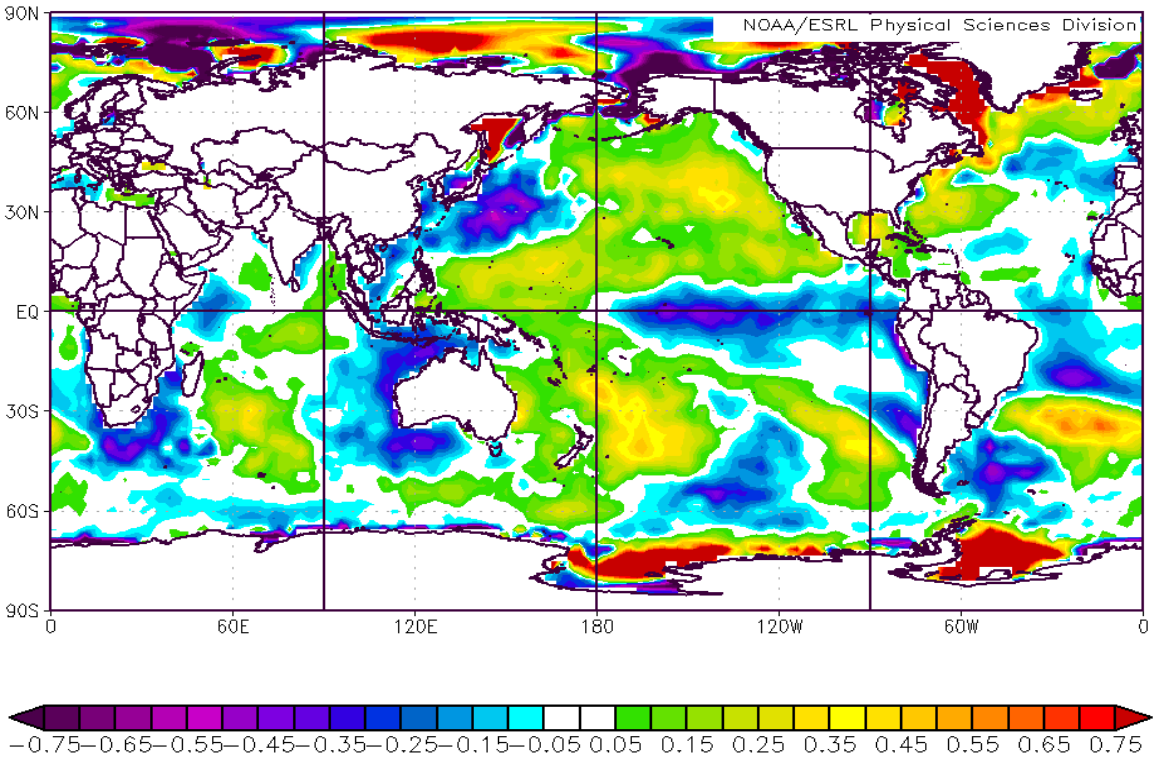

Figure 63. SST Anomalies (°C) for MJO Phase 8 and Neutral Years during JFM.

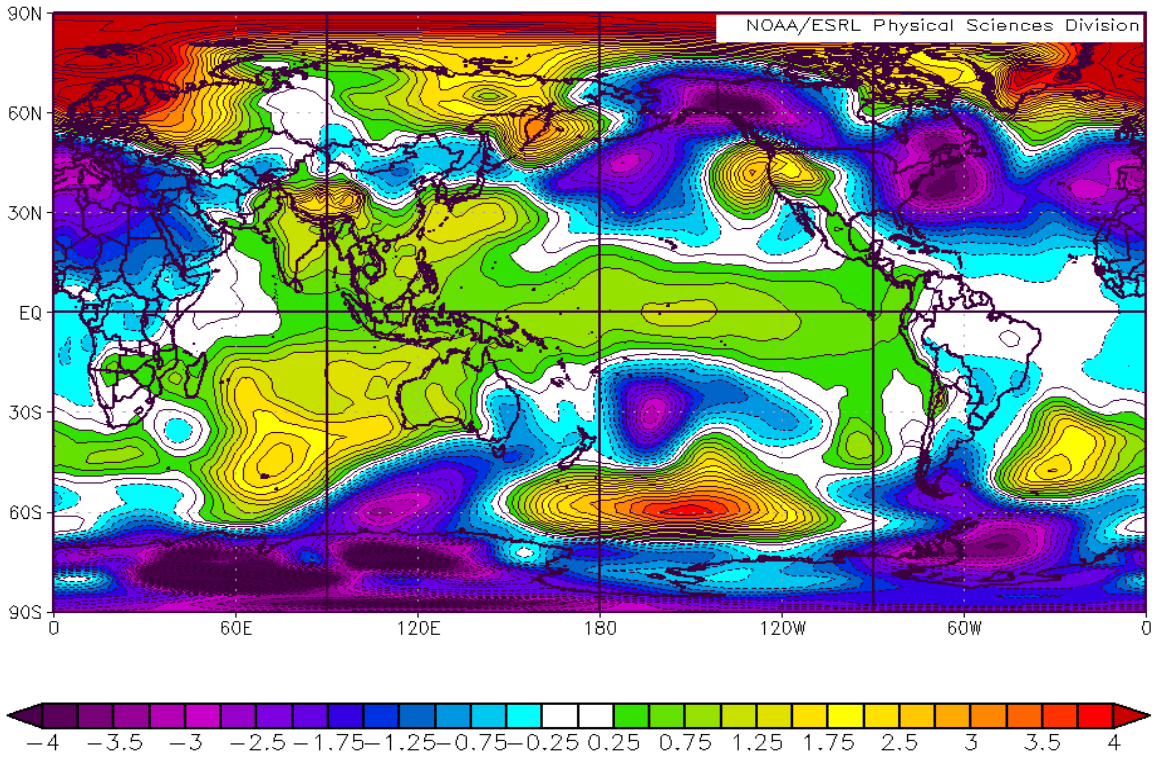

Figure 64. SLP Anomalies (mb) for MJO Phase 8 and Neutral Years during JFM.

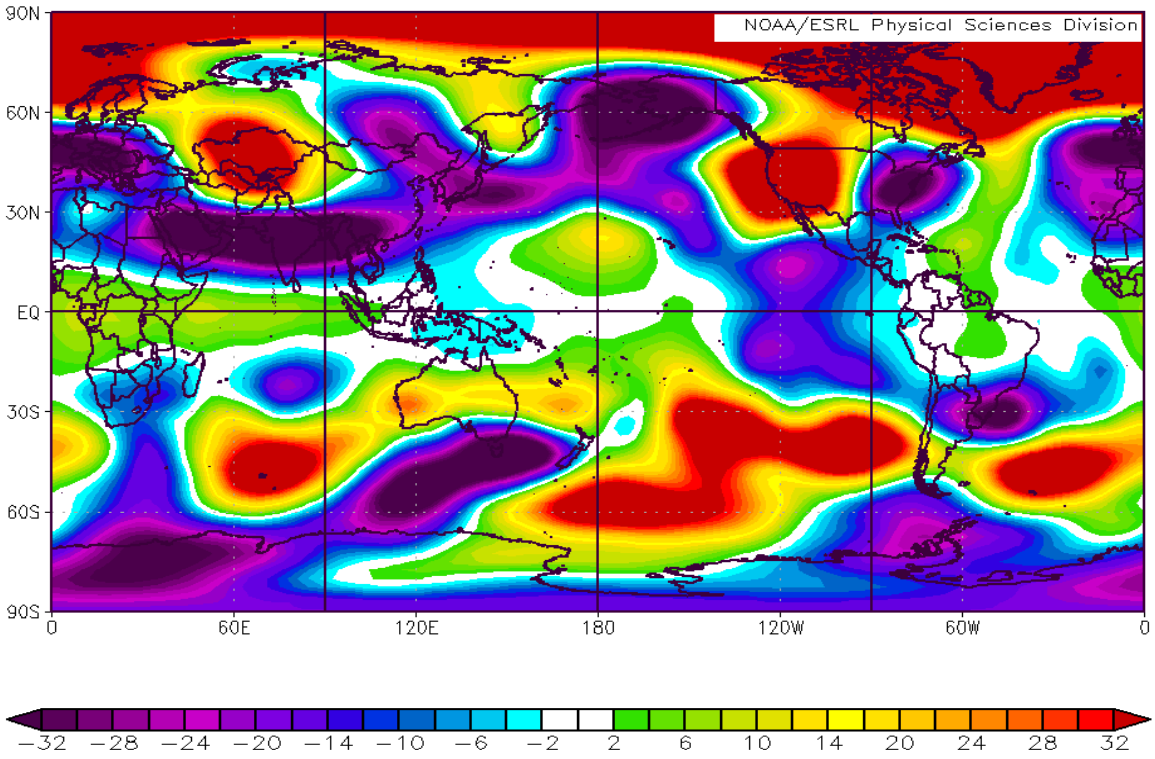

Figure 65. Z200 Anomalies (mb) for MJO Phase 8 and Neutral Years during JFM.

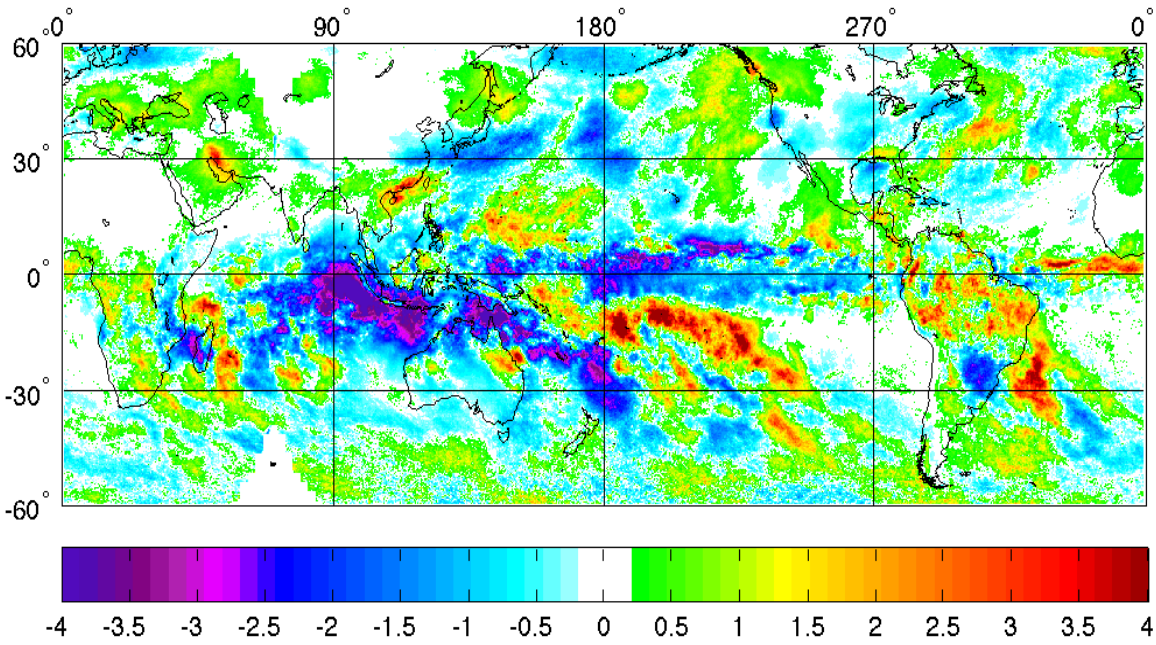

Figure 66. PR Anomalies (mm/day) for MJO Phase 8 and Neutral Years during JFM.

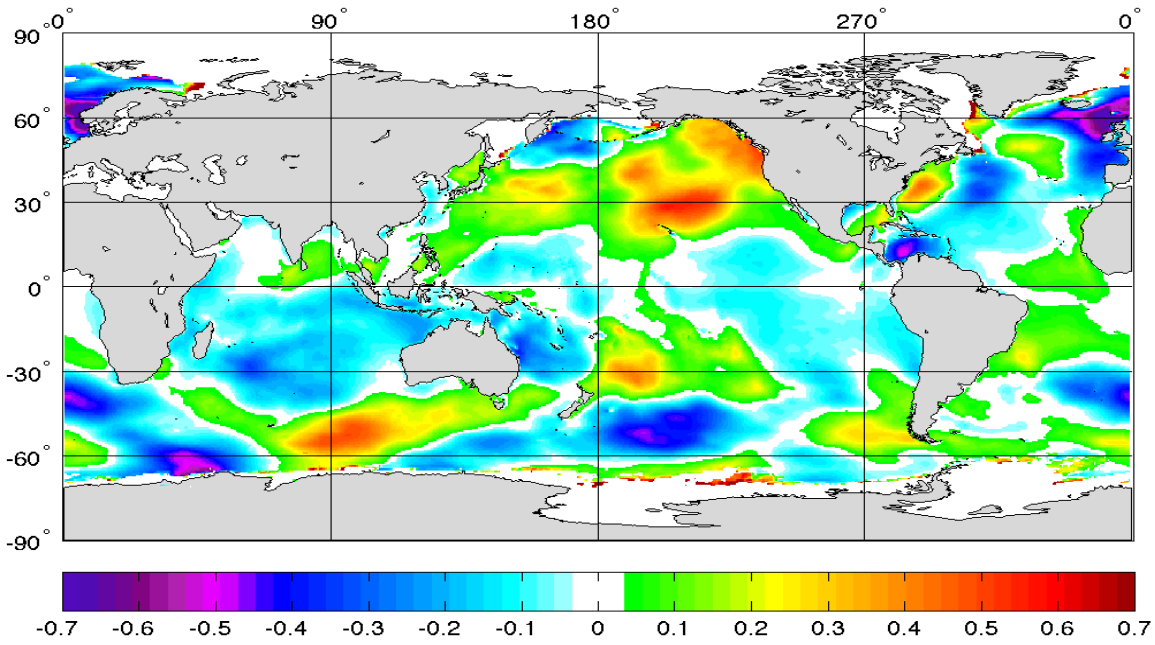

Figure 67. SWH Anomalies (m) for MJO Phase 8 and Neutral Years during JFM.

APPENDIX B. JAS RESULTS

A. CASE 13: CHARACTERISTIC JAS LONG TERM MEANS

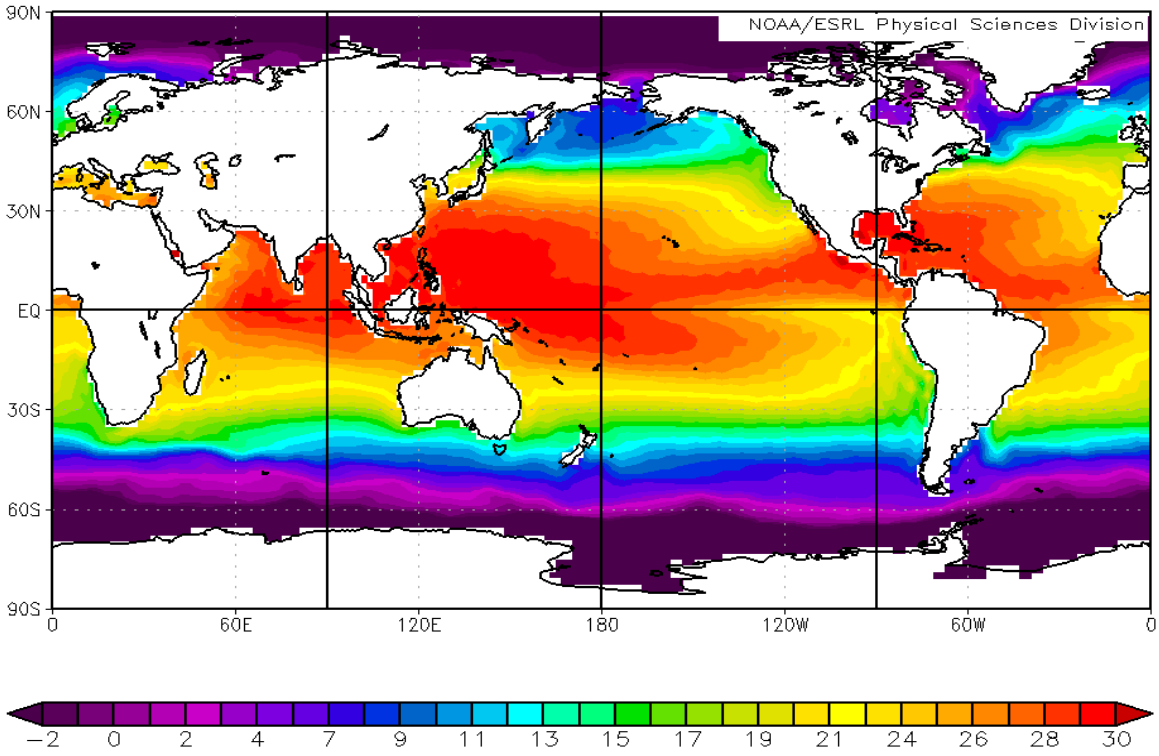

Figure 68. LTM Sea Surface Temperature (SST; °C) for JAS.

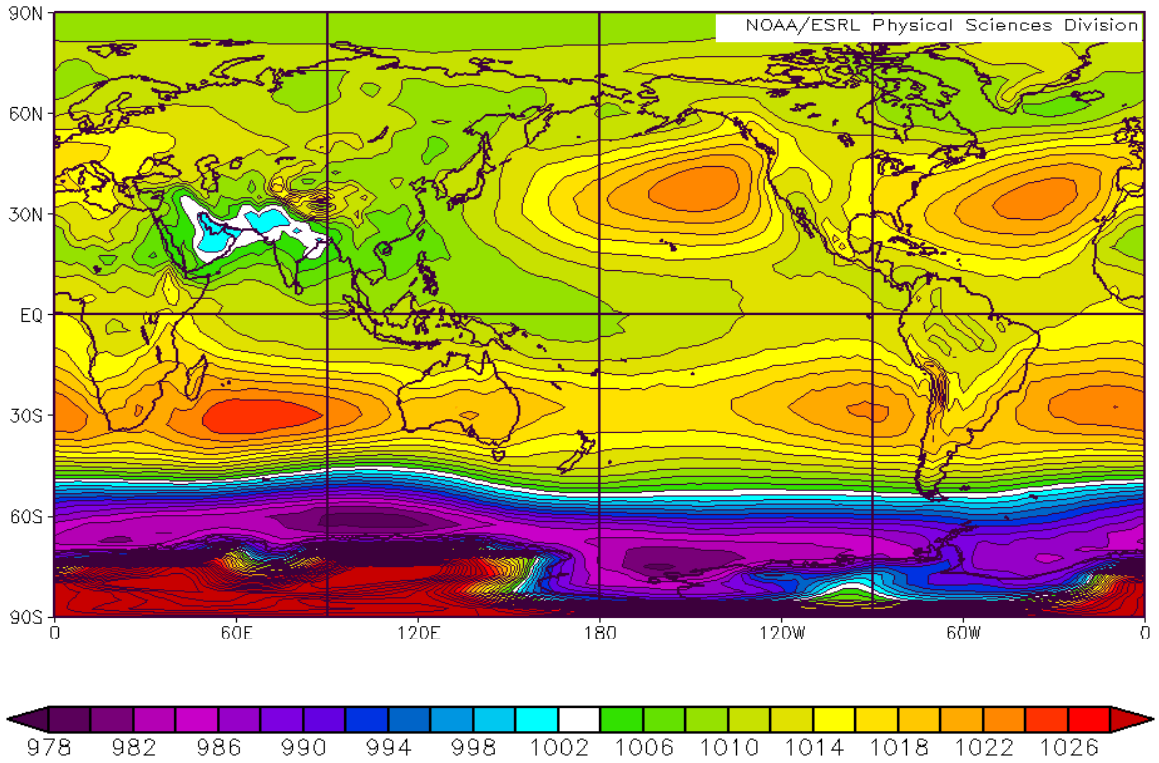

Figure 69. LTM Sea Level Pressure (SLP; mb) for JAS.

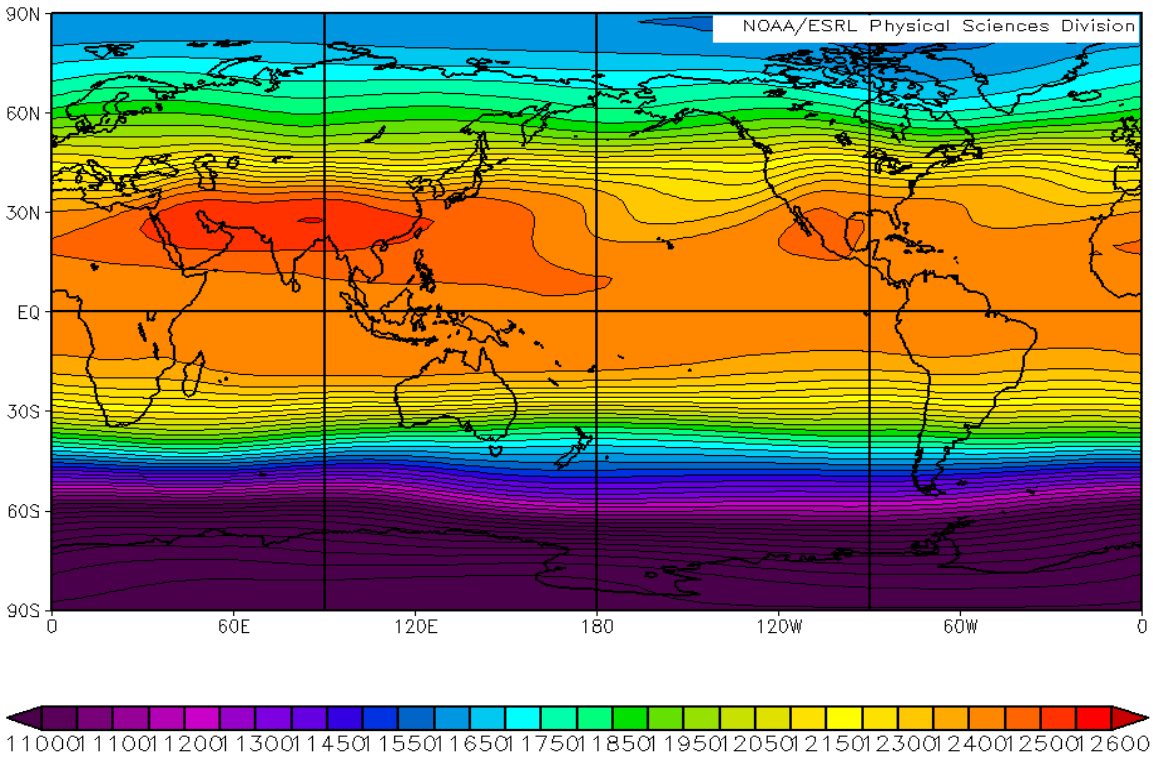

Figure 70. LTM 200 mb Geopotential Height (Z200; m) for JAS.

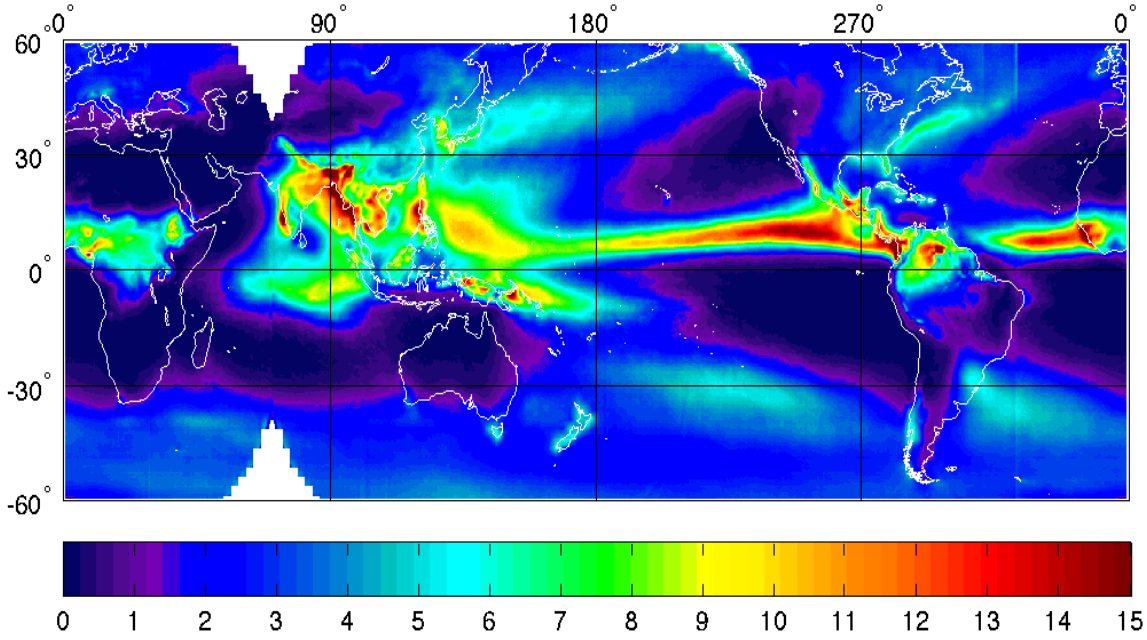

Figure 71. LTM Precipitation Rate (PR; mm/day) for JAS.

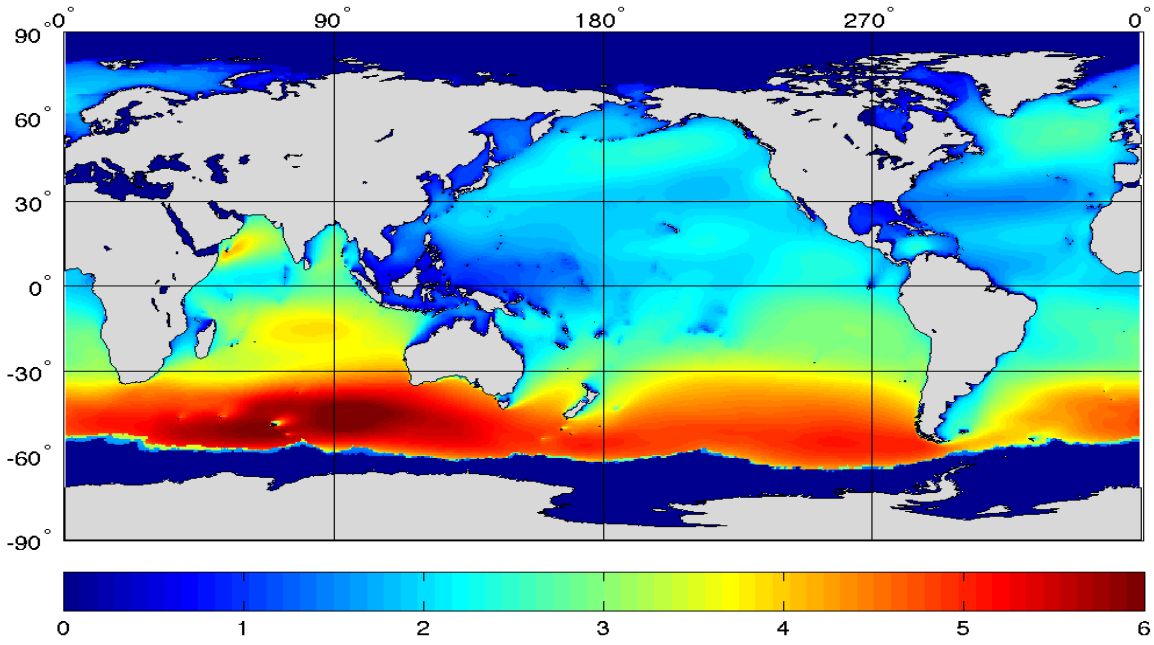

Figure 72. LTM Significant Wave Height (SWH; m) for JAS.

B. CASE 14: CHARACTERISTIC JAS EN ANOMALIES

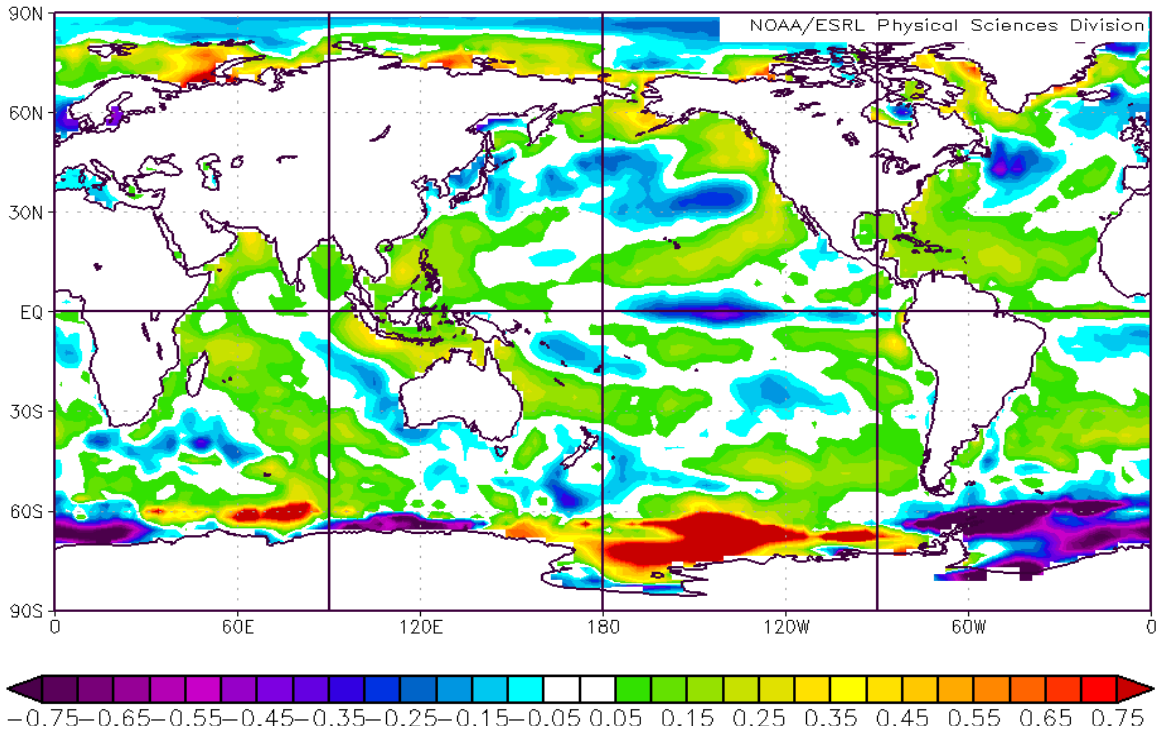

Figure 73. SST Anomalies (°C) for EN Years during JAS.

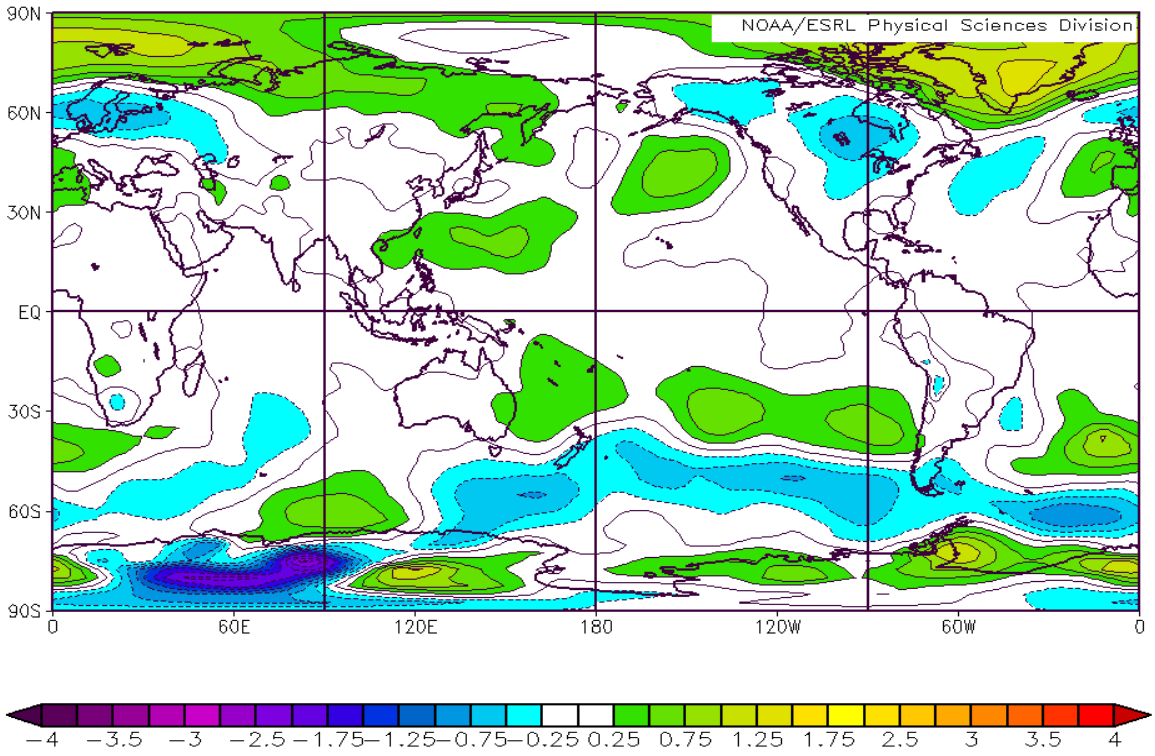

Figure 74. SLP Anomalies (mb) for EN Years during JAS.

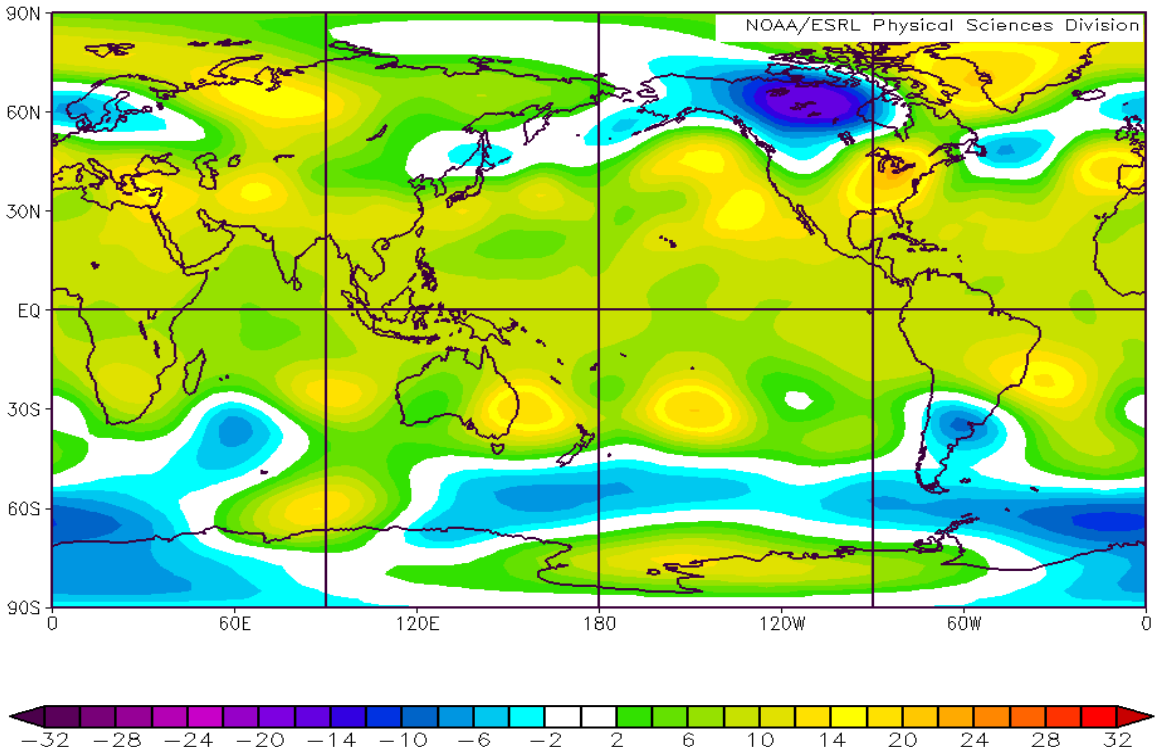

Figure 75. Z200 Anomalies (m) for EN Years during JAS.

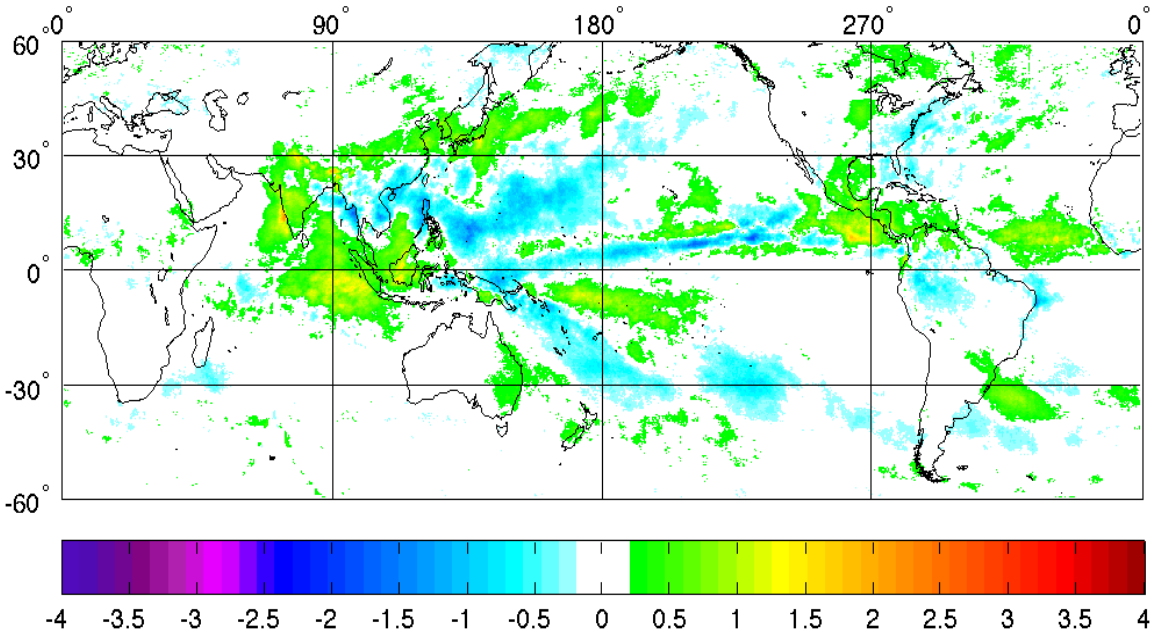

Figure 76. PR Anomalies (mm/day) for EN Years during JAS.

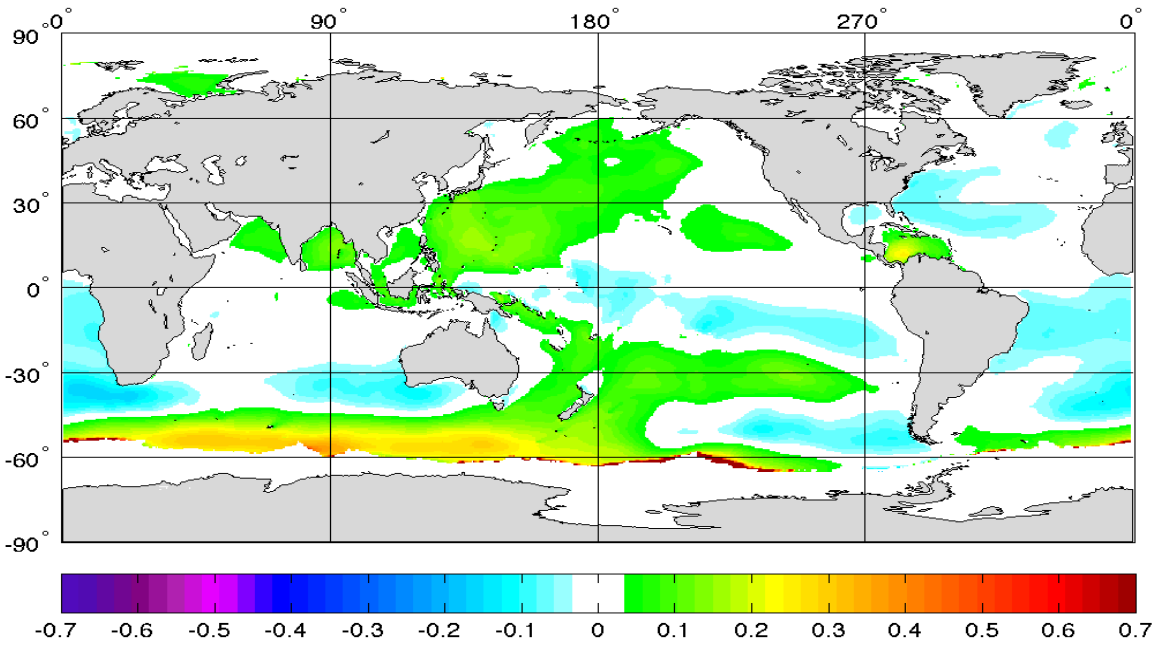

Figure 77. SWH Anomalies (m) for EN Years during JAS.

C. CASE 15: CHARACTERISTIC JAS LN ANOMALIES

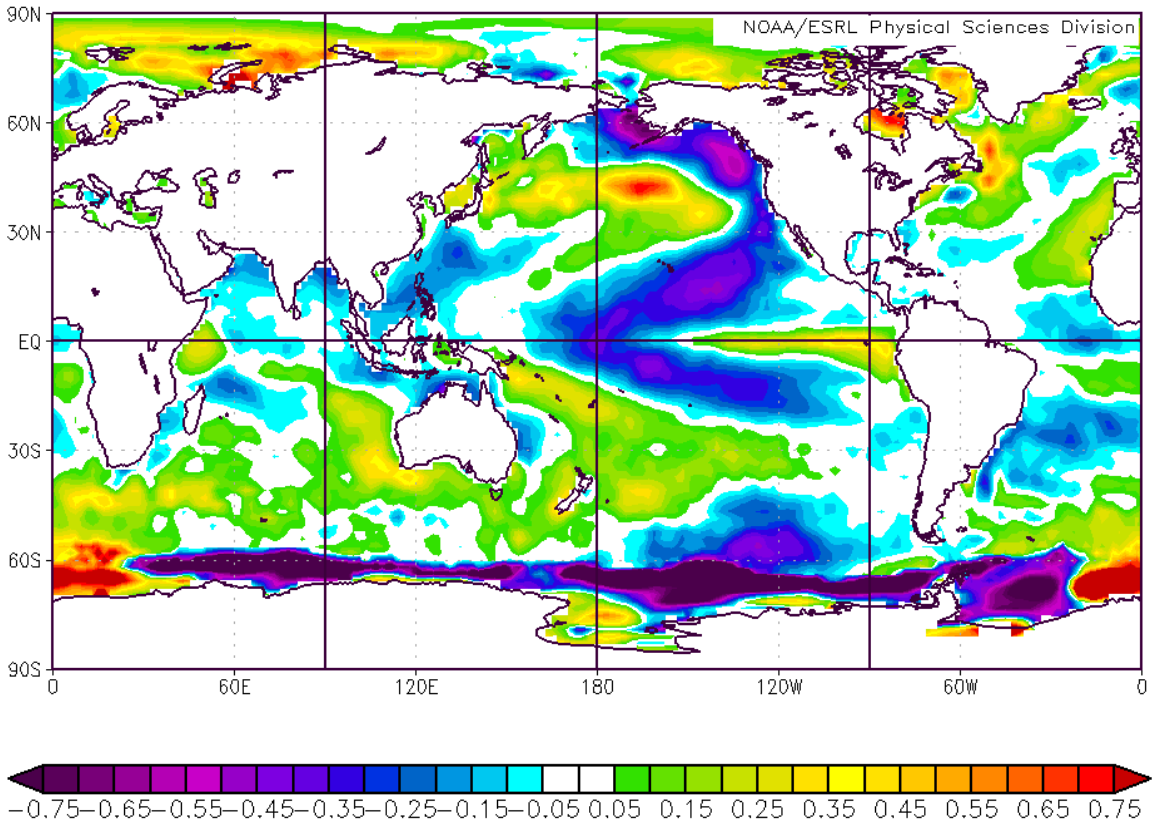

Figure 78. SST Anomalies (°C) for LN Years during JAS.

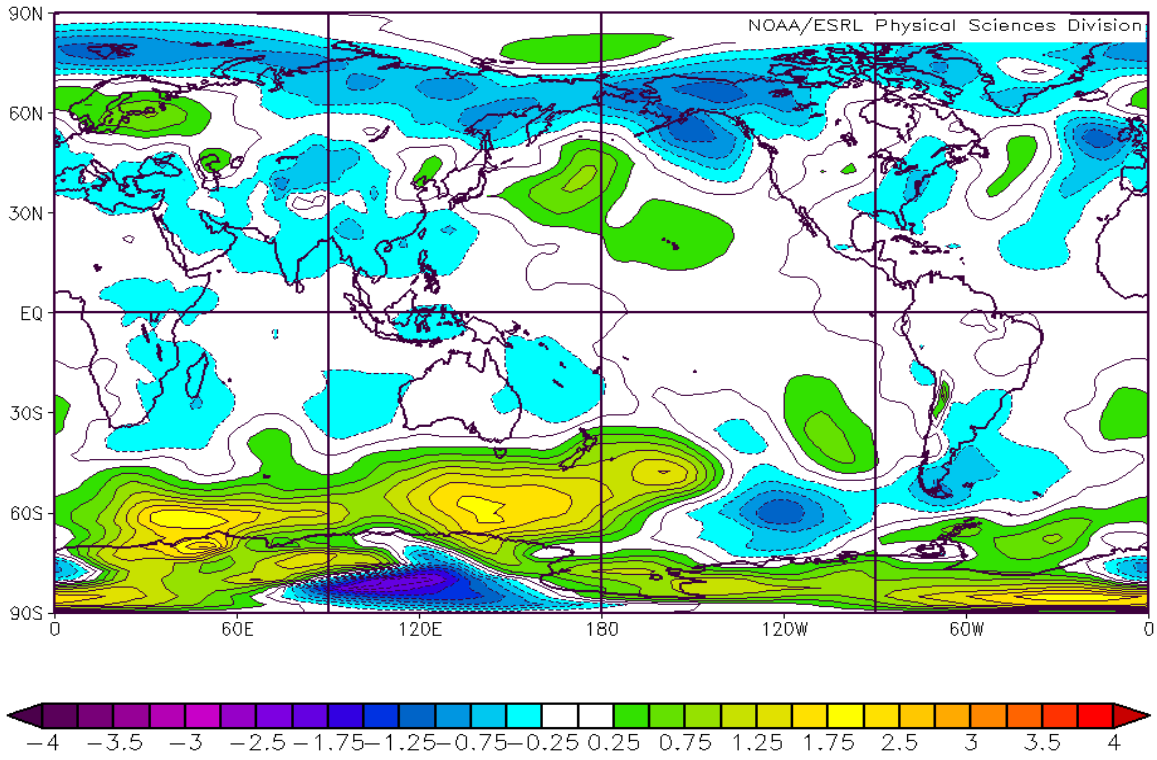

Figure 79. SLP Anomalies (mb) for LN Years during JAS.

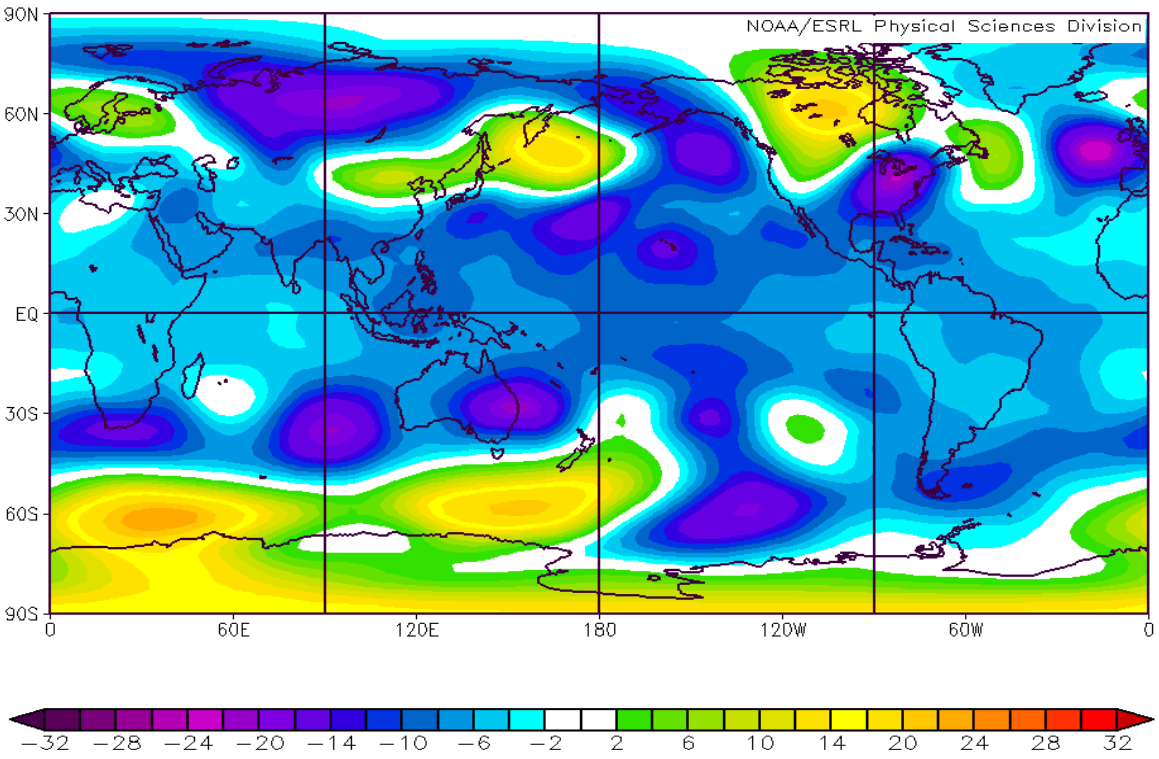

Figure 80. Z200 Anomalies (m) for LN Years during JAS.

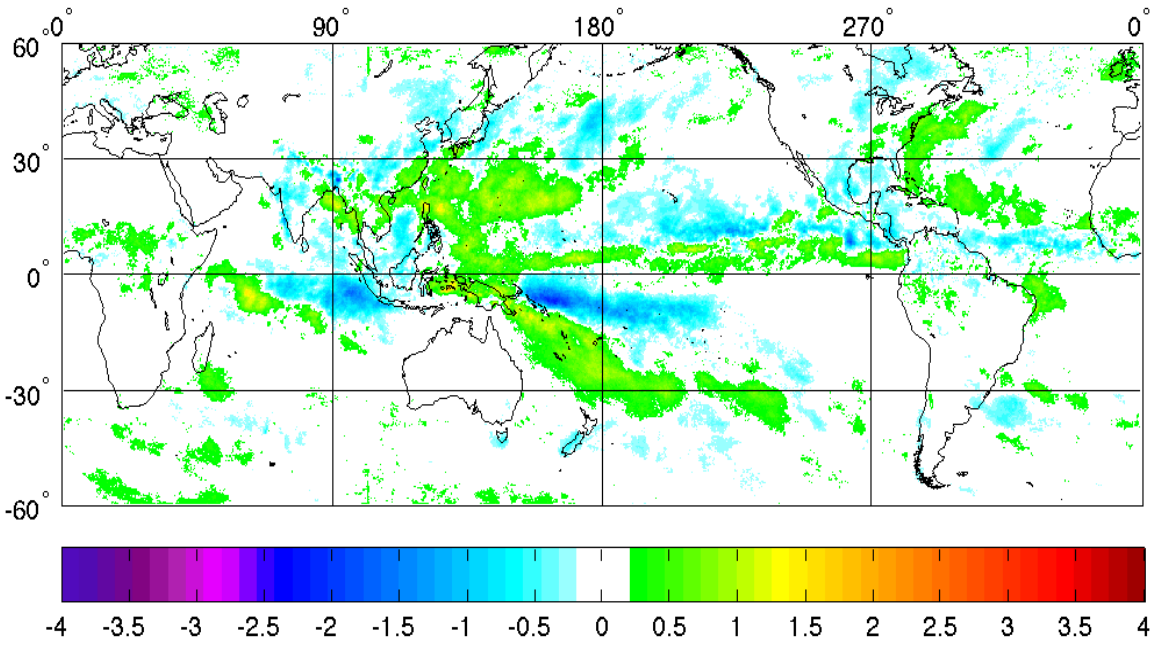

Figure 81. PR Anomalies (mm/day) for LN Years during JAS.

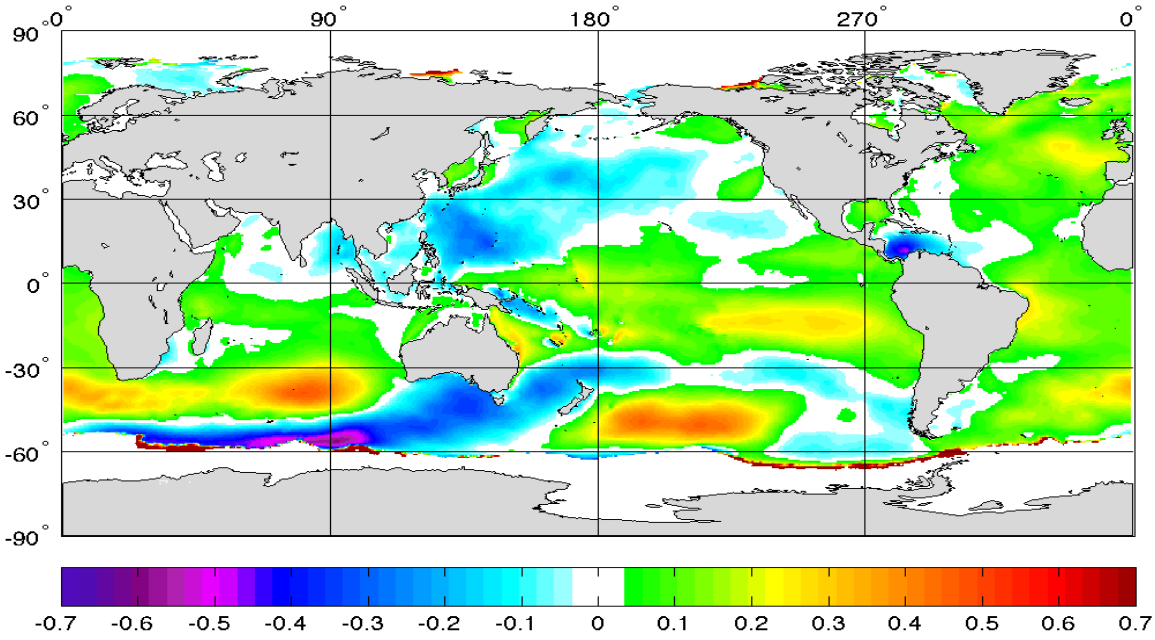

Figure 82. SWH Anomalies (m) for LN Years during JAS.

D. CASE 16: CHARACTERISTIC JAS NEUTRAL ANOMALIES

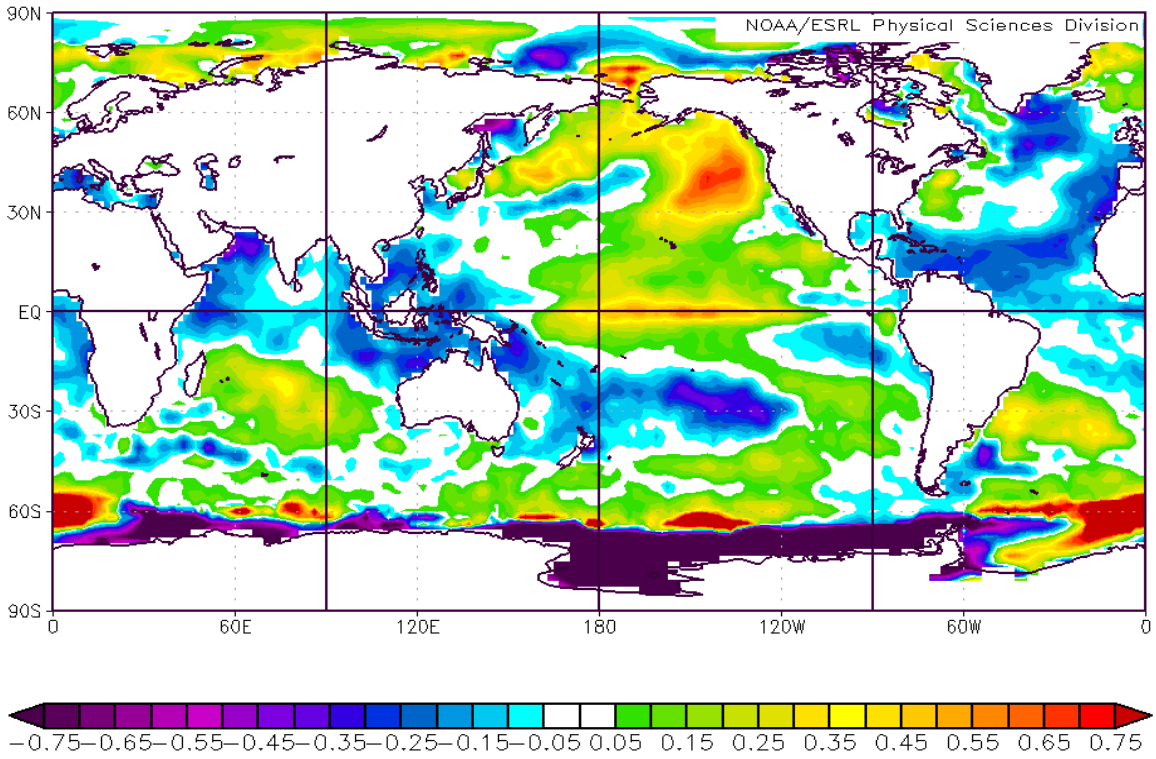

Figure 83. SST Anomalies (°C) for Neutral Years during JAS.

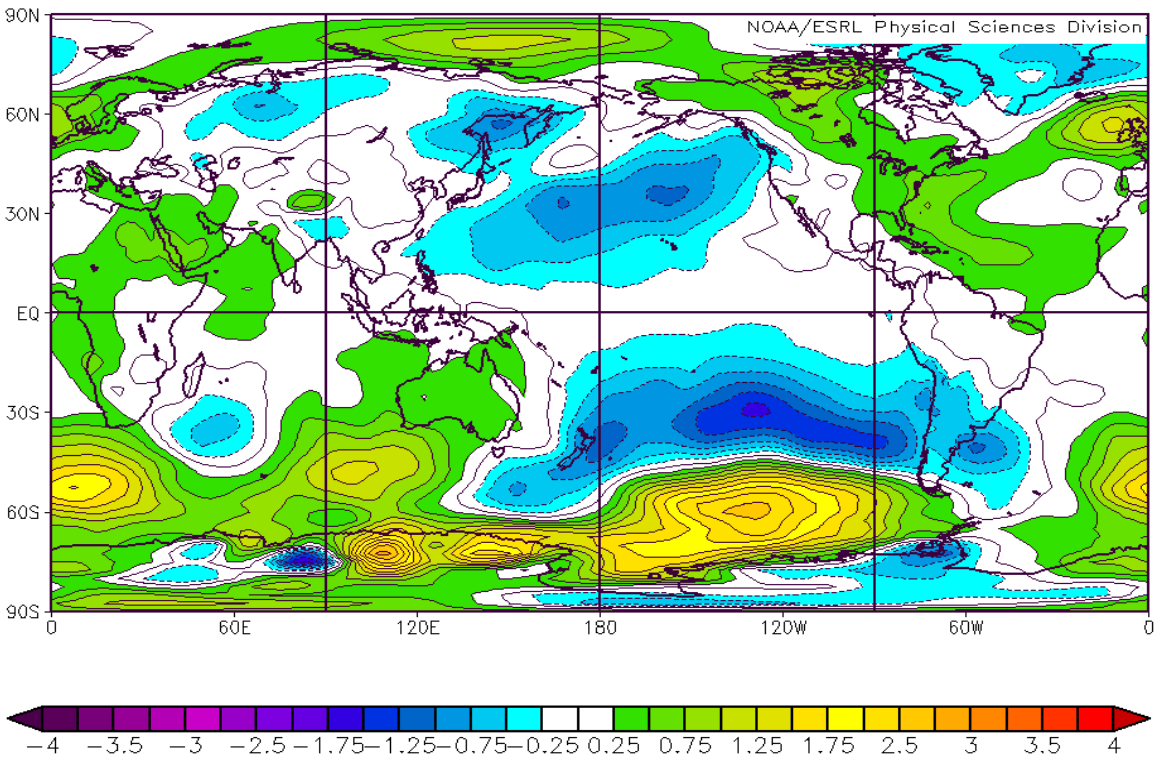

Figure 84. SLP Anomalies (mb) for Neutral Years during JAS.

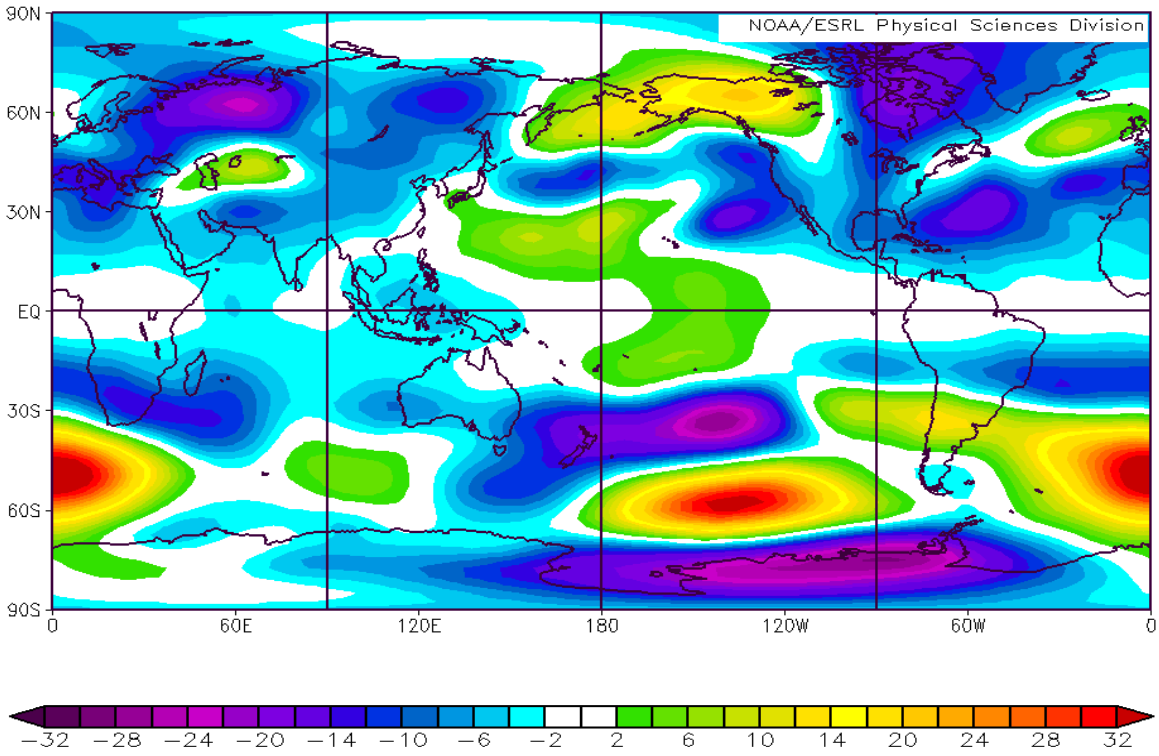

Figure 85. Z200 Anomalies (m) for Neutral Years during JAS.

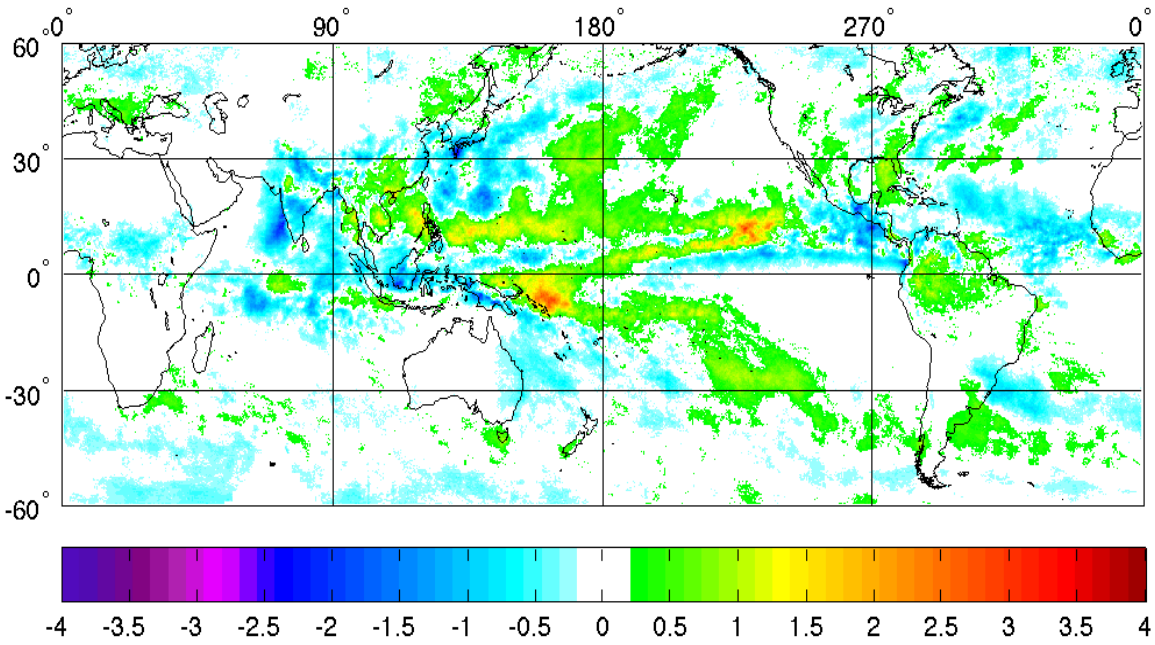

Figure 86. PR Anomalies (mm/day) for Neutral Years during JAS.

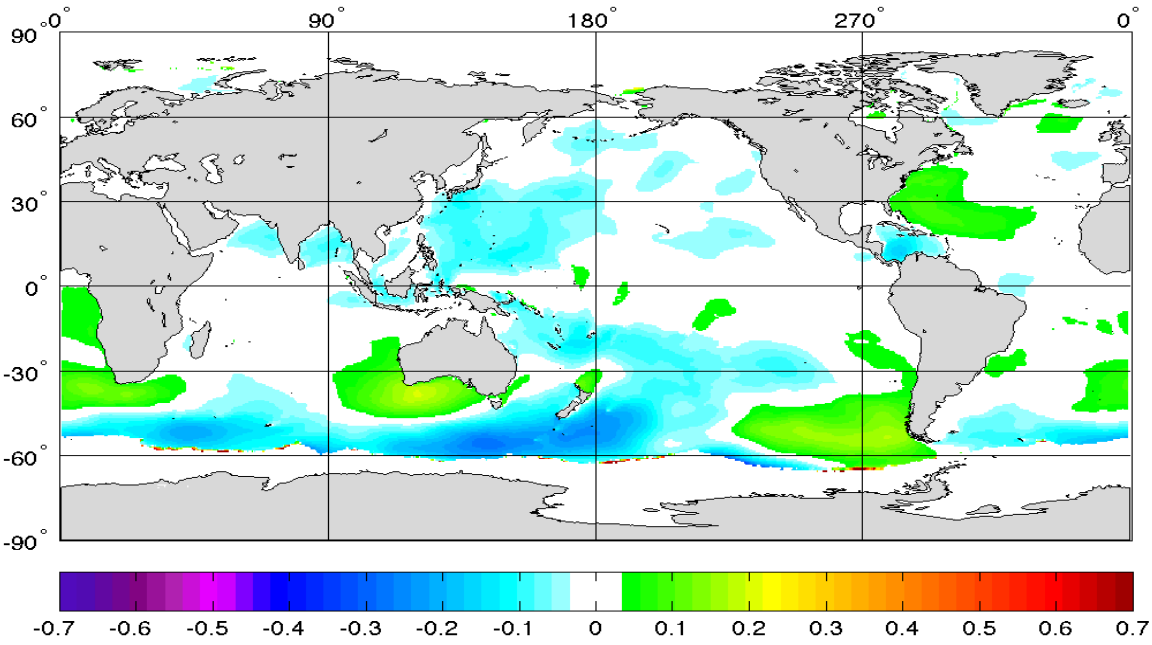

Figure 87. SWH Anomalies (m) for Neutral Years during JAS.

E. CASE 17: CHARACTERISTIC JAS PHASE 4 ANOMALIES

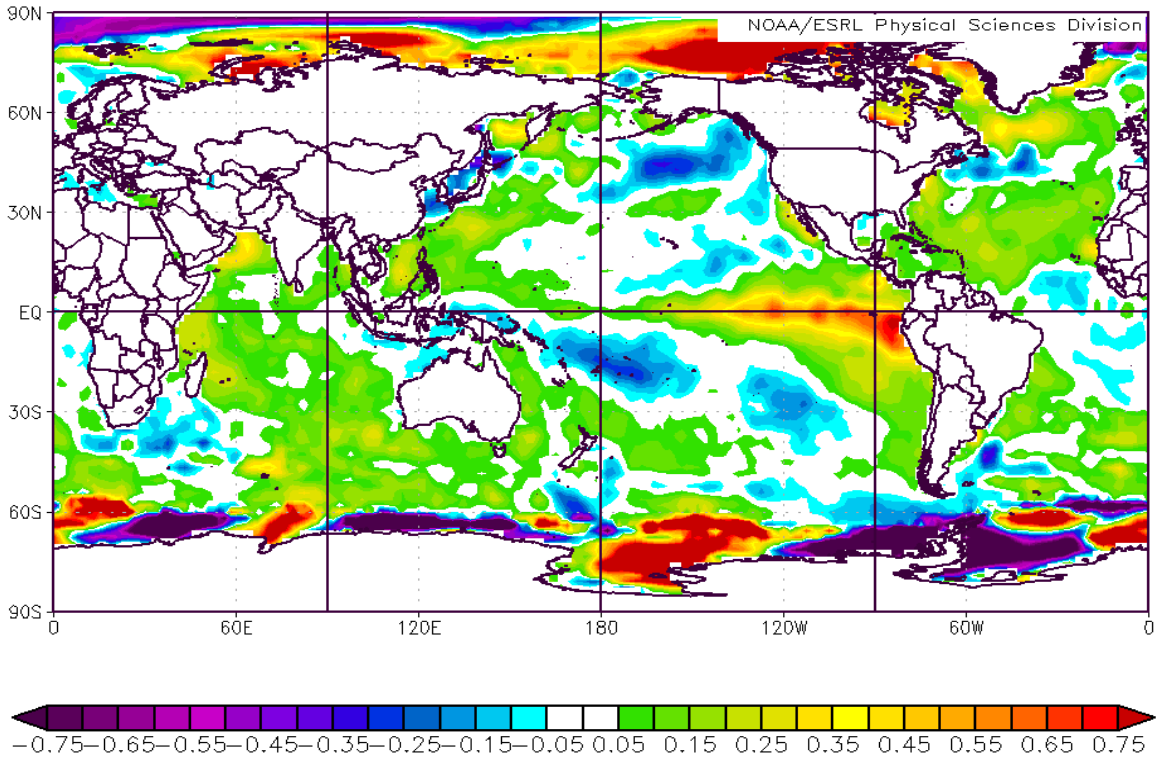

Figure 88. SST Anomalies (°C) for MJO Phase 4 and all EN, LN, and Neutral Years during JFM.

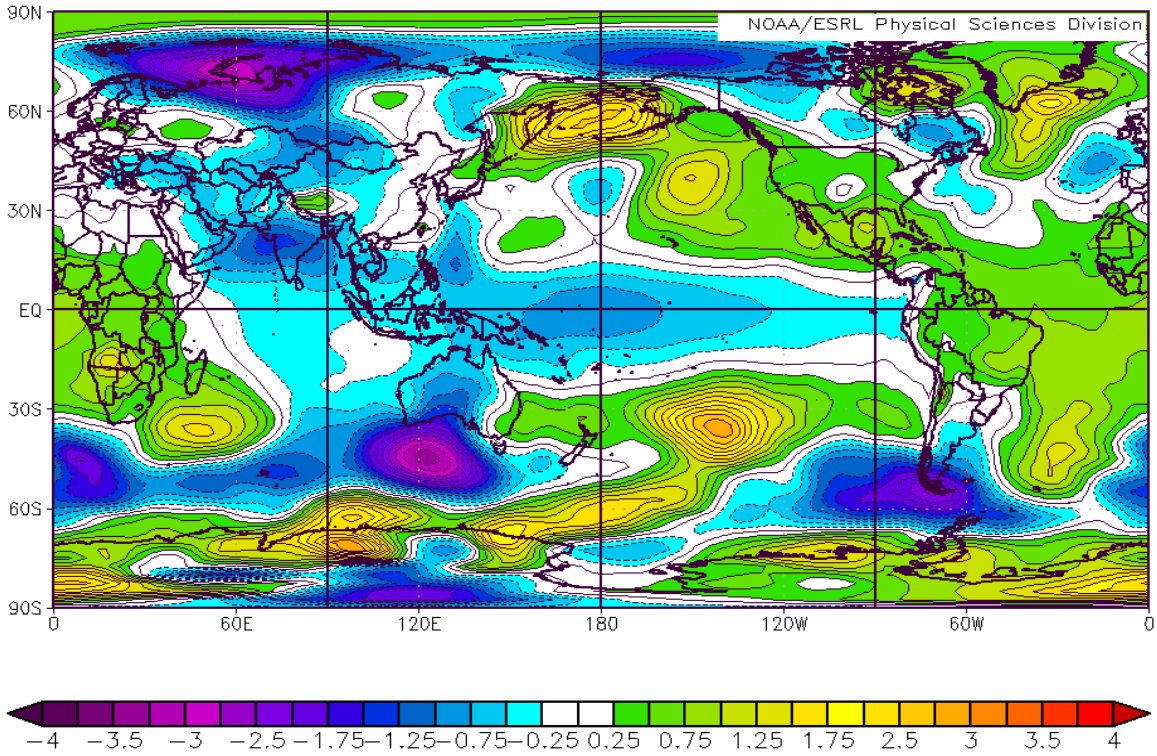

Figure 89. SLP Anomalies (mb) for MJO Phase 4 and all EN, LN, and Neutral Years during JFM.

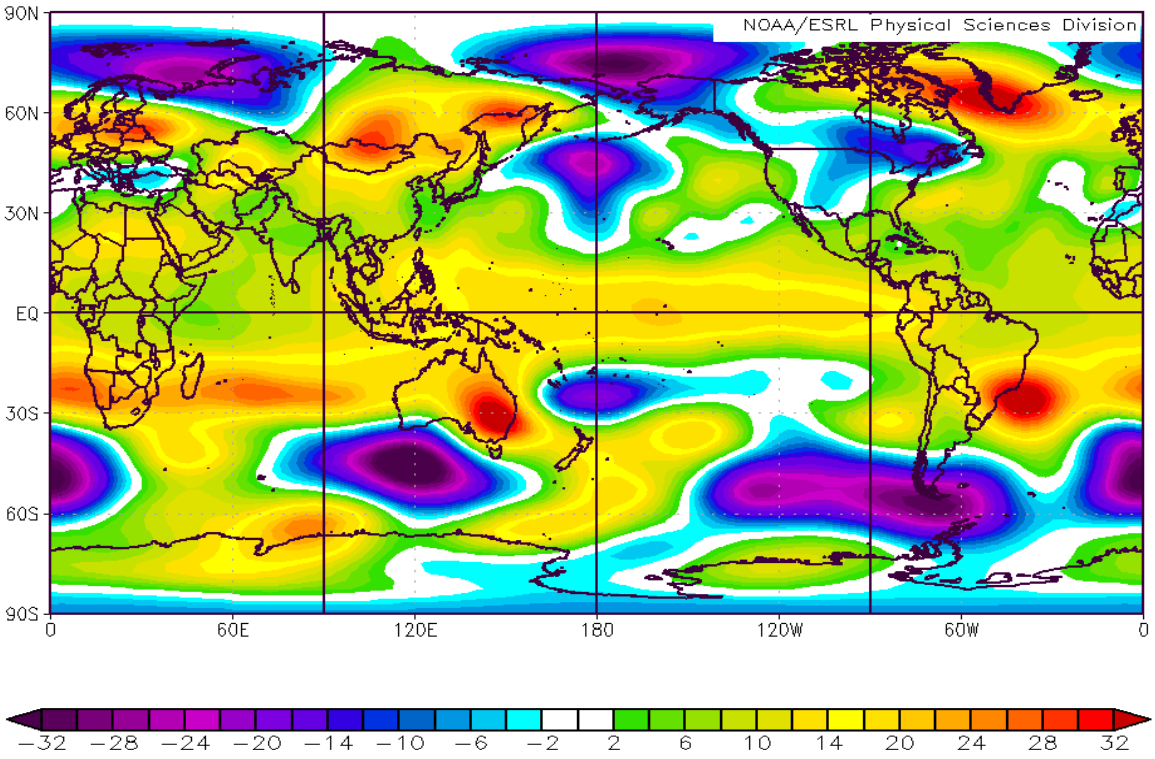

Figure 90. Z200 Anomalies (mb) for MJO Phase 4 and all EN, LN, and Neutral Years during JFM.

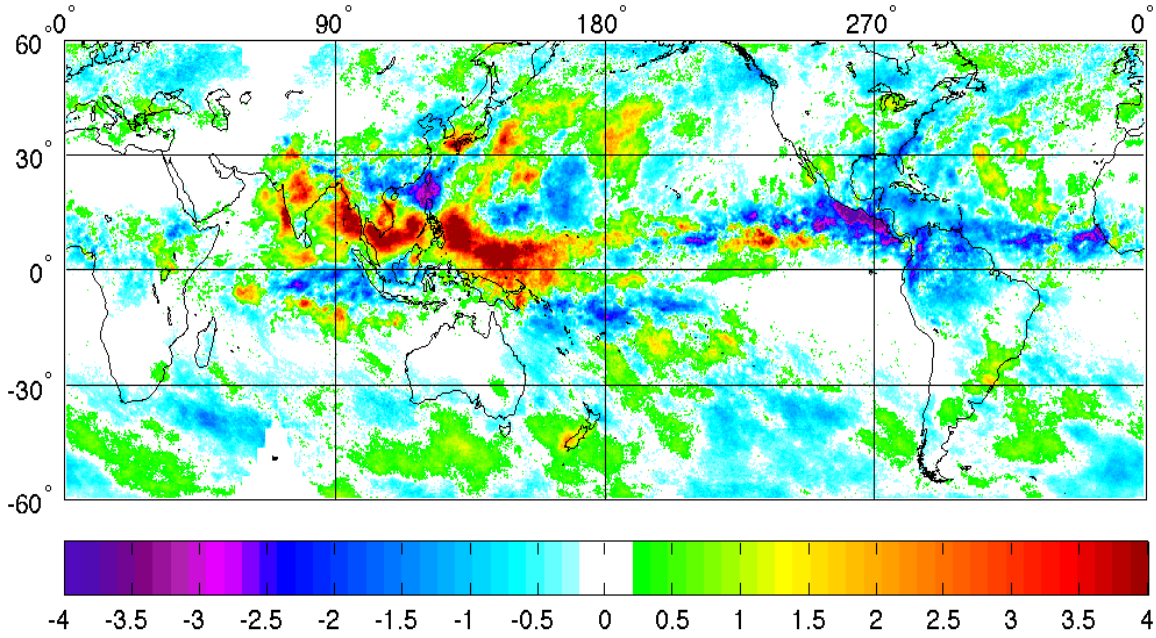

Figure 91. PR Anomalies (mm/day) for MJO Phase 4 and all EN, LN, and Neutral Years during JAS.

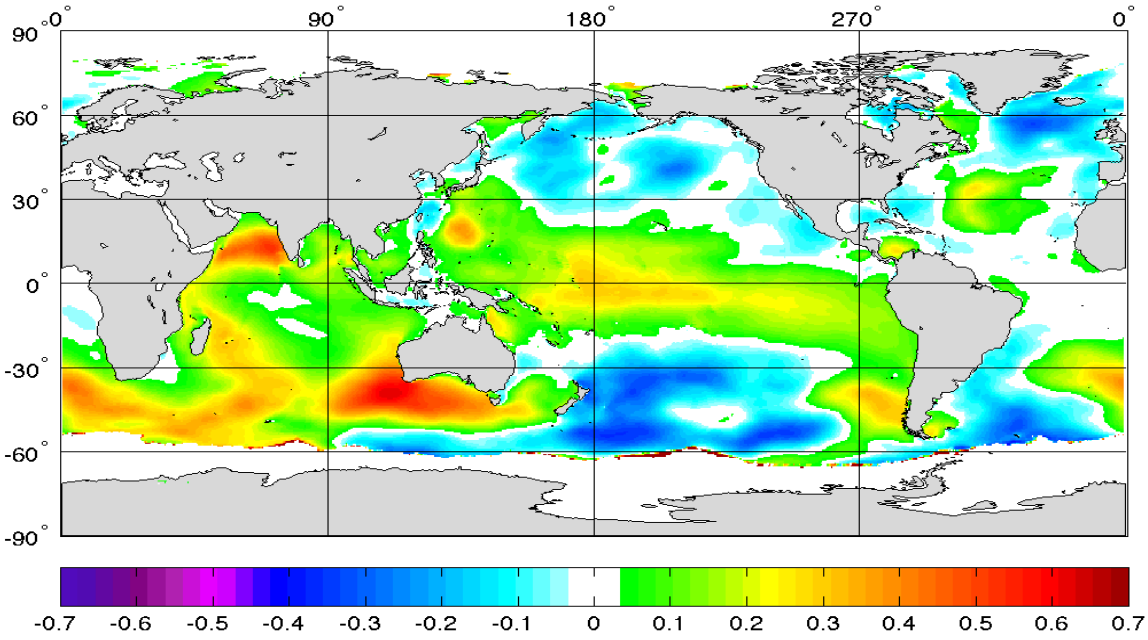

Figure 92. SWH Anomalies (m) for MJO Phase 4 and all EN, LN, and Neutral Years during JAS.

F. CASE 18: CHARACTERISTIC JAS EN PHASE 4 ANOMALIES

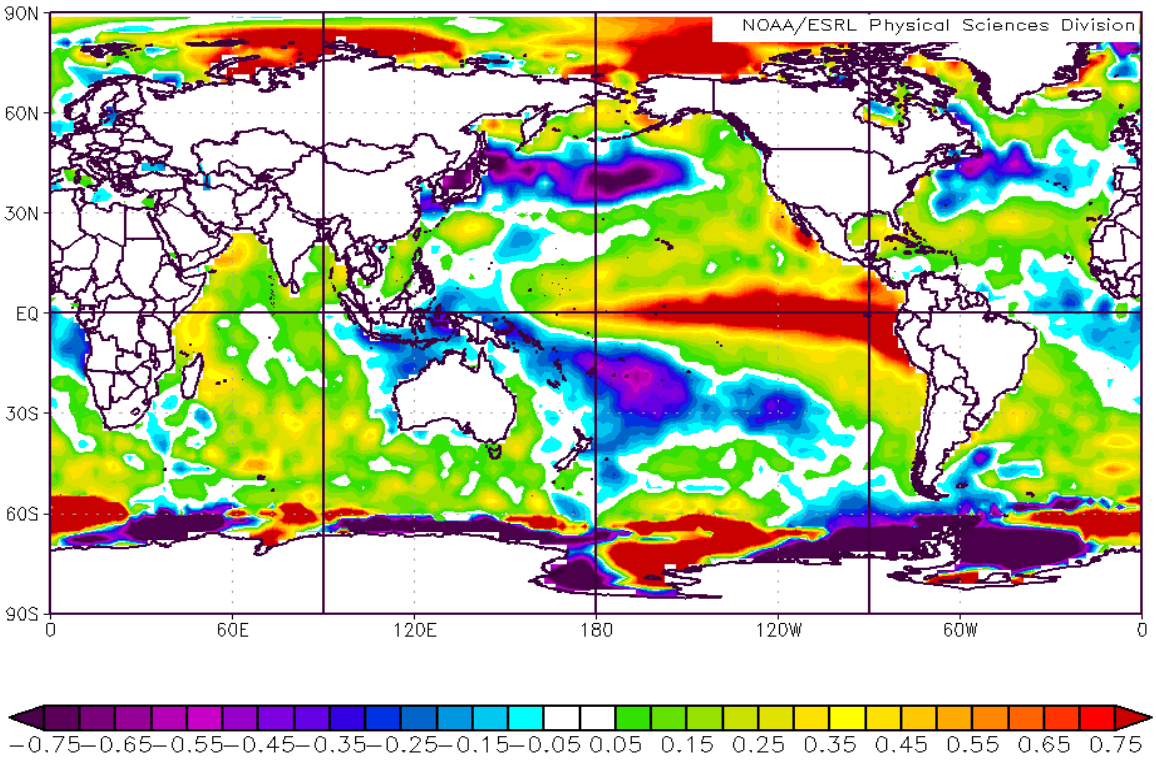

Figure 93. SST Anomalies (°C) for MJO Phase 4 and EN Years during JAS.

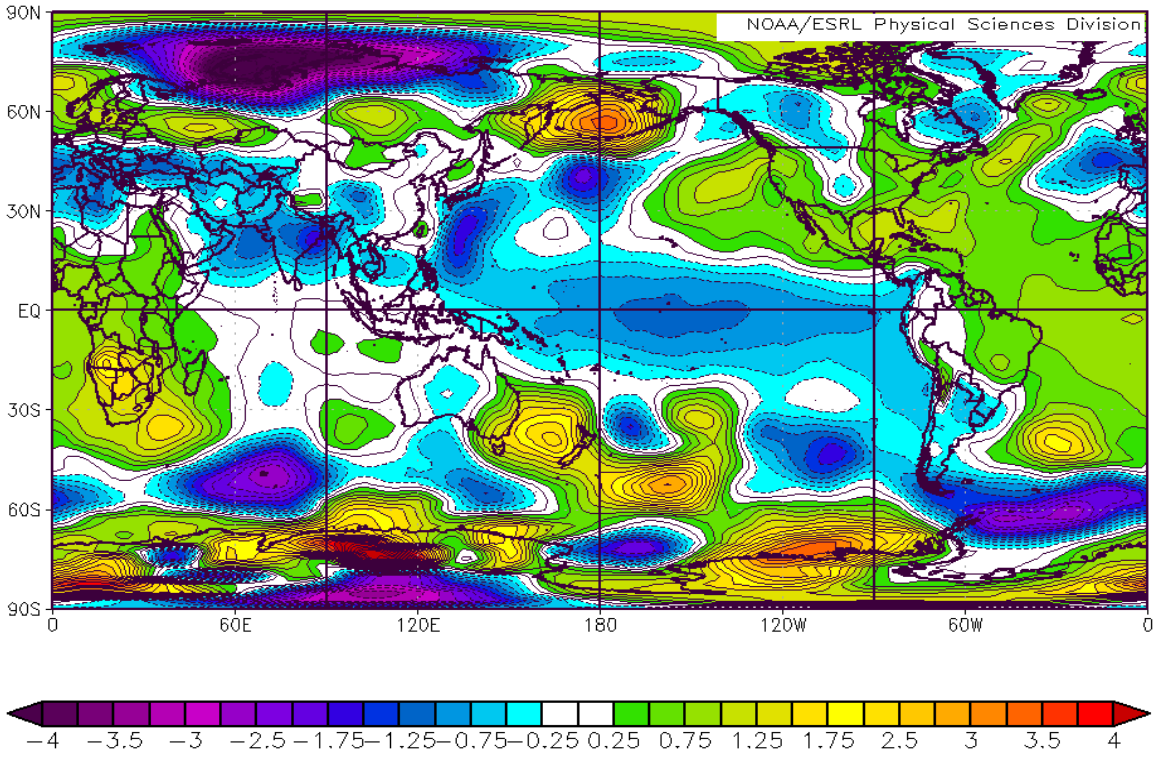

Figure 94. SLP Anomalies (mb) for MJO Phase 4 and EN Years during JAS.

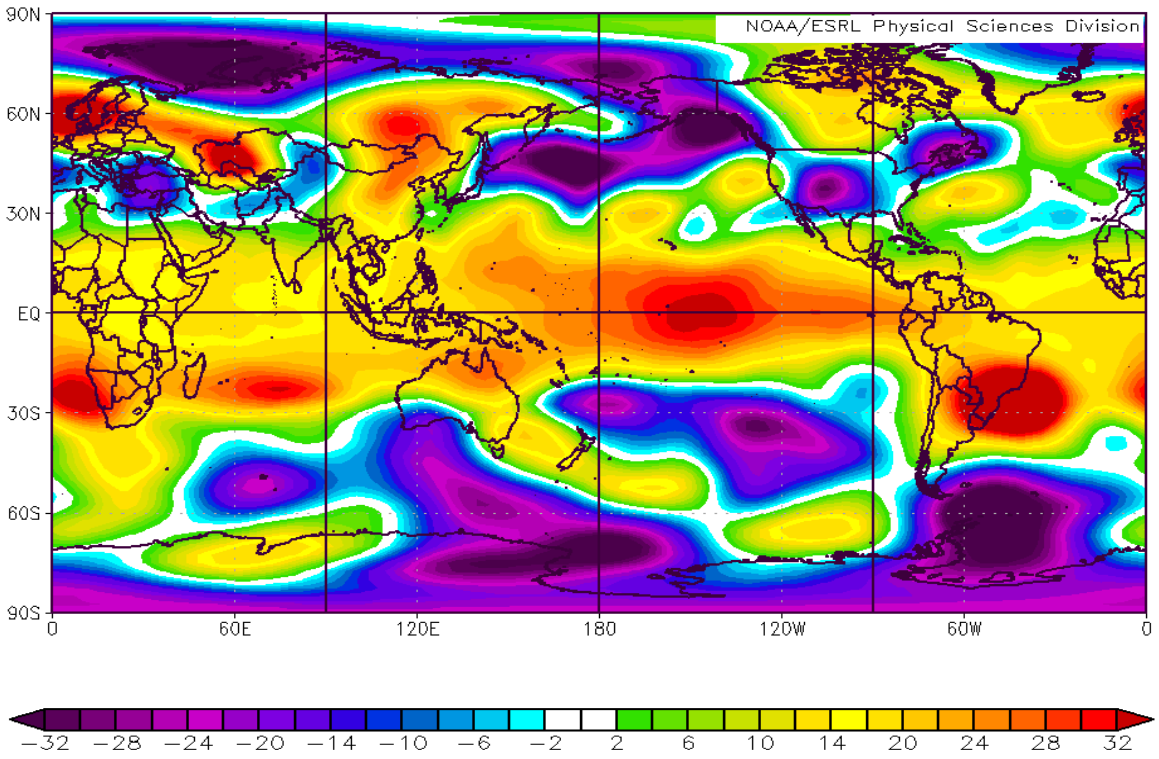

Figure 95. Z200 Anomalies (mb) for MJO Phase 4 and EN Years during JAS.

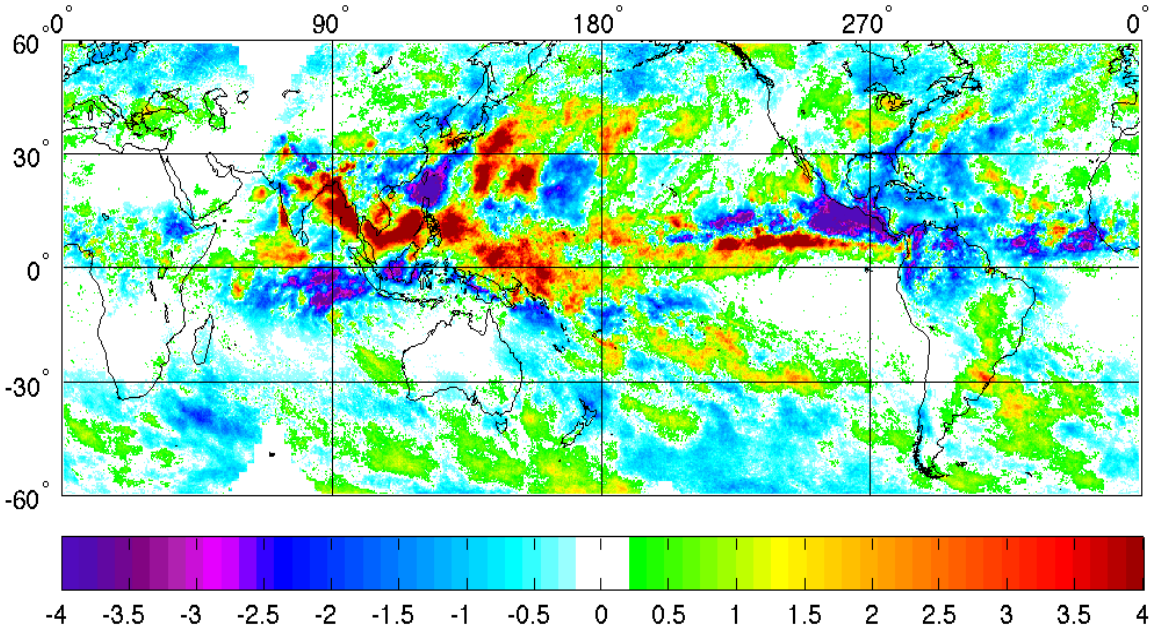

Figure 96. PR Anomalies (mm/day) for MJO Phase 4 and EN Years during JAS.

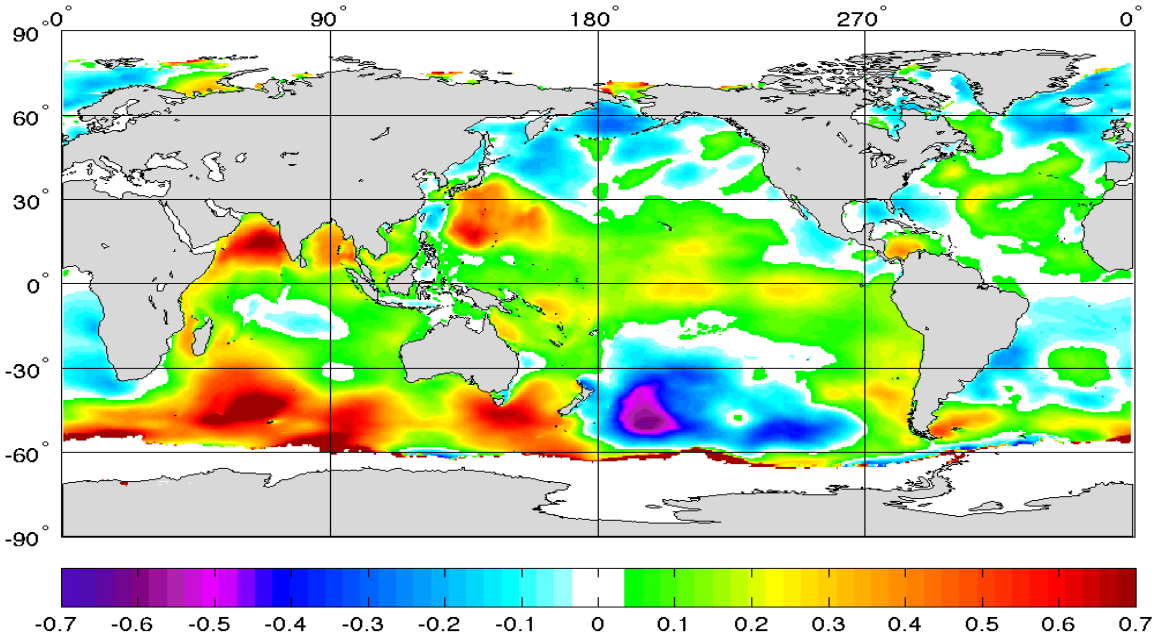

Figure 97. SWH Anomalies (m) for MJO Phase 4 and EN Years during JAS.

G. CASE 19: CHARACTERISTIC JAS LN PHASE 4 ANOMALIES

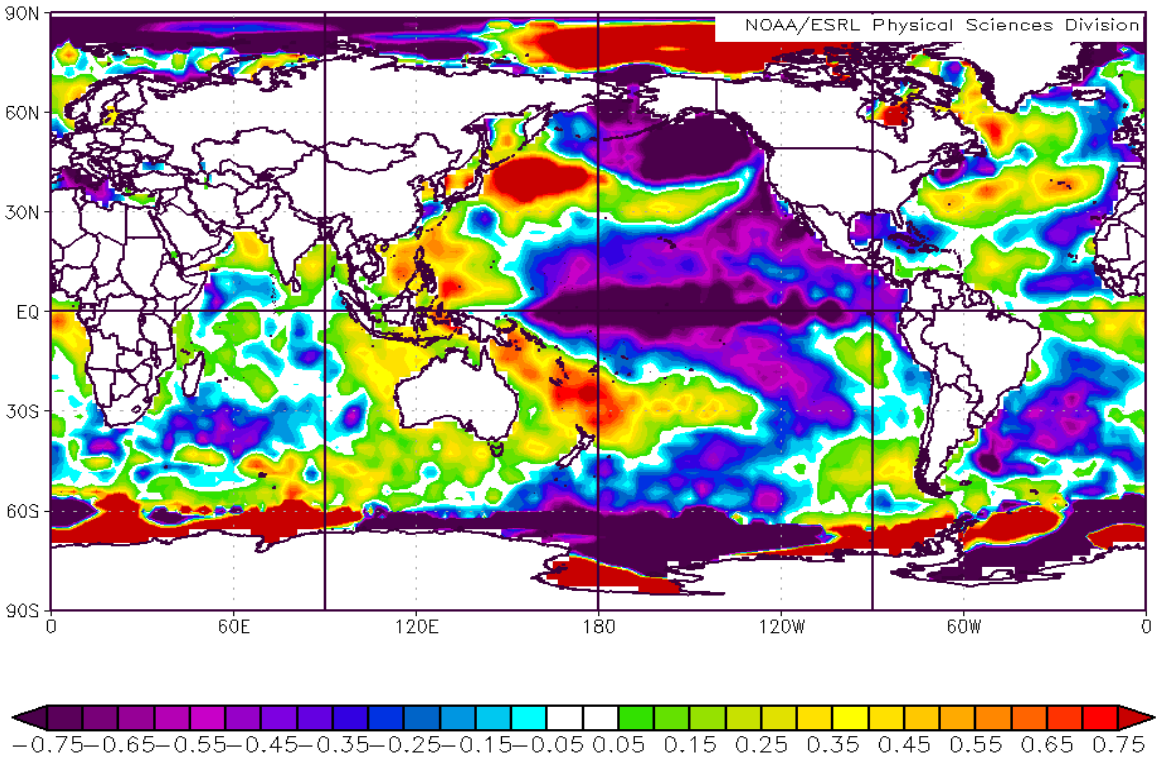

Figure 98. SST Anomalies (°C) for MJO Phase 4 and LN Years during JAS.

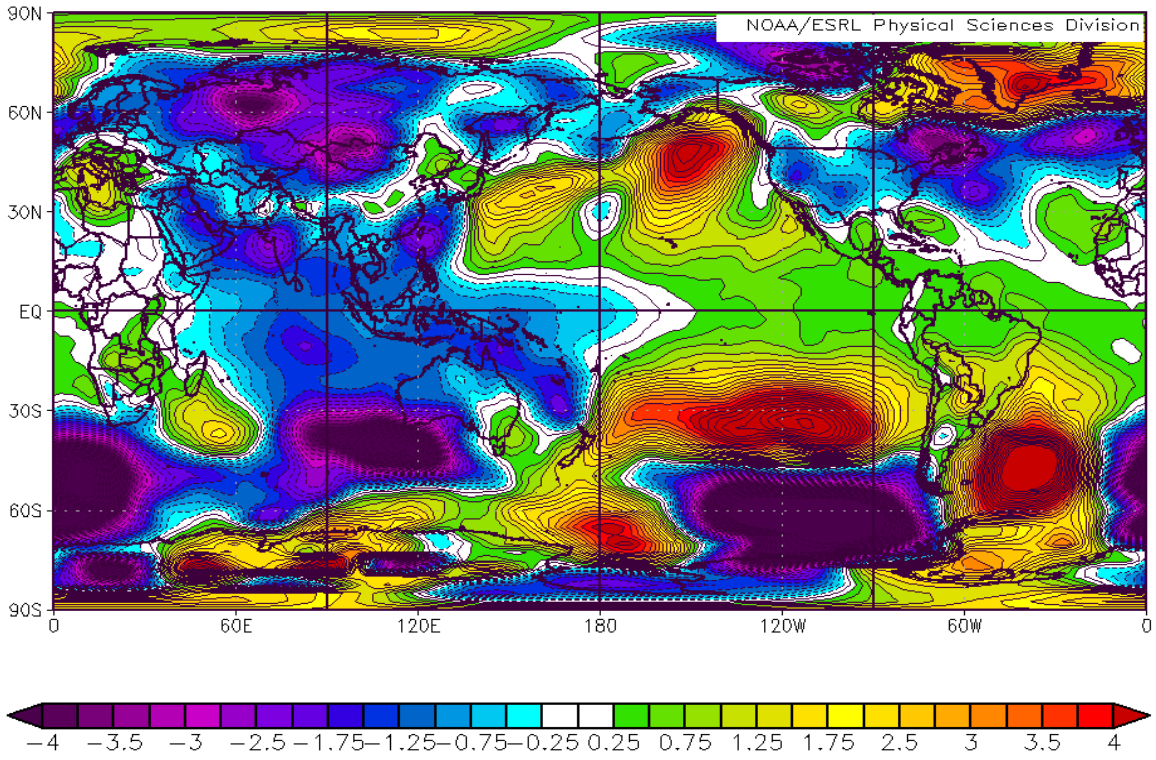

Figure 99. SLP Anomalies (mb) for MJO Phase 4 and LN Years during JAS.

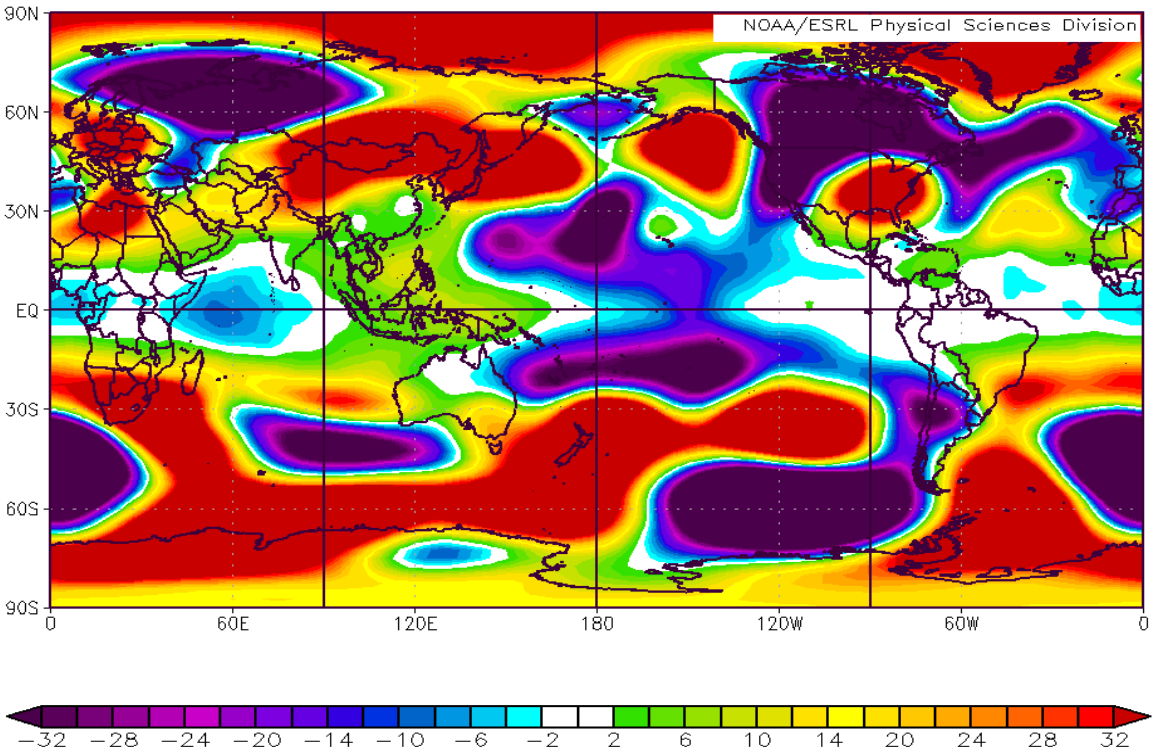

Figure 100. Z200 Anomalies (mb) for MJO Phase 4 and LN Years during JAS.

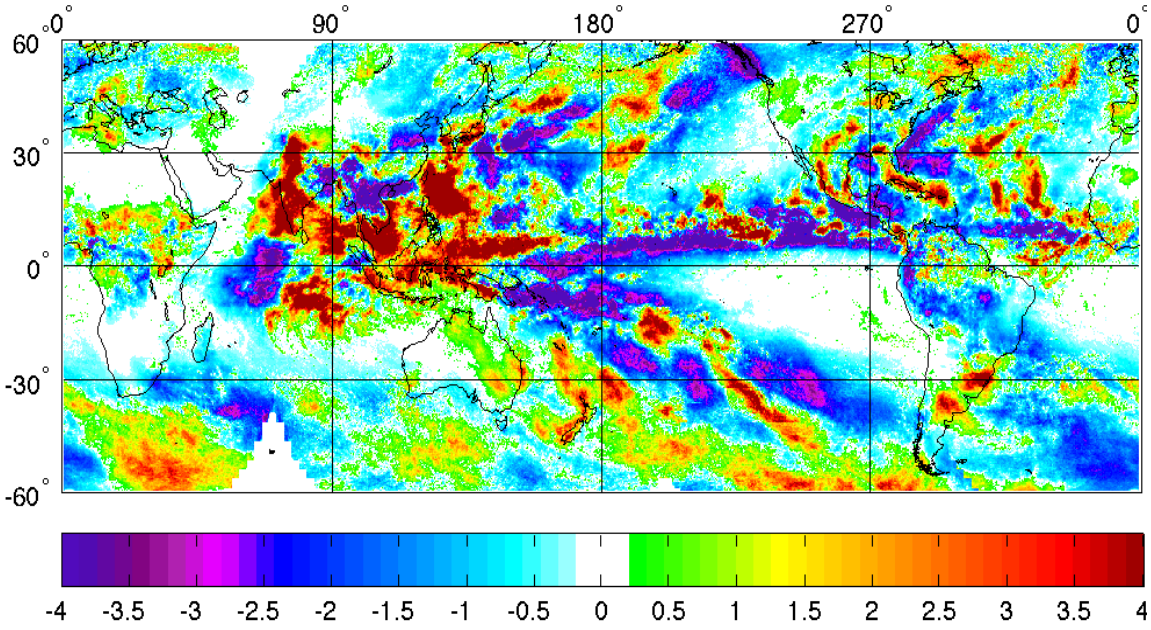

Figure 101. PR Anomalies (mm/day) for MJO Phase 4 and LN Years during JAS.

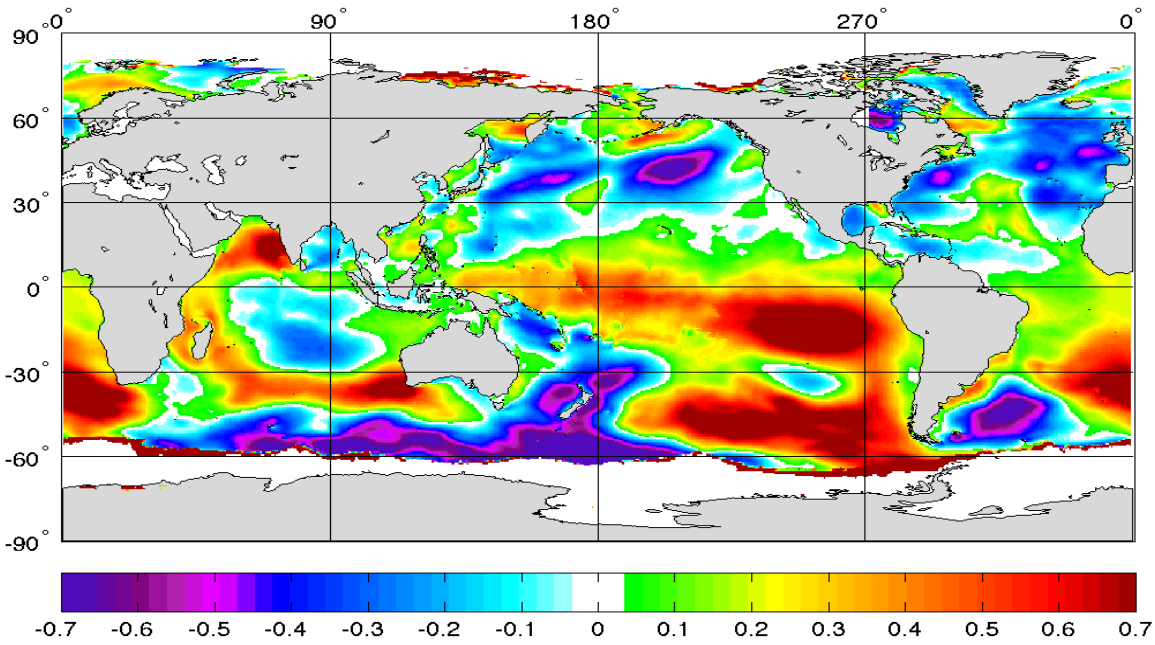

Figure 102. SWH Anomalies (m) for MJO Phase 4 and LN Years during JAS.

H. CASE 20: CHARACTERISTIC JAS NEUTRAL PHASE 4 ANOMALIES

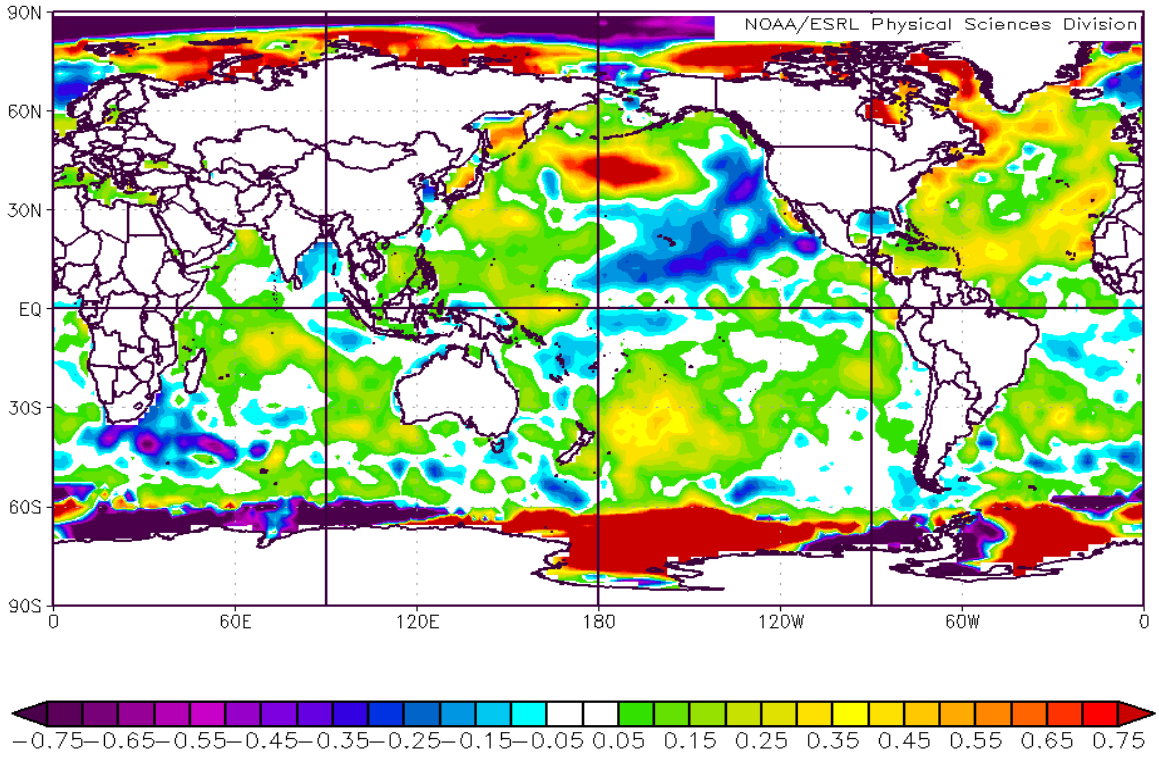

Figure 103. SST Anomalies (°C) for MJO Phase 4 and Neutral Years during JAS.

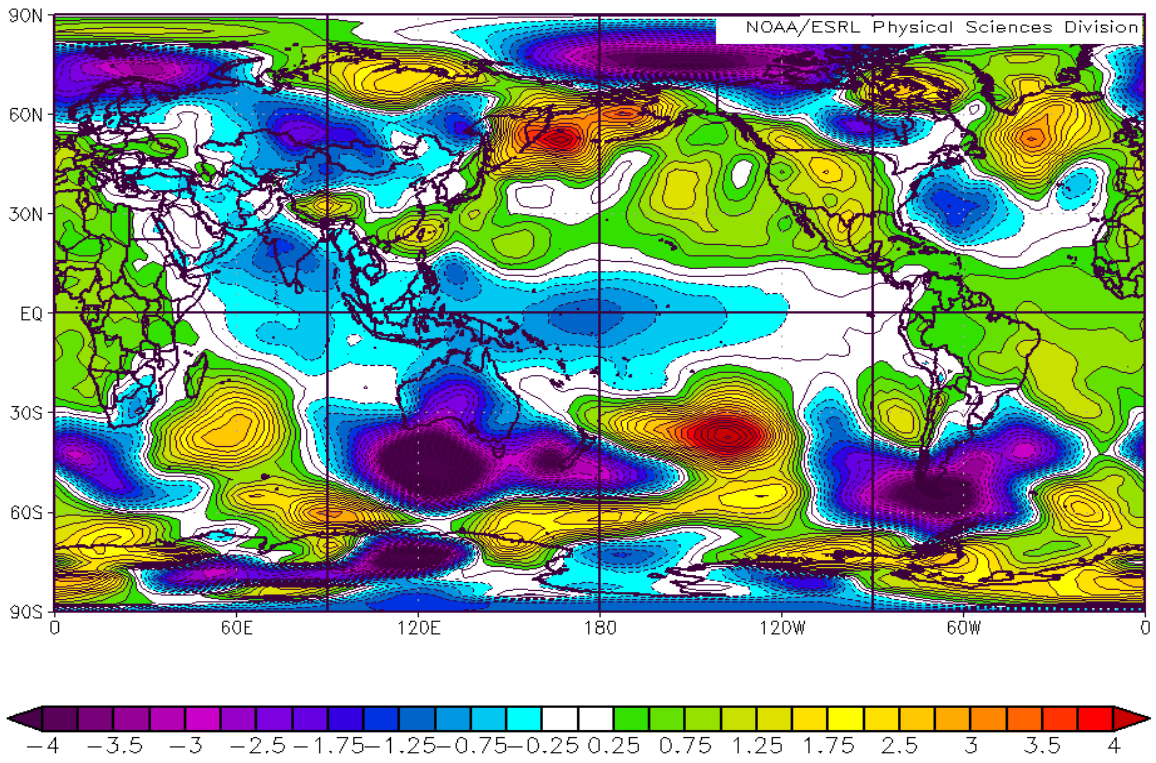

Figure 104. SLP Anomalies (mb) for MJO Phase 4 and Neutral Years during JAS.

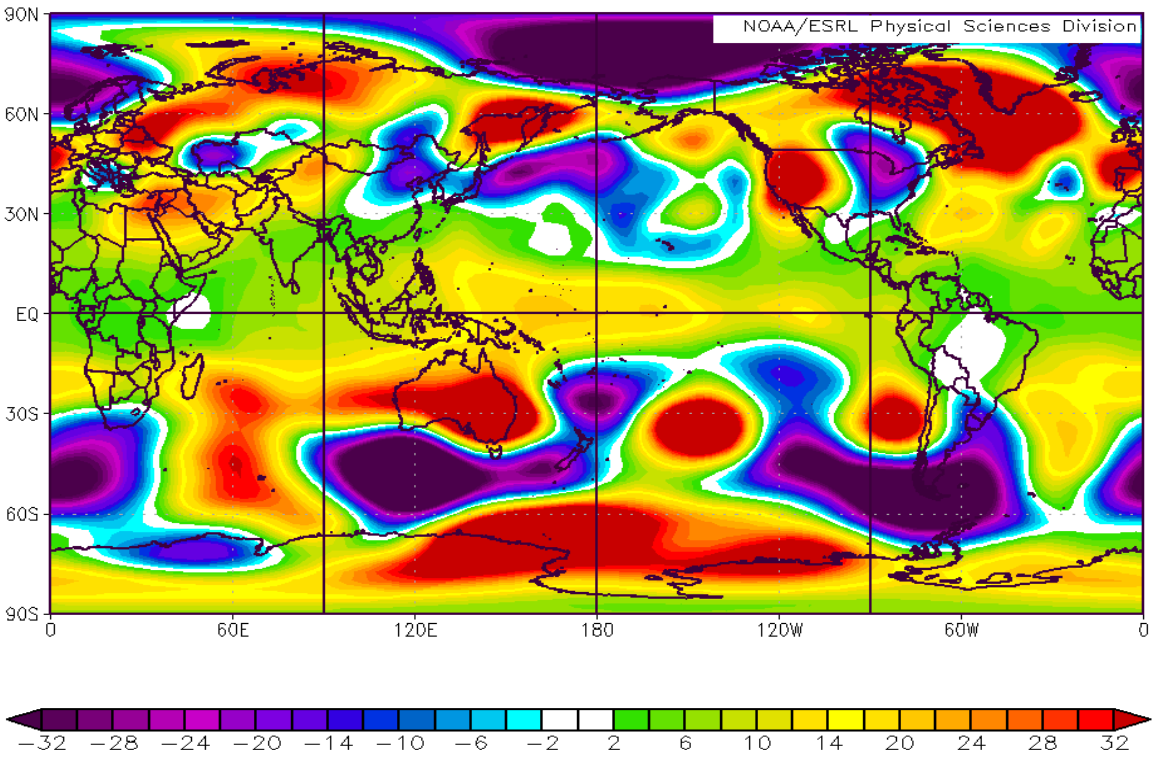

Figure 105. Z200 Anomalies (mb) for MJO Phase 4 and Neutral Years during JAS.

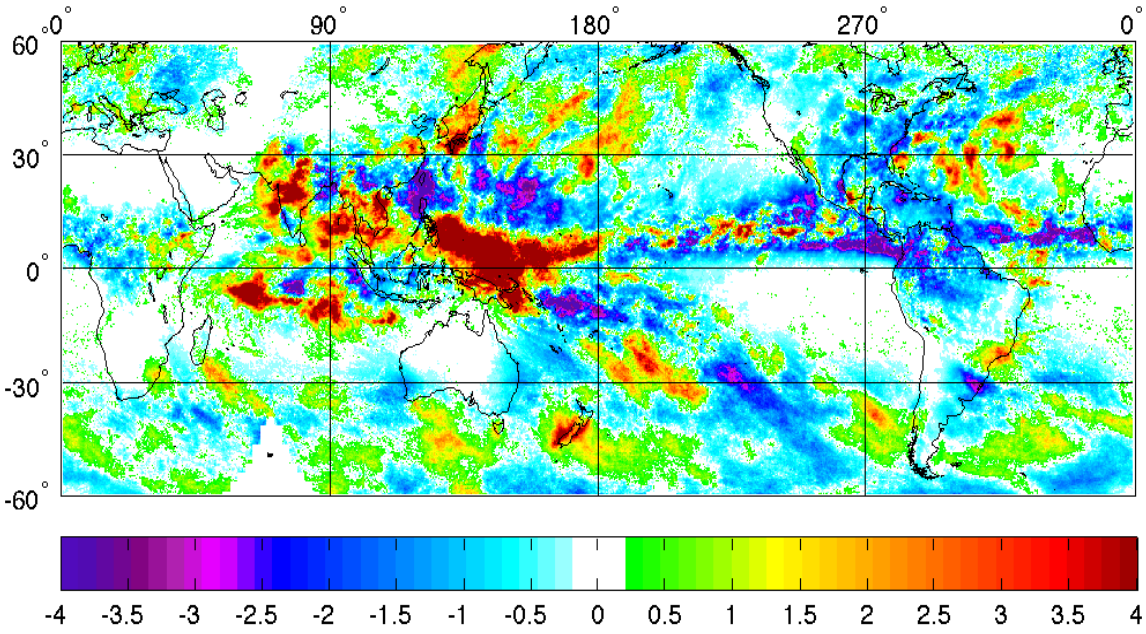

Figure 106. PR Anomalies (mm/day) for MJO Phase 4 and Neutral Years during JAS.

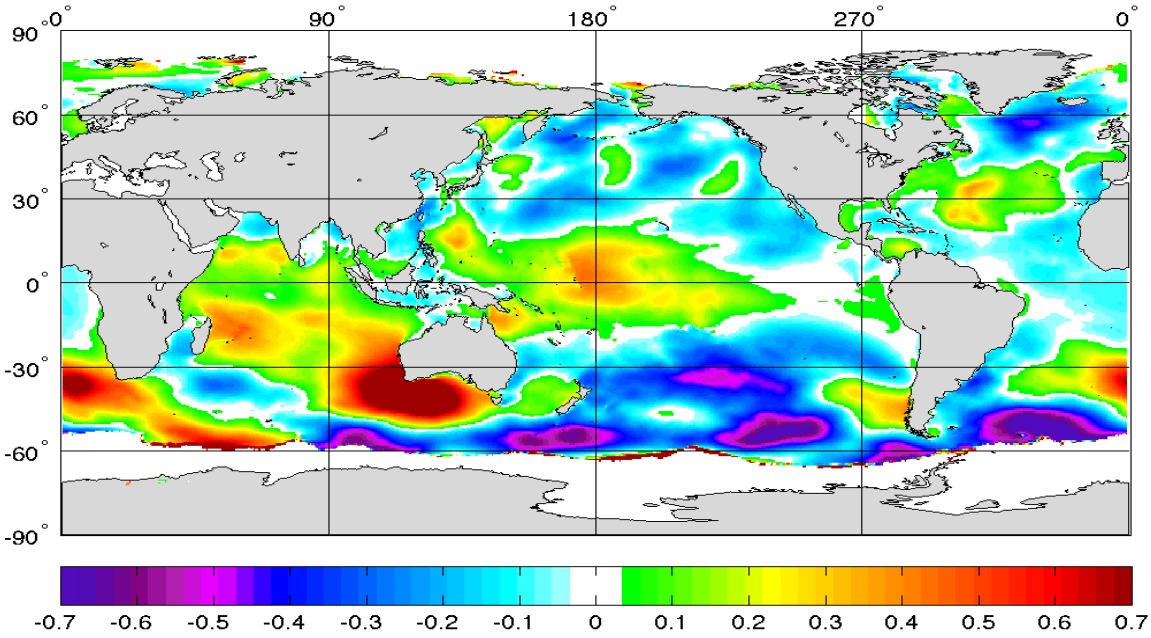

Figure 107. SWH Anomalies (m) for MJO Phase 4 and Neutral Years during JAS.

I. CASE 21: CHARACTERISTIC JAS PHASE 8 ANOMALIES

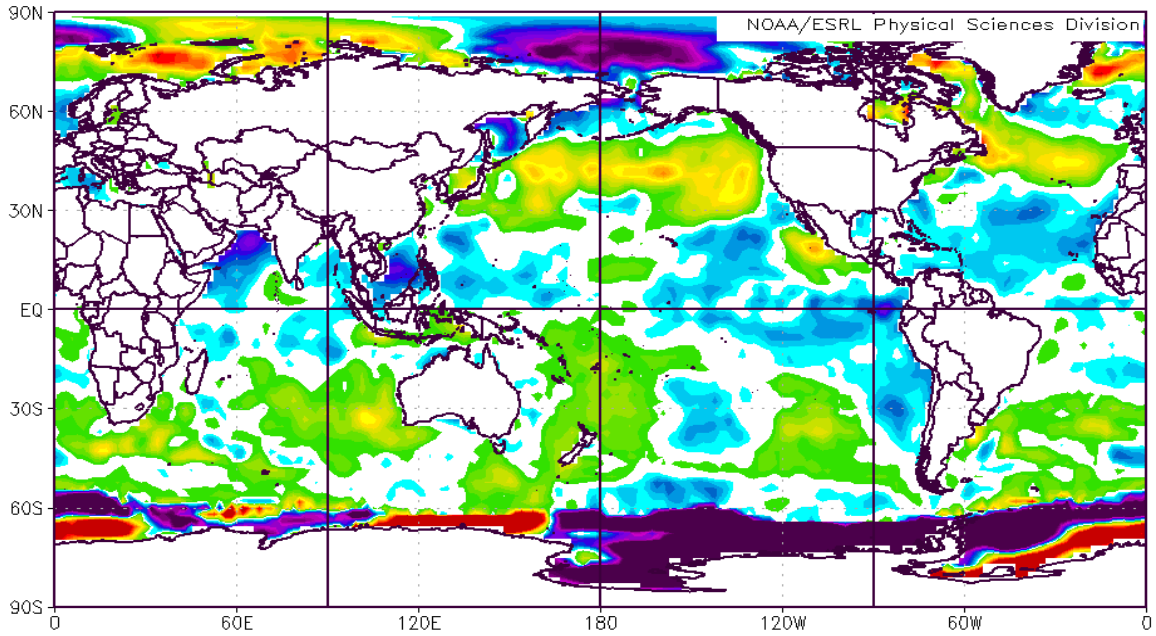

Figure 108. SST Anomalies (°C) for MJO Phase 8 and all EN, LN, and Neutral Years during JAS.

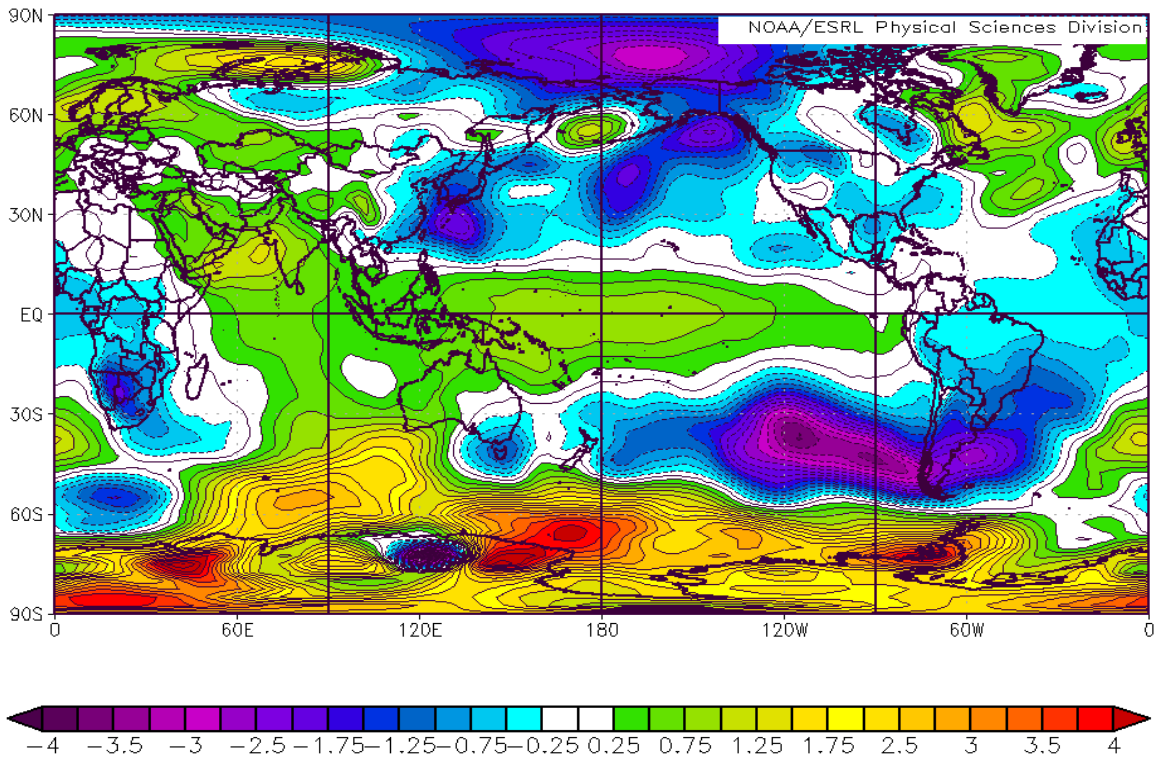

Figure 109. SLP Anomalies (mb) for MJO Phase 8 and all EN, LN, and Neutral Years during JAS.

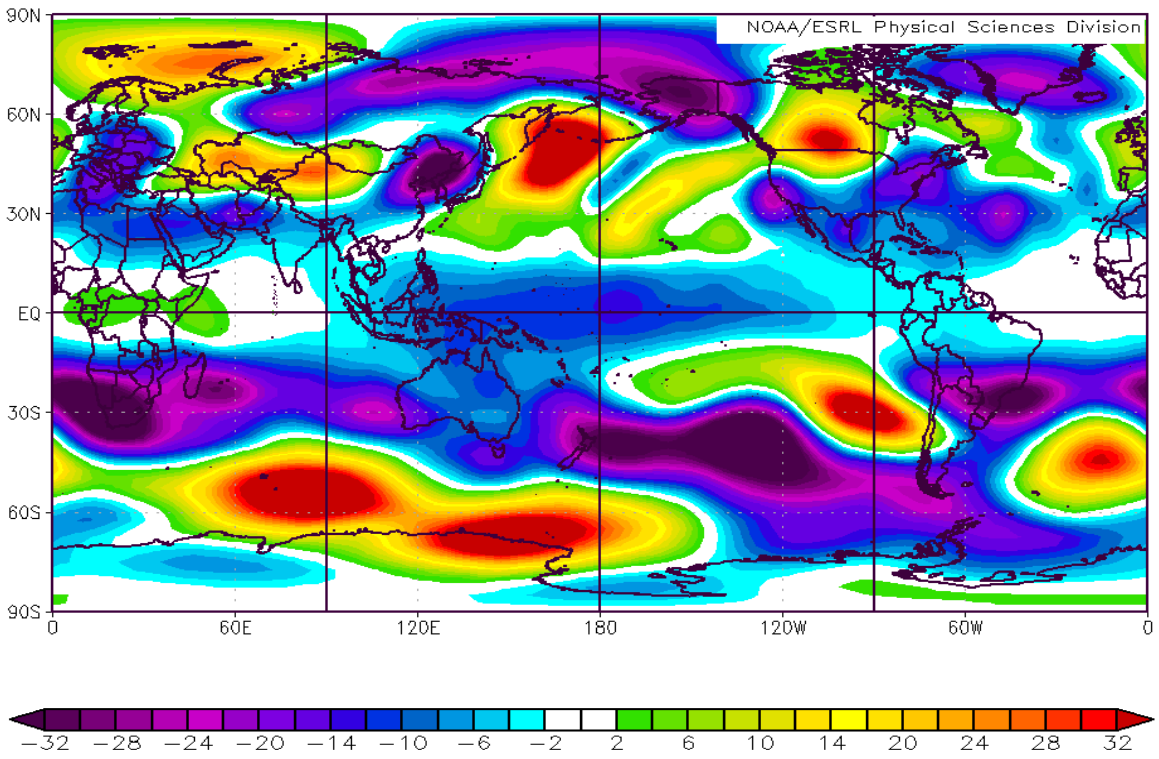

Figure 110. Z200 Anomalies (mb) for MJO Phase 8 and all EN, LN, and Neutral Years during JAS.

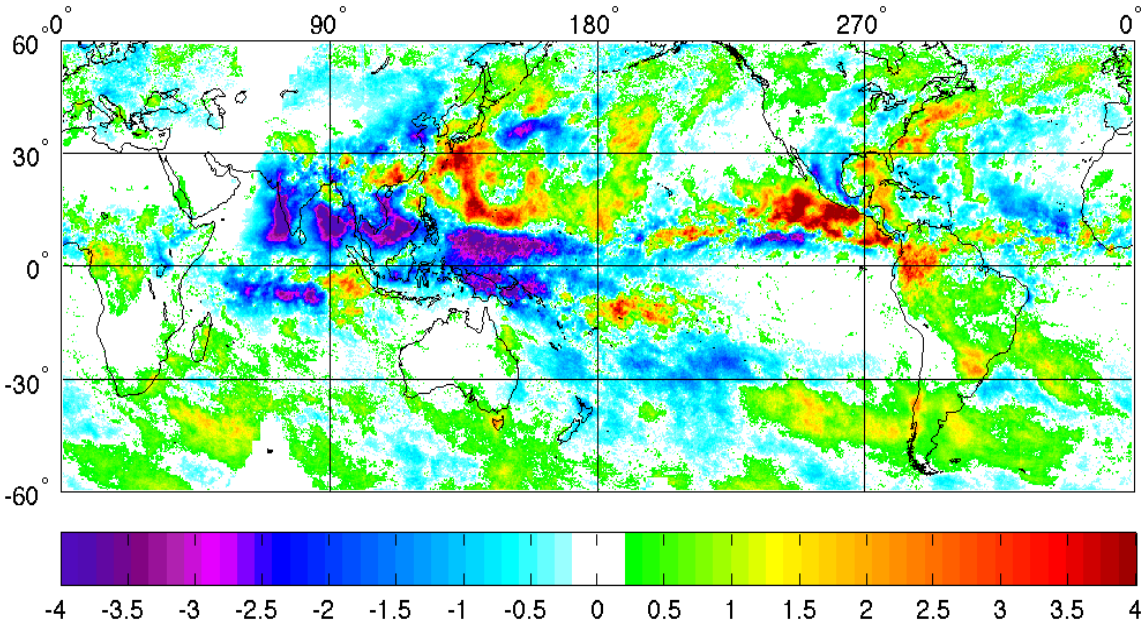

Figure 111. PR Anomalies (mm/day) for MJO Phase 8 and all EN, LN, and Neutral Years during JAS.

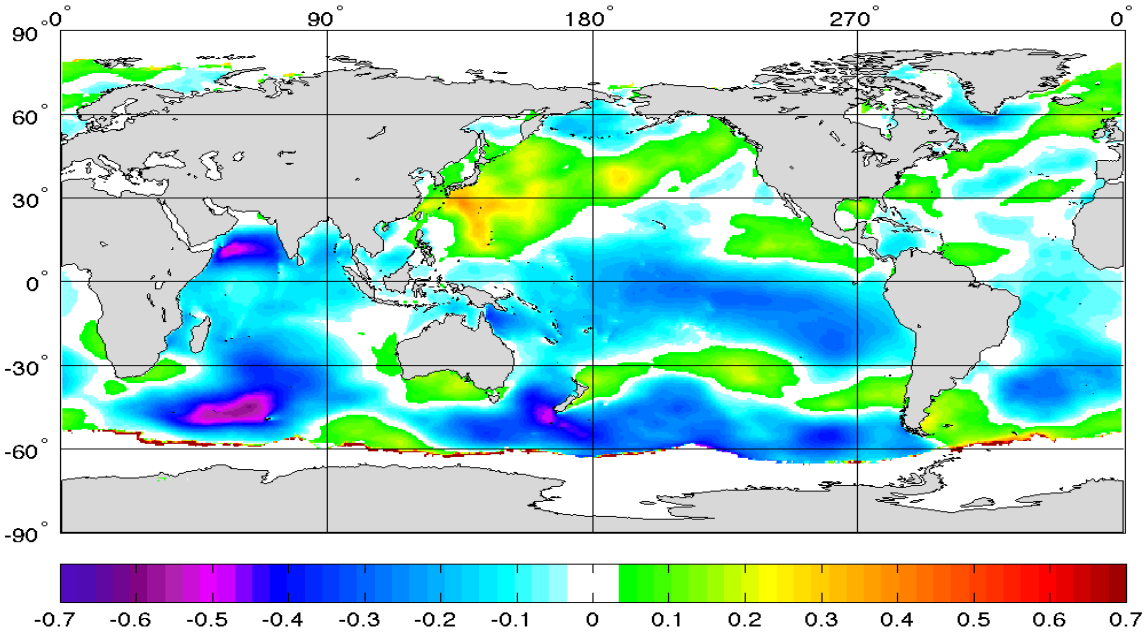

Figure 112. SWH Anomalies (m) for MJO Phase 8 and all EN, LN, and Neutral Years during JAS.

J. CASE 22: CHARACTERISTIC JAS EN PHASE 8 ANOMALIES

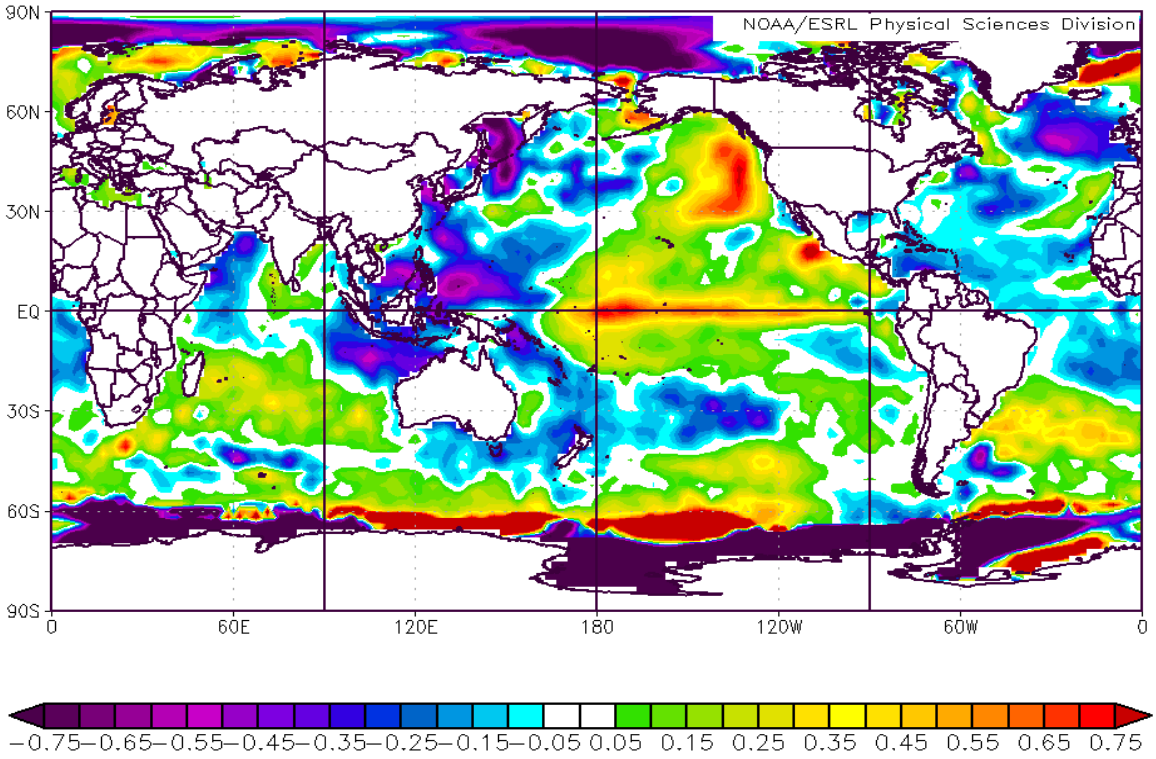

Figure 113. SST Anomalies (°C) for MJO Phase 8 and EN Years during JAS.

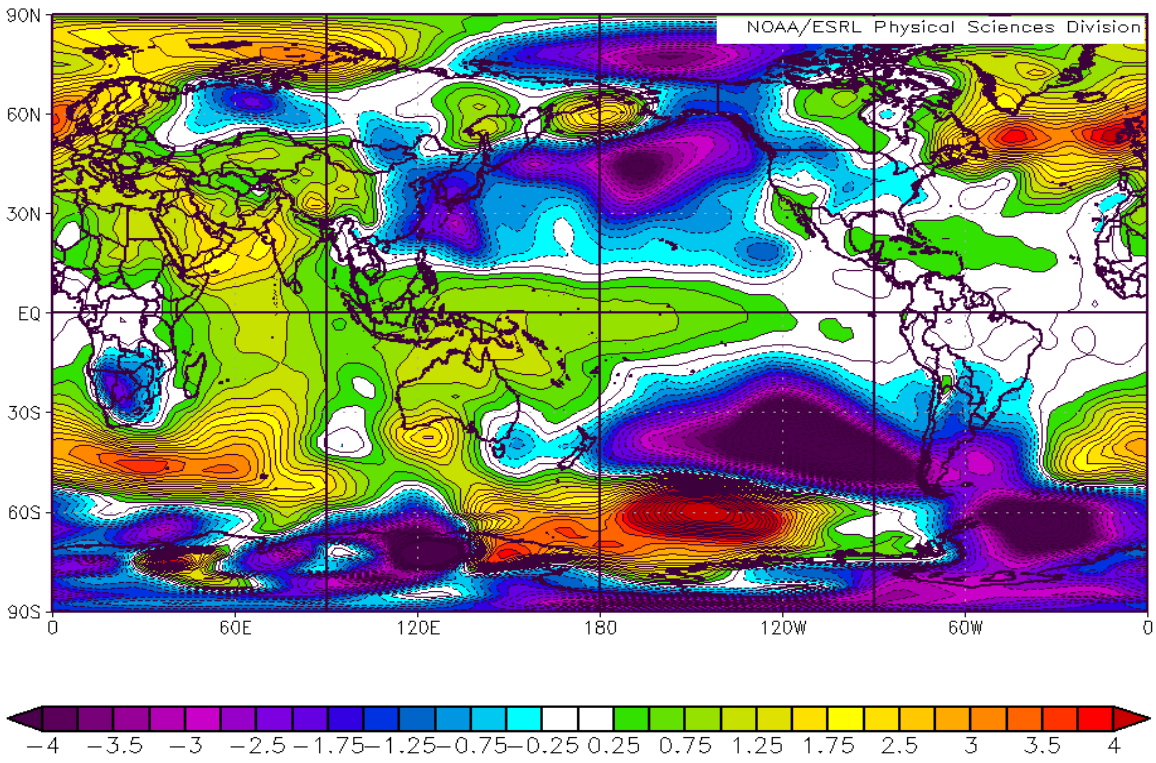

Figure 114. SLP Anomalies (mb) for MJO Phase 8 and EN Years during JAS.

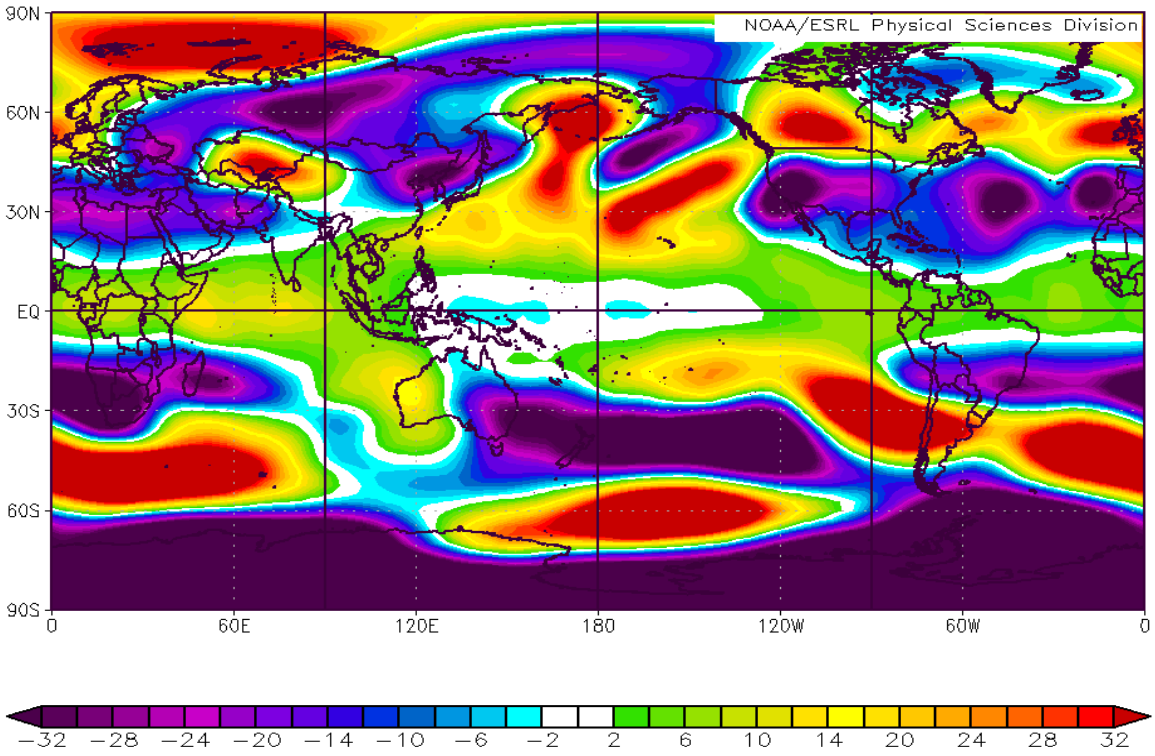

Figure 115. Z200 Anomalies (mb) for MJO Phase 8 and EN Years during JAS.

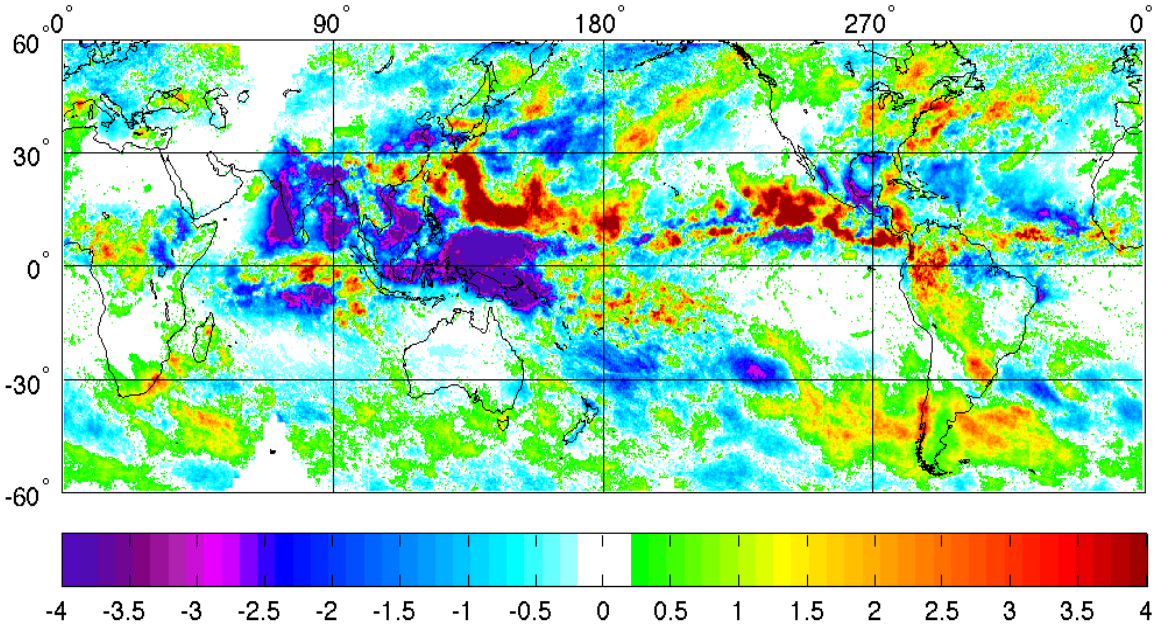

Figure 116. PR Anomalies (mm/day) for MJO Phase 8 and EN Years during JAS.

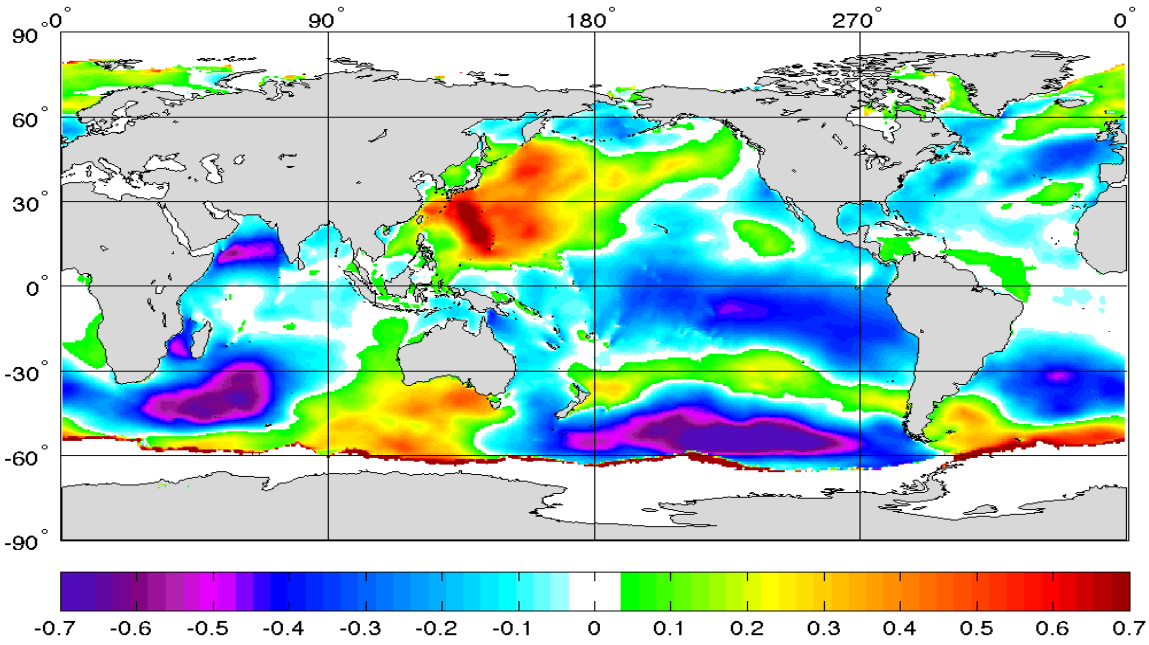

Figure 117. SWH Anomalies (m) for MJO Phase 8 and EN Years during JAS.

K. CASE 23: CHARACTERISTIC JAS LN PHASE 8 ANOMALIES

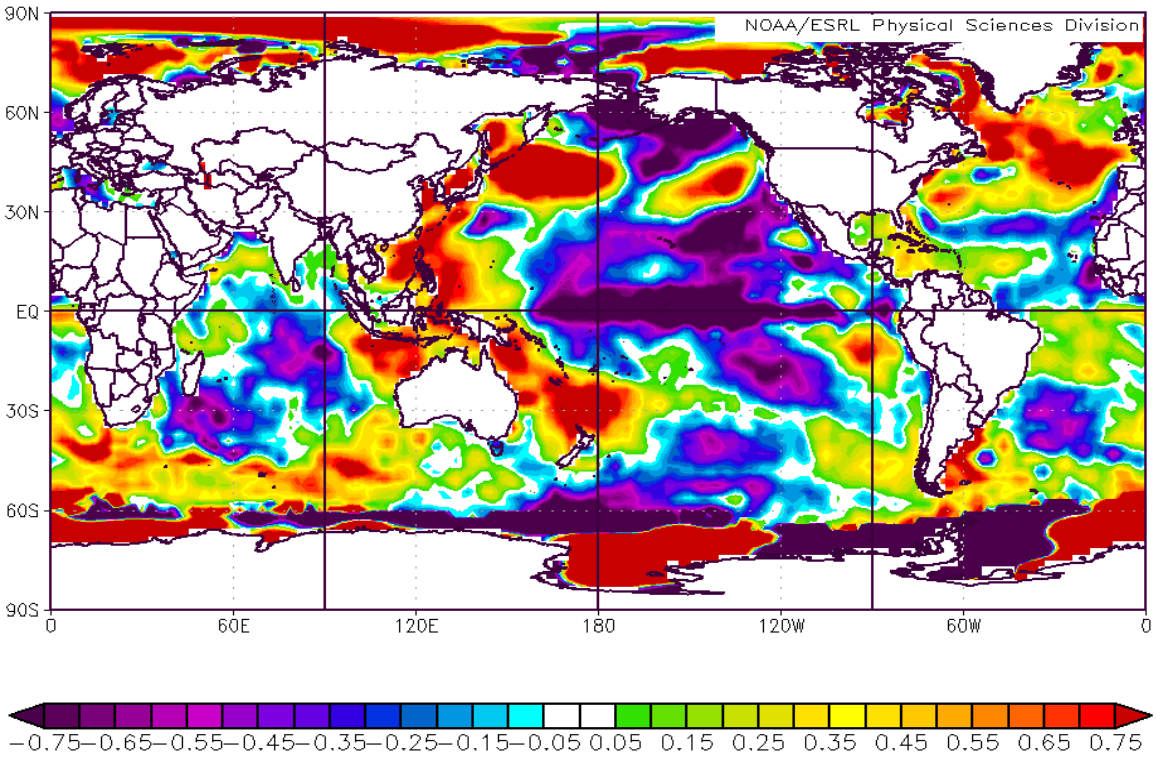

Figure 118. SST Anomalies (°C) for MJO Phase 8 and LN Years during JAS.

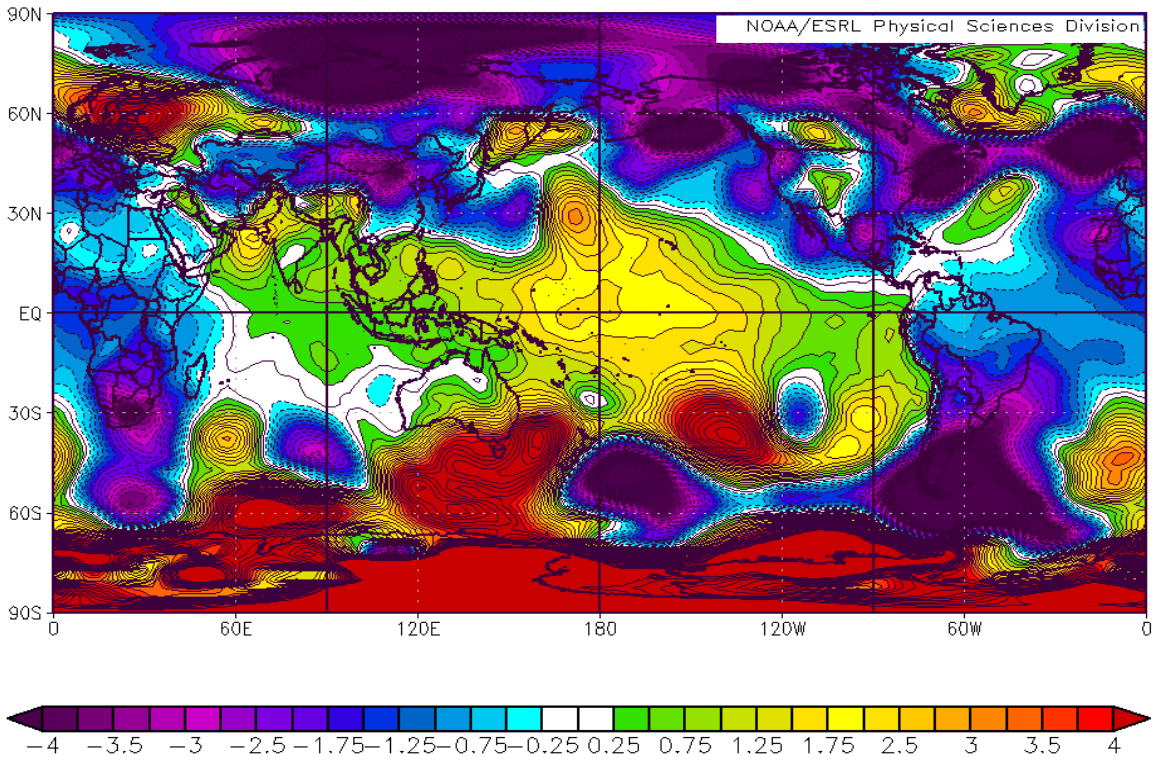

Figure 119. SLP Anomalies (mb) for MJO Phase 8 and LN Years during JAS.

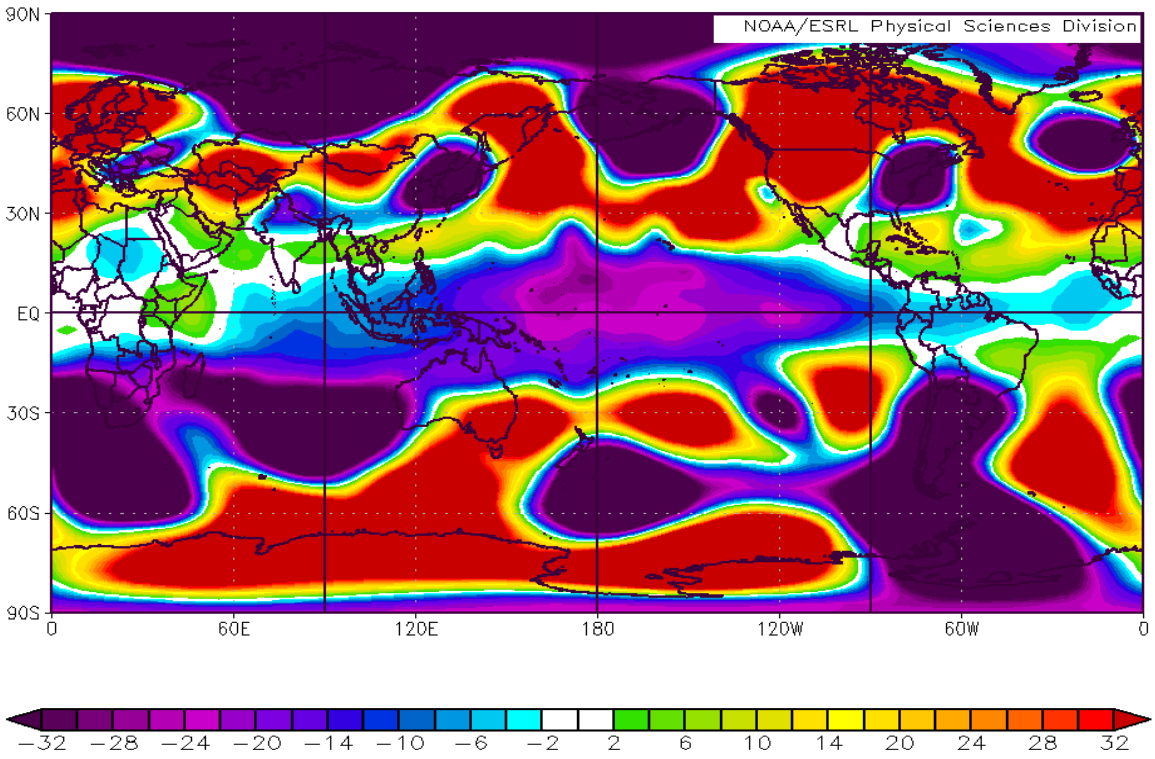

Figure 120. Z200 Anomalies (mb) for MJO Phase 8 and LN Years during JAS.

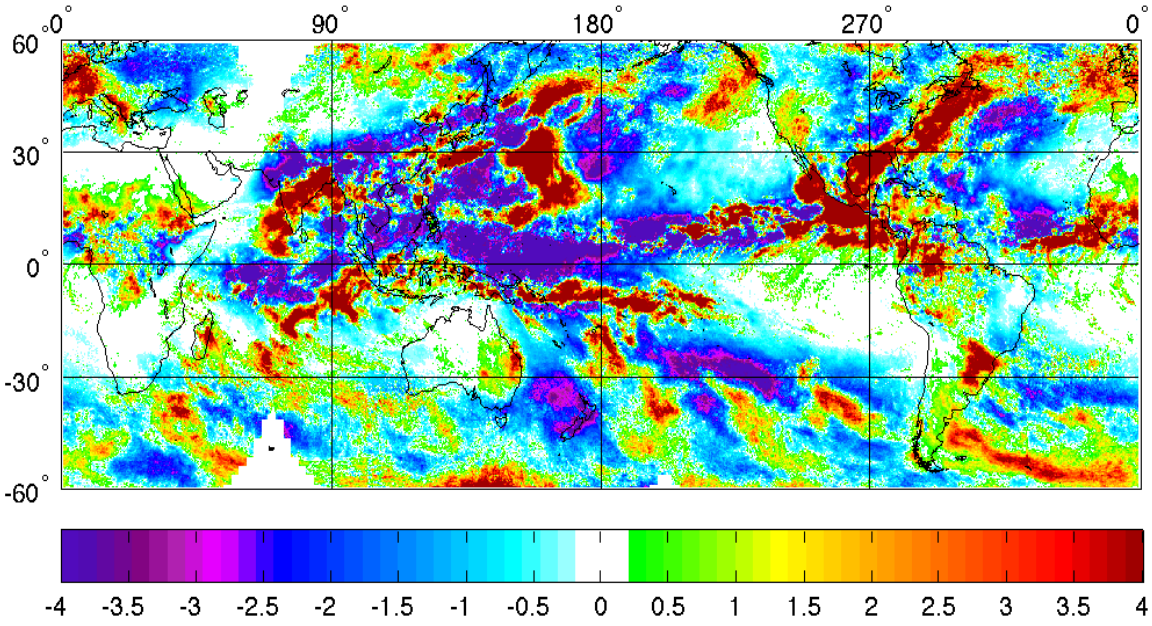

Figure 121. PR Anomalies (mm/day) for MJO Phase 8 and LN Years during JAS.

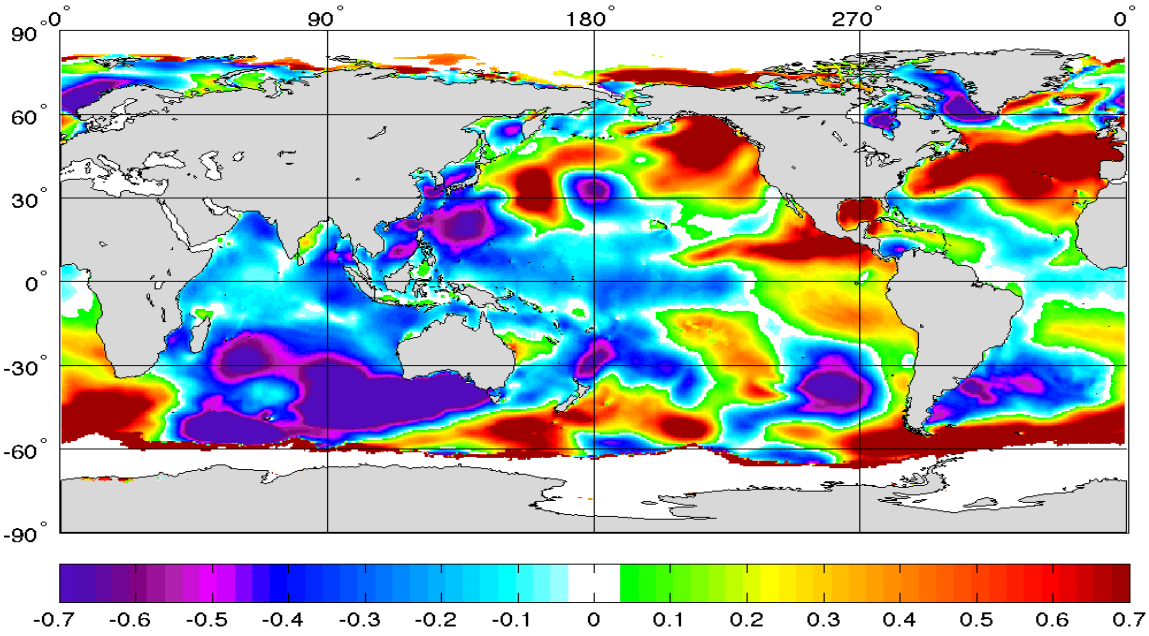

Figure 122. SWH Anomalies (m) for MJO Phase 8 and LN Years during JAS.

L. CASE 24: CHARACTERISTIC JAS NEUTRAL PHASE 8 ANOMALIES

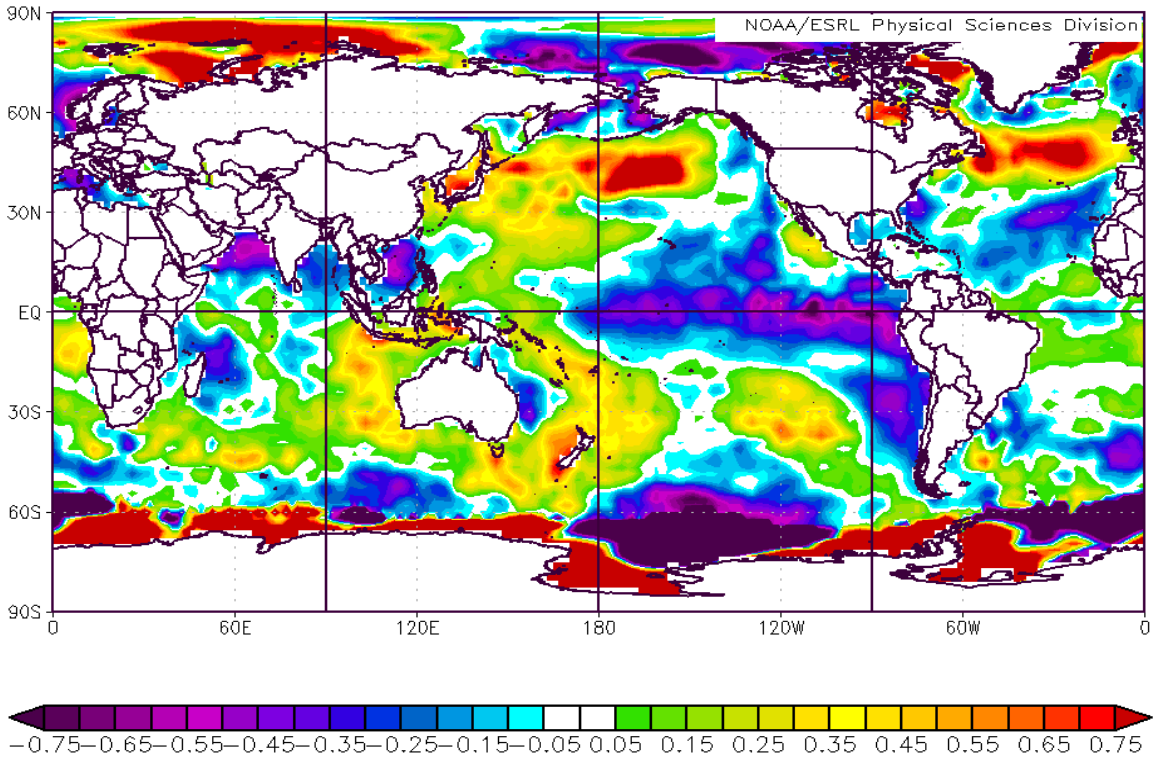

Figure 123. SST Anomalies (°C) for MJO Phase 8 and Neutral Years during JAS.

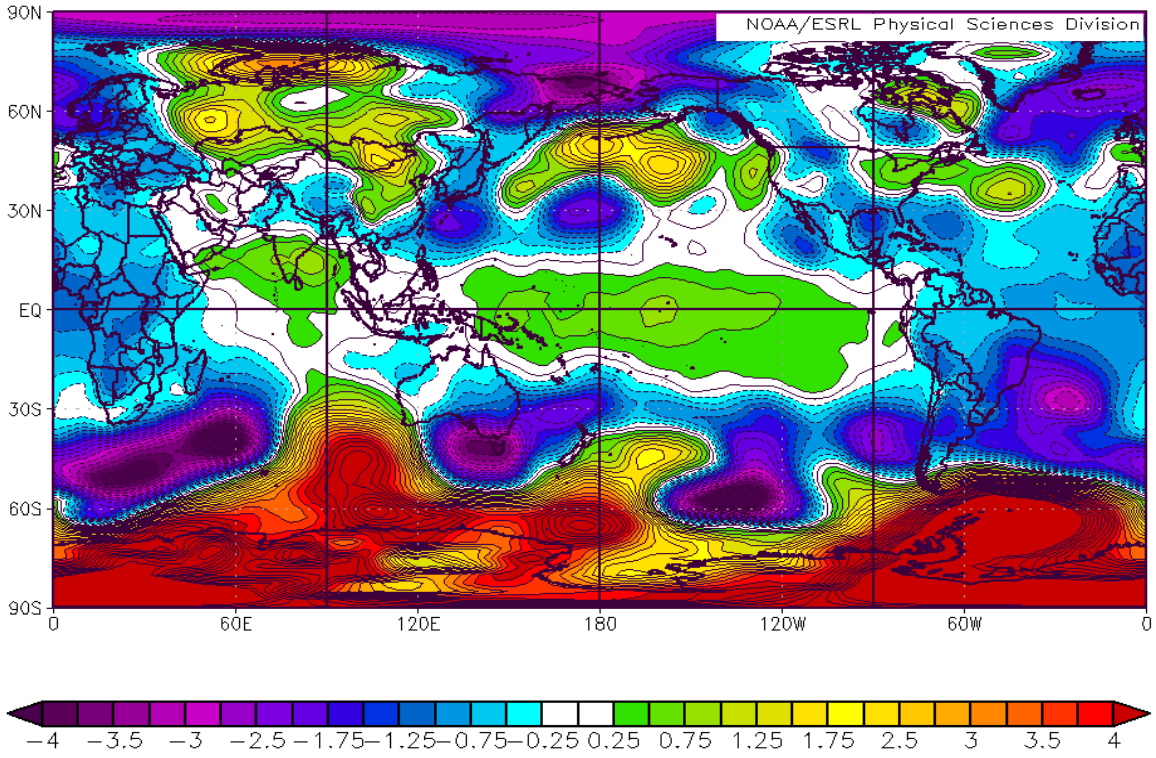

Figure 124. SLP Anomalies (mb) for MJO Phase 8 and Neutral Years during JAS.

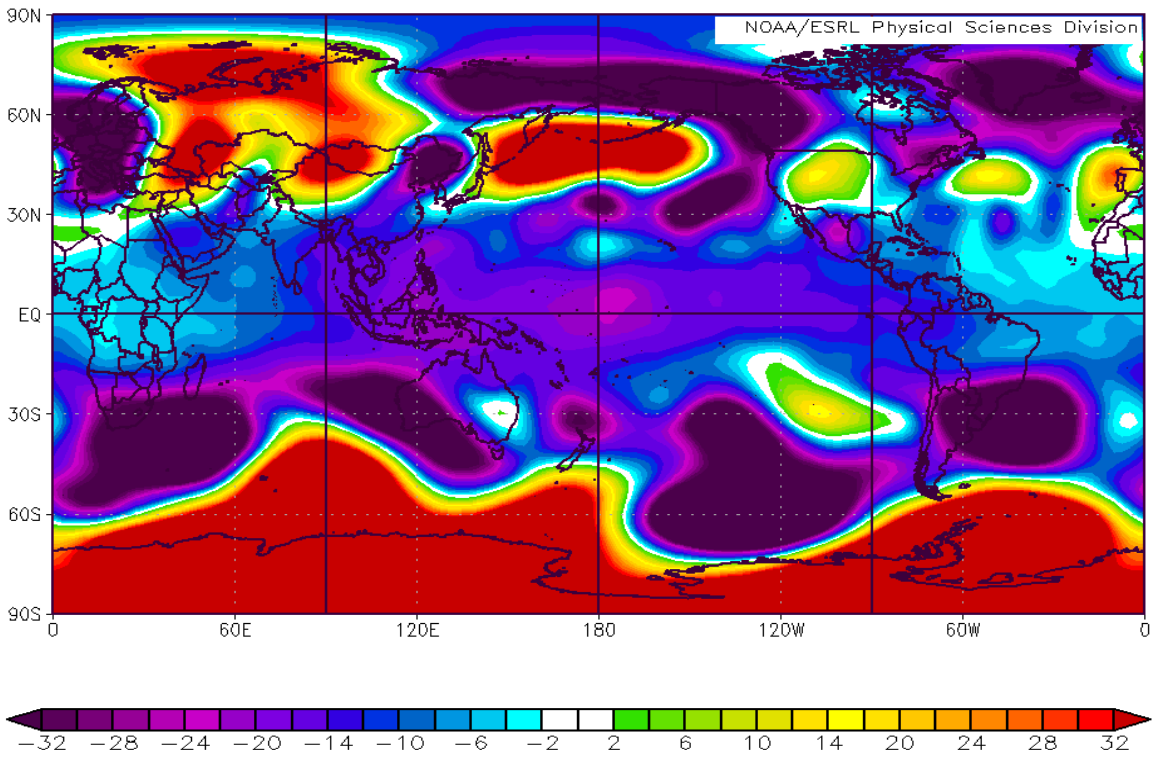

Figure 125. Z200 Anomalies (mb) for MJO Phase 8 and Neutral Years during JAS.

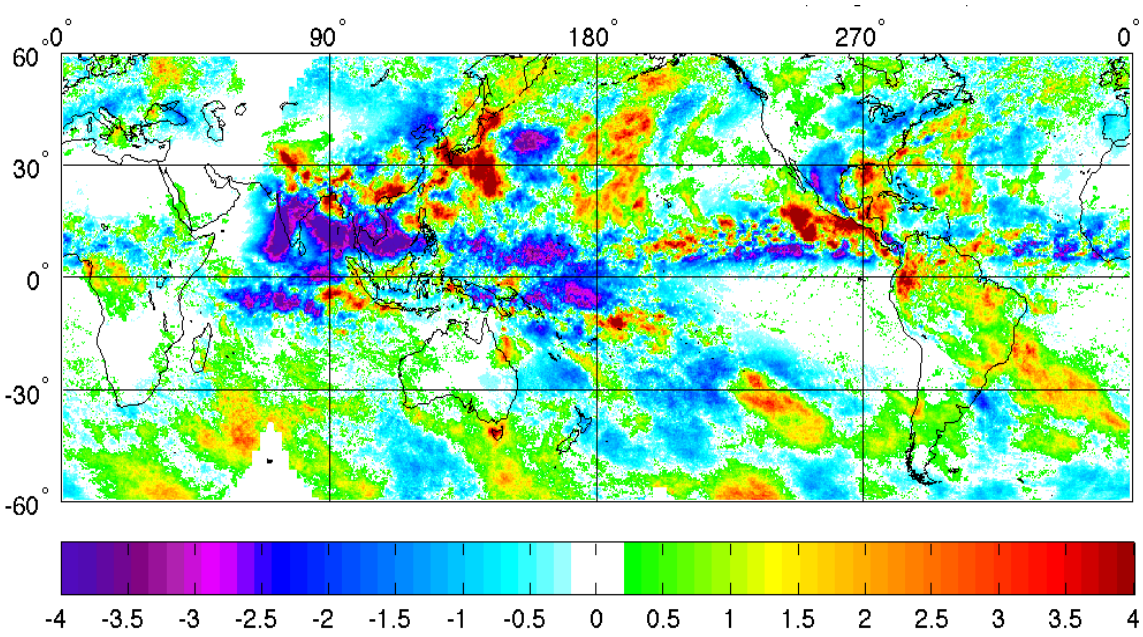

Figure 126. PR Anomalies (mm/day) for MJO Phase 8 and Neutral Years during JAS.

THIS PAGE INTENTIONALLY LEFT BLANK

APPENDIX C. CASE 25: SOUTHWEST ASIA RESULTS

A. CHARACTERISTIC SWA JFM EN ANOMALIES

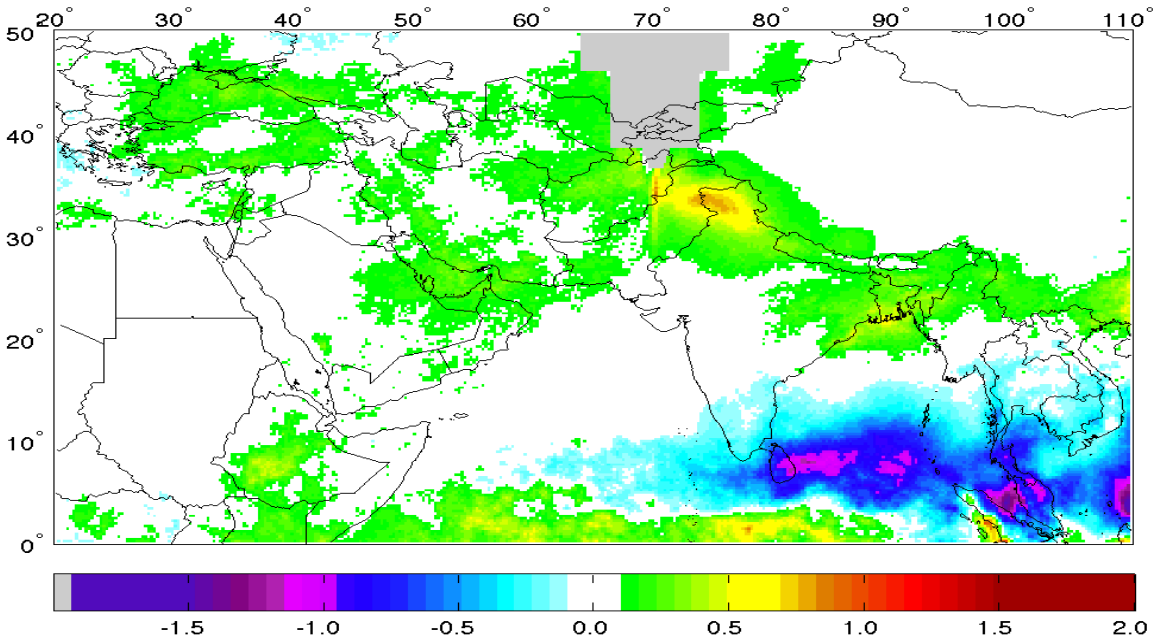

The grey area centered near 70°E is an area of insufficient data. The grey areas in the Indian Ocean indicate PRA values less than -1.95 mm/day.

Figure 127. SWA PR Anomalies (mm/day) for EN Years during JFM.

B. CHARACTERISTIC SWA JFM LN ANOMALIES

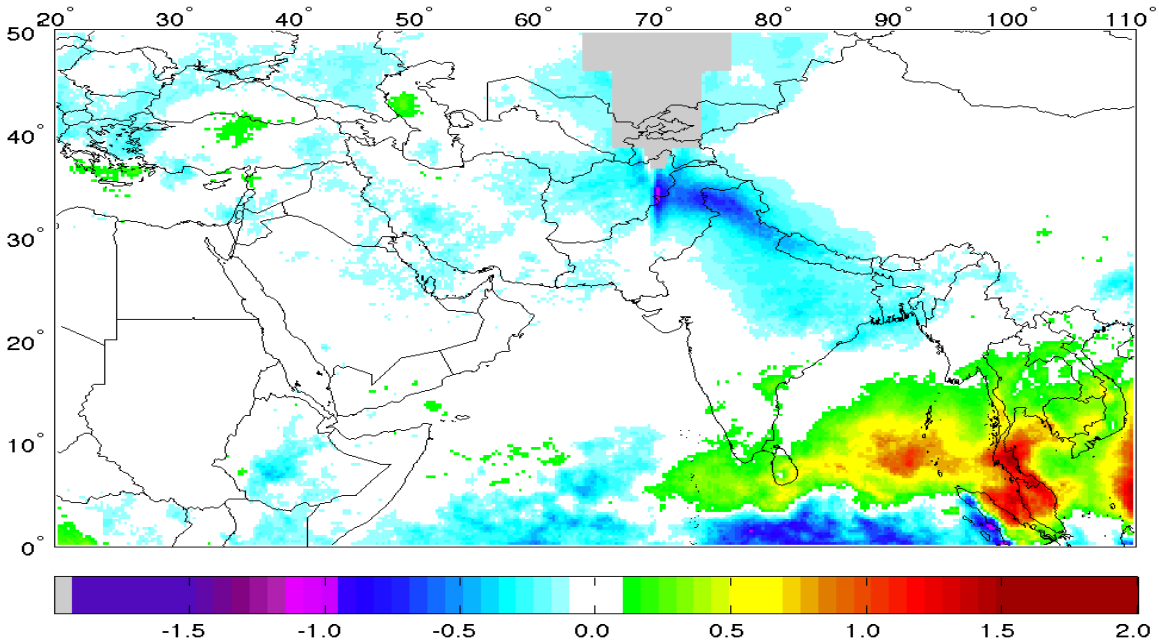

The grey area centered near 70°E is an area of insufficient data.

Figure 128. SWA PR Anomalies (mm/day) for LN Years during JFM.

C. CHARACTERISTIC SWA JFM EN PHASE 4 ANOMALIES

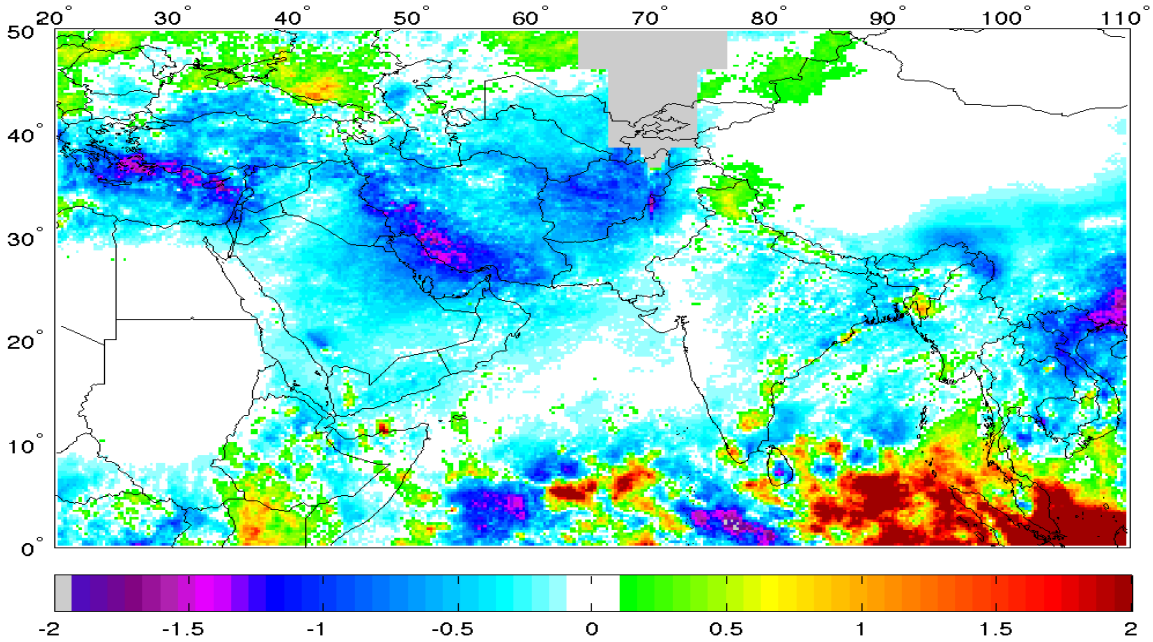

The grey area centered near 70°E is an area of insufficient data.

Figure 129. SWA PR Anomalies (mm/day) for MJO Phase 4 and EN Years during JFM.

D. CHARACTERISTIC SWA JFM EN PHASE 8 ANOMALIES

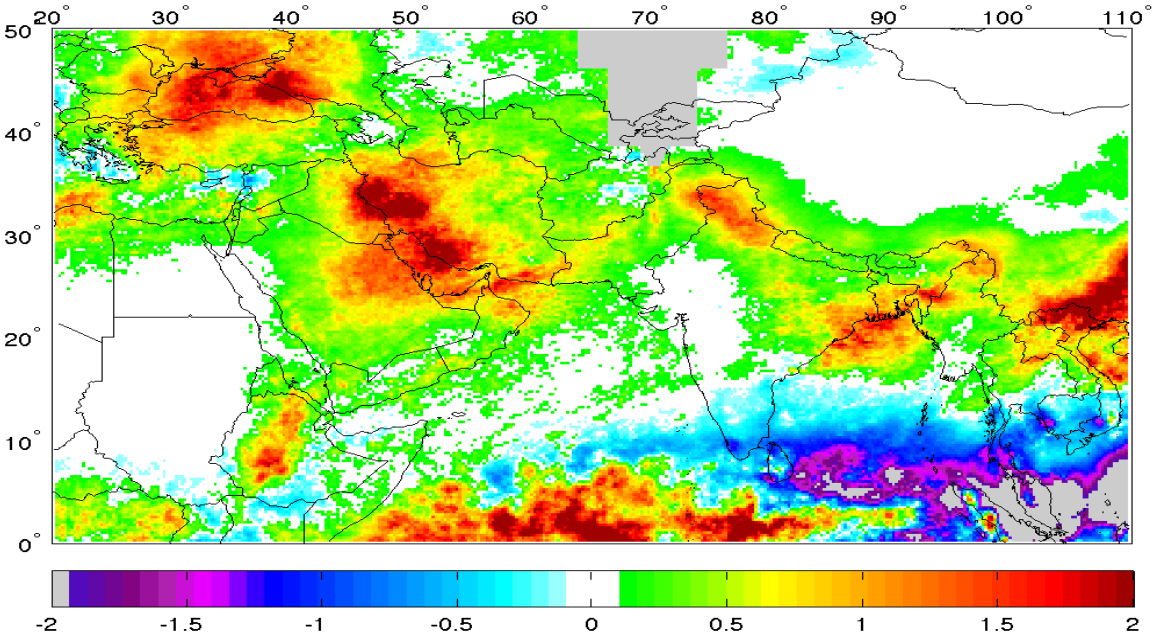

The grey area centered near 70°E is an area of insufficient data. The grey areas in the Indian Ocean indicate PRA values less than -1.95 mm/day.

Figure 130. SWA PR Anomalies (mm/day) for MJO Phase 8 and EN Years during JFM.

E. CHARACTERISTIC SWA JFM LN PHASE 4 ANOMALIES

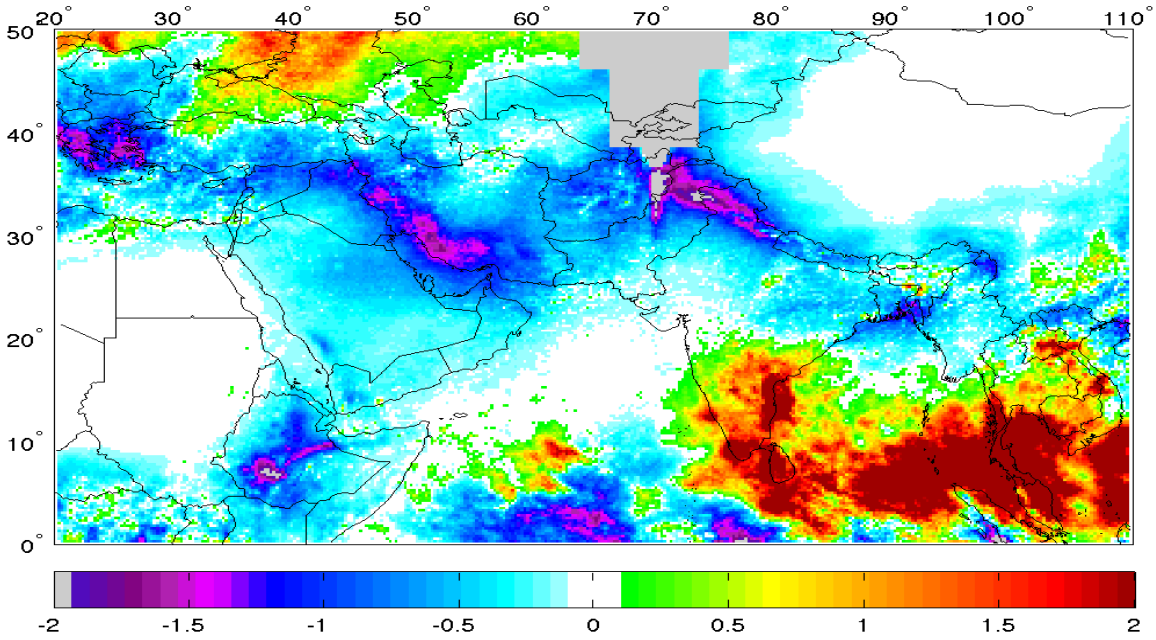

The grey area centered near 70°E is an area of insufficient data.

Figure 131. SWA PR Anomalies (mm/day) for MJO Phase 4 and LN Years during JFM.

F. CHARACTERISTIC SWA JFM LN PHASE 8 ANOMALIES

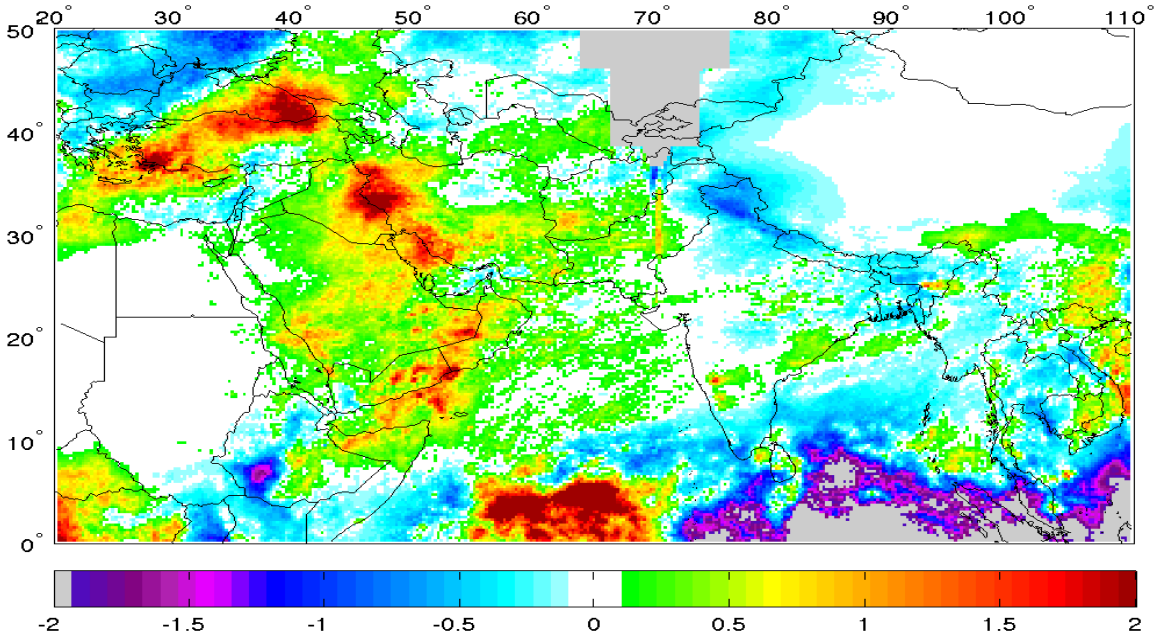

The grey area centered near 70°E is an area of insufficient data. The grey areas in the Indian Ocean indicate PRA values less than -1.95 mm/day.

Figure 132. SWA PR Anomalies (mm/day) for MJO Phase 8 and LN Years during JFM.

G. CHARACTERISTIC SWA JFM NEUTRAL PHASE 4 ANOMALIES

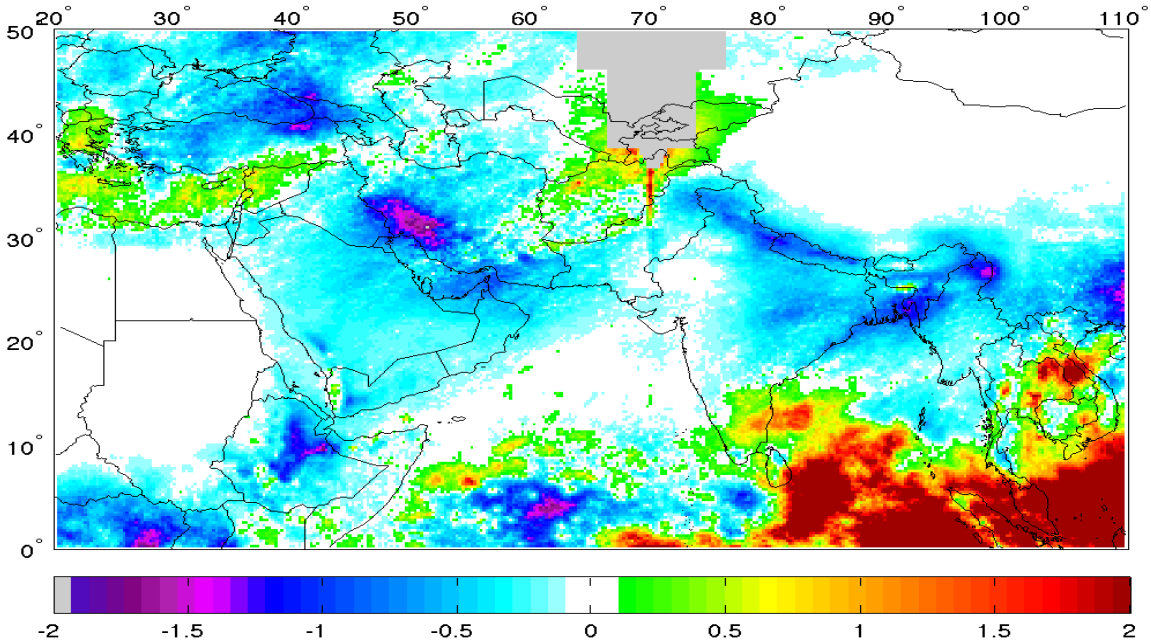

The grey area centered near 70°E is an area of insufficient data.

Figure 133. SWA PR Anomalies (mm/day) for MJO Phase 4 and Neutral Years during JFM.

H. CHARACTERISTIC SWA JFM NEUTRAL PHASE 8 ANOMALIES

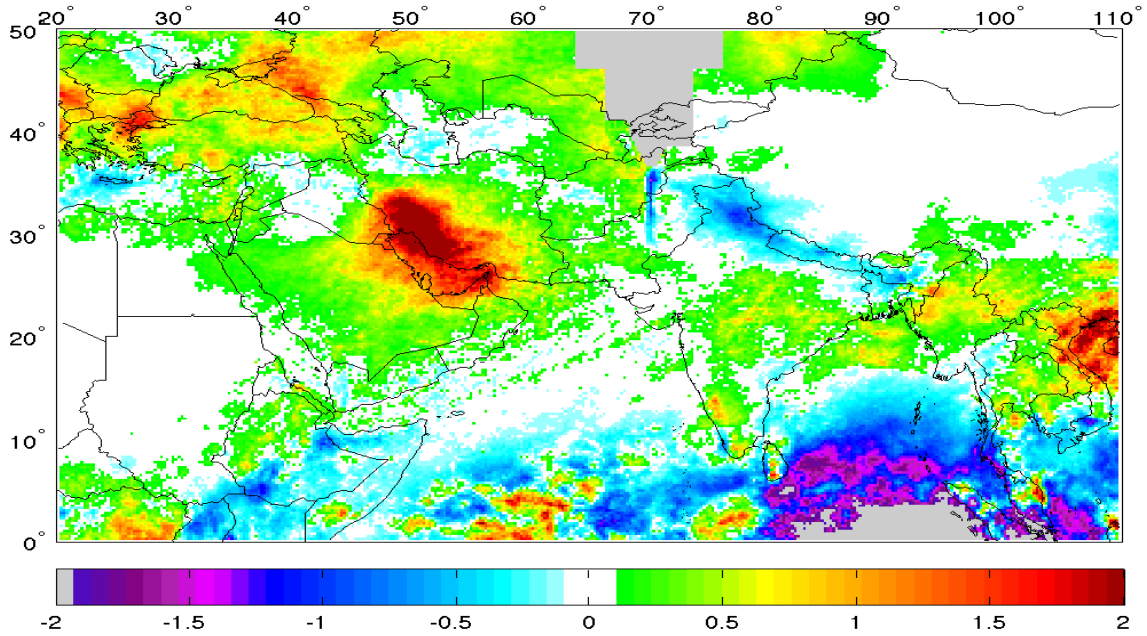

The grey area centered near 70°E is an area of insufficient data. The grey areas in the Indian Ocean indicate PRA values less than -1.95 mm/day.

Figure 134. SWA PR Anomalies (mm/day) for MJO Phase 8 and Neutral Years during JFM.

LIST OF REFERENCES

Ashouri, H., K. Hsu, S. Sorooshian, D. K. Braithwaite, K. R. Knapp, L. D. Cecil, B. R. Nelson, and O. P. Prat, 2014: PERSIANN-CDR: Daily precipitation climate data record from multi-satellite observations for hydrological and climate studies. *Bull. Amer. Meteor. Soc.*, **96,** 69–83.

Australian Government Bureau of Meteorology, 2016: Madden–Julian Oscillation (MJO). Accessed 03 November 2016. [Available online at http://www.bom.gov.au/climate/mjo/.]

Bridgman, H. A., J. E. Oliver, and M. H. Glantz, 2006: *The Global Climate System: Patterns, Processes, and Teleconnections*. Cambridge University Press, 331 pp.

Camargo, S. J., A. G. Barnston, P. J. Klotzbach and C. W. Landsea, 2007: Seasonal Tropical Cyclone Forecasts. *WMO Bull.*, **56,** 297–309.

Chawla, A., D. M. Spindler, and H. L. Tolman, 2013. 30 Year Wave Hindcasts using WAVEWATCH III with CFSR winds Phase 1. MMAB Tech. Note 302, 23 pp.

Chung, C. T. Y., and S. B. Power, 2016: Modelled impact of global warming on ENSO-driven precipitation changes in the tropical Pacific. *Clim. Dyn.,* **47,** 1303–1323.

Gill, A. E., 1982. *Atmosphere-Ocean Dynamics*. Academic Press, 662 pp.

Gottschalck, J., V. Kousky, R. W. Higgins, and M. L. L'Heureux, 2016: Madden Julian Oscillation (MJO) Summary. Accessed 16 January 2016. [Available online at http://www.cpc.ncep.noaa.gov/products/precip/CWlink/MJO/MJO_summary.pdf]

Heidt, S. L., 2009: Long-range atmosphere-ocean forecasting in support of undersea warfare operations in the western north Pacific. M.S. thesis, Dept. of Meteorology, Naval Postgraduate School, 75 pp.

Hendon, H. H., and M. L. Salby, 1994: The Life Cycle of the Madden–Julian Oscillation. *J. Atmos. Sci.,* **51,** 2225–2237.

Horel, J. D., and J. M. Wallace, 1981: Planetary-Scale Atmospheric Phenomena Associated with the Southern Oscillation. *Mon. Wea. Rev.,* **109,** 813–829.

Hu, Q., and S. Feng, 2010: Influence of the Arctic oscillation on central United States summer rainfall, *J. Geophys. Res.*, **115,** D01102, 1–13.

Johnson, S. A., 2011: Modeling the impacts of intraseasonal to interannual climate variations on tropical cyclone formations in the western North Pacific. M.S. thesis, Dept. of Meteorology, Naval Postgraduate School, 87 pp.

Leathers, D. J., B. Yarnal, and M. A. Palecki, 1991: The Pacific/North American Teleconnection Pattern and United States Climate. Part I: Regional Temperature and Precipitation Associations. *J. Climate,* **4,** 517–528.

Kalnay, E., and Coauthors, 1996: The NCEP/NCAR 40-Year Reanalysis Project. *Bull. Amer. Meteor. Soc.*, **77**, 437–471.

Kayano, M. T., and V. V. Kousky, 1999: Intraseasonal (30–60 day) variability in the global tropics: principal modes and their evolution. *Tellus,* **51A**, 373–386.

Kessler, W. S., and R. Kleeman, 1999: Rectification of the Madden–Julian Oscillation into the ENSO Cycle. *Bull. Amer. Meteor. Soc.,* **13,** 3560–3575.

Kistler, R., and Coauthors, 2001: The NCEP–NCAR 50-Year Reanalysis: Monthly Means CD-ROM and Documentation. *Bull. Amer. Meteor. Soc.*, **82**, 247–267.

Madden, R., and P. Julian, 1971: Detection of a 40–50 Day Oscillation in the Zonal Wind in the Tropical Pacific. *J. Atmos. Sci.,* **28,** 702–708.

Madden, R., and P. Julian, 1994: Observations of the 40–50-day Tropical Oscillation – A Review. *Mon, Wea. Rev.*, **122,** 814–837.

Marshall, A. G., H. H. Hendon, T. H. Durrant, and M. A. Hemer, 2015: Madden Julian Oscillation impacts on global ocean surface waves. *Ocean Modeling,* **96,** 136–147.

Marshall, A. G., H. H. Hendon, and G. Wang, 2016: On the role of anomalous ocean surface temperatures for promoting the record Madden–Julian Oscillation in March 2015. *Geophys. Res. Lett.,* **43,** 472–481.

Matsuno, T., 1966. Quasi-Geostrophic Motions in the Equatorial Area. *J. Meteor. Soc. Japan*, **44**, 25–43.

McKeon, B., 2013: Climate analysis of evaporation ducts in the South China Sea. M.S. thesis, Dept. of Meteorology, Naval Postgraduate School, 89 pp.

Moon, J. –Y., B. Wang, and K. –J. Ha, 2011: ENSO regulation of MJO teleconnection. *Clim. Dyn.*, **37,** 1133–1149.

Murphree, T., 2016: Modern Climatology. Naval Postgraduate School, lecture notes for MR3610.

Murphree, T., 2016: Dynamic Meteorology. Naval Postgraduate School, lecture notes for MR4322.

NOAA, 2016: Coastal and Marine Spatial Planning. Accessed 2016. [Available online at https://www.cmsp.noaa.gov/activities/.]

NOAA, 2016: Multivariate ENOS Index. Accessed 2016. [Available online at http://www.esrl.noaa.gov/psd/enso/mei/.]

NOAA, 2016: Daily Mean Composites. Accessed 2016. [Available online at http://www.esrl.noaa.gov/psd/data/composites/day.]

NOAA, 2016: Monthly/Seasonal Climate Composites. Accessed 2016. [Available online at http://www.esrl.noaa.gov/psd/cgi-bin/data/composites/printpage.pl.]

Obama, B. H., 2010: Executive Order 13547-Stewardship of the Ocean, Our Coasts, and the Great Lakes. Accessed 20 November 2016. [Available online at https://www.whitehouse.gov/the-press-office/executive-order-stewardship-ocean-our-coasts-and-great-lakes.]

PIRPB, 2016: Pacific Islands Regional Planning Body. Accessed 16 March 2016. [Available online at https://pacificislandsrpb.org/.]

Philander, S. G. H., 1990: *El Nino, La Niña, and the Southern Oscillation*. Academic Press, 293 pp.

Pohl, B., and A. J. Matthews, 2007: Observed Changes in the Lifetime and Amplitude of the Madden Julian Oscillation Associated with Interannual ENSO Sea Surface Temperature Anomalies. *J. Climate,* **20,** 2659–2674.

Rui. H., and B. Wang, 1990: Development Characteristics and Dynamic Structure of Tropical Intraseasonal Convection Anomalies. *J. Atmos. Sci.,* **47,** 357–379.

Ramsaur, D., 2009: Climate analysis and long range forecasting of radar performance in the western North Pacific. M.S. thesis, Dept. of Meteorology, Naval Postgraduate School, 93 pp.

Saha, S., and Coauthors, 2006: The NCEP Climate Forecast System. *J. Climate*, **19**, 3483–3517.

Saha, S., and Coauthors, 2010: The NCEP Climate Forecast System Reanalysis. *Bull. Amer. Meteor. Soc.*, **91,** 1015–1057.

Saha, S., and Coauthors, 2014: The NCEP Climate Forecast System Version 2. *J. Climate,* **27,** 2185–2208.

Sardeshmukh, P. D., and B. J. Hoskins, 1988: The Generation of Global Rotational Flow by Steady Idealized Tropical Divergence. *J. Atmos. Sci.,* **45,** 1228–1251.

Stepanek, A. J., 2006: North Pacific – North American Circulation and Precipitation Anomalies Associated with the Madden – Julian Oscillation. M.S. thesis, Dept. of Meteorology, Naval Postgraduate School, 119 pp.

Turek, A. G., 2008: Smart climatology applications for undersea warfare. M.S. thesis, Dept. of Meteorology, Naval Postgraduate School, 95 pp.

Van den Dool, H. M., 2007: *Empirical Methods in Short-Term Climate Prediction*. Oxford University Press, 215 pp.

Wang, B., and J. C. L. Chan, 2002: How strong ENSO Events Affect Tropical Storm Activity over the Western North Pacific. *J. Climate*, **15,** 1643–1658.

Wheeler, M. C., and H. H. Hendon, 2004: An All-Season Real-Time Multivariate MJO index: Development of an Index for Monitoring and Prediction. *Mon. Wea. Rev.*, **132,** 1917–1932.

Wilks, D. S., 2006: *Statistical Methods in the Atmospheric Science*, 2nd ed., Academic Press, 627 pp.

Wolter, K., and M. S. Timlin, 2011: El Niño/Southern Oscillation behaviour since 1871 as diagnosed in an extended multivariate ENSO index (MEI.ext). *Intl. J. Climatology*, **31,** 14 pp., in press.

Zhang, C., 2005: Madden–Julian Oscillation. *Rev. Geophys.*, **43,** 1–36.

Zhang, C., 2013: Madden–Julian Oscillation: Bridging Weather and Climate. *Bull. Amer. Meteor. Soc.*, **94,** 1849–1870.

INITIAL DISTRIBUTION LIST

1. Defense Technical Information Center
   Ft. Belvoir, Virginia

2. Dudley Knox Library
   Naval Postgraduate School
   Monterey, California